AN INVESTIGATION INTO THE ATOMISATION OF EMULSIFIED FUELS

By

PEI LIN ZHOU

A Thesis Submitted In Application

For Admission To The Degree Of

DOCTOR OF PHILOSOPHY

Department Of Marine Technology

Faculty Of Engineering

University Of Newcastle upon Tyne

December 1992

NEWCASTLE UNIVERSITY LIBRARY

092 50645 X

Thesis L4081

CONTENTS

AN INVESTIGATION INTO THE ATOMISATION OF WATER-IN-OIL EMULSIFIED FUELS

ABSTRACT

It has been recognised for a number of years that the use of water-in-oil emulsified fuels in diesel engines provides the advantages of improved engine combustion and emissions. At the present time, it is a general practice to burn W/O emulsions on shipboard propulsion diesel engines. To meet the requirements of environmental protection, there exists the possibility of using emulsified fuels on road vehicles in the future.

The Department of Marine Technology of The University of Newcastle upon Tyne has been involved in this subject for many years, initially concentrating on the production of emulsions using surfactants, and later using mechanical devices, subsequently concentrating on the engine performance study using W/O emulsions. A multiplicity of experimental data has been obtained from a broad range of diesel engines. In the mean time, there have been many reports in this field from other investigators. It is safe to say that the research on engine performance using emulsified fuels has been comprehensive.

This project is a continuation of the application of W/O emulsions in diesel engines. As there is a lack of investigation into W/O emulsion atomisation and combustion, the project aims to a).study the effect of water on fuel atomisation; b).develop the mathematical models for spray atomisation of emulsified fuels; c).investigate the phenomena concerned with the combustion and emissions observed by previous researchers.

In the atomisation study of emulsified fuels, it has generally been assumed that the benefits associated with improvements in fuel atomisation are brought about by what is termed the "micro-explosions" effect as observed in boiler/furnace applications. It

has been reported that the positive effect of the micro-explosions in an engine combustion chamber exists only under limited conditions. It is therefore questionable as to whether micro-explosions actually occur in the real engine combustion chamber or not. Even if they do take place it is likely that the explosions are very weak. There is some justification to support the thesis that the perceived benefits of using emulsified fuels may be derived from sources other than micro-explosions.

This thesis presents a systematic and detailed investigation on the atomisation of water-in-oil emulsified fuels, which includes the properties of W/O emulsions, atomising fundamentals, test rigs for fuel spray atomisation, mathematical model development and regression of the models, etc.. A novel, less expensive and effective method for studying fuel atomisation, is achieved by a high speed camera with a micro lens and an extensive tube, and this has successfully been used in the tests. Test results obtained from the non-combusting bomb indicate that the atomisation of emulsified fuel contributes a major part in the improvements of engine combustion and emissions in the following respects: 1).longer spray penetration; 2).larger spray angle; 3).larger fuel specific area/small Sauter mean diameter; 4).more air is available in the spray for combustion. Results are in good agreement with the theoretical study, and explain the mechanisms of the phenomena observed in engine tests by previous researchers. There is also a good consistency between the results and the quantitative descriptions of the models.

ACKNOWLEDGEMENTS

The author would like to express his gratitude to his supervisor, Mr. I. Thorp, Head of the Department of Marine Technology, for his advice, patience, and encouragement throughout this project.

Thanks to Mr. J. Smith for his kind cooperation and assistance with the test rig manufacture and the whole experimental programme.

Thanks to all members of staff in the Department of Marine Technology for all sorts of help during the period of the author's study.

The author is very grateful to the Government of the People's Republic of China and the British Council for their financial support.

Special thanks to my wife Li Wang, my son Xin Zhou and my family at home for their care, patience and understanding.

DECLARATION

This is to declare that no part of the work presented in this thesis has been submitted in application for another degree in this or any other university or educational institute.

CHAPTER ONE:

INTRODUCTION

1.1 Introduction

The diesel engine has more than a hundred years history. Now, almost all ships, heavy duty trucks and many locomotives are driven by diesel engines. In the small vehicle area, cars, buses etc., diesel engines also stand as a strong competitor with petrol engines. To investigate the performance of diesel engines has long been a favoured topic for researchers in the internal combustion engine field.

During the last 50 years considerable efforts have been made to increase the thermal efficiency and reliability of diesel engines ,and to decrease noise and harmful emissions. Normally, methods to increase thermal efficiency are contrary to those of decreasing noise and emissions. For example, in order to increase thermal efficiency by increasing the combustion pressure, methods of increasing the compression ratio and advancing the injection timing, etc. have been adopted. These are generally contrary to the requirement for reducing noise and emissions. A requirement arises from this to investigate methods which help to solve both of the problems at the same time. Emulsified fuel (water added into the fuel) may go some way to satisfy this requirement. Actually, the effect of using emulsified fuel in reducing emissions is much greater than its effect on increasing thermal efficiency.

1.2 The Historical Application Of Water-in-Oil Emulsions

The application of emulsified fuel in internal combustion engines has shown that the injection of water into a combustion engine improves the engine performance. Direct water spray injection into high performance spark-ignition engines for cooling and reducing detonation has been used since at least 1913[1]. In the past, it was used to

increase the octane rating of gasoline, and to reduce nitrogen oxide emissions in gas turbines, and particulate emissions in oil furnaces. In World War II, it was general practice to increase power output in aircraft by injecting water into the engines.

Preliminary findings indicate that during combustion the internal water droplets vaporize, causing micro-explosions of fuel drops, leading to much finer atomisation and very thorough mixing of air and fuel. This allows complete combustion with much less air and a reduction in soot production. It is reported [2], that in boiler furnaces the soot reduction was 80-90% in some cases. Less excess air means that less heat is carried out by the exhaust gases.

The addition of water into the fuel improves atomisation, and permits a leaner air/fuel ratio. A reduction in combustion temperature by the vaporization of water limits exhaust valve burning and engine overheating. A leaner ratio permits reduction of CO emissions. The reduction of combustion zone temperature will also reduce NO_x emissions. The lower combustion temperature can also reduce heat loss through the cylinder wall. The net result is to improve engine efficiency.

1.3 The Utilization Of Water-in-Oil Emulsions In Diesel Engines

The Department of Marine Technology at the University of Newcastle upon-Tyne has been doing research on emulsified fuel for many years, initially concentrating on the production of emulsions using surfactants, and later, using mechanical devices. Tests were undertaken in different engines and with different fuels. Gas oil and heavy fuels up to 120cSt were used. A multiplicity of experimental data had been obtained from a broad range of diesel engines and boiler systems. A series of extensive tests have been undertaken with the Department's own Ruston 6APC medium speed diesel engine. An extensive test was also undertaken on a Doxford 58JS slow speed diesel engine.

The tests clearly demonstrated the practicability of running marine diesel engines on non-stabilized water-in-oil emulsions. Significant reductions in fuel consumption up

to a maximum of 7.5 percent, were achieved with moderate water contents, up to 10 percent. At the same time, the engines were reported to be cleaner, the exhaust emissions reduced and exhaust temperatures lowered.

Many reports agree that the utilization of emulsified fuel in a diesel engine can reduce the emission of NOx by 25% to 50% [1,2,3,4,5,6,7,8]. The unburnt hydrocarbons increased in most tests, while exhaust temperatures were lowered.

The reports about specific fuel consumption vary. Most researchers reported reduction in fuel consumption from 1% to 8%. The use of emulsified fuel resulted in 3% to 5% saving in shipboard applications [5]. Some tests showed that there was no remarkable improvement in specific fuel consumption [7] and others a worsening effect [8].

The combustion theory of emulsified fuel is not yet fully understood, since the phenomena of hydrocarbon combustion are so complex.

In 1988, Dr. H.Z. Sheng published a series of reports [9,10,11,12] about the investigation of spray jet, vaporization, combustion process and combustion models of emulsion in a diesel engine. Dr. Sheng's tests confirmed that micro-explosions did occur in the high temperature and pressure combustion chamber. The strength of micro-explosion varied as the test conditions changed, which gave a reasonable explanation as to why the tests results for emulsified fuel in a diesel engine may vary.

Dr. Sheng found that when the high pressure chamber was heated to about 500°C, the micro explosions were much stronger. When the temperature was below 460°C, the micro explosions could hardly be observed, the energy of the explosion being very weak if it took place at all. At 550°C, the explosion took place early and was weaker as well. Dr. Sheng's explanations of these phenomena are: If the environmental temperature is not high enough, the water particles in the droplets will not be superheated and will evaporate gently. If the temperature is too high, the heat transfer between gas and droplets is too rapid and the temperature gradient of the droplet is so

steep that the particles in the droplets can not be evenly superheated. Only the outer layer is superheated and explodes, while the inner parts of water particles are still "cold". If the environmental temperature is suitable, the water particles in the droplets will all be rapidly heated into the superheated state, which is a pseudo-stable state. When the water particles near the outer layer of the spray achieve the limit of superheat and vaporization, the other water particles will also vaporize and expand rapidly at the same time. In this case, the explosive strength will be strong enough to emit fragments of torn droplets several millimetres away from the spray, and greatly enlarge the spray from a macroscopical point of view.

From the above explanations about the micro-explosions of water particles in droplets, it is understood that the micro-explosions are able to expand the spray and homogenize the fuel air mixture. However its occurrence and strength is totally dependent on the environmental conditions and water percentage, etc. and the effect of the micro-explosion is also related to the environmental pressure. Thus the positive influence of the emulsion is fully conditional on the applied situation. Because of that, sometimes the effect may be negative. That is the reason why the economic benefits to engine application reported by different researchers are often different, some are even worse than pure fuel according to the different test conditions.

Until now, all the investigations of the application of emulsified fuel have been limited to the engine's performance. Some researchers did observe the phenomena of atomisation and combustion of emulsified fuel, but only qualitatively. Even in Dr. Sheng's reports [13], only a qualitative explanation of emulsified fuel atomisation and combustion was given.

It is questioned therefore how emulsified fuel behaves in an engine combustion chamber. Do micro-explosions occur in a real engine combustion chamber? According to Dr. Sheng's tests, the positive effect of micro-explosions only exists when the temperature is about 500°C(460-540°C) in a still pressure bomb. However in a real

engine all the events are carried out at high speed. The time interval within which the cylinder temperature is about 500°C is very short. There might not be enough time for heat transfer from the hot surroundings to the water particles which are covered by fuel. So it is hard to say whether micro-explosions would occur in the a engine combustion chamber or not. If they do occur, the explosion strength must be very weak. There could be other reasons which might explain where the benefits of applying emulsified fuel are achieved other than by micro-explosions.

It is evident that the addition of water into fuel changes the properties of fuel, e.g. density, viscosity, surface tension etc., which are the key parameters influencing fuel atomisation. The studies of engine performance and atomisation for pure fuel have been extensive [14,15,16,17,18,19,20,21,22,23,24], and many mathematical models have been built up to describe the atomisation process. What are the characteristics of emulsified fuel atomisation? What are the quantitative descriptions of emulsified fuel atomisation?

1.4 The Objectives Of This Project

The investigation of emulsified fuel atomisation is the continuation of previous studies. The objectives are: i) to find out the effects of water on fuel atomisation based on the fundamental study of the atomisation, ii) to develop the atomisation mathematical models based on the experimental results obtained from a non-combustion bomb and the test data regression. iii) to predict the combustion and emissions of emulsified fuels in real diesel engines.

1.5 Survey Of Previous Work On The Fuel Atomization In Diesel Engines

1.5.1 Introduction

The properties of a pressure spray jet can be divided into two categories: these are injection property and atomisation property. The injection one property is associated

with time and refers to the fuel injection rate, injection time and injection duration which are determined by the high pressure pump, high pressure pipe, injector and so on. In other words, the injection property is determined by the combination of the individual property of the parts which form the injection system. To determine the injection property, one must first measure the properties of individual parts. Since the introduction of the computer, data retrieval has been greatly enhanced, the injection property being calculated from a mathematical model by only the input of pressure wave and needle lift, etc..

The injection property is a very important parameter for influencing the engine's performance, but it is not considered in this project.

The atomisation property refers to the spatial property of the spray, i.e. spray penetration, spray angle, droplet size and distribution, etc.. It has been verified by theory and experiment that, in order to obtain intensive and effective combustion, a large specific fuel area must be provided by the atomisation before its combustion. The quality of spray atomisation directly affects the formation of gas/fuel mixture in the combustion chamber, therefore affecting the combustion process. The requirements of a spray for "good" combustion are:

1). Good atomisation: For the same volume fuel, the larger the specific area, the faster the vaporization and combustion. For example, the surface area of 1 ml fuel of spherical shape is 483 mm^2. If it is atomized into droplets of 40 μm in diameter, the droplet number is $2.99x10^7$, and the total surface area is $1.5x10^5$ mm^2, the increased surface area being 310 times of its initial value. The increase of surface area means an increase in combustion rate. Therefore, for the purpose of "good" combustion, fuel must be atomised into small and homogeneous droplets. This does not mean that the smaller the droplets are, the better the combustion process, since the momentum of droplets is proportional to D^3, where D is the droplet diameter. If the droplet diameter is too small that will reduce the penetration of spray.

In a spray jet, fuel droplets have a wide range in diameter. The mean droplet diameter cannot be used to indicate the total fuel surface area. The concept of the Sauter Mean Diameter (SMD) has extensively been employed to express the total fuel droplets surface area. The definition of SMD is $D_{32} = (\Sigma d_i^3)/(\Sigma d_i^2)$, which corresponds to (not equal to) the ratio of total droplets volume to their surface area. The ideal SMD is normally under or about 25 μm.

2). Proper spray penetration: If the burning droplets are still, they would be covered by the burned gas and hence the combustion would be stopped due to the shortage of oxygen. Therefore the droplets must have a certain momentum to break up the burned gas, and contact the fresh air. As mentioned above, the droplet momentum is $\propto D^3$, while the resistance to droplet progression is $\propto D^2$. In order to increase the spray penetration, the droplet size has to be increased. This is contrary to the requirement for a large specific area. Of course, the increase in the momentum can be obtained by increasing the droplet velocity, but this is restricted by the injection system and the engine itself. How to organize the injection and atomisation has long been one of the problems in diesel engine combustion.

3). Proper spatial distribution: For the purpose of increase of the mean effective pressure, and reduction of the equivalent rate of air to fuel rate, all the air in the combustion chamber should participate in the combustion. It is easy to realize this in the gasoline engine because of its very homogeneous air/fuel mixture. In a diesel engine combustion chamber, the air in the areas where the droplets cannot approach cannot be utilized, while, in the areas where the fuel is too rich, gas carbon (CO_2 and CO) will be produced which stops the fuel combustion due to the shortage of oxygen. Thus, the fuel droplets should be distributed homogeneously throughout the whole combustion chamber to fully utilize the air for combustion. For this purpose, some methods have been proposed, e.g. increasing the injection pressure to achieve a more homogeneous atomisation and longer penetration, introducing or

creating air swirl and turbulence in the combustion chamber to promote the mixing of fuel with air, improving the shape of combustion chamber to achieve a good spatial match with fuel sprays, etc..

Most of the previous work on fuel atomisation in diesel engines has been concerned with the measurement of spray penetration, spray angle and the development of their models. Little work has dealt with the spray droplets and their distribution because of the problem of high density and velocity. Recently, laser techniques and very high speed photography have been introduced into this area, which allows accurate measurement of droplet size, distribution and vaporization. Their utilization will be discussed in a following section.

1.5.2 Test Rig For Fuel Atomization And Combustion Study

There has been a wide range of test rigs for investigating the spray atomisation of diesel engines, with each set-up having its own merits. Researchers, with a strong desire to validate their mathematical models on diesel injection spray, mixture of fuel/air and combustion, have used fixed volume chambers [25,26,27,28, 29,30,31, 32]. These test rigs often have the advantages of providing excellent optical access, and allowing independent control of the major influencing parameters. They are thus suitable for fundamental studies of spray formation, ignition delay and combustion. However, they cannot simulate the real engine running conditions, since there is no piston movement or inlet and exhaust valves similar to that of a reciprocating engine. Absence of the above, no doubt changes the air flow characteristics significantly.

To simulate the air flow characteristics, some researchers have used rapid compression machines with an optical access on the combustion chamber as the test rig (Fig. 1.1) [32]. But rapid compression machines still have no inlet and outlet valves.

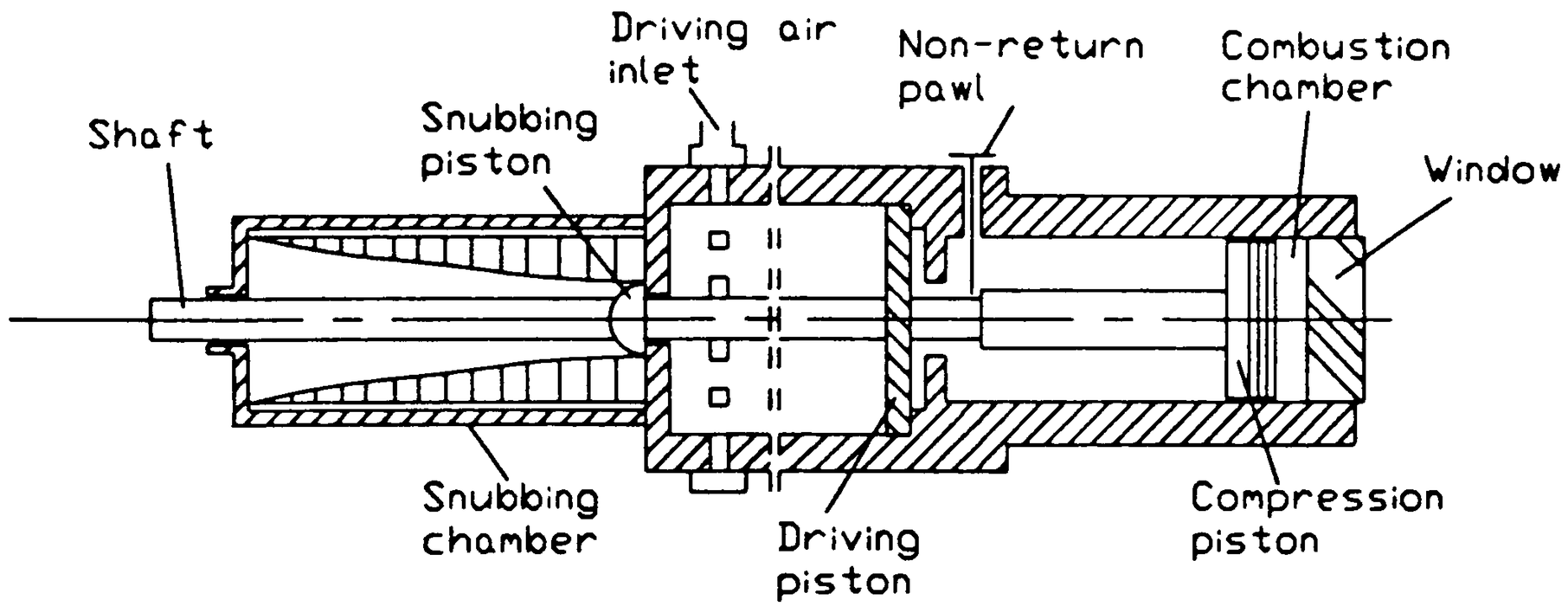

Fig 1.1 Rapid compression machine

Real engines have also been used for fuel spray and combustion photography. In general there are two types: the ones viewing the injection and combustion phenomena from the top through a transparent cylinder head, with or without ports and valves (Fig. 1.2) [33]; and those viewing from the underneath through an elongated piston with transparent crown (Fig. 1.3) [34,35]. Some researchers used test rigs with transparent windows on both the cylinder head and piston crown [36]. In [37], the optical openings were on the side of the cylinder wall.

The test rigs mentioned above, originally conceived for fundamental investigations, suffer from being slightly different from real engines as far as operating conditions and hardware is concerned.

The AVL company developed a new technique in 1985 which circumvents these disadvantages [38]. The system shown in Fig 1.4 is a combination of endoscopes and an optical linkage mechanism to transmit the image from the combustion chamber

of an engine to a high speed camera without any major modifications of the engine. This system can even be used on a production engine to investigate the realistic injection and combustion processes.

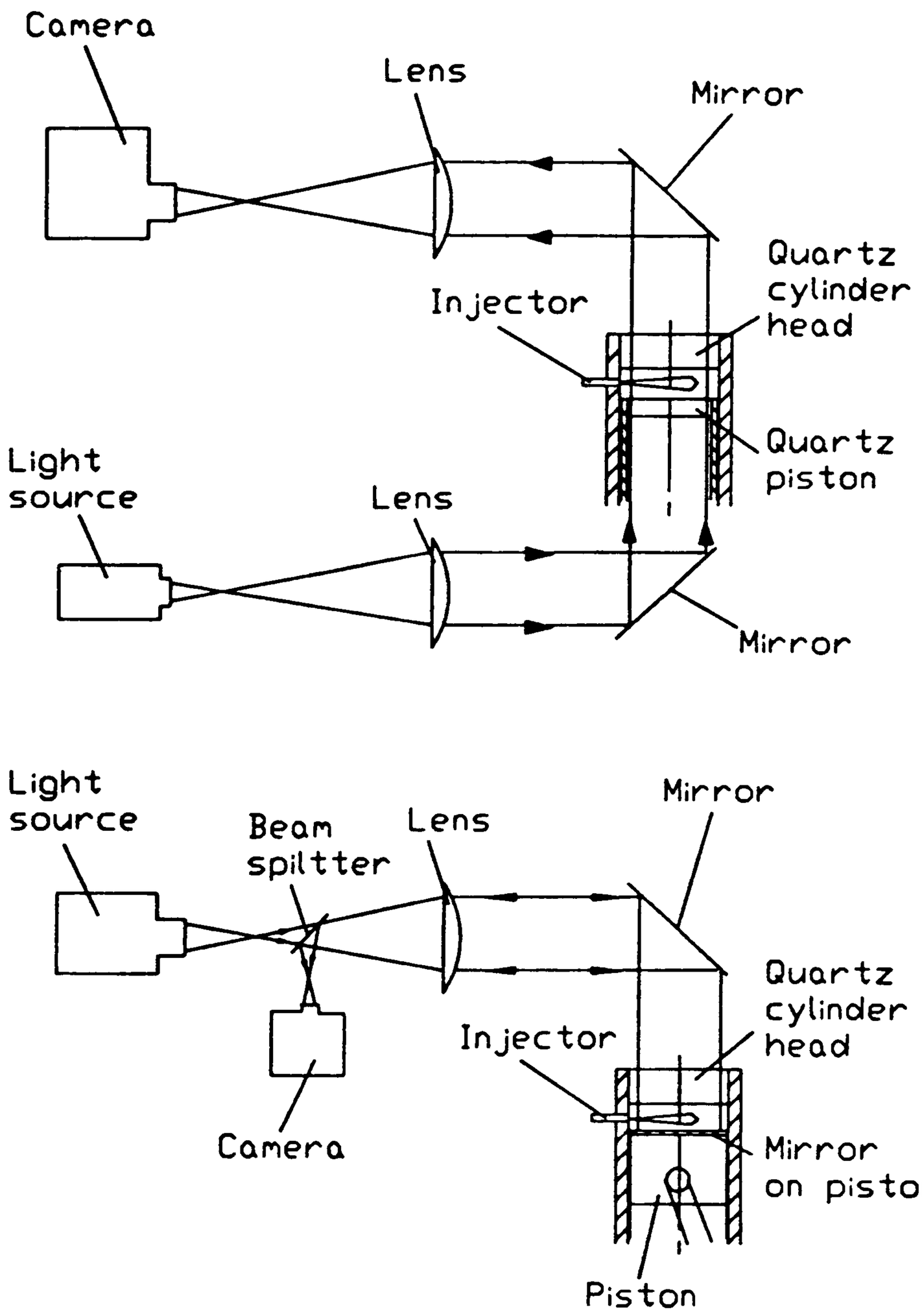

Fig 1.2 Viewing the atomising and combustion from cylinder head

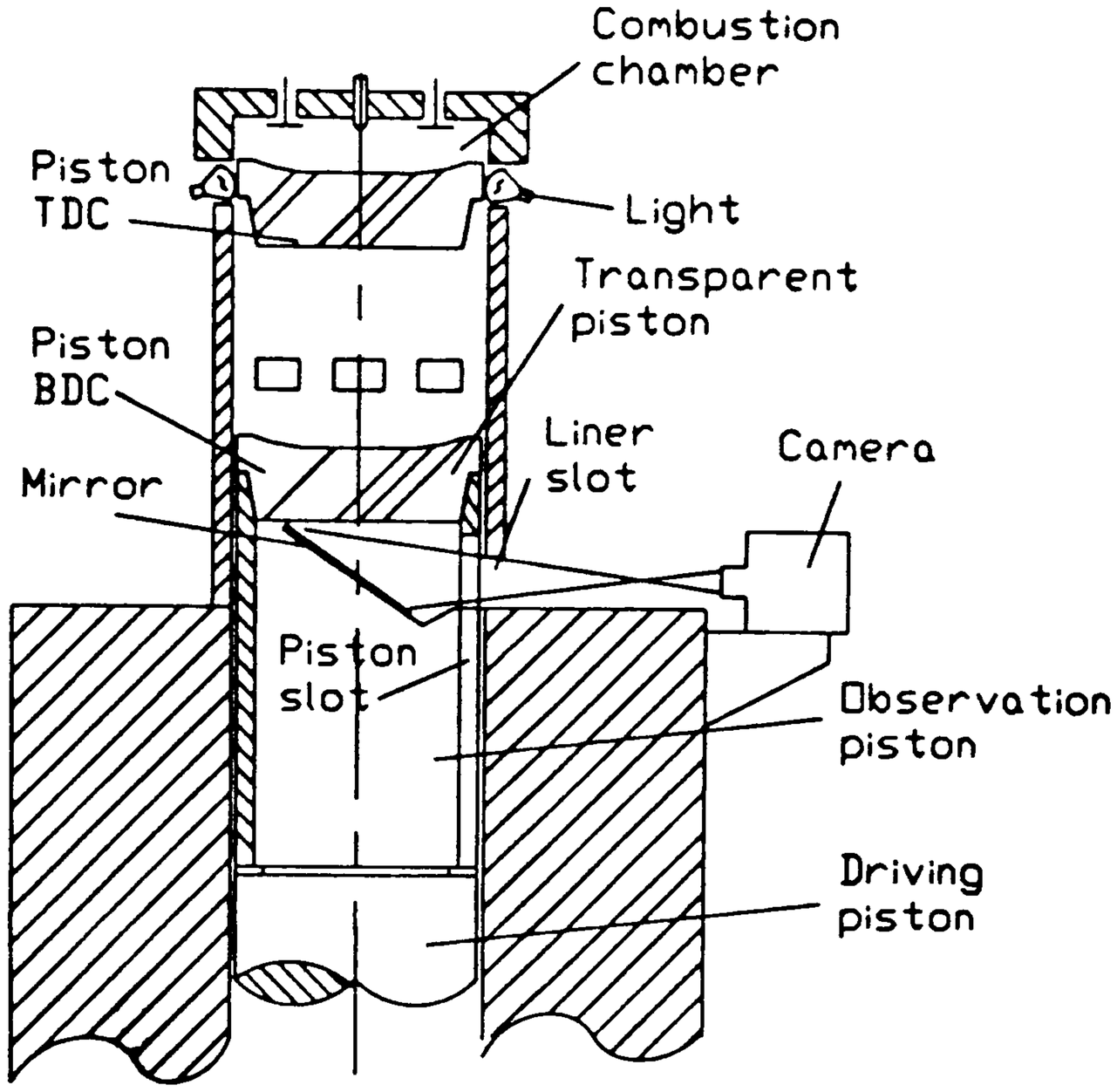

Fig 1.3 Viewing the atomising and combustion from the transparent piston

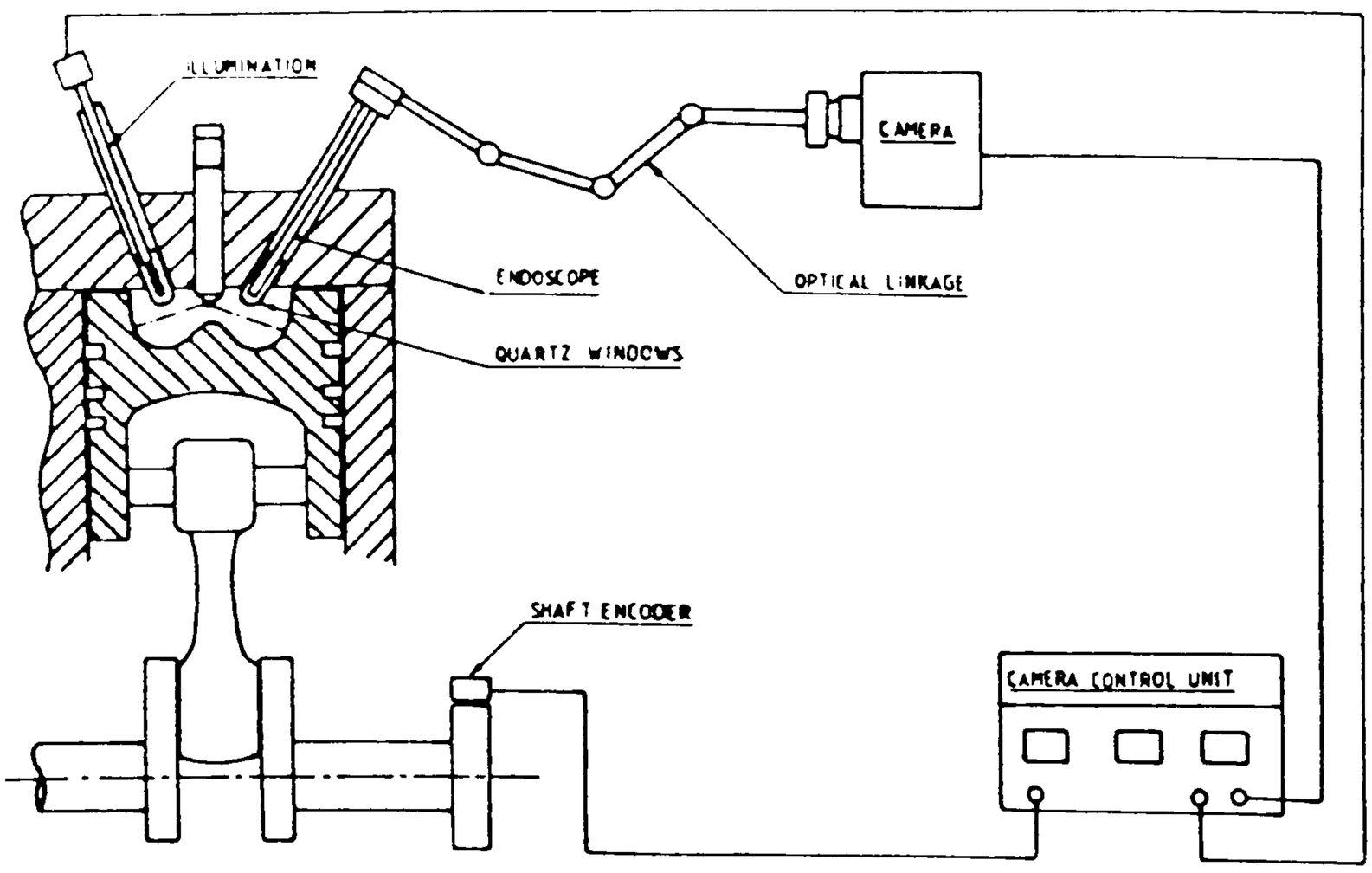

Fig 1.4 AVL high speed camera system

1.5.3 Instrumentation Techniques For Studying Atomization And Combustion

The study of atomisation and combustion involves: (a) The measurement of the time dependent local properties of spray and its combustion, i.e. droplets size, velocity and vaporization, combustion temperature and rates, gas species concentration, etc.. (b) The measurement analysis and modelling.

The techniques applied for this purpose [26,31,32,33,34,35,37,38,39,40,41,42, 43,44,45,46,47,48,49,50,51,52] can be essentially classified as intrusive and non-intrusive, in other words, solid probes and optical methods.

The intrusive techniques, consisting of thermocouples and suction probes, have a long history of usage for measurements of temperature in flames, particle size and velocity, and gas species of concentration [39,40,41]. By directly linking the output from fine wire thermocouples to a computer, measurements of local time constants are made, followed immediately by direct compensation of temperature variation. Measurement of the time dependent local gas temperature can be made in flames with particulates. Suction probes are fitted with filters to allow separation of particles and gas. Physical and chemical analyses are made of particles after removal from the probe. Concentration measurements of gas species are made by chromatography, chemiluminescence and flame ionization.

It is evident that the intrusive techniques disturb the flow characteristics and the probes are easily damaged by the fluid flow. Amongst these techniques, the computer compensated thermocouple causes minimum disturbance.

The non-intrusive techniques can be classified into laser and image techniques. Fig. 1.5 summarises the non-intrusive techniques in detail.

Laser anemometry has now become a well-established technique for the measurement of velocity of individual particles, velocity variation with time and particle size [33,37]. The vaporization rates can be derived from the particle size variation with time.

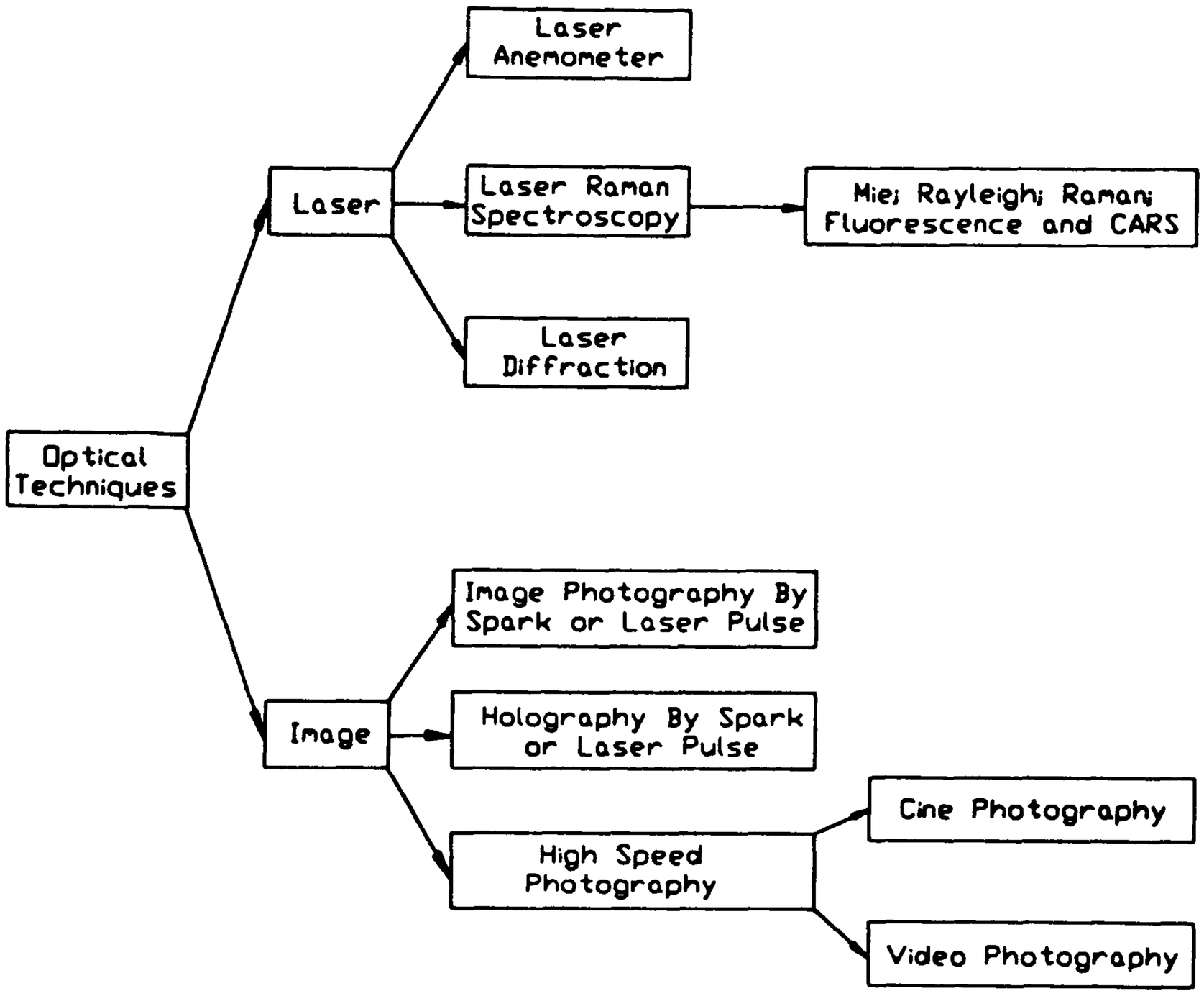

Fig. 1.5 The non-intrusive technology

The basic principle of laser anemometry is to produce two crossed laser beams. The intensity of the scattered light is a function of the particle size. The velocity of particles is determined directly from the analysis of the measurement of frequency from the modulated signal. Thus signals are analysed to derive information on particle diameter and particle velocity. The laser diffraction technique provides size distribution of clouds of particles in a spray. Laser Raman spectroscopy [15,20]

allows simultaneous measurement of gas temperature and gas species concentration in non-absorbing gas (N_2, O_2, CO, CO_2, H_2O and unburnt fuel fragments in combustion products).

A summary of the techniques based on laser beams is given as follows in table 1.1

Table 1.1 Laser Measurement Techniques

Name of techniques:	**Measurement:**
Laser Anemometer:	gas velocity, size and velocity of individual particles, spray boundaries
Laser Diffraction:	size distributions of sprays
Laser Raman Spectroscopy:	local gas temperature and species concentration
Mie Scattering [42]:	particle size distributions and number densities
Raman Scattering:	temperature and concentrations of major species
Fluorescence Scattering [43]:	minor constituents (ppm concentration) OH, C_2
Coherent Anti-Stokes Raman (CARS):	species concentration and temperature

Compared with the other measurement techniques, laser instrumentation provide simultaneous, flexible and accurate measurements of particle size and velocity, flame temperature and velocity and gas species concentration. However, these systems are

too expensive, and the absorption of light by particles from the intensive laser beam can raise particle temperature to the vaporization point and this increases the thermal radiation from the particles.

Photography is the earliest technique used to study combustion [43]. The earlier usage was mostly on S.I. engines of low compression ratio. At present, photography is commonly used for investigating spray atomisation and combustion.

The most detailed information in liquid spray and combustion has been obtained from the use of high speed photography [25,28,29,34,35,36,38,53]. With a micro-lens, photographic recordings are made of the images of individual particles moving through a narrow depth of field within the spray. When two sparks are used with different light intensities and the sparks are triggered at micro-second intervals, double images are formed on the photographic plate. Magnification of the images allows visual and digital analysis of diameter, shape, velocity and angle of flight of individual particles without probe interference. From the colour interpretation, the flame temperature can be obtained by high speed colour movie film and this allows the direct interpretation of measurements of variation of flame properties with time, with clearly visible movements of liquid and solid particles, as well as large eddy structures.

The basic photographic technique is being extended by the following means:

1) Use of TV camera and video tape to record image and carry out subsequent analysis by image analysis computer. These two operations can be directly coupled so as to provide on-line image analysis.

2) Replacement of spark sources by pulsed lasers so as to provide shorter duration light sources with more uniform background lighting. This allows particles to be measured more accurately down to a size of 2 microns.

3) Holography in conjunction with a pulsed laser offers a possibility to view the whole atomisation field. A single hologram covers a wide depth of field. By reconstructing this hologram, using a TV camera, the sections of spray can be brought into focus under controlled conditions, allowing more detailed analysis of spray.

From the above discussion, it is evident that image techniques possess the characteristics of direct visual observation, a great deal of information being contained in one measurement at less expense than laser instrumentation.

The major problem with photographic techniques is the image analysis. It is extremely lengthy, laborious and costly to analyse the photographs and measure droplets size, often by using back projection and manual or semi-automated data logging equipment. Attempts have been made to fully automate the micro-photographic technique by using extremely expensive purpose built computer systems interfaced with holographic instrumentation or television cameras. However, in many institutions, powerful image analysis computers now exist which are used for a wide range of purposes other than determining particle size.

An image analysis computer carries out automatic analysis of approximately 25 photographs per hour. It provides an accurate measurement of particle size and distribution. It is essential that the computer is programmed with all necessary information on the properties of the photographic image of a particle as a function of the size of the particle and its position in the field of view of the camera.

CHAPTER TWO:

THE ATOMIZATION OF WATER/FUEL EMULSION

2.1 Introduction

As discussed in chapter one, the micro-explosions of emulsified fuel have been observed in a pressure bomb with a constant volume [13], where it occurred conditionally, therefore, it is questioned whether or not the micro-explosions occur in a real engine, since the injection and combustion events are so fast even if the air temperature is higher than the saturation temperature of water. In other words, if the micro-explosions do occur in a real engine, the explosive energy is likely to be weak. So where does the benefit of applying emulsified fuel on an engine come from?

This chapter will discuss the W/O emulsion atomising behaviour in diesel engines, that is, the properties of emulsified fuel and its effects on the atomization process.

2.2 The Properties Of W/O Emulsion [54]*

In the following discussion, it is assumed that the water droplets (globules) are homogeneously distributed in the fuel (continuous phase). When performing the quantitative calculation, 10% water added into fuel (by volume) is taken as the example. The mean water droplets diameter varies from 4 to 5 μm depending on the types of emulsifiers [22].

2.2.1 Surface Tension

Generally, in an emulsion, various forces operate. These include: a) cohesion between molecules of the continuous phase, b) interaction between disperse phase globules, c) interaction between the globules and the continuous phase.

---

*Equations discribing emulsion properties in reference [54], e.g. surface tension and viscosity, are general expressions for emulsions. The accuracy for a particular emulsion has not been given in the reference. Since it is not in the scope of this project, the author has not done any experiment on emulsified fuel properties. The specifications of the fuel used in the tests are supplied by the British Fuel Company Limited.

a). The cohesion between molecules of the continuous phase is represented by its surface tension σ_f**.

b). Interaction between the water globules (V):

Interaction between globules in an emulsion can be interpreted in terms of prevailing forces of repulsion and attraction, which can be expressed in the form:

$$V = V_R - V_A$$

where: V_R is repulsion force and V_A is attraction force.

Fig 2.1 shows the potential energy (ε) of interaction curves for W/O emulsions with γ ranging from 0.40 to 0.74. Where D_m is the droplet mean diameter, H_0 is the distance between droplets.

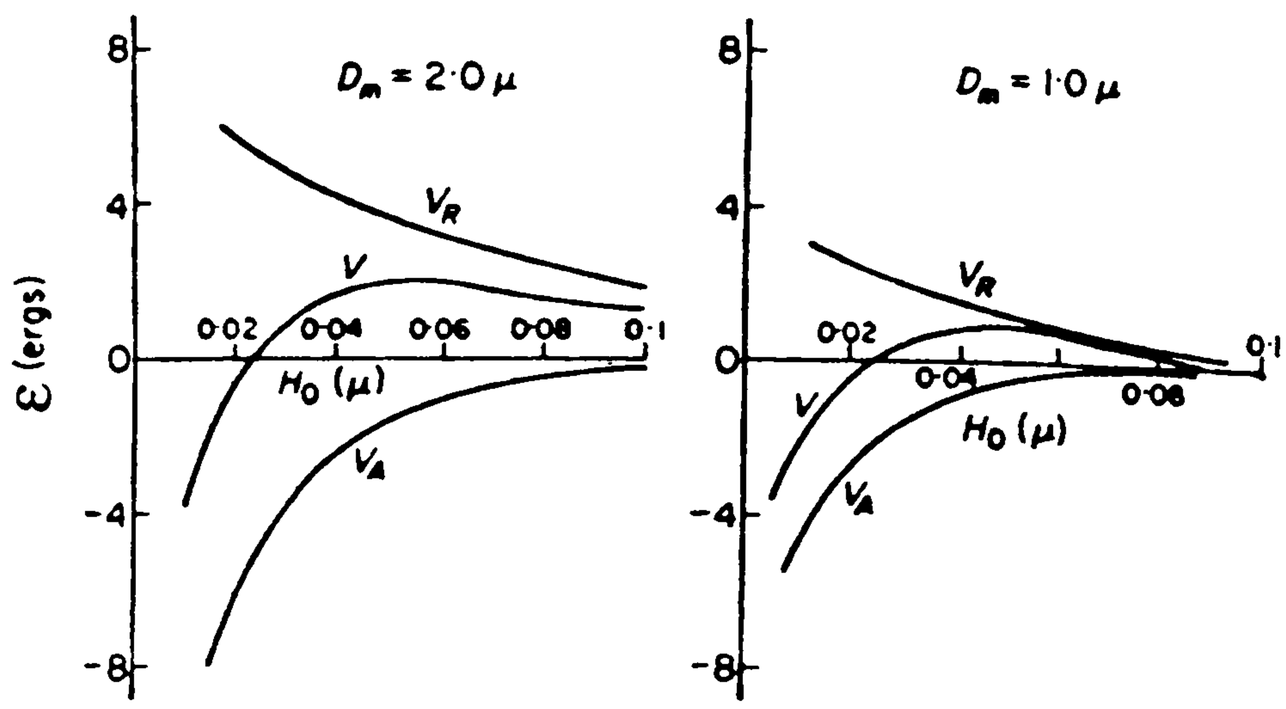

Fig. 2.1 Potential energy curves for W/O emulsions

**Notation:
σ - surface tension (dynes/cm or N/m);
ν - viscosity (cm^2/Sec. or m^2/S);
γ - ratio of water to fuel by volume;
F, f - fuel; W, w - water; E, e - emulsion.

The interaction forces between globules are a function of the distance between the globules. If γ=0.1 and the mean globule diameter is 4 μm, the distance between globules is about 18 μm. According to Fig. 2.1, the interaction force is very small when the distance between globules is greater than 0.1 μm. Thus, for γ=0.1 emulsion the interaction forces can be ignored since the distance between globules is much greater than 0.1 μm.

c). The interfacial tension (the tension at the interface of water droplets and fuel):

The interfacial tension is represented by inter molecular forces between water and fuel. The main intermolecular forces in water are hydrogen bonding (β^h) and dispersion forces (β^v), so that the surface tension can be represented by:

$$\sigma_w = \beta_w^h + \beta_w^v$$

For a saturated hydrocarbon (fuel), the dispersion forces are predominant, so $\sigma_f = \beta_f^v$. It has been testified that the interfacial tension between fuel and water is mainly due to the dispersion forces between hydrocarbon and water molecules, the expression is [54]:

$$\sigma_{w/f} = \sigma_w + \sigma_f - 2 \cdot \sqrt{\beta_f^v \cdot \beta_w^v} \qquad ---2.1$$

Experiments [54] show that the interfacial tension is much smaller than the surface tension of water or fuel. Normally, it is less than one third of the smallest of the liquid's surface tensions.

The surface tension of W/O emulsion:

According to Gibbs' absorption theory [54], the surface tension of two liquids can be written as follow:

$$\sigma_e = \sigma_w + \sigma_f - 2 \times \Phi \times \sqrt{\sigma_w \cdot \sigma_f} \qquad ---2.2$$

where Φ is a constant.

For water with diesel emulsion:

Φ= 0.51 ~ 0.78;

σ_w= 73.0 dynes/cm;

σ_f= 23.9 dynes/cm,

Substitute σ_w and σ_f into Eq. 2.2 and take Φ= 0.65, then the surface tension of water/diesel oil emulsion is: σ_e= 42.6 dynes/cm .

2.2.2 Viscosity

When water is added into fuel, the viscosity of fuel increases. Guth and Simha (1936) [54] gave the first quantitative definition of this increment.

$$\frac{\nu_e}{\nu_f} = 1 + a \cdot \gamma + 14.1 \cdot \gamma^2 \qquad ---2.3$$

where "a" is a constant, which varies with different emulsions.

For W/O emulsion, mean drop diameter D_m= 3 μm [22], then a=2.3 ~ 2.8.

After that, Simha (1952) [54] considered the hydrodynamic interaction between globules and related it to the Newtonian component of non-Newtonian flow. He developed two other alternative equations for viscosity as follows:

$$\frac{\nu_e}{\nu_f} = 1 + 2.5 \cdot \gamma\left[1 + \frac{25}{4 \cdot f^3} \cdot \gamma - \frac{21}{2 \cdot f^5} \cdot \gamma^{5/3} + \frac{625}{16 \cdot f^6} \cdot \gamma^2 + \cdots\right] \qquad ---2.3.1$$

$$\frac{\nu_e}{\nu_f} = 1 + 2.5 \cdot \gamma\left[1 + \frac{25}{4 \cdot f^3} \cdot \gamma + \frac{75}{4 \cdot f^4} \cdot \gamma^{4/3} + \frac{27}{f^5} \cdot \gamma^{5/3} + \frac{785}{16 \cdot f^6} \cdot \gamma^2 + \cdots\right] \qquad ---2.3.2$$

where f is a constant and changes between 1.3 and 2, the typical value being 1.81 or 1.61, respectively.

For the water/diesel emulsion of 10% water,

$\nu_f = 1.8 \sim 7.0$ c stoke;

$\gamma = 0.1$.

Then :

The viscosity of emulsion from Eq. 2.3 is: $\nu_e = 2.5 \sim 9.7$ cst,

from Eq. 2.3.1 is: $\nu_e = 2.3 \sim 8.9$ cst,

and from Eq. 2.3.2 is: $\nu_e = 2.5 \sim 9.7$ cst.

The viscosity of emulsion increases as the water droplet size decreases. When $D_m < 0.5$ μm, the water droplet size has a strong influence on ν_e, while the influence could be ignored when $D_m > 2$ μm.

2.2.3 Density

The emulsion density is given by:

$$\rho_e = \frac{M_e}{V_e};$$

The emulsion mass and volume are given by:

$$M_e = M_f + M_w$$

$$V_e = V_f + V_w$$

where: M -- mass; V -- volume.

Then: $$M_e = \rho_f \cdot V_f + \rho_w \cdot V_w = \left[\rho_f + \rho_w \cdot \frac{V_w}{V_f}\right] \cdot V_f;$$

Let: $$\gamma = \frac{V_w}{V_f}$$

now: $$\rho_e = \frac{(\rho_f + \rho_w \cdot \gamma) \cdot V_f}{(1+\gamma) \cdot V_f} = \frac{\rho_f + \rho_w \cdot \gamma}{1+\gamma} \qquad ---2.4$$

To summarise the above discussion, for a water/diesel oil emulsion, the interaction forces between water droplets can be ignored since their distances apart (about 18 μm) are far greater than 0.1 μm where within it the repulsion and attraction forces are affected. The interfacial tension between water droplets and fuel can also be ignored, since it is too small (less than one third of the smallest of one of the liquid's surface tension). Thus only surface tension and viscosity are considered when discussing the properties of water/diesel oil emulsion, i.e.

Surface tension: $$\sigma_e = \sigma_w + \sigma_f - 2 \times \Phi \times \sqrt{\sigma_w \cdot \sigma_f}$$

Viscosity: $$\nu_e = (1 + a \cdot \gamma + 14.1 \cdot \gamma^2) \times \nu_f$$

Where: σ_w = 73.0 dynes/cm;

σ_f = 23.9 dynes/cm;

μ_f = 1.8 ~ 7.0 c stoke;

Φ = 0.51 ~ 0.78, constant;

a = 2.3 ~ 2.8, constant;

γ = ratio of water to fuel by volume.

2.3 W/O Emulsion Atomization Fundamentals

This section discusses the principles of pure fuel atomization and the influence of water droplets on the atomization of fuel. The theoretical conclusion is that a high atomization efficiency and 'finer' fuel drops will be achieved with water addition into fuel.

2.3.1 Atomization Efficiency [55]

The definition of atomization efficiency is:

$$\eta_A = \frac{theoretical \quad minimum \quad input \quad power}{actual \quad input \quad power \quad to \quad atomizer}$$

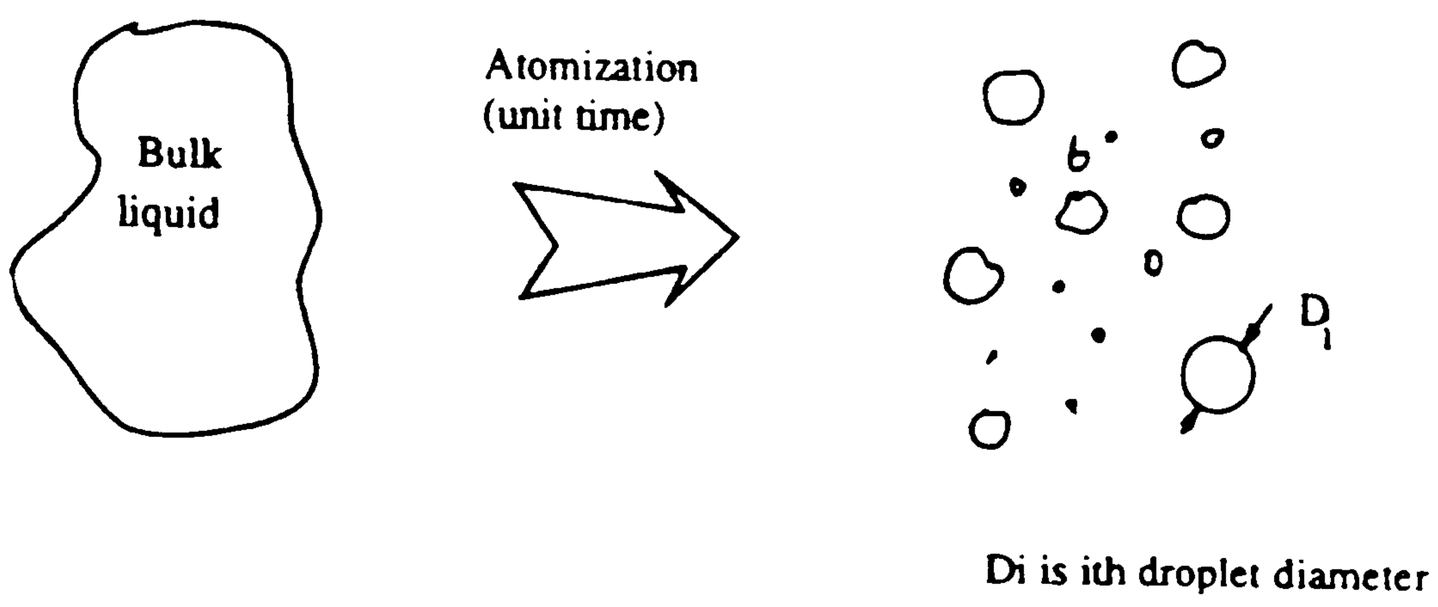

Fig. 2.2 Theoretical minimum energy required for atomization

The theoretical minimum energy (ε_{min}) required to produce the i_{th} droplet from bulk liquid is:

$$\varepsilon_{min} = \sigma_{liquid} \cdot \pi \cdot D_i^2$$

In a unit time the total energy required is:

$$\varepsilon_{total} = \sigma \cdot \pi \cdot \sum_{i=1}^{N} D_i^2$$

where N is the number of droplets atomized in unit time

For a pressure jet atomizer, the liquid is forced at high velocity through a small orifice. The total energy input is in the form of the pressure head supplied to the liquid. Thus the total input power to the atomizer is the product of ΔP and the liquid flow rate,

$$P_{inp} = \Delta P \times V$$

where ΔP is the pressure drop across the nozzle and V is the droplets volume atomized in unit time.

$$V_i = \frac{\pi}{6} \cdot D_i^3 \qquad V = \sum_{i=1}^{N} V_i$$

then:

$$\eta_A = \left(\sigma_f \cdot \pi \cdot \sum_{i=1}^{N} D_i^2\right) \Big/ \left(\Delta P \cdot \frac{\pi}{6} \cdot \sum_{i=1}^{N} D_i^3\right) \qquad ---2.5$$

Let:

$$D_{32} = \sum_{i=1}^{N} \frac{D_i^3}{D_i^2}$$

---Sauter Mean Diameter (the definition of SMD is in chapter 3).

Equation 2.5 can be rewritten as follow:

$$\eta_A = \frac{6 \cdot \sigma_f}{\Delta P \cdot D_{32}} \qquad ---2.5.1$$

Equation 2.5.1 shows that the atomization efficiency of emulsion is greater than that of pure fuel since $\sigma_e > \sigma_f$ (σ_e= 42.6 dynes/cm; σ_f=23.9 dynes/cm). The physical meaning of this is that the energy supplied to an emulsion spray is greater than that applied to pure fuel if the input energy of an injector is constant. Hence the emulsion jet spray will be finer and have greater penetration energy.

2.3.2 Break Down Of Sheet And Ligament

The mechanism of atomization of the bulk liquid involves sheets and/or ligaments formation near the atomizer, followed by their break-up into small droplets. The formation of a thin layer of liquid is required for efficient and rapid atomization to a desired droplet size.

The condition for "good" atomisation was described by Dombroski and Munday (1968) [55], which stated that the most effective way of utilizing energy imparted to a liquid is to arrange that the liquid has a large specific surface area before it commences to break down into drops. Thus the primary function of an atomizer is to transpose bulk liquid into thin sheets or ligaments. The instability of liquid ligaments is perhaps the fundamental physical phenomenon of the atomization process. Fig. 2.3 shows the models of ligament break up.

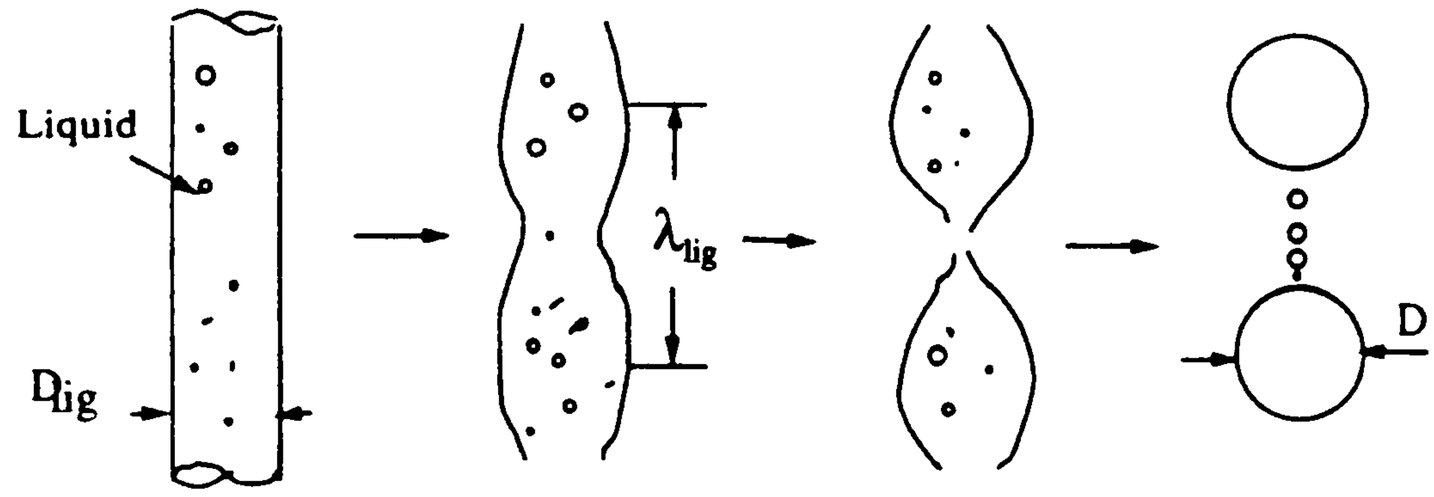

Fig. 2.3 "O" Mode of ligament disintegration

Lord Rayleigh (1878, 1894) [55] studied mathematically the instability of an inviscid column of liquid (ligament), considering only inertial and surface tension forces. He found that a free liquid column is unstable to axisymmetric disturbances with wavelength greater than the circumference of the ligament and that the most amplified wave-length is: $\lambda_{lig} = \sqrt{2} \cdot \pi \cdot D_{lig}$, where D_{lig} is the diameter of ligament.

Weber (1931) [55] showed that when viscous forces are involved in the analysis, the most amplified wave-length is:

$$\lambda_{lig} = \sqrt{2} \cdot \pi \cdot D_{lig} \cdot \left[1 + \frac{3 \cdot \nu_l}{(\rho_l \cdot \sigma_l D_{lig})^{1/2}} \right]^{1/2} \qquad ---2.6$$

where: subscript 'l' signifies any liquid.

As shown in Fig. 2.3, a uniform thread or ligament breaks down into a uniform stream of droplets which are separated by smaller satellite droplets, sometimes referred to as "plateau's spherules".

Castleman (1932), Henlin (1932) and Ohnesorge (1937) [55] studied, by photography, liquid columns with variation in liquid properties. Their qualitative observations are shown in Fig. 2.4, where 'U' is the jet velocity.

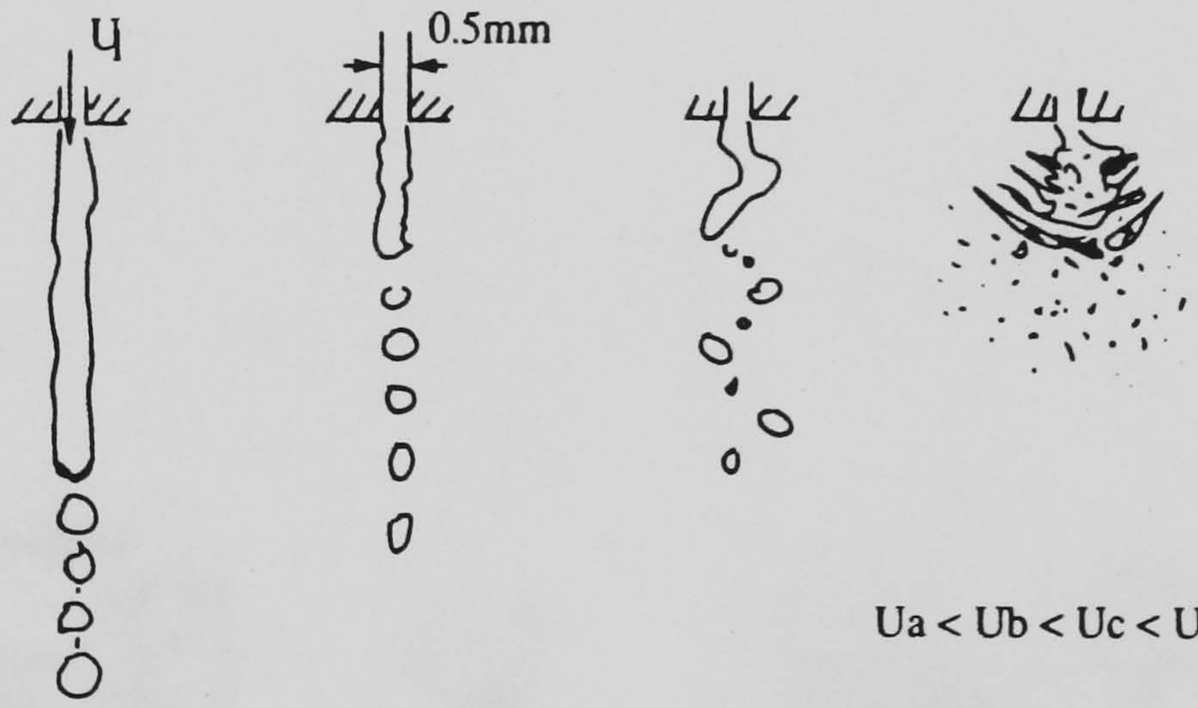

Fig. 2.4 Ligament break up

As the jet velocity increases, the "break-point" for droplets formation moves nearer to the orifice, the fundamental wavelength decreases and droplet size also decreases

in reasonable agreement with the theoretical treatment. At high relative velocity the shearing forces due to the air strip small ligaments from the main liquid column which in turn break down into small droplets.

Applying the "O" Mode of ligament disintegration to a W/O emulsion, there are two possible explanations for the emulsion ligament break up.

a). According to equation 2.6, the emulsion ligament wavelength should suffer no significant change, since both fuel viscosity and surface tension are increased, the item $\frac{3 \cdot \nu_e}{(\rho_e \cdot \sigma_e D_{lig})^{1/2}}$ being almost the same for diesel and emulsified fuels.

b). Since the interfacial tension of water drops and fuel is much smaller than pure fuel surface tension ($\sigma_{w/f}$= 0.1 ~ 0.3 σ_f), the interface of water drops and fuel is much easier to separate because of the unstable contact. In this case, the wavelength of the emulsion ligament decreases and droplets size will decrease, Fig. 2.5.

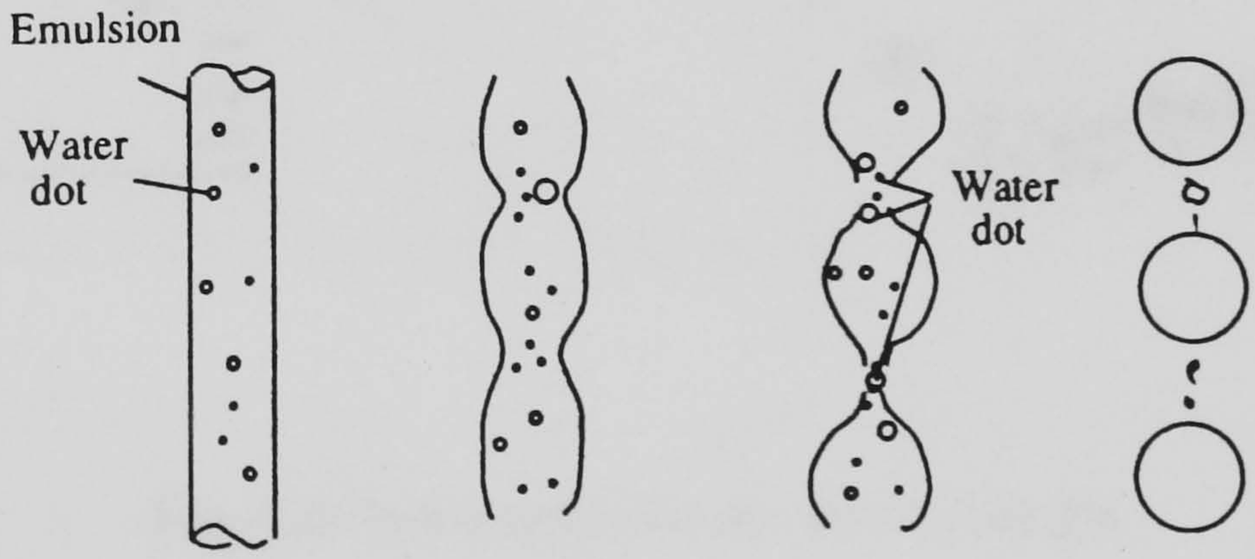

Fig. 2.5 Emulsion ligament disintegration

Case "a" is based on the theoretical discussion, while case "b" is on assumption. The real situation will be derived from the experimental results.

2.3.3 Droplet Break Up

As discussed earlier, when a bulk liquid is pressed out of a small orifice, ligaments and droplets which form a spray are stripped off from the bulk liquid by the relative velocity of liquid to air. There is a wide range of droplet size distribution in the spray. The larger drops can break up again. This is important in creating fine sprays and increasing specific surface area of the spray.

B.J. Azzopardi [55] has studied droplets break up phenomenon by high speed photography. The method he used is that of dropping a liquid drop into a jet of gas with a flat velocity profile Fig. 2.6

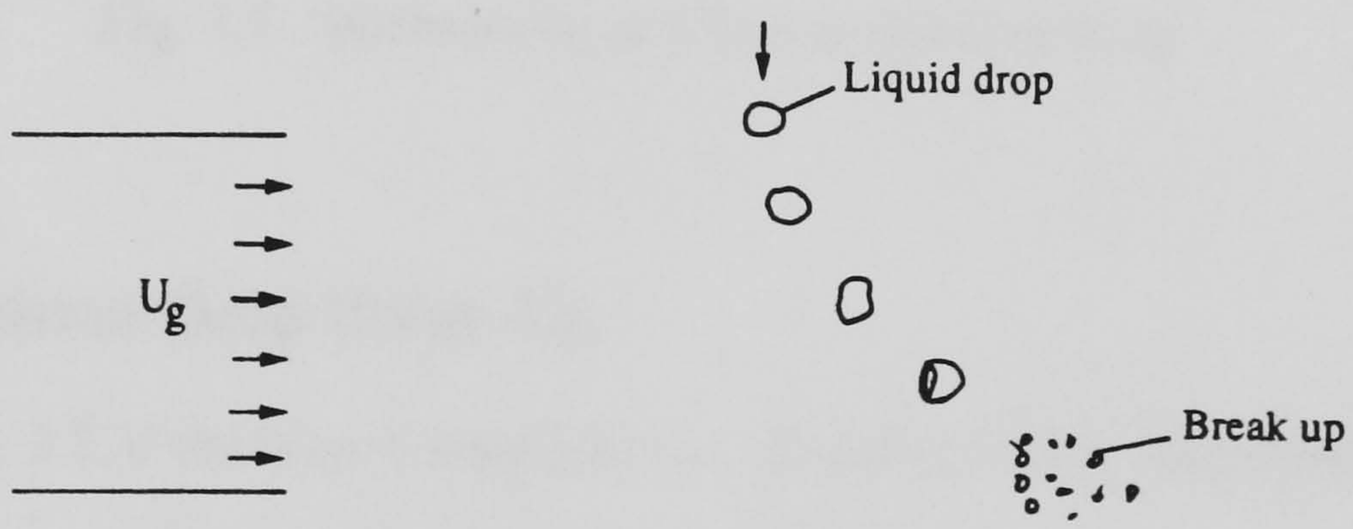

Fig. 2.6 Fuel droplet breaks up in a gas jet

The mechanisms of drop break up are different at different Weber numbers ($W_e = \rho \cdot D \cdot u^2/\sigma$). Fig. 2.7 shows the break up mechanisms at the lowest and highest

Weber numbers studied. In both cases, the drop is first flattened into a disk by the pressure difference across it. At lower W_e the middle is thinned out and blown out like bubble gum. The thin skin breaks up into fine drops whilst the rim produces larger drops. At higher W_e, the edges of the disk are dragged forward and atomization occurs there.

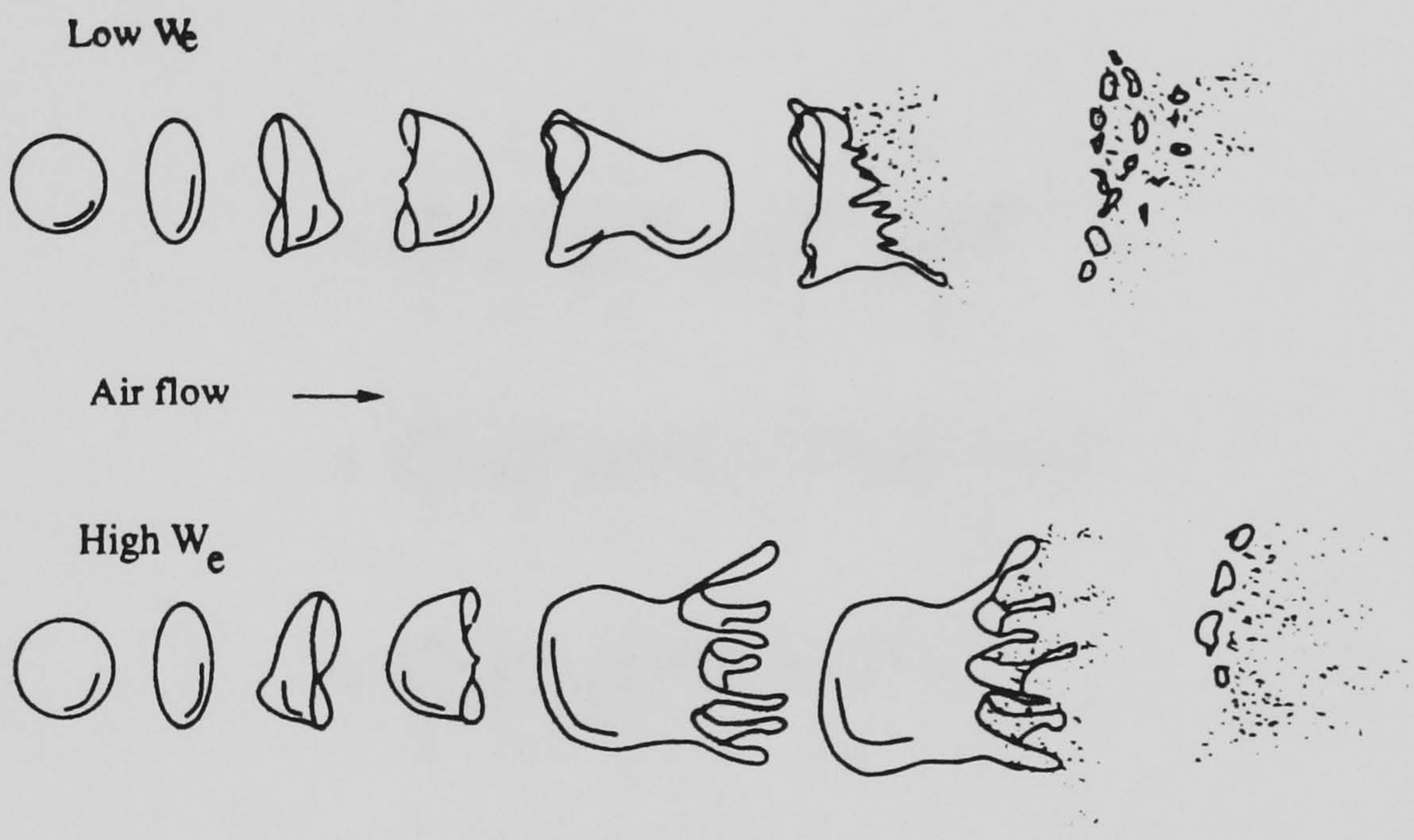

Fig. 2.7 Mechanisms of a fuel droplet break up

2.3.4 Emulsion Drop Break Up

Based on Fig. 2.7, if the drop is emulsion fuel, it means that the drop contains some minute-sized water drops. What is the change in Fig. 2.7?

Rumscheidt and Mason (1961) [55] investigated the deformation of liquid globules in a continuous phase with different viscosity ratios. It was found at high rates of shear that fluid globules deformed and might even burst depending on the magnitude of the viscosity ratios. As shown in Fig. 2.8, when the viscosity ratio was 0.03 ~ 1.00 and the velocity gradient attained the value for drop rupture, the central part

of the drop extended into a cylinder while a narrow neck formed in the middle. The neck thinned continuously until the drop disintegrated into two equally-sized smaller drops, and it was accompanied by the release of several very small drops. This is the case for water/diesel oil emulsion, since W/O emulsified fuels have $\nu_{drop}/\nu_{cont} = 1.01/1.80\sim7.0 = 0.56\sim0.16$, where ν_{drop} is the viscosity of water drops and $\nu_{cont.}$ is the visosity of continuous phase.

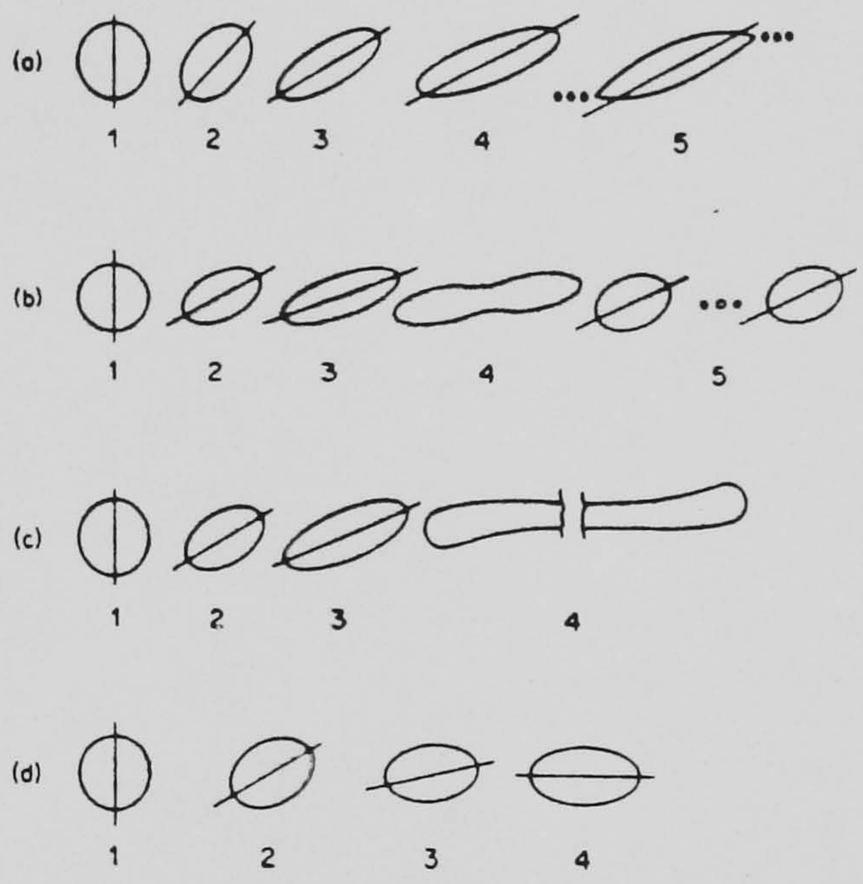

Fig. 2.8 Globule deformation in a continuous phase

where: a). $\nu_{drop}/\nu_{cont} = 1.3x10^{-4}\sim0.19$ c). $\nu_{drop}/\nu_{cont} = 0.70\sim2.20$

b). $\nu_{drop}/\nu_{cont} = 0.03\sim1.00$ d). $\nu_{drop}/\nu_{cont} = 3.80\sim29.00$

As assumed earlier, the water percentage in the fuel is 10%, the mean water droplet size is 4 ~ 5 μm in diameter and all the water droplets are homogeneously distribute in the fuel. Then, an emulsion drop of 1 mm in diameter contains about one million water droplets. If a percentage of water droplets burst, at the time of the fuel drops breaking up (Fig. 2.7), that will make the atomization of spray even finer.

2.4 Conclusions

Theoretically, there will be a reduction in the number of big diameter droplets by the addition of water into fuel. The emulsified fuel sprays have higher atomising energy, and permit the formation of a good mixture of fuel and air. This may explain the source of the improvement in engine performance by using emulsified fuel even if micro-explosion does not occur.

CHAPTER THREE:

MATHEMATICAL MODELS FOR AN INJECTION SPRAY

3.1 Introduction

To describe a spatial spray, generally there are three mathematical models required, namely, spray penetration, mean droplet diameter and spray angle. In addition, other models may have to be involved, namely, the length of spray break up, droplet size distribution, spray vaporization and fuel vapour density, etc. [53,56,57,58,59,60,61,62, 63,64,65,66]. For the purpose of building these models, general mathematical models should be developed by use of non-dimensional theory combined with the analysis of the physical phenomena of the injection spray. The mathematical models for a particular spray can then be derived from experimental data analysis and mathematical regression.

3.2 Penetration Of Spray Jet

Fig. 3.1 illustrates the model of a spray jet.

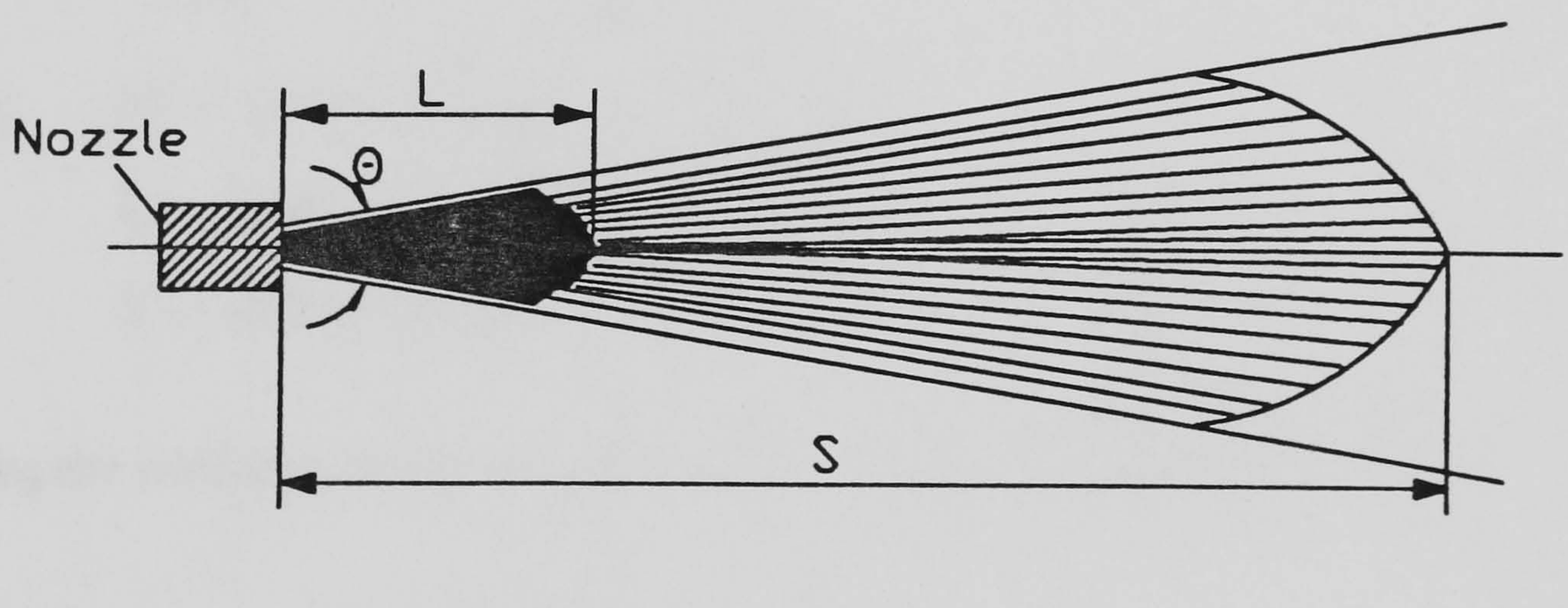

L -- break up length
S -- spray penetration
θ -- spray angle

Fig. 3.1 Fuel spray model

From the previous experiments in this area [52,58,67], it is known that the penetration of a spray jet is a function of following parameters:

ΔP: Pressure difference across the nozzle hole;
D_0: Diameter of nozzle hole;
L_0: Length of nozzle hole;
ρ_f Density of fuel;
ρ_g: Density of gas;
μ_f: Viscosity of fuel;
σ_f: Surface tension of fuel.

The units associated with these parameters are:

	Units	Fundamental Dimension
ΔP:	N/m^2	M/T^2L
D_0:	m	L
L_0:	m	L
ρ_f:	Kg/m^3	M/L^3
ρ_g:	Kg/m^3	M/L^3
μ_f:	Ns/m^2	M/TL
σ_f:	N/m	M/T^2

where: M --- symbol of mass,
L --- symbol of length,
T --- symbol of time.

Applying the similarity theory [68], the matrix of fundamental dimensions is:

	S_*	ΔP	D_0	ρ_f	ρ_g	μ_f	σ_f
M:	0	1	0	1	1	1	1
L:	1	-1	1	-3	-3	-1	0
T:	0	-2	0	0	0	-1	-2

---3.1

* S represents spray penetration

The rank of the matrix given by Eq. 3.1 is 3.

To simplify, let:

a_1 represents S; a_2 represents ΔP; a_3 represents D_0; ...; a_7 represents σ_f .

According to non-dimensional theory,

$$\begin{pmatrix} M & = & 0 \\ L & = & 0 \\ T & = & 0 \end{pmatrix} \qquad \text{---3.2}$$

Then the dimensional determinant is:

$$\begin{pmatrix} 0 & = & a_2 & + & a_4 & + & a_5 & + & a_6 & + & a_7 & & \\ 0 & = & a_1 & - & a_2 & + & a_3 & - & 3a_4 & - & 3a_5 & - & a_6 \\ 0 & = & -2a_2 & - & a_6 & - & 2a_7 & & & & & & \end{pmatrix} \qquad \text{---3.3}$$

The variable number of Eq. 3.3 is 7 and rank is 3,

$$7 - 3 = 4$$

So 4 or more terms are needed to solve Eq. 3.3.

Applying the "PI" theory [56], assume that a_1, ..., a_4 are known,

giving:

$$\begin{array}{lllllllll} \rho_g & : & a_5 & = & a_1 & - & a_2 & + & a_3 & - & a_4 \\ \mu_f & : & -a_6 & = & 2a_5 & + & 2a_4 & & & & \\ \sigma_f & : & a_7 & = & -a_2 & + & a_5 & + & a_4 & & \end{array}$$

$$\Rightarrow \begin{pmatrix} a_5 & = & a_1 & - & a_2 & + & a_3 & - & a_4 \\ a_6 & = & -2a_1 & + & 2a_2 & - & 2a_3 & & \\ a_7 & = & a_1 & - & 2a_2 & + & a_3 & & \end{pmatrix} \qquad \text{---3.4}$$

Substituting for a_5, a_6, and a_7 in a statement of dimensional homogeneity and collecting exponents with the same coefficients,

gives:

$$\left(\frac{S\cdot\sigma_f\cdot\rho_g}{\mu_f^2}\right)^{a_1}\cdot\left(\frac{\Delta P\cdot\mu_f^2}{\sigma_f^2\cdot\rho_g}\right)^{a_2}\cdot\left(\frac{D_0\cdot\sigma_f\cdot\rho_g}{\mu_f^2}\right)^{a_3}\cdot\left(\frac{\rho_f}{\rho_g}\right)^{a_4}=M^0\cdot L^0\cdot T^0 \qquad ---3.5$$

Let:
$$\pi_1=\frac{S\cdot\sigma_f\cdot\rho_g}{\mu_f^2};\qquad \pi_2=\frac{\Delta P\cdot\mu_f^2}{\sigma_f^2\cdot\rho_g};$$

$$\pi_3=\frac{D_0\cdot\sigma_f\cdot\rho_g}{\mu_f^2};\qquad \pi_4=\frac{\rho_f}{\rho_g}, \qquad ---3.6$$

and assuming:

$$\pi_2^{'}=\pi_2\cdot\pi_3^2;$$

$$\pi_1^{'}=\pi_1/\pi_3,$$

gives:
$$\pi_2^{'}=\frac{\Delta P\cdot D_0^2\cdot\rho_g}{\mu_f^2};\qquad \pi_1^{'}=\frac{S}{D_0}, \qquad ---3.6.1$$

Plus three non-dimensional parameters: L_0/D_0 ; t/t_0; and γ , then:

$$\pi_1^{'}=f\left[\pi_2^{'},\pi_3,\pi_4,\frac{L_0}{D_0},\frac{t}{t_0},f(\gamma)\right];$$

$$\frac{S}{D_0}=f\left[\frac{\Delta P\cdot D_0^2\cdot\rho_g}{\mu_f^2},\frac{\rho_g\cdot\sigma_f\cdot D_0}{\mu_f^2},\frac{\rho_f}{\rho_g},\frac{L_0}{D_0},\frac{t}{t_0},f(\gamma)\right] \qquad ---3.7$$

where: t -- time from the start of injection to a certain point;

t_0-- reference time;

γ -- percentage of water in fuel by volume.

Rewriting equation 3.7, gives:

$$\frac{S}{D_0} = f[K_1, K_2, K_3, K_4, K_5, K_6] \qquad ---3.7.1$$

where:

$$K_1 = \frac{\Delta P \cdot D_0^2 \cdot \rho_g}{\mu_f^2}; \qquad K_2 = \frac{\rho_g \cdot \sigma_f \cdot D_0}{\mu_f^2};$$

$$K_3 = \frac{\rho_f}{\rho_g}; \qquad K_4 = \frac{L_0}{D_0};$$

$$K_5 = \frac{t}{t_0}; \qquad K_6 = f(\gamma),$$

Each of K_i (i=1,...,6) has a physical meaning which vitally controls the formation of the atomization spray. The explanations of K_i (i=1, 2,..., 6) are as follows:

K_1: $(\Delta P \cdot D_0^2 \cdot \rho_g)/\mu_f^2$

The theoretical velocity of fuel at the nozzle is: $V_0^2 = 2 \cdot g \cdot \Delta P/\rho_f$, so K_1 is proportional to the square of the initial velocity of fuel, a measure of the kinetic effect of the jet.

K_2: $(\rho_g \cdot D_0 \cdot \sigma_f)/\mu_f^2$

In equation 3.6, if let, $\pi_3 \cdot \pi_4 = \pi_3^{'}$,

then: $\pi_3^{'} = \frac{\rho_f \cdot D_0 \cdot \sigma_f}{\mu_f^2} = Lp;$ --- Laplace number

L_p is a ratio of surface tension effect to viscous effect.

Since:

$$R_e = V_0 \cdot D_0 \cdot \rho_f/\mu_f; \qquad \text{--- Reynolds number}$$

$$W_e = V_0^2 \cdot D_0 \cdot \rho_f/\sigma_f; \qquad \text{--- Weber number}$$

then: $K_2 = \frac{R_e^2}{W_e} \cdot \frac{1}{K_3}$,

So, K_2 indicates the characteristic of spray jet flow, i.e. the ratio of the square of the inertial effect to the kinetic effect.

K_3: (ρ_f/ρ_g)

Ratio of fuel to gas mass, i.e. the ratio of initial effective forces of fuel to gas.

K_4: (L_0/D_0)

Geometric property.

K_5: (t/t_0)

Time property.

K_6: $f(\gamma)$

The effect of water on spray penetration.

According to the above explanation, it is evident that all K_i (i=1, 2,..., 6) are key parameters for controlling the spray penetration.

From the observation and analysis of experimental data, the relationship between spray penetration and K_i (i=1,...,5) is of an exponential type. So the non-dimensional expression of penetration is:

$$\frac{S}{D_0} = C \cdot K_1^{B_1} \cdot K_2^{B_2} \cdot K_3^{B_3} \cdot K_4^{B_4} \cdot K_5^{B_5} \cdot K_6 \qquad ---3.8$$

where C -- Constant and B_i-- Exponential constants (i=1,...,5).

C and B_i are determined from experimental data, while K_i (i=1,...,6) are derived from test conditions. The function of the effect of water on fuel atomisation (last item in Eq. 3.8) will be determined by the analysis of experimental results.

Taking logs of both sides of equation 3.8,

gives:

$$\ln\frac{S}{D_0} = \ln C + B_1 \cdot \ln K_1 + B_2 \cdot \ln K_2 +, \cdots, + \ln K_6 \qquad ---3.9$$

Let: $Y = \ln(S/D_0)$;

$B_0 = \ln C$;

$X_i = \ln K_i$, i=1, 2, ..., 6;

then:

$$Y = B_0 + B_1 \cdot X_1 + B_2 \cdot X_2 + B_3 \cdot X_3 + B_4 \cdot X_4 + B_5 \cdot X_5 + X_6$$

$$---3.9.1$$

When function $f(\gamma)$ is known, equation 3.9.1 is a multidimensional regression expression.

3.3 Droplet Diameters And Distributions

Droplet size and distribution are very important parameters for investigating the vaporization properties of spray jets. Normally, the mean diameter of droplets is used to express the droplet size. Therefore the mean droplet diameter and its distribution are the vital parameters for vaporization and combustion of the fuel spray.

3.3.1 Droplet Mean Diameters

The generalised expression for droplet mean diameter is [69]:

$$D_{pq} = \left[\frac{\int_0^\infty d_i^p \cdot n_i \cdot d(d_i)}{\int_0^\infty d_i^q \cdot n_i \cdot d(d_i)} \right]^{\frac{1}{p-q}} \Rightarrow \left[\frac{\sum_{i=1}^{N} d_i^p}{\sum_{i=1}^{N} d_i^q} \right]^{\frac{1}{p-q}} \quad ---3.10$$

Where the range of droplet diameters is divided into k classes. The ith class has a midpoint diameter d_i and a width Δd_i. The upper and lower size boundaries of the ith class are thus $d_i-\Delta d_i/2$ and $d_i+\Delta d_i/2$. The number of droplets counted which have diameters within the ith class is n_i, so that the total number of droplets is $N = \sum_{i=1}^{K} n_i$.

In Eq. 3.10, where p and q are normally equal to 0, 1, 2 and 3. There are different physical meanings when p and q have different values.

For examples, when p=1 and q=0, then D_{10} is the mean droplet diameter given by:

$$D_{10} = \frac{\sum_{i=1}^{N} d_i^1}{\sum_{i=1}^{N} d_i^0} = \left(\sum_{i=1}^{N} d_i \right) / N \quad \text{--- Mean droplet diameter}$$

when p=3 and q=0,

$$D_{30} = \left[\left(\sum_{i=1}^{N} d_i^3 \right) / N \right]^{\frac{1}{3}} \quad \text{--- Volume mean diameter}$$

when p=3 and q=2,

$$D_{32} = \frac{\sum_{i=1}^{N} d_i^3}{\sum_{i=1}^{N} d_i^2} \quad \text{--- Sauter mean diameter}$$

The Sauter mean droplet diameter is one of the well understood and widely used mathematical expressions for mean droplet diameter. It is a measure of the ratio of total volume to the total surface area of droplets in a spray, which is very important for predicating the mass transfer and combustion efficiency, etc..

3.3.2 The Sauter Mean Diameter (D_{32})

Considering the previous work in this area, the key parameters which control the SMD are pressure drop ΔP, fuel and gas densities ρ_f, ρ_g and the geometric size of the nozzle. From the view point of atomization analysis, the atomization process is a co-action process of kinetic, inertial, surface tension and viscous effects. So μ and ρ also play an important role in the atomization process.

For the purpose of the explanation of physical meaning, the initial velocity is used instead of ΔP to array the dimensional matrix. This gives:

	a_1 D_{32}	a_2 V_0	a_3 μ_f	a_4 D_0	a_5 ρ_g	a_6 ρ_f	a_7 σ_f
L:	1	1	-1	1	-3	-3	0
M:	0	0	1	0	1	1	1
T:	0	-1	-1	0	0	0	-2

---3.11

Applying the "PI" theory, assuming a_1, a_5, a_6 and a_7 are known, the non-dimensional equation is:

$$\left(\frac{D_{32}}{D_0}\right)^{a_1}\cdot\left(\frac{\rho_g\cdot D_0\cdot V_0}{\mu_f}\right)^{a_5}\cdot\left(\frac{D_0\cdot V_0\cdot\rho_f}{\mu_f}\right)^{a_6}\cdot\left(\frac{\sigma_f}{V_0\cdot\mu_f}\right)^{a_7}=L^0\cdot M^0\cdot L^0$$

---3.12

Let: $\pi_1=\dfrac{D_{32}}{D_0}$; $\pi_2=\dfrac{\rho_g\cdot D_0\cdot V_0}{\mu_f}$;

$\pi_3=\dfrac{D_0\cdot V_0\cdot\rho_f}{\mu_f}$; $\pi_4=\dfrac{\sigma_f}{V_0\cdot\mu_f}$,

and assuming:

$$\pi_2^{'} = \frac{\pi_3}{\pi_2} = \frac{\rho_f}{\rho_g};$$

$$\pi_4^{'} = \pi_3 \times \pi_4 = \frac{D_0 \cdot \rho_f \cdot \sigma_f}{\mu_f^2};$$

$$\pi_5 = f(\gamma).$$

then:

$$\pi_1 = f\left[\pi_2^{'}, \pi_3, \pi_4^{'}, \pi_5\right];$$

$$\frac{D_{32}}{D_0} = f\left[\frac{D_0 \cdot V_0 \cdot \rho_f}{\mu_f}, \frac{D_0 \cdot \rho_f \cdot \sigma_f}{\mu_f^2}, \frac{\rho_f}{\rho_g}, f(\gamma)\right]$$

---3.13

The physical meanings of the items on the right hand side of equation 3.13 are as follows:

$\frac{D_0 \cdot V_0 \cdot \rho_f}{\mu_f} = R_e$: Reynolds number, which is the ratio of inertial effect to viscous effect.

$\frac{D_0 \cdot \sigma_f \cdot \rho_f}{\mu_f^2} = L_p$: Laplace number, the ratio of surface tension effect to viscous effect.

$\frac{\rho_f}{\rho_g} = M$: Ratio of densities, i.e. ratio of inertial effects of fuel to gas.

So, $$\frac{D_{32}}{D_0} = C \cdot (R_e)^{B_1} \cdot (L_p)^{B_2} \cdot (M)^{B_3} \cdot f(\gamma)$$

---3.13.1

Constant C and exponentials B_i (i=1, 2, 3) will be determined from the experimental data by means of multidimensional regression.

3.3.3 Droplet Distributions

The measured droplet diameters from a spray sample, or in fact the data from all types of particle sizing techniques, are generally converted into a finite difference (histogram) approximation of the required size distribution as indicated by the step functions representing number distribution of droplet diameters $n(d_i)$ and volume distribution of droplet diameters $V(d_i)$ as shown in Fig. 3.2.

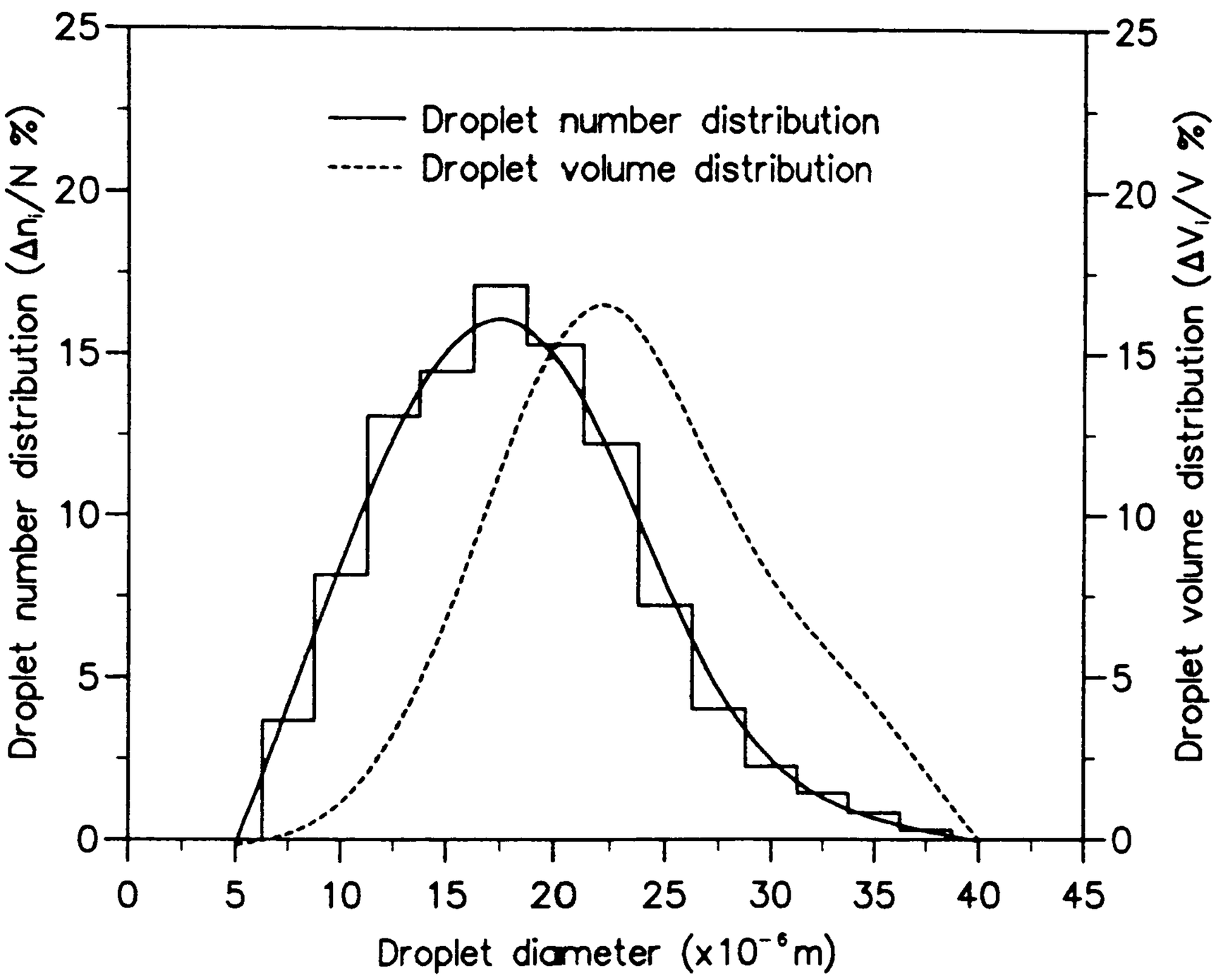

Fig. 3.2 Number/Volume distributions of droplet diameters

There are, normally, many ways to express the distributions of droplet diameters. In addition to $n(d_i)$ and $V(d_i)$, cumulative distributions of droplet diameter are often adopted to express the distributions of droplet diameters (Fig. 3.3). In Fig. 3.2, if $n(d_i)$ and $V(d_i)$ are divided by N (total number of droplets) and V (total volume of droplets) respectively, then they become the number/volume frequency distributions of droplet diameters.

When calculating or drawing the distributions of droplet diameters, it is not essential to take all the class widths as the same for the normalization of each class 'height' by the class width Δd_i. However many measurement techniques necessitate non-constant Δd_i and it is often necessary to increase Δd_i, with increasing d_i, to counteract the effect of the long 'tail' towards the large droplet end of the size distribution.

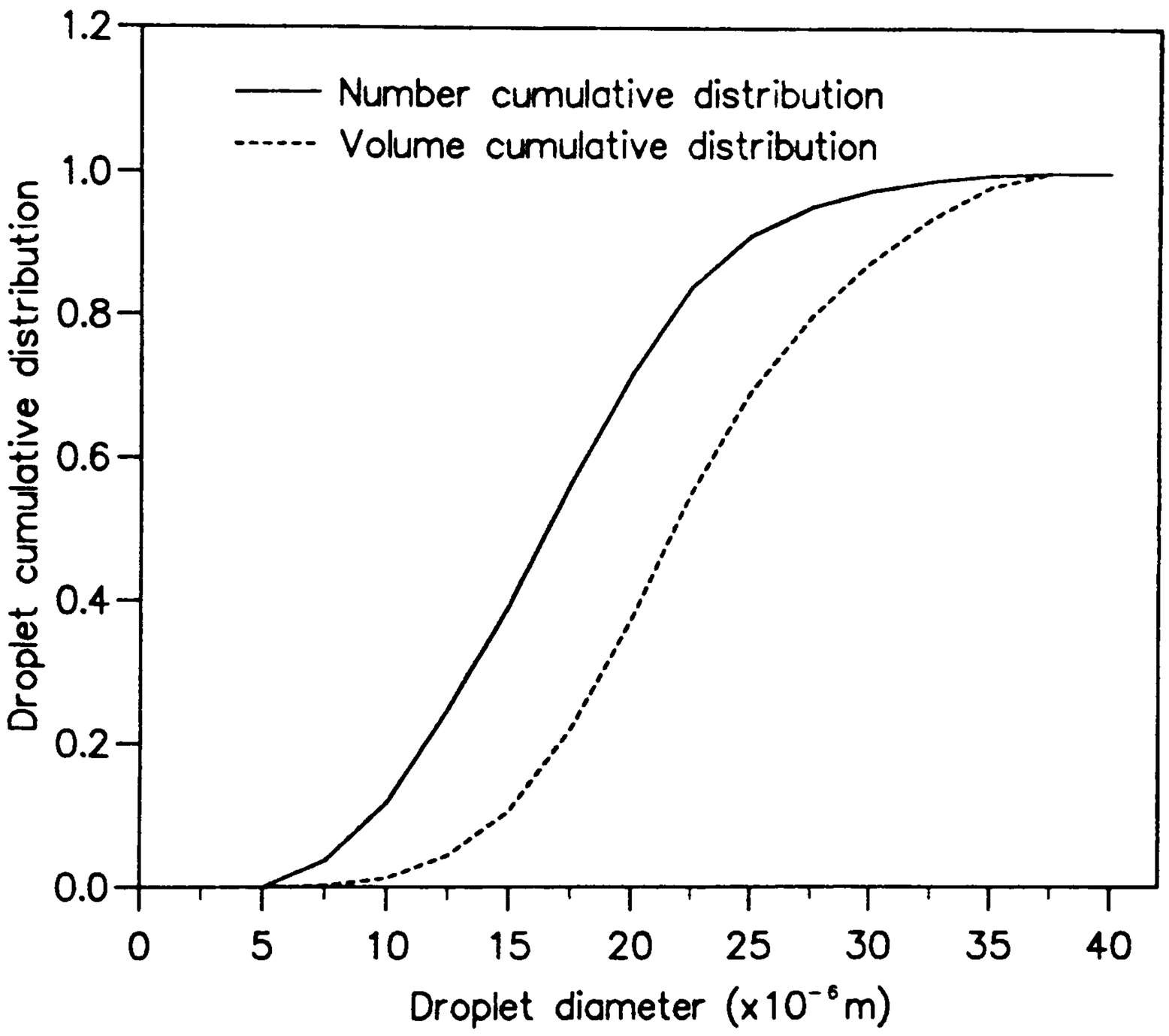

Fig 3.3 Cumulative distributions of droplet diameters

There are also many empirical size distributions which have been suggested for fitting and correlating measured droplet size distribution in the sprays. The empirical nature of these distributions is emphasised; there is in general no physical reason why one particular distribution should perform better than the others. At the same time, no distribution has been found to be universally applicable and in general, the larger the number of the adjustable constants in an empirical equation, the closer fit can be obtained with the experimental results.

Different empirical curves may perform best with different requirements and different types of atomisers.

1). The Rosin-Rammler (R-R) Distribution [55]

The statement of R-R distribution is as follow:

Defining $V_c(d_i)$ as the cumulative volume undersize distribution so that $100(1-V_c(d_i))=V_1\%$, where $V_1\%$ is the volume percentage of droplets which are larger than the diameter d_i.

The R-R distribution expression is:

$$1 - V_c(d_i) = \exp\left[-\left(\frac{d_i}{D}\right)^{\alpha}\right] \qquad ---3.14$$

where D is a droplet size parameter, usually referred to as 'the R-R mean diameter' and α is a measure of the dispersion of droplet size, usually referred to as 'the R-R exponent'.

Thus, the volume distribution of droplet diameter is:

$$V(d_i) = \frac{d(V_c(d_i))}{d(d_i)}$$

$$V(d_i) = \frac{\alpha}{D^{\alpha}} \cdot d_i^{\alpha-1} \cdot \exp\left[-\left(\frac{d_i}{D}\right)^{\alpha}\right] \qquad ---3.15$$

The R-R distribution gives a good fit to droplet volume distributions, in particular the cumulative volume distribution, for sprays from most types of twin fluid and pressure jet atomisers, but often gives a rather poor fit to droplet number or surface area distributions.

2). The Gaussian Probability Distribution [69]

The expression of Gaussian probability distribution is :

$$V(d_i) = \alpha \cdot \exp(-\alpha^2 \cdot y^2) \qquad ---3.16$$

where α is a constant and y varies with the different definitions and researchers. One of the definitions is the Logarithm of the droplet diameter, that is $y=\ln(d_i/D_v)$, where D_v is the median volume diameter.

Gaussian distribution is symmetrical and is seldom valid for either the number or volume size distributions of most sprays (with the exception of certain specialised atomizers). However it often gives a better fit for smaller size droplets than the R-R distribution.

3). The Nukiyama-Tanasawa (N-T) Distribution [69]

The N-T empirical distribution is generally used in a number distribution and gives a quite good fit for pressure jet atomisers. The standard expression of the N-T distribution is:

$$\frac{d(n_i)}{d(d_i)} \cdot \frac{1}{N} = A \cdot (d_i)^{\alpha} \cdot \exp(-B \cdot d_i^{\beta}) \qquad ---3.17$$

where: A, α, B and β are the atomization parameters.

n_i is the number of droplets counted which have diameters within the ith class.

d_i is the midpoint diameter of the ith class.

Several empirical distributions of droplet diameters have been briefly discussed above. Each of them has its own merits and demerits. The decision to select which distribution to use depends upon the type of atomiser and the purpose of the research. When one distribution has been developed (such as the distribution of droplet diameters), the other distributions, e.g. droplets surface area, droplets volume and droplets weight, etc., can be derived from the mathematical conversions, as well as

the droplet mean diameters D_{pq}, droplets dispersion, accumulative curves and median diameters. Therefore, the droplet diameter distribution functions are very important for analysing the spray atomization processes.

The following discussion will concentrate on the number frequency distribution of droplet diameters. Since the atomiser used in this project is a pressure jet atomiser, the Nukiyama-Tanasawa empirical distribution will be employed. Thus, the objective of following discussion is to investigate the relationships of parameters A, α, B and β in Eq. 3.17.

From the definition of SMD:

$$D_{32} = \frac{\int_0^\infty d_i^3 d(n_i)}{\int_0^\infty d_i^2 d(n_i)} \qquad ---3.18$$

and also from Eq. 3.17, we have,

$$\int_0^\infty d_i^3 d(n_i) = \int_0^\infty N \cdot A \cdot d_i^{\alpha+3} \cdot \exp(-B \cdot d_i^\beta) \cdot d(d_i) \qquad ---3.19$$

$$\int_0^\infty d_i^2 d(n_i) = \int_0^\infty N \cdot A \cdot d_i^{\alpha+2} \cdot \exp(-B \cdot d_i^\beta) \cdot d(d_i) \qquad ---3.20$$

Let:

$$B \cdot d_i^\beta = y,$$

then:

$$d_i = \left(\frac{y}{B}\right)^{\frac{1}{\beta}}$$

$$d(d_i) = d\left[\left(\frac{y}{B}\right)^{\frac{1}{\beta}}\right] = \frac{1}{\beta \cdot B} \cdot \left(\frac{y}{B}\right)^{\frac{1-\beta}{\beta}} \cdot d(y) \qquad ---3.21$$

Substituting Eq. 3.21 and $d_i = (y/B)^{(1/\beta)}$ into Eq. 3.19,

gives:

$$\int_0^\infty d_i^3 \cdot d(n_i) = \int_0^\infty N \cdot A \cdot \left(\frac{y}{B}\right)^{\frac{\alpha+3}{\beta}} \cdot \exp(-y) \cdot \frac{1}{\beta \cdot B} \cdot \left(\frac{y}{B}\right)^{\frac{1-\beta}{\beta}} \cdot d(y)$$

$$= \frac{N \cdot A}{\beta \cdot B^{\frac{\alpha+4}{\beta}}} \int_0^\infty \exp(-y) \cdot y^{\left(\frac{\alpha+4}{\beta}-1\right)} \cdot d(y)$$

$$= \frac{N \cdot A}{\beta \cdot B^{\frac{\alpha+4}{\beta}}} \cdot \Gamma\left(\frac{\alpha+4}{\beta}\right) \qquad ---3.22$$

where $\Gamma\left(\frac{\alpha+4}{\beta}\right)$ is the gamma function, $\Gamma(c) = \int_0^\infty e^{-x} \cdot x^{c-1} \cdot d(x)$, the value being obtained from standard reference tables.

In the same way,

$$\int_0^\infty d_i^2 \cdot d(n_i) = \frac{N \cdot A}{\beta \cdot B^{\frac{\alpha+3}{\beta}}} \cdot \Gamma\left(\frac{\alpha+3}{\beta}\right) \qquad ---3.23$$

Thus,

$$\int_0^\infty d_i^p \cdot d(n_i) = \frac{N \cdot A}{\beta \cdot B^{\frac{\alpha+1+p}{\beta}}} \cdot \Gamma\left(\frac{\alpha+1+p}{\beta}\right) \qquad ---3.24$$

Substituting Eq. 3.22 and Eq. 3.23 into Eq. 3.18,

then:

$$D_{32} = B^{-\frac{1}{\beta}} \cdot \frac{\Gamma\left(\frac{\alpha+4}{\beta}\right)}{\Gamma\left(\frac{\alpha+3}{\beta}\right)} \qquad ---3.25$$

and $$B = \left[\frac{\Gamma\left(\frac{\alpha+4}{\beta}\right)}{D_{32} \cdot \Gamma\left(\frac{\alpha+3}{\beta}\right)} \right]^{\beta} \qquad ---3.26$$

Since:

$$N = \int_0^{\infty} d(n_i) = \int_0^{\infty} d_i^0 \cdot d(n_i), \qquad ---3.27$$

From Eq. 3.24:

$$N = \frac{N \cdot A}{\beta \cdot B^{\frac{\alpha+1}{\beta}}} \cdot \Gamma\left(\frac{\alpha+1}{\beta}\right) \qquad ---3.28$$

then:

$$A = \frac{\beta \cdot B^{\frac{\alpha+1}{\beta}}}{\Gamma\left(\frac{\alpha+1}{\beta}\right)} \qquad ---3.29$$

Substituting Eq. 3.26 into Eq. 3.29, gives:

$$A = \frac{\beta}{\Gamma\left(\frac{\alpha+1}{\beta}\right)} \cdot \left[\frac{\Gamma\left(\frac{\alpha+4}{\beta}\right)}{D_{32} \cdot \Gamma\left(\frac{\alpha+3}{\beta}\right)} \right]^{\alpha+1} \qquad ---3.29.1$$

Dividing D_{32} by D_{10} where,

$$D_{10} = \frac{\int_0^{\infty} d_i \cdot d(n_i)}{\int_0^{\infty} d_i^0 \cdot d(n_i)} = B^{-\frac{1}{\beta}} \cdot \frac{\Gamma\left(\frac{\alpha+2}{\beta}\right)}{\Gamma\left(\frac{\alpha+1}{\beta}\right)} \qquad ---3.30$$

then:

$$\frac{D_{32}}{D_{10}} = \frac{\Gamma\left(\frac{\alpha+4}{\beta}\right)}{\Gamma\left(\frac{\alpha+3}{\beta}\right)} \cdot \frac{\Gamma\left(\frac{\alpha+1}{\beta}\right)}{\Gamma\left(\frac{\alpha+2}{\beta}\right)} = f(\alpha, \beta) \qquad ---3.31$$

Thus there are the simultaneous equations:

$$A = \frac{\beta}{\Gamma\left(\frac{\alpha+1}{\beta}\right)} \cdot \left[\frac{\Gamma\left(\frac{\alpha+4}{\beta}\right)}{D_{32} \cdot \Gamma\left(\frac{\alpha+3}{\beta}\right)} \right]^{\alpha+1}$$

$$B = \left[\frac{\Gamma\left(\frac{\alpha+4}{\beta}\right)}{D_{32} \cdot \Gamma\left(\frac{\alpha+3}{\beta}\right)} \right]^{\beta}$$

$$\frac{D_{32}}{D_{10}} = f(\alpha, \beta) \qquad ---3.32$$

where D_{32} and D_{10} are determined from the experimental data.

Thus, there are three equations and four unknown parameters. To solve the equations, one parameter must be assumed first, then the solutions are found by trial-and-error.

3.4 Spray Angle (θ)

It is understood that the spray angle is a function of the following parameters:

ΔP: Pressure drop across the nozzle hole;

μ_f, σ_f: Viscosity and surface tension of fuel;

L_0, D_0: Length and diameter of nozzle hole;

ρ_f, ρ_g: Densities of fuel and gas.

There are many mathematical expressions concerning the spray angle which have been developed by different researchers by means of either theoretical or experimental methods (table 3.1). All of them are derived under the conditions of static gas and normal temperature. Some modifications are required when they are used in practice.

Generally speaking, there are only two kinds of parameters controlling the spray angle, i.e. kinetic parameters of the fuel and resistance parameters of the gas (inertial effect of gas), since only kinetic and resistive forces exist after the fuel leaves the nozzle. All

the other parameters, such as injection pressure, nozzle hole diameter, nozzle discharge coefficient, injection amount, etc., are the effective elements (factors) which are formed by the kinetic parameters.

Table 3.1 Mathematical expressions for spray angle [52]

Researchers	**Methods**	**Expressions**
Waguri, 1960	momentum theory, spray penetration	$2\theta' = 2\tan^{-1}\frac{\sqrt{C\rho_f/\rho_g}}{\left(\frac{K}{\sqrt{V_0 d}}\right)^2}$ C and K are constants, K can be determinate by spray penetration and ρ_f/ρ_a
Abramovich, 1963	efflux theory	$\tan(\theta/2) = 0.13(1+\rho_g/\rho_f)$
Sitkei, 1964	efflux theory	$\theta = 2\tan^{-1}(A + B\sqrt{\rho_g})$ A, B -- constants
Sitkei, 1964	dimension analysis	$\theta = 0.03\left(\frac{l}{d}\right)^{-3}\left(\frac{\rho_f}{\rho_g}\right)^{0.1} R_e^{0.7}$ $\theta = \alpha_z + C\left(\frac{l}{d}\right)^{n}\left(\frac{\rho_f}{\rho_g}\right)^{b} R_e^{c}$ l/d -- ratio of hole length and diameter, α_z -- angle of needle tip
Hiroyasu, 1974	empiric formula, high pressure vessel	$\theta = \tan^{-1}(0.07 + 0.053\sqrt{\gamma_a - 0.8})$
Yakota and Matsuoka, 1977	empiric formula, high pressure vessel	$\theta = \frac{1}{7.4} R_e^{0.64}\left(\frac{l}{d}\right)^{-\beta}\left[1-\exp\left(-\frac{1}{43.6}\frac{\rho_f}{\rho_g}\right)\right]^{-1}$ $\beta = 0.0284(\rho_f/\rho_g)^{0.39}$
Reitz and Bracco, 1979	Taylor theory and experiment	$\tan(\theta/2) = \frac{4\pi}{A}\left(\frac{\rho_g}{\rho_f}\right)^{0.5} f\left(\frac{\rho_f}{\rho_g}\frac{R_{ef}}{W_{ef}}\right)^2$ A -- experimental constant
Hiroyasu and Arai, 1980	empiric formula, dimension analysis, high pressure vessel	$\theta = 0.05\left(\frac{\rho_g \Delta P D_0^2}{\mu_g^2}\right)^{0.25}$

It would be very convenient if only the kinetic effect of fuel and inertial effect of gas are considered for studying the spray angle.

Thus, the Reynolds Number is used to represent the kinetic effect and the gas density to represent the inertial effect of gas, giving:

$$\theta = C \cdot R_e^{a_1} \cdot \left(\frac{\rho_g}{\rho_f}\right)^{a_2} \qquad ---3.33$$

Considering the effect of water, Eq. 3.33 can be rewritten as follow:

$$\theta = C \cdot R_e^{a_1} \cdot \left(\frac{\rho_g}{\rho_f}\right)^{a_2} \cdot f(\gamma) \qquad ---3.34$$

where: R_e -- Reyonlds number ($=\frac{V_0 \cdot D_0 \cdot \rho_f}{\mu_f}$).

ρ_g, ρ_f -- densities of gas and fuel.

C, a_1 and a_2 -- constants.

$f(\gamma)$ -- modifying function of water on the spray angle, which remains to be determined from the analysis of experimental data.

3.5 Summary

From the above derivations and analysis, the expressions for spray penetration, angle, Sauter mean diameter and distributions of droplet diameter of emulsified fuel spray have been established. At the moment, these equations remain only in the form of qualitative expressions. The quantitative expressions will be derived from the regression of experimental data. The differences in atomization between emulsified fuel and pure fuel can be determined from the comparison of quantitative expressions.

CHAPTER FOUR:

TEST RIGS AND INSTRUMENTATION DESCRIPTION

4.1 Introduction

Two kinds of test rigs are involved in this project. One is concerned with investigating the fundamentals of atomization; the other is concerned with the high speed photography for studying the atomization of a spray in a non-combustion bomb and developing its mathematical models.

The most difficult aspects in studying high pressure jet spray atomization are its high velocity and density. The objectives of the first test were to lower the jet velocity and study the atomisation phenomena of low speed jets. The results obtained from this could be used to predict the atomisation of the high speed spray jet. The second test involved photographing the high pressure jet in a non-combustion bomb to study the spray penetration, angle, droplet size and distributions. Based on the test results and data regression, the mathematical models for spray atomisation could be developed

4.2 Test Rig For Investigating The Fundamentals Of Atomization

As discussed in Chapter two, the primary function of an atomizer is to transpose bulk liquid sheets to ligaments (threads of liquid) to drops. Therefore, the unstable ligament break up is a basic phenomena of spray atomization. The biggest obstruction to studying pressure jet atomisation is its high velocity and density. In order to observe and analyse this basic phenomena of jet atomisation, it is necessary to lower the jet velocity. The results derived from this low velocity jet provide a prediction of the atomization of a real spray jet. The test rig used toward this end is shown in Fig. 4.1.

The fuel jet is forced out of the nozzle by the compressed nitrogen. The jet velocity is in turn controlled by the nitrogen pressure which is controlled by the pressure regulator.

The emulsifier has two functions in this test: to emulsify water with fuel and to circulate/pump the fuel round the system. In order to get a well-mixed emulsion, the fuel is forced by the emulsifier to circulate round the system for some time before tests began. The fuel jet speed is controlled by the regulating valve which controls the pressure in the pressure tank. A 30mm measuring scale was fitted under the tank along the axis of the jet to provide a quantitative reference. A nozzle plate with an orifice of 0.5mm in diameter and 5mm in length was fixed at the bottom of the nozzle body. The volume of the pressure tank was 1.178 litre. Fig. 4.2 shows the pressure tank. A Pentax camera body with a 55mm micro-lens was used for this test.

Fig. 4.1 Fundamental study test rig

1.fuel tank;
2.emulsified fuel tank;
3.emulsifier;
4.pressure fuel tank;
5.nozzle;
6.flash;
7.measuring scale;
8.camera;
9.pressure gauge;
10.pressure regulator;
11.nitrogen bottle;
12.nozzle plate.

4.3 Test Rig And Instrumentation For The High Speed Camera Test

The schematic illustration of the test rig and instrumentation for this test is presented in Fig. 4.3, a more general view being shown in Fig. 4.4. In Fig. 4.3, the upper case number represents the test rig and instrumentations, while the italic number represents the signal wires.

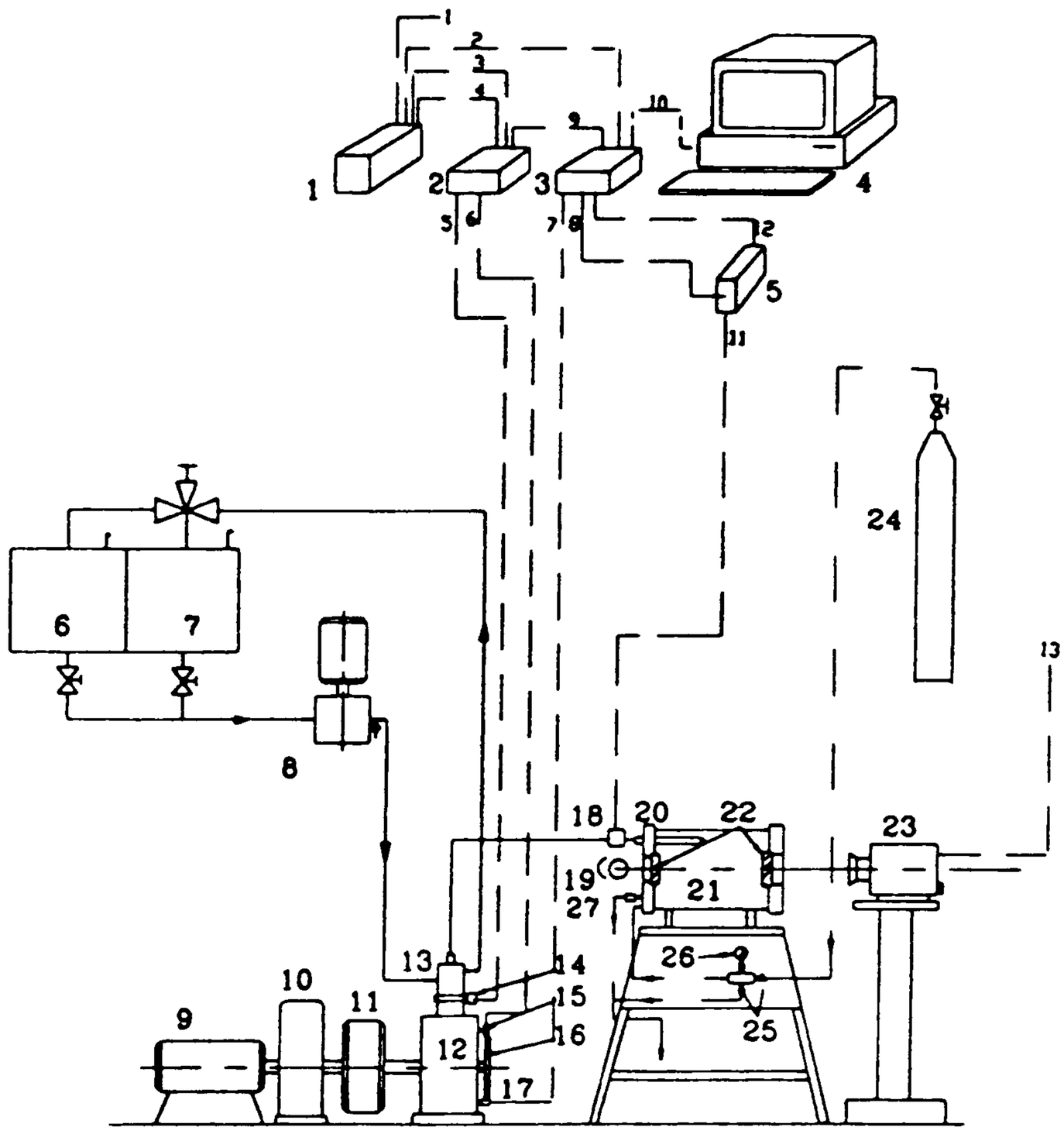

Fig. 4.3 High speed camera test rig and instrumentation

1.camera controller;
2.event sequence timing controller;
3.analog digital conversion;
4.computer;
5.charge amplifier;
6.fuel tank;
7.emulsified fuel tank;
8.emulsifier;
9.driving motor;
10.gear box;
11.fly wheel;
12.cam house;
13.high pressure pump;
14.solenoid;
15.magnetic pick-up;
16.slotted wheel;
17.micro-swicth;
18.pressure transducer;
19.illumination light;
20.injector;
21.bomb;
22.quartz glasses;
23.high-speed camera;
24.nitrogen bottle;
25.needle valves;
26.pressure gauge;
27.relief valve.

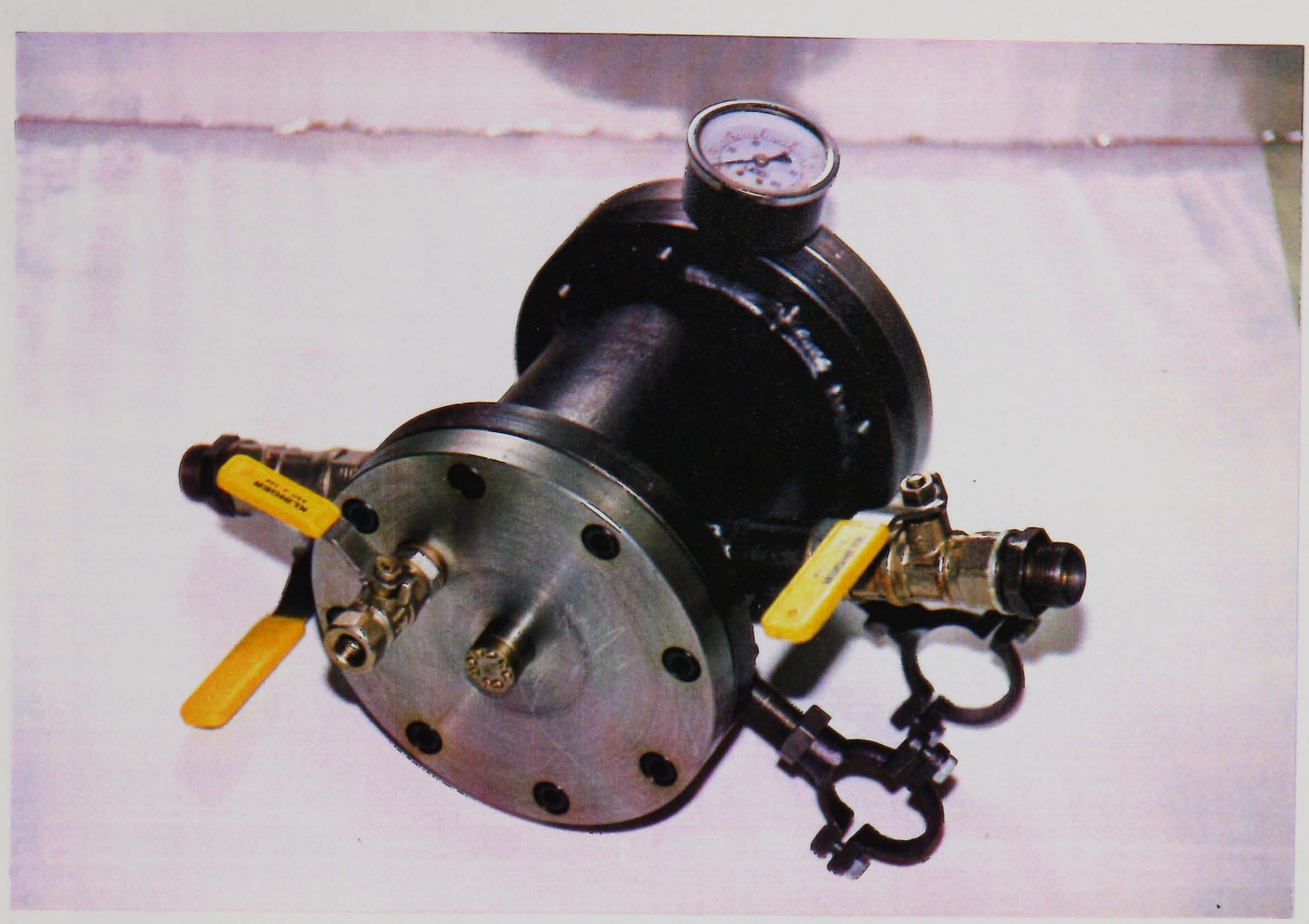

Fig. 4.2 Pressure tanker for atomising fundamentals study

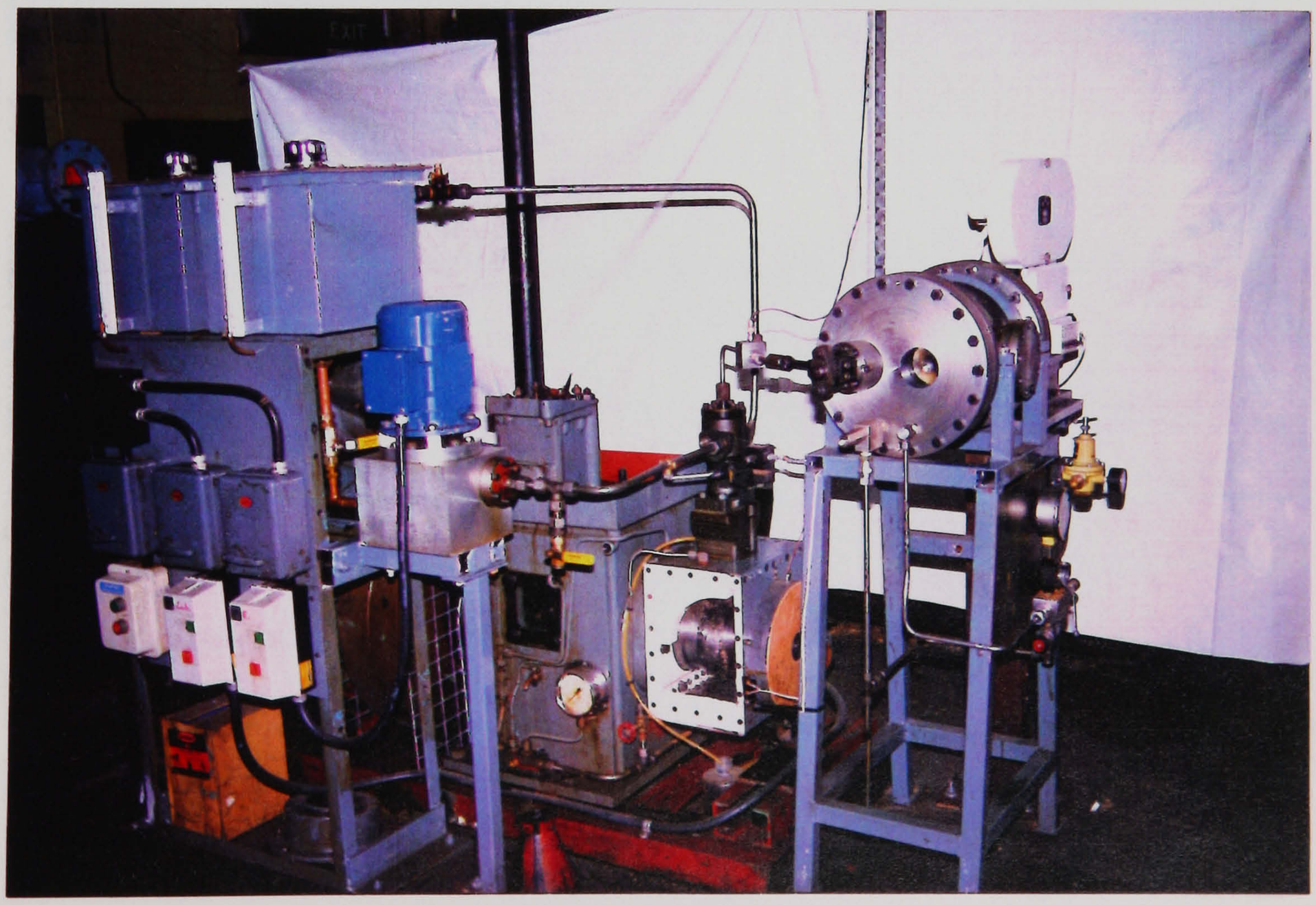

Fig. 4.4 High speed camera test rig

Table 4.1 Signal direction and functions

No	From	To	Functions
1	Camera controller	High speed camera	Camera power/operating
2	Computer	Camera controller	Remote controls camera start
3	Events sequence timing Controller(ESTC)	Computer controller	Event marker in
4	Camera controller	ESTC	Event synchronising
5	ESTC	Solenoid	Pulling rack to inj. position
6	Micro switch	ESTC	Inj. sequence control
7	Magnetic pick up	ADC	Time marker
8	Charge amplifier	ADC	Inj. pressure
9	ESTC	ADC	Camera stop signal
10	ADC	Computer	Inj. pressure
11	Pressure transducer	Charge amplifier	Inj. pressure
12	ADC	Charge amplifier	Charge amplifier reset
13	Camera controller	High speed camera	Camera power/operating

Non-combusting bomb:

The non-combusting bomb was specially designed to simulate the combustion chamber of a Ruston 6APC engine as shown in Fig 4.5 (dimensions shown in mm). Two quartz glasses were fitted on the two side covers for illuminating the spray and taking photographs. The illumination light, quartz glasses and camera were arranged for correct alignment. The injector was fitted on the cover at the illumination side with a 15° angle to the central line of the bomb. With such an arrangement, one of the injection sprays is perpendicular to the camera axis. To prevent fuel combustion, nitrogen was used to pressurise the bomb. The bomb pressure could be adjusted by the needle valves. The opening pressure of the relief valve was set at 80 bar. The bomb was tested hydraulically to 130 bar with quartz glasses in place.

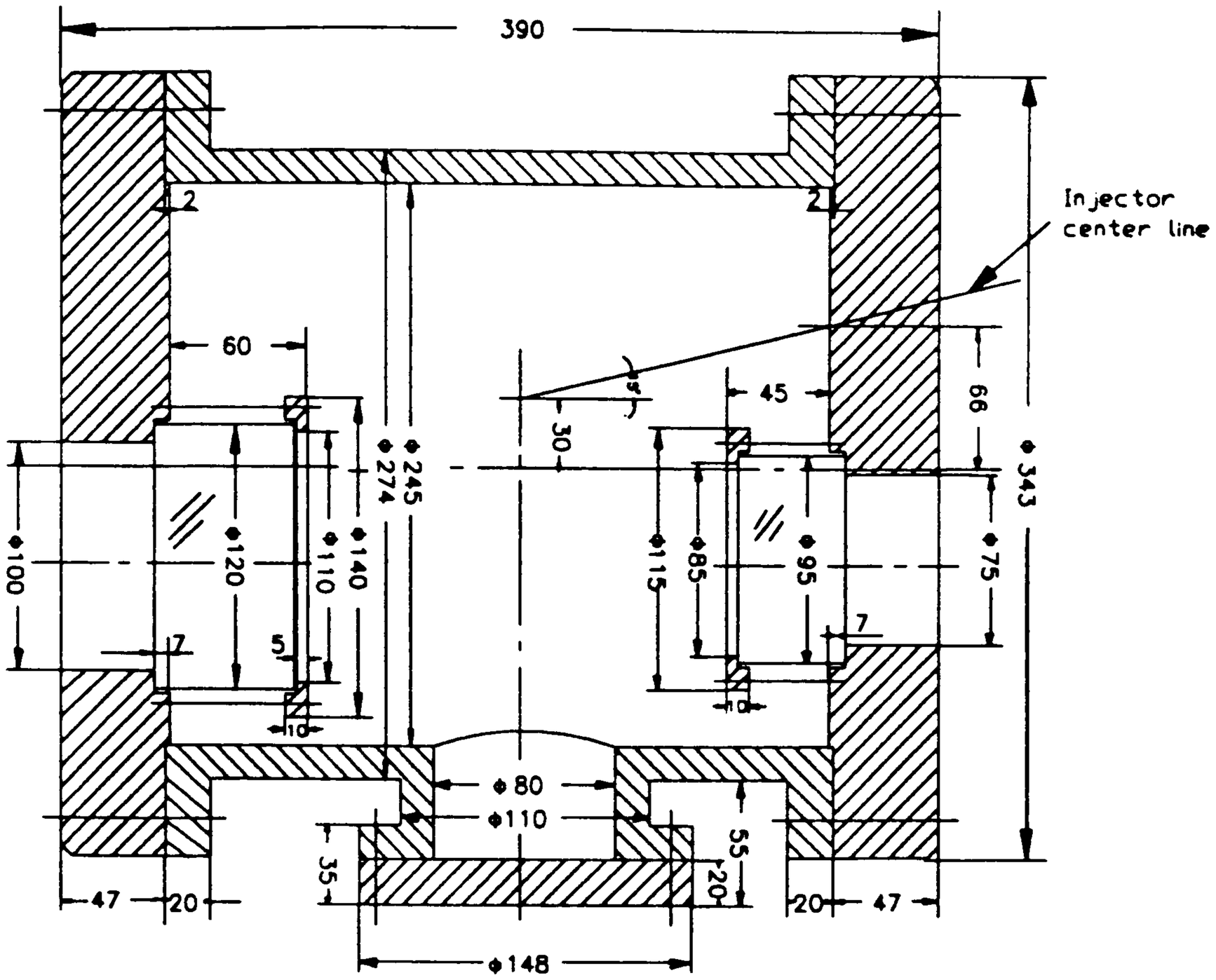

Fig. 4.5 Non-combusting bomb

Injector:

The injector used was a Lucas Bryce fuel injector for a Ruston 6 APC engine (Fig. 4.6). Three nozzles were used for the tests with different hole diameters (Fig. 4.7).

The emulsified fuel trapped in the high pressure pipe and injector body will separate if it is not injected immediately. The separation of water from the fuel is very quick for water/diesel oil emulsion, normally in minutes or seconds. In this case, it is necessary to bleed off the remaining fuel in the high pressure system and to feed fresh emulsion as close as possible to the nozzle before the tests.

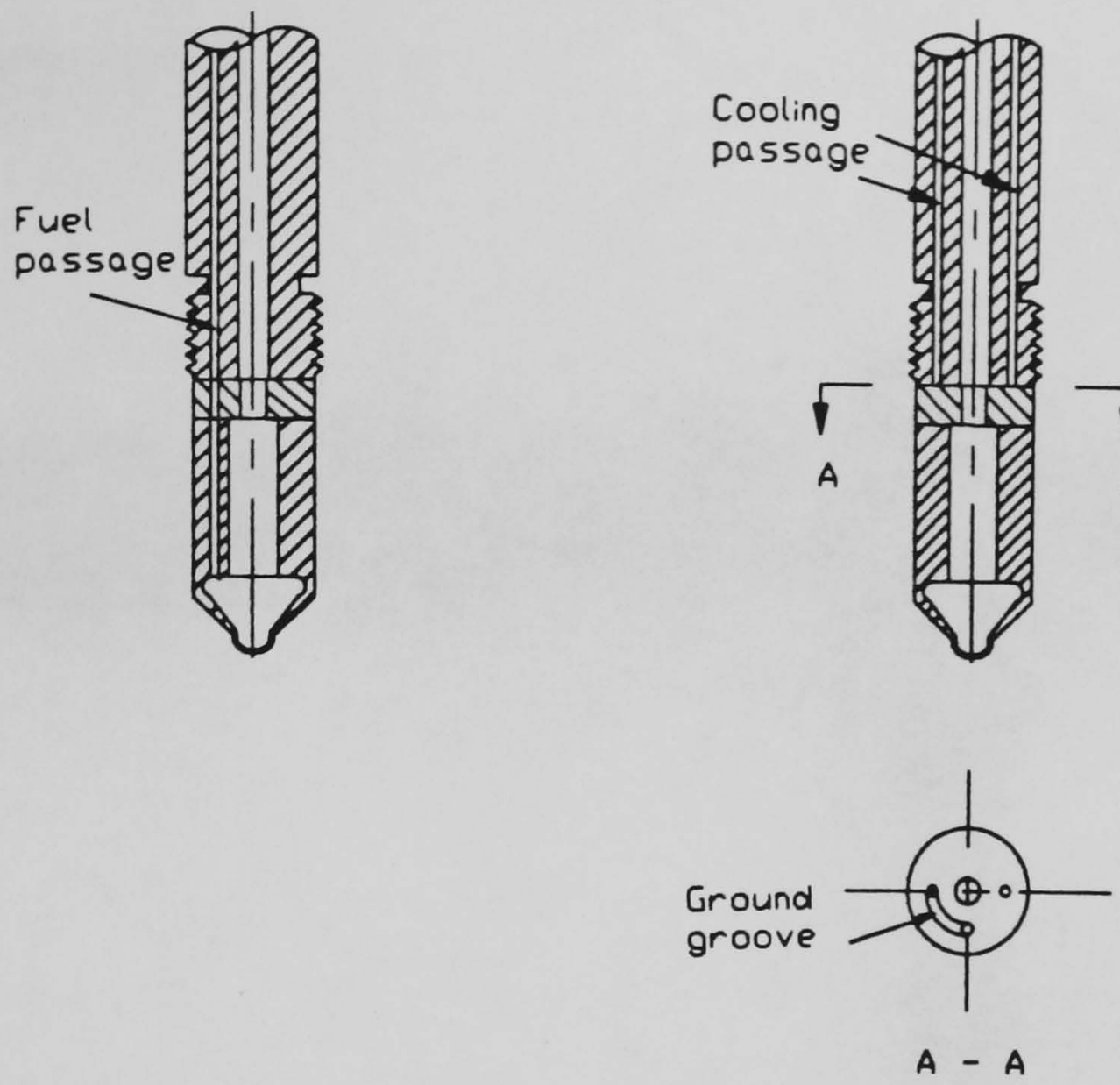

Fig. 4.6 Injector

The nozzle parameters:

Nozzle:	$1_{\#}$	$2_{\#}$	$3_{\#}$
Hole No.:	9	9	9
Hole diameter:	0.35 mm	0.37 mm	0.39 mm
Spray angle:	150°	150°	150°
Opening Pre.:	210 bar	210 bar	210 bar

For the purpose of these tests, the injector had to be modified. The injector has a cooling system for burning heavy fuel. In Fig. 4.6, the block "A" is interchangeable with or without the cooling passages. A groove was ground on the block without cooling passages to connect the fuel cell with one of the cooling passages on the injector body as shown in Fig. 4.8. Thus the fuel trapped in the high pressure pipe and injector body could be bled off from the cooling passage. After bleeding, the fuel amount remaining

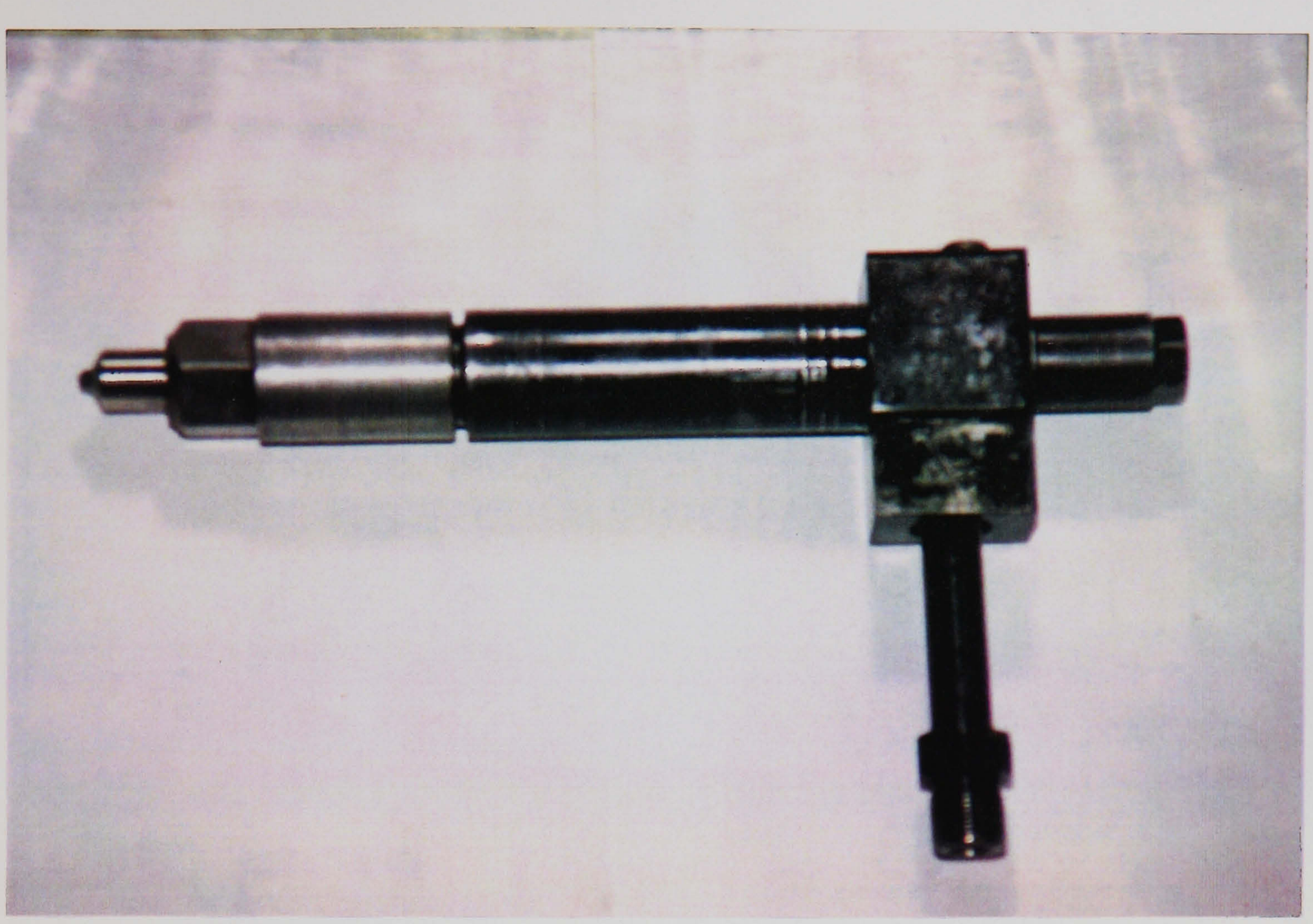

Fig. 4.7 Injector and nozzles used in the tests

Fig. 4.8 Injector block with ground groove for bleeding fuel

Fig. 4.10 Lenses used in the tests

at the top of the nozzle is only about one injection's amount. One roll of film (30.5m) can catch 3 or 4 injection events at the film speed of 6000 fps (frames per second), so the last two sprays on the film will be the emulsified fuel sprays.

High pressure pump and pump cam:

Both the pump and its cam used were spare parts for the Ruston 6APC engine. They were directly fitted on the rig without any modification. The cam was driven by an electric motor with a non-step variable speed gear box. The rack was operated by the solenoid pulled on to the injection position and returned by a spring. Fig. 4.9 shows the calibration curve for the pump. At full load, the injection amount is 0.70 ml per cycle and the rack position is at 12.5mm.

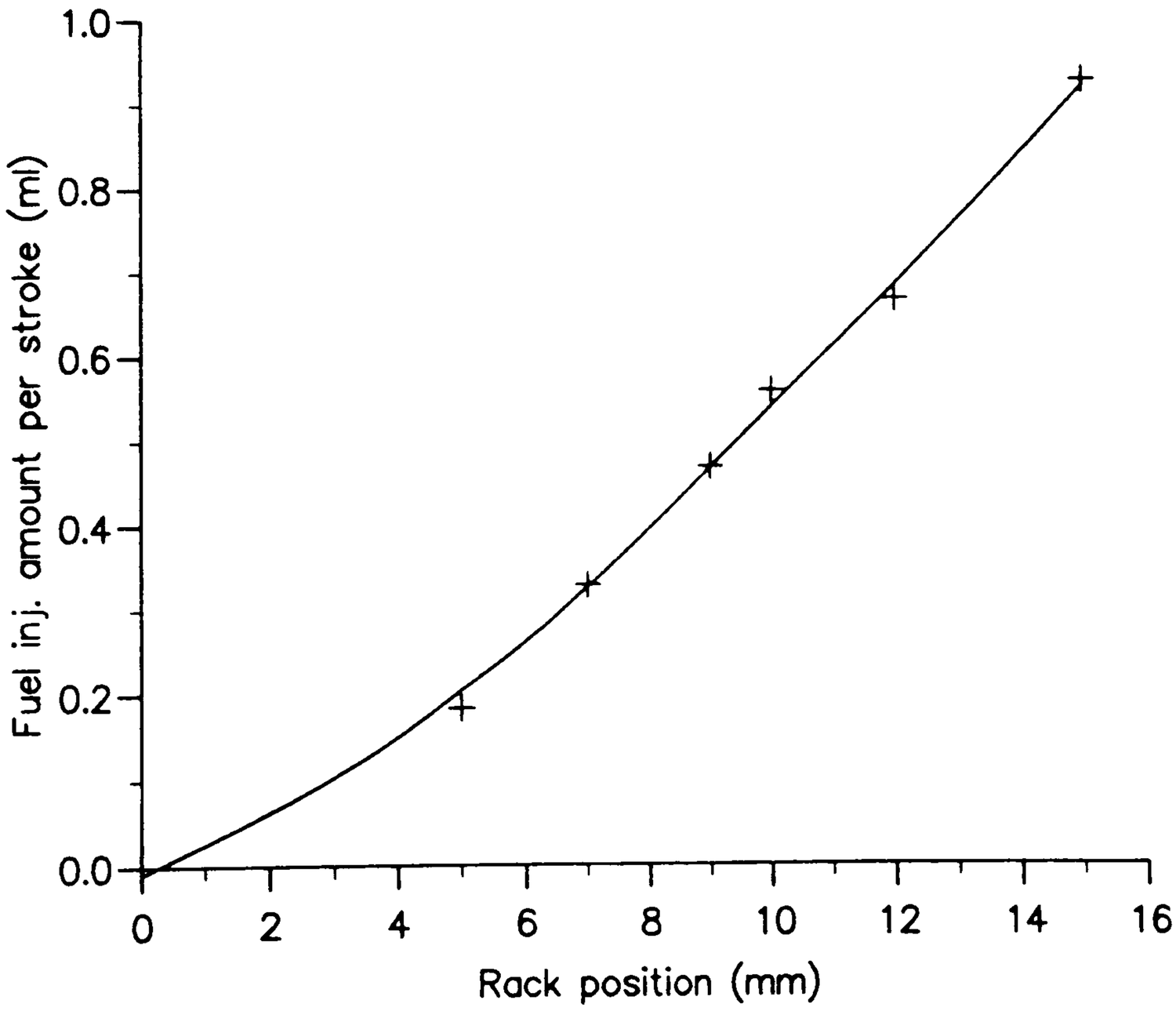

Fig 4.9 Calibration curve for the fuel pump

Instrumentation:

1). Camera:

The camera used was a NAC-E10 of International IMC Ltd. This is a 16mm rotating prism high speed camera, normal speed is 300 to 10,000 frames per second. With a 16 side prism, the film speed can reach 40,000 fps. The camera is controlled by a camera controller which is operated by computer.

2). Lens:

A 25mm Nikon lens with the rotating shutter of shutter constant K5 was used for taking the pictures of whole sprays, while for picturing the droplets in sprays, a micro-lens model TAMRON SP 90mm F/2.5 with an extension tube and a shutter of shutter constant K40 were used.

The exposure time $T = 1/(K \cdot S)$(sec.), where K is shutter constant and S is film speed (fps). Fig. 4.10 shows the picture of the lenses used in this test.

3). Illumination:

A 1 KW Photographic bulb was fitted in a specially built light housing for illuminating the spray. When shooting the droplet size in the spray, a very short camera exposure time was required to obtain a sharp image on films. In this test, the exposure time was 6.25×10^{-6} second. An extremely strong light was needed for illumination as the exposure time was so short. Normal light sources cannot satisfy this requirement. For this purpose, a condensing lens was fitted in front of the quartz glass at the illumination side to concentrate the light beam.

4). Camera controller:

The camera controller has the following functions: a). starting and stopping the camera; b). setting up film speed; c). producing the Event Synchronous signal to trigger the injection event. The event can be triggered before or after the starting of the camera

with a pre-set time; d). providing a signal for making time reference markers on the edge of film with the frequency of 100 Hz or 1,000 Hz; e). stopping the camera at a designed film length. Fig. 4.11 illustrates the camera controller and computer

5). Computer:

A PC computer of COLUMBIA DATA PRODUCTS, INC was used for remote-controlling of the camera and collecting the injection line pressure data.

6). Pressure transducer and charge amplifier:

The fuel line pressure was picked up by a Kistler [type 6227 SN212849] piezo pressure transducer fitted on the high pressure line at the injector end. The charge amplifier used was also made by Kistler [type 5007 SN264667].

7). Events sequence timing controller(ESTC):

The ESTC was specially designed for controlling all the signal sequences in the extremely short time available. Fig. 4.12 shows the circuit diagram of the ESTC.

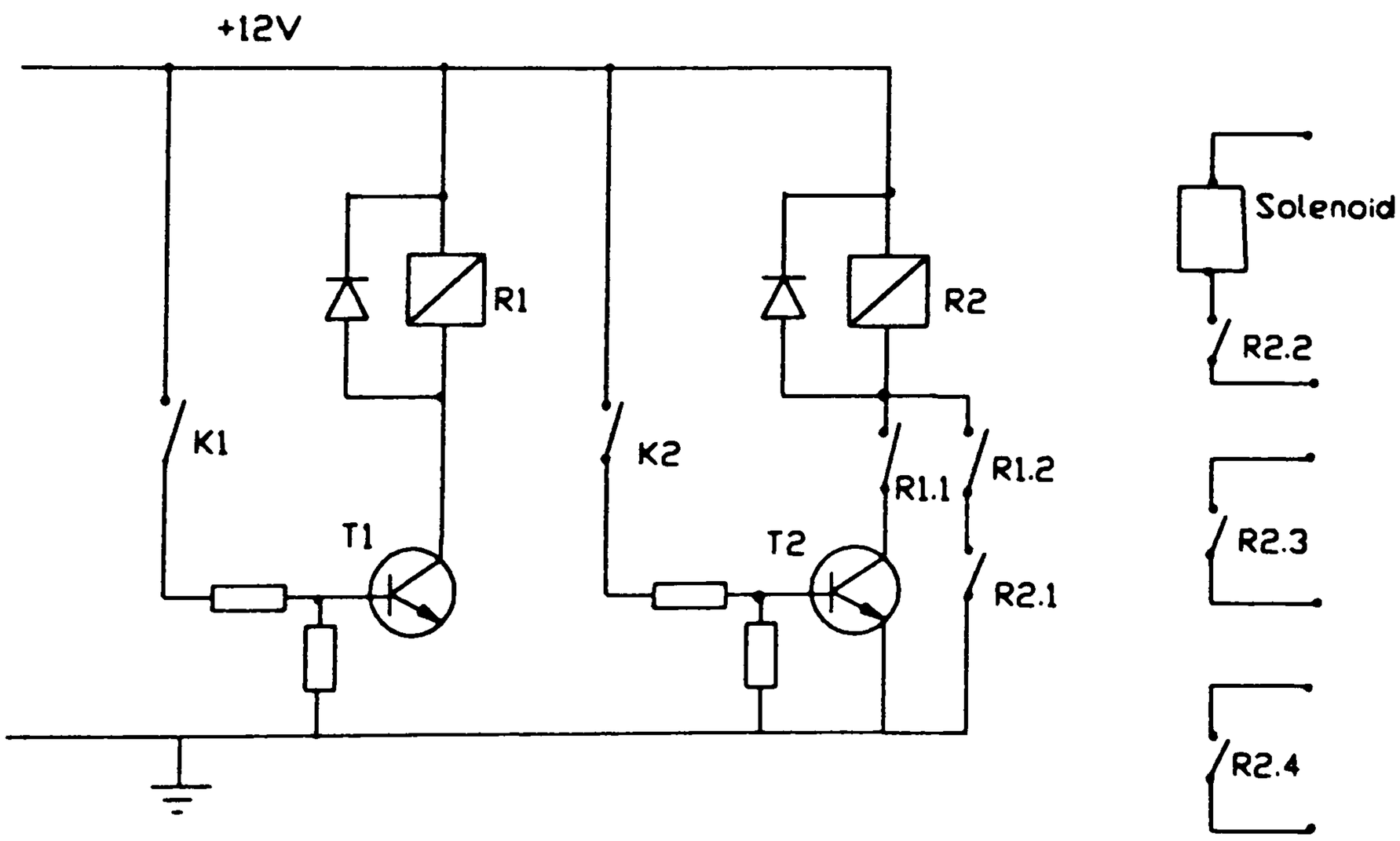

Fig. 4.12 The diagram of ESTC circuit

In Fig. 4.12, where:

K_1: Event sync. switch from camera controller.

K_2: Micro-switch (No.17 on Fig. 4.3) fitted on the side of cam house, controlled by slotted wheel.

R_1,R_2: Normal open relays.

$R_{1.1}$,$R_{1.2}$,$R_{2.1}$: Relay switches for self-locking.

$R_{2.2}$: Relay switch in the solenoid power line, operating the solenoid to pull the fuel rack to start injection.

$R_{2.3}$: Relay switch to "Event Marker In" on the camera controller for making time reference markers on the edge of film.

$R_{2.4}$: Relay switch to ADC for starting and stopping of computer sampling.

The micro-switch is closed at the time when the cam follower sits on the base of cam. Thus the pump rack is pulled to the on injection position during the pump suction stroke, so that the first spray caught on the film is a whole spray.

8). Analog digital conversion (ADC):

The ADC provides a means of connecting all the signals in or out of the computer. These are: a). voltage signal from the charge amplifier to computer, b). signal from computer to camera controller to start the camera, c). signal from the ESTC to start and stop the computer sampling, d). signal from the magnetic pick up to mark the start point of injection, e). signal to charge amplifier to reset it. Fig 4.13 shows the charge amplifier, ESTC and ADC used in the tests.

The signal sequences are as follows:

Fig. 4.11 Camera control and computer

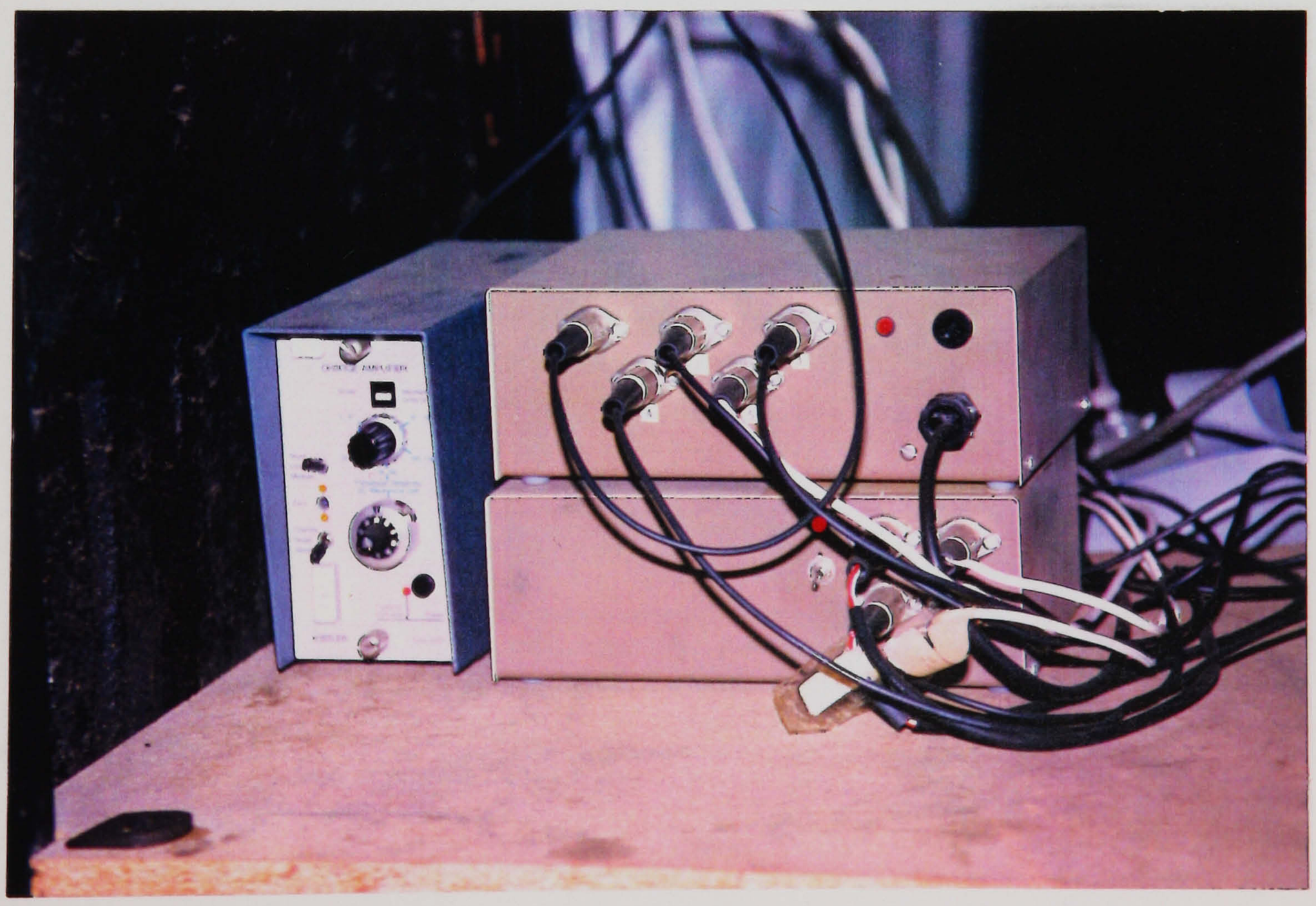

Fig. 4.13 Charger amplifier, ESTC and ADC

a) Press key "S" on computer key board to trigger the remote control switch on camera controller for starting the injection events.

b) Event sync. signal generated by the camera controller to ESTC, so that K_1 is closed (see Fig. 4.12), R_1 is connected on power, $R_{1.1}$ and $R_{1.2}$ are closed.

c) When micro switch is closed, $R_{2.n}$ (n=1,2,3,4) are closed, then ESTC produces three signals, i) to camera controller "event marker in", ii) to trigger the solenoid, iii) to start computer sampling.

d) Solenoid pulls the pump rack to the pre-set position, then injection starts.

e) Computer records injection pressure and pump delivery time where the signal comes from the magnetic pick up.

f) When the film runs out, the camera stops automatically, event sync. is off, signals from ESTC are off and computer stops sampling.

CHAPTER FIVE:

TEST RESULTS AND ANALYSIS

5.1 Test Results From Atomisation Fundamentals Study

5.1.1 Test Conditions

The test conditions for this test are listed as follows:

Fuels:	diesel fuel, 10% water emulsion, 20% water emulsion.
Inj. pressure:	1.0, 1.5, 2.0 bar,
Nozzle diameter:	0.5 mm,
Nozzle hole length	5.0 mm,
Camera body:	Pentax,
Lens:	55 mm micro-lens,
Camera aperture:	f8.0,
Film:	Kodak Ektachrome 100 positive colour film,
Flash:	Metz 45 CT 5.

The liquid jet is forced out of the nozzle by the compressed nitrogen as shown in Fig. 4.1. The jet velocity is controlled by the pressure of nitrogen which is controlled by the regulator. Each fuel sample was tested at three different pressures. The test procedure was as follows:

When pure fuel was used the pressure tank was first filled and pressurised to the desired pressure using the regulator. When the jet flow was judged to be stable the camera was used to record the jet reproduced. For emulsified fuel, before each test the fuel was circulated for some time through the system and the fuel near the bottom of the tank bled off to ensure that what was forced from the nozzle was emulsified fuel and that no separation had taken place. The measurement of flow rate was recorded at the same time in order to calculate the jet velocity.

5.1.2 Test Results

Fig. 5.1 shows three samples of the pictures taken in this test. One spray jet consists of three pictures (see Fig. 5.1). Since the jet was a continuous and time-independent flow, it was possible to take pictures at different sections and times. On the pictures, the bright "bars" are the length of fuel ligaments or the travel distances of ligaments at the time of flash duration. Since the flash duration is very short, the ligaments' travel distance can be ignored. Therefore the bright bars represent the lengths of the ligaments.

Table 5.1 gives the experimental data obtained from the analysis of these pictures.

Table 5.1 The data of atomizing fundamentals test

	Presure (bar)	Countable No. of ligaments	Mean diameter of ligaments(mm)	Mean length of ligaments(mm)	Jet velocity at nozzle (m/s)	Break up length (mm)
A*	2.0	25	0.18-0.20	10.62	16.30	90
	1.5	27	0.20	9.50	14.38	90
	1.0	26	0.16	8.07	11.53	140-150
B	2.0	46	0.22	6.25	17.78	within 40
	1.5	66	0.25	3.63	14.95	within 40
	1.0	58	0.33	2.59	12.26	within 40
C	2.0	47	0.4	5.48	10.37	within 40
	1.5	49	0.5	5.18	7.70	within 40
	1.0	52	0.5	4.44	7.16	within 40

* where: A -- pure diesel; B -- emulsified fuel with 10% water; C -- emulsified fuel with 20% water.

In table 5.1, the countable droplet number refers to the droplets or ligaments number which can be counted in one jet. The jet velocity is calculated as follow:

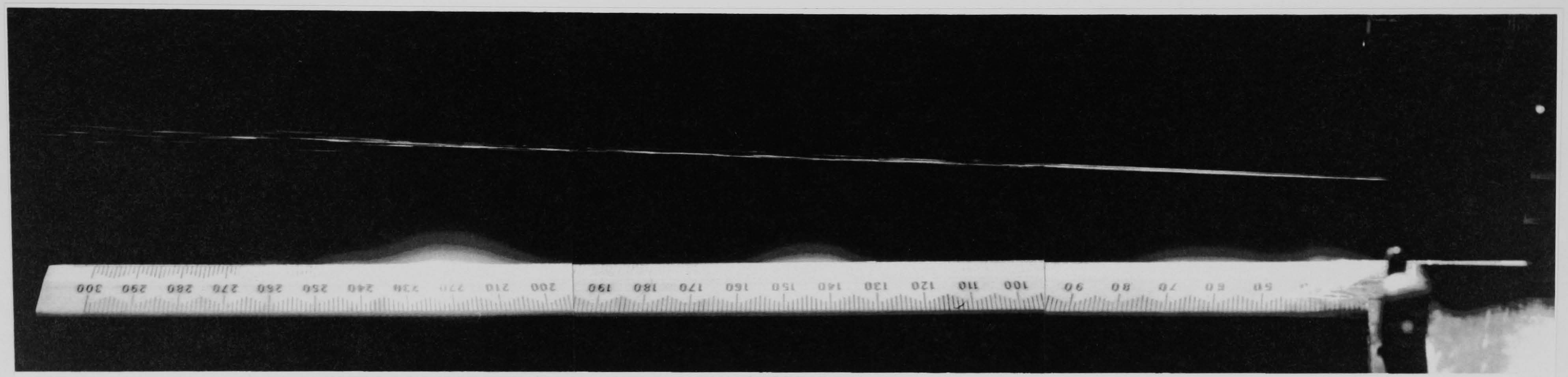

Fig. 5.1(a) Fuel spray obtained from the atomising fundamental study rig

Test conditions: Fuel sample: Pure fuel;

Injection pressure: 1.5 bar (gauge pressure);

Nozzle hole diameter: 0.5 mm;

Nozzle hole length: 5.0 mm.

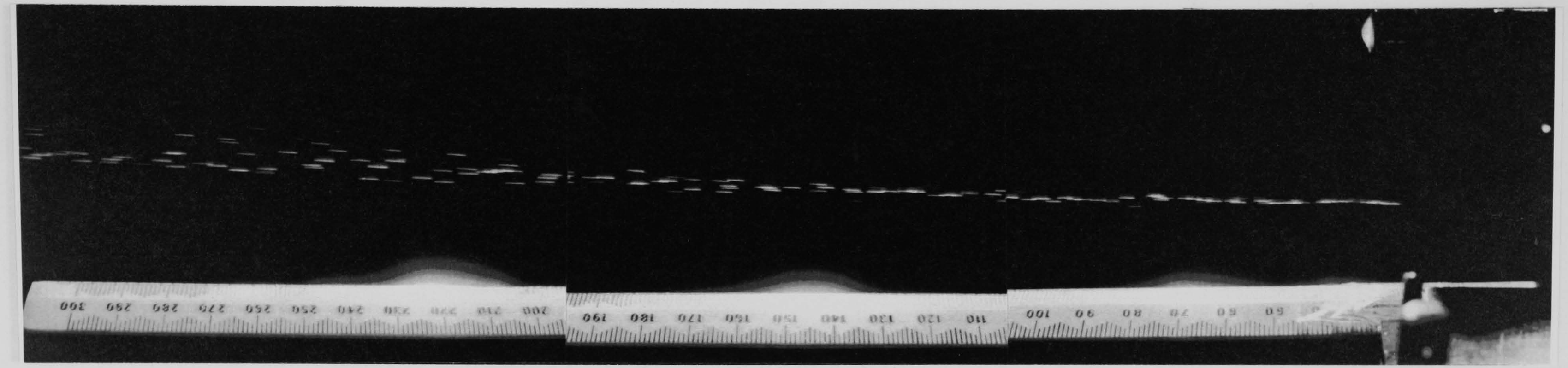

Fig. 5.1(b) Fuel spray obtained from the atomising fundamental study rig

Test conditions: Fuel sample: 10% water emulsified fuel;

Injection pressure: 1.5 bar (gauge pressure);

Nozzle hole diameter: 0.5 mm;

Nozzle hole length: 5.0 mm.

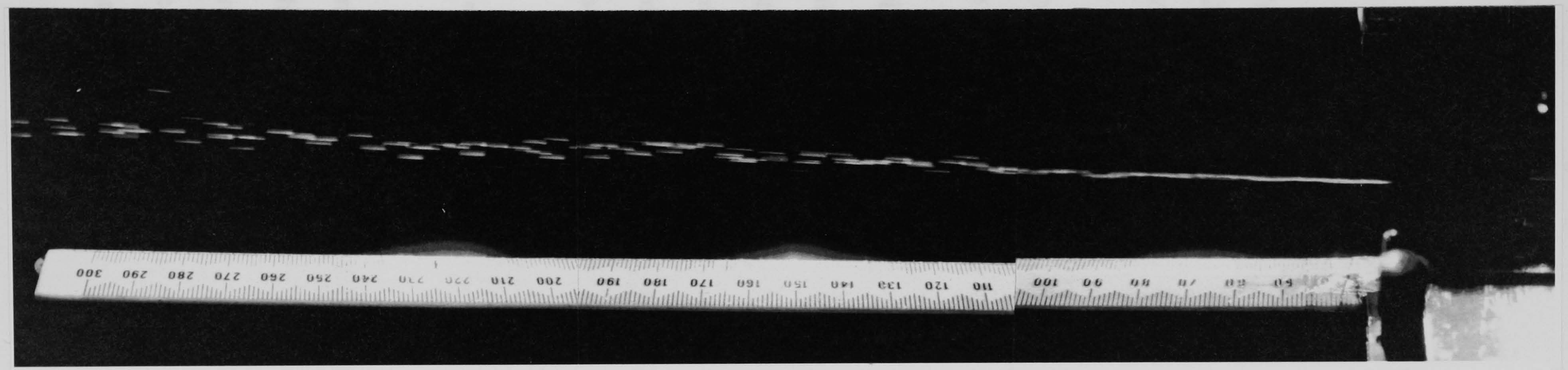

Fig. 5.1(c) Fuel spray obtained from the atomising fundamental study rig

Test conditions: Fuel sample: 20% water emulsified fuel;

Injection pressure: 1.5 bar (gauge pressure);

Nozzle hole diameter: 0.5 mm;

Nozzle hole length: 5.0 mm.

$$v_{jet} = \frac{Q}{A}; \qquad Q = \frac{V}{t};$$

$$A = \frac{\pi}{4} \cdot D_0^2 \cdot \phi,$$

Where: v_{jet} -- Fuel jet velocity ;

Q -- Jet flow rate;

V -- The volume of fuel through the nozzle during the time t;

t -- Time;

D_0-- Nozzle diameter;

ϕ -- Nozzle discharge coefficient.

5.1.3 Discussion Of Test Results

1). The third column in table 5.1 indicates that the ligament diameter of emulsified fuel is greater than that of pure diesel fuel and Fig. 5.1 shows that the ligament lengths of emulsified fuels are shorter. Theoretically, the ligament length (equivalent to wavelength) is a function of fuel viscosity, density and surface tension as expressed in Eq. 2.6,

$$\lambda_{lig} = \sqrt{2} \cdot \pi \cdot D_{lig} \cdot \left[1 + \frac{3 \cdot \nu_l}{(\rho_l \cdot \sigma_l \cdot D_{lig})^{1/2}} \right]^{1/2} \qquad ---2.6 repeat$$

The parameters ν, ρ and σ are increased as water is added to the fuel. The calculated result of the term $3\nu_l/(\rho_l\sigma_l D_{lig})^{1/2}$ shows almost no change for 10% water emulsified fuel. Therefore the ligament lengths of emulsified fuels should, theoretically, show no change. The possible reason for the change in ligament length is the unstable contact inter-surface between water droplets and fuel. This proves the assumption in section 2.3.2, Fig. 2.5.

According to the atomisation theory, these ligaments will further break down to droplets at a high-shear rate. The droplet diameter is proportional to the diameter of the broken-up ligament. Thus, in a high-speed jet, the emulsified fuel will have a bigger mean droplet diameter.

2). Due to the unstable contact of water droplets with fuel, the emulsified fuel is easy to break up. This results in an increase in countable ligament (droplet) numbers in emulsified fuel jets which will result in an increase in the total surface area of the spray jet.

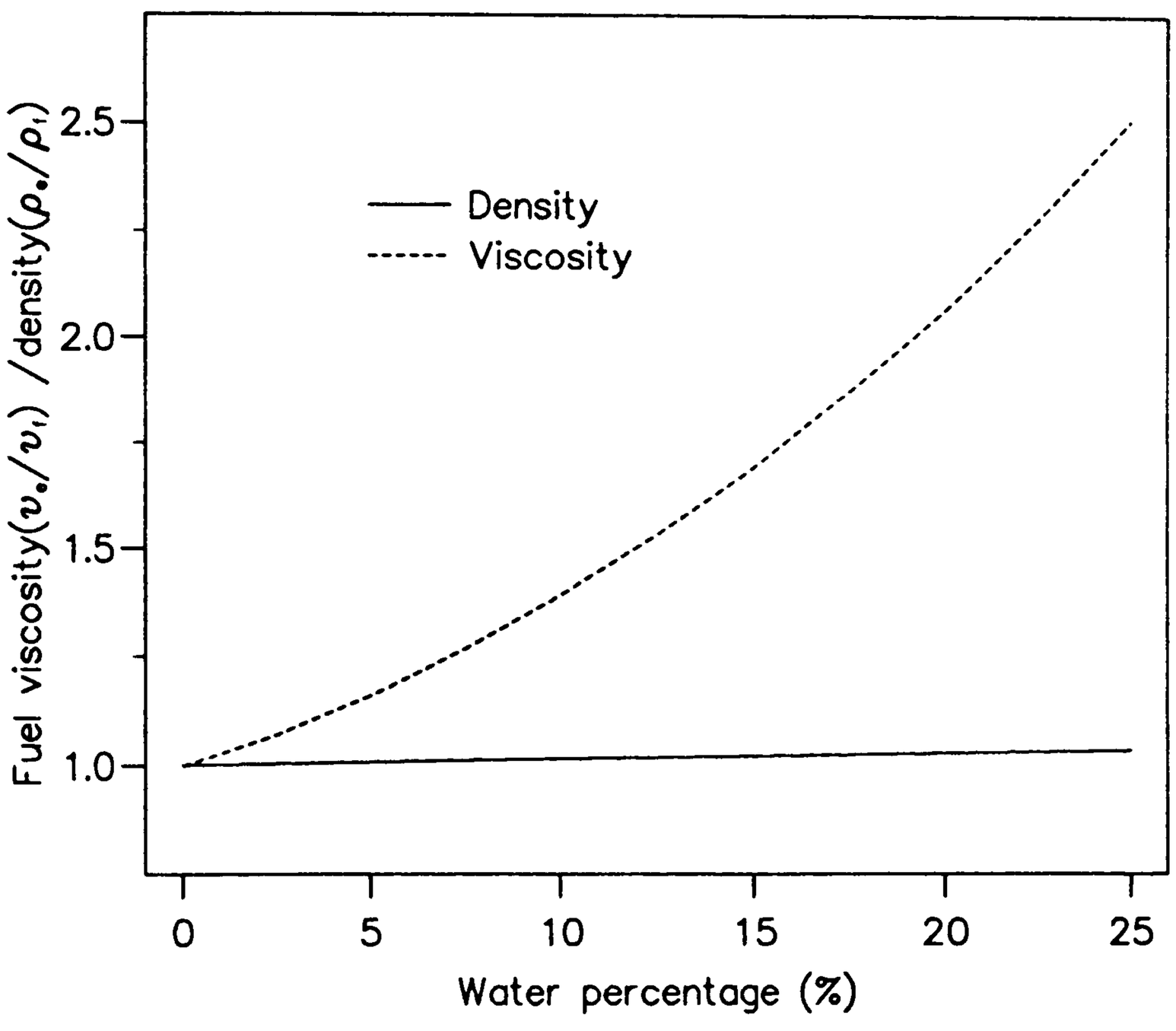

Fig. 5.2 The curves of ρ_e and ν_e change with γ

where, $\rho_e = \frac{\rho_f + \rho_w \cdot \gamma}{1+\gamma}$; $\nu_e = (1 + 2.5 \cdot \gamma + 14.1 \cdot \gamma^2) \cdot \nu_f$; $\gamma = V_w/V_f$.

3). As discussed in Chapter 2, both the inertial and viscous forces are increased when water is added into the fuel (Fig. 5.2). The velocity of the emulsified fuel with 10% water is slightly greater than that of diesel fuel, but it decreases very much for the emulsified fuel of 20% water. This is because the inertial force of fuel, F_i

$\propto \rho L^3$, is proportional to its density, while its viscous force, $F_v \propto \tau L^2 \propto \nu(u/L)L^2$, is proportional to the viscosity. As shown in Fig 5.2, compared with the density, the increase of viscosity of emulsified fuel is rapid as the water percentage increases. In the other words, the Reynolds number of the emulsified fuel decreases rapidly as the water content increases. However the decrease of Reynolds number means an increase in the coefficient of friction. Thus, for emulsified fuel of 20% water, the increment of viscous resistance is much greater than that of inertial force, which further results in a low jet velocity. These test results imply that for the small water content emulsified fuels (lower than 10%), the jet velocity would be fast (at least as fast as 10% water emulsion) due to their viscosity increments being relatively small.

This might not occur in a real engine, since the ratio (L/D_0) of orifice length to diameter of an injector is only between 2 and 5, while L/D_0 in this test is 10. Thus the friction loss on the orifice wall would not be so significant in the real injector.

4). The break up point gets nearer to the nozzle as the pressure increases; for the emulsified fuel, the break up points are much closer to the nozzle. Unfortunately, the flash light at that area was blocked by the bleed valve and therefore the exact points can not be seen on the pictures. However, it is recognized that the break up points of emulsified fuel are closer to the nozzle, compared with diesel oil at the same test conditions.

For "good" atomisation, the spray break up length is required to be as short as possible. A lot of effort has been made to meet this requirement. It is evident that emulsified fuel can solve this problem by a certain degree without any additional effort.

In Dr. Sheng's report [22], it is stated that the atomization of emulsified fuel gets worse, because of increase of droplet size. This statement seems rather doubtful, since the specific area of the emulsified fuel jet is enlarged at the same time due to

the increased number of droplets or ligaments. The objective of atomization is to produce fine droplets. but this does not mean that finer droplets are necessarily better. Good atomization (as defined by Dombrowski [55]) utilises the energy imparted to the liquid so that the liquid has a large specific surface before it commences to break down into drops. According to this definition, the atomization of emulsified fuel is more effective.

The earlier spray break up enlarges the jet spray angle, and provides more opportunities for air and fuel to mix with each other. Thus, it will improve the combustion process.

It has been found by other researchers that the ignition delay of emulsified fuel is longer than that of pure fuel, since the vaporization of water lowers the temperature of the combustion chamber. Here, in addition to lower temperature, the increase of droplet diameter and larger specific area gives another explanation for this phenomenon. The longer ignition delay gives more time for the air and fuel to mix and this results in a better preparation for combustion, what is often called the physical and chemical preparation. That is the reason why the combustion process of emulsified fuel is faster and improved.

From the above discussion, the prediction of the characteristics of emulsified fuel atomization in a real engine can be worked out as follows. Compared with diesel fuel, emulsified fuel atomization has the following characteristics:

a). the mean droplet diameter of the spray gets bigger, but its specific area is increased because of the increased droplet numbers. b). The spray angle is enlarged due to the earlier break up of the spray. c). The jet velocity is a function of the amount of water added to the fuel.

The results concerning jet velocity from this test can not be used to predict the events in a real engine, since the geometric difference between the nozzles is too great. It seems that, at low water percentages, the spray velocity will increase as the water amount increases.

5.2 Spray Penetration Test Results

5.2.1 The Measurement Of Test Data

The measurement of spray penetration data was done manually from the 16mm negative film. The facility used for this purpose was a micro-fiche viewer. To obtain an accurate measurement, several instruments, such as micro-scopes, projectors and micro-fiche viewers, were tried to enlarge the film. Among them, the micro-fiche viewer was the most suitable one. When the micro-scopes were used, only a small part of the picture could be seen at any one time, and the object on the film lost its concentration (blurring) due to the large magnification. When the film was projected onto a wall, the whole spray could be seen clearly, but the edge of the enlarged spray, especially the spray tip, did not produce a sharp image. Besides this, it was not convenient to stand by the wall and take readings from the large number of films. Although the magnification of micro-fiche viewer (40 times) is the smallest compared with the other two, it was enough to magnify the film to the size in which the spray configuration image was clear and sharp, hence the measurements could be taken accurately.

Fig. 5.3 shows the print of one injection spray. The progress of the spray with time is clearly presented on the print. For the purpose of calibration, a fork with post widths of 10mm was fixed in a position where the spray was not disturbed. The actual perpendicular distance from the post at the nozzle side to the nozzle is 60mm. In this case, the calculation of magnification of film is not needed.

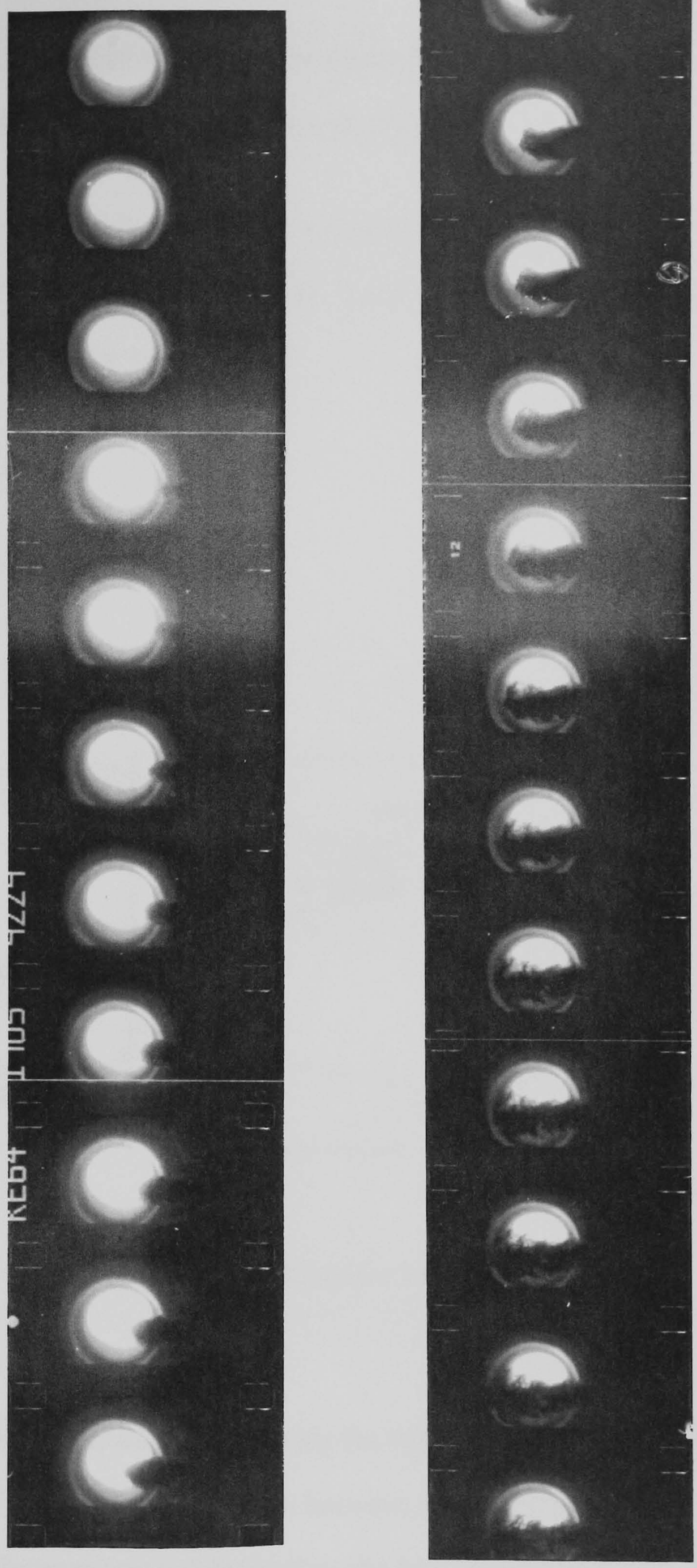

Fig. 5.3 Fuel injection spray obtained from the high speed camera test rig

Test conditions: Fuel sample: pure fuel;
P_{inj}: 180 bar;
P_g: 55 bar;
D_0: 0.37 mm;
Film speed: 6000 frames per second

Unfortunately, the initial section of the injection spray can not be seen on the film due to darkness in that area as indicated by Fig. 5.4.

This was caused by a deficiency in the initial bomb design. The problem was found after the test rig was completely built. Lack of time and resources prevented a complete reconstruction of the bomb.

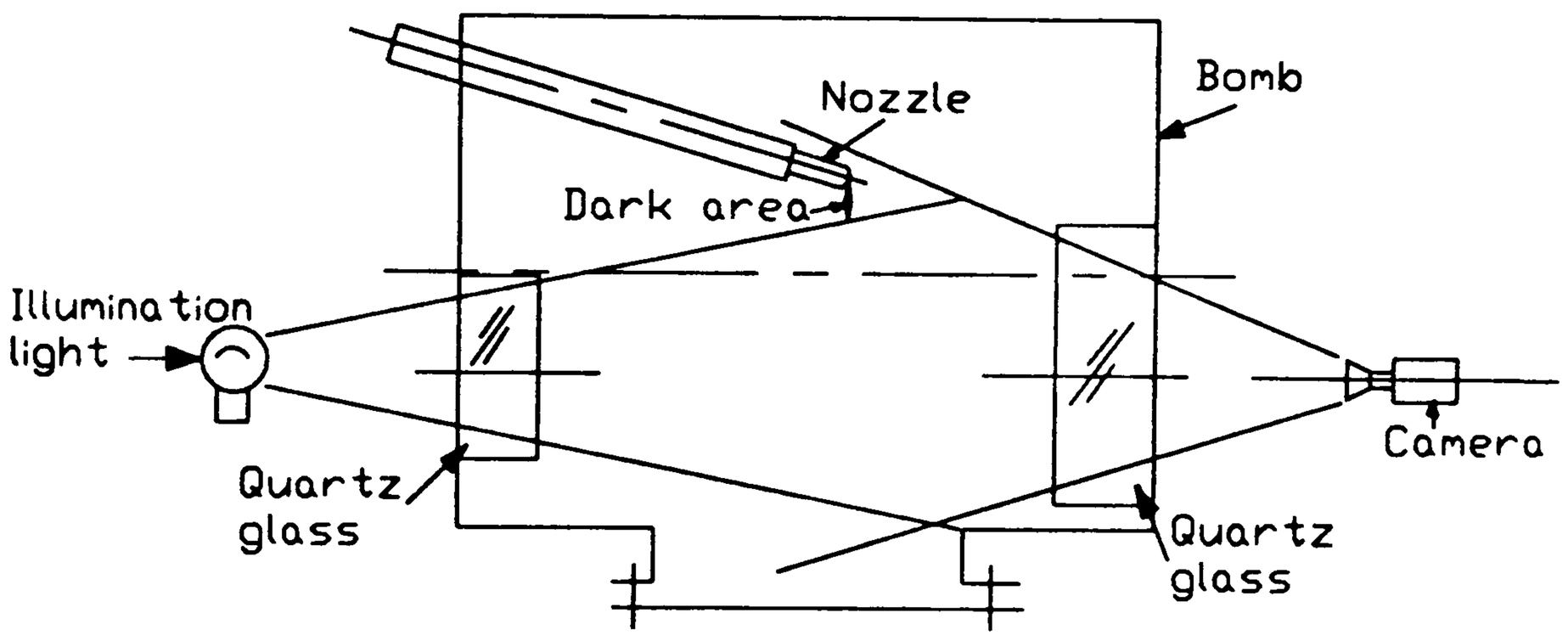

Fig. 5.4 Illumination of the bomb

A remedial method was used for locating the injection start point on film. See Fig. 5.5. The actual perpendicular distance between the nozzle and the post A is 60mm. An equivalent distance can be obtained on the film, and a line B may then be drawn to connect the points of the nozzle on the film. According to the test results analysis and previous researchers' reports [52,53,56,65], the spray speed at beginning of the injection is constant, therefore a line C can be drawn to link several spray tips formed at the beginning of injection and this will meet line B at point D. Thus, point D can be considered as the injection start point. In this way, the estimated error in the

measurement of the injection starting point is likely to be less than one frame. At a film speed of 6000 fps, the time interval of each frames is 1/6000 = 0.16 ms and since the pump cam shaft speed is 325 rpm the cam shaft rotation during this would be 0.312° (0.624° crank shaft). Thus the location of point D does provide an accurate represention for the start point of injection.

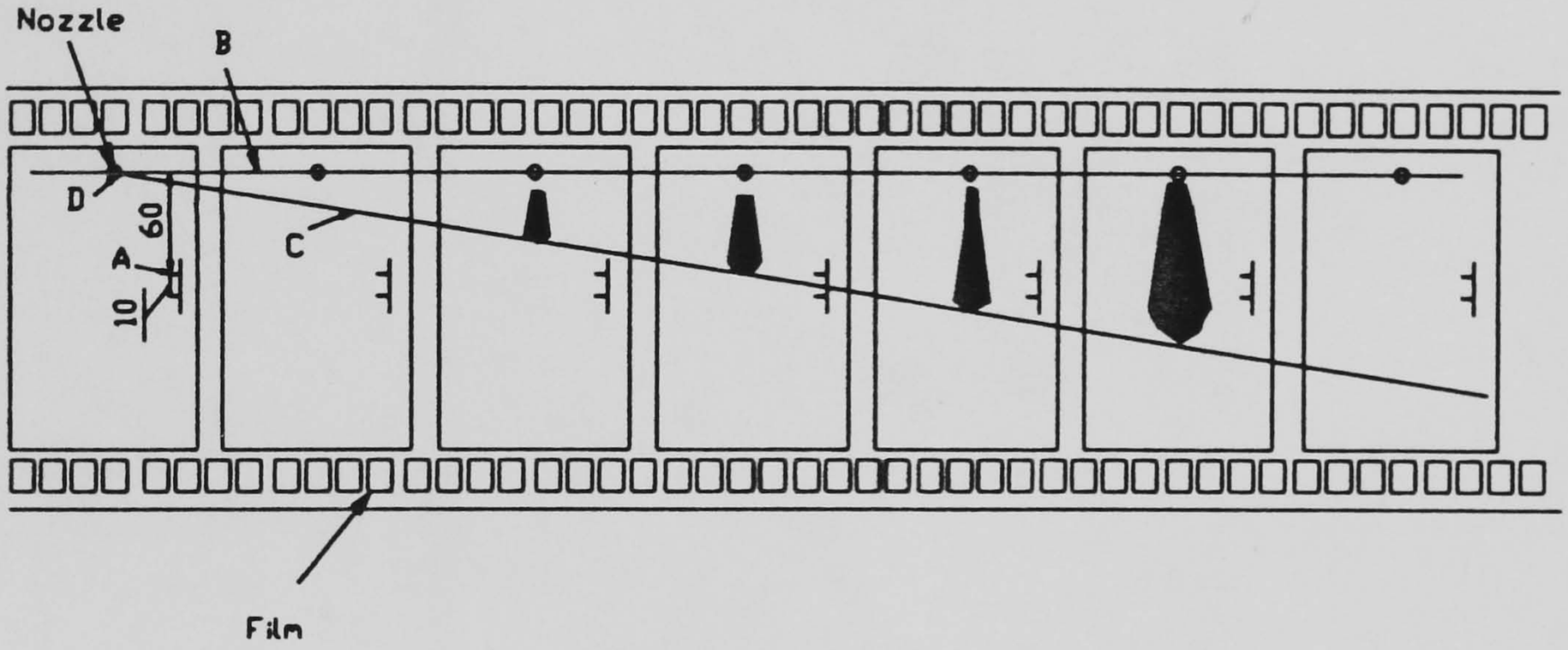

Fig. 5.5 Remedial method for locating the injection start point

5.2.2 Interpretation Of Readings From The Film

After the injection start point (ISP) has been decided, every frame on the film represents a corresponding time from the ISP.

Fig 5.6 represents what could be seen on the screen of the micro-fiche viewer. Taking post A as the zero point for measurement, x_i is the distance from post A to the tip of the spray on the screen.

Then the spray penetration S is calculated as follows:

$$S_i = 60 + 0.435 \cdot x_i \quad \text{(mm)} \qquad ---5.1$$

where 0.435 is scaling factor which obtained by 10(mm)/23(mm), where 10mm is the actual distance of the two posts of the the fork and 23mm is the distance of the two posts on screen.

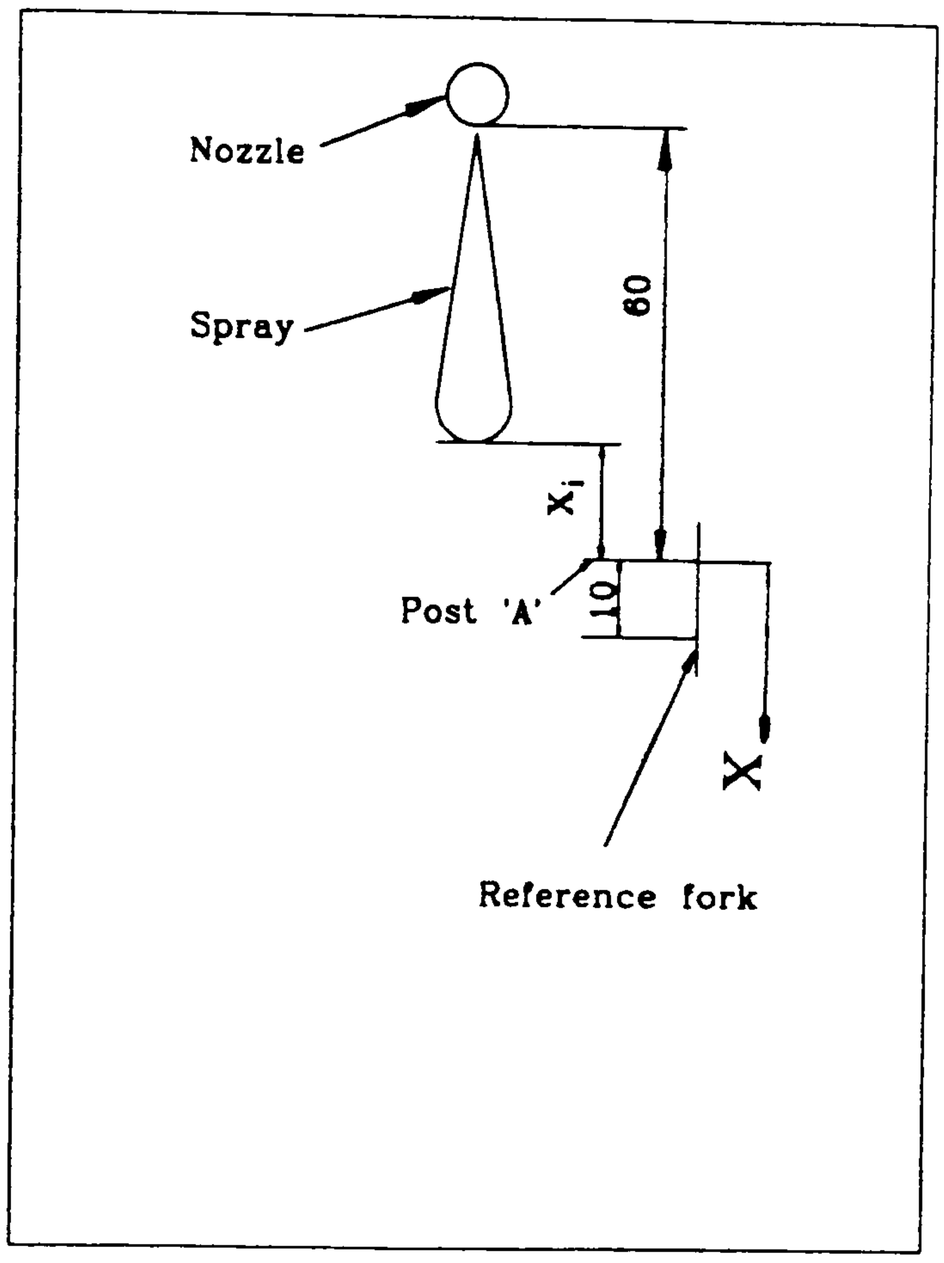

Fig. 5.6 Reading measurement from the micro-fiche viewer screen

Table 5.2 is an example of the original reading obtained from the screen.

Table 5.2 the spray penetration readings obtained from micro-fiche viewer screen

Frames:	6	7	8	9	10	11	12	13	14	15	16	17	18	19	20	21	22	23	24
x_i(mm):	-45	-37	-30	-21	-16	-8	-2	5	10	16	20	22	27	34	40	41	44	47	50
Time (ms):	1.00	1.16	1.33	1.50	1.66	1.83	2.00	2.16	2.33	2.50	2.66	2.83	3.00	3.16	3.33	3.50	3.66	3.83	4.00

* Test conditions for the above table:

P_{inj}=210 bar; P_g=50 bar; D_0=0.35 mm; q=0.70 ml; γ=0.

Errors in measurement are unavoidable and the results must be smoothed to remove the experimental and reading errors to whatever degree possible. For this purpose, a five points of degree three smoothing polynomial function was employed to smooth the measurement readings. Appendix A gives the spray penetration data after smoothing.

5.2.3 Test Conditions

It was discussed in chapter 3 that the main parameters which affect the spray penetration are:

ΔP -- pressure difference at the front and back of the nozzle hole,
D_0 -- diameter of nozzle hole,
L_0 -- length of nozzle hole,
ρ_g and ρ_f -- densities of gas and fuel,
μ_f -- viscosity of fuel,
σ_f -- surface tension of fuel,
γ -- percentage of water in fuel by volume.

For the existing test rig, only the parameters ΔP, D_0, ρ_g and γ were considered. To obtain the changing tendency of the spray penetration with the parameters mentioned above, each parameter must be measured at least at three test points. Now, there are four parameters to be considered in the test, and each of them has three test points (levels), so that the total test numbers would be $3^4 = 81$, if only one parameter was changed in every test.

Table 5.3 Orthogonal design table for 4 variables with 3 levels

Test No.		1 2 3	4 5 6	7 8 9
Variables	1	1 1 1	2 2 2	3 3 3
	2	1 2 3	1 2 3	1 2 3
	3	1 2 3	2 3 1	3 1 2
	4	1 2 3	3 2 1	2 3 1

To reduce the test work, an orthogonal design table was employed. The main idea of an orthogonal design table is to obtain the maximum information from the minimum number of tests by different combinations of test variables. Table 5.3 is the orthogonal design table for four variables with three levels.

Rewriting Table 5.3 with the corresponding parameters where P_{inj} (injection pressure) represents variable 1, P_g represents variable 2, D_0 and γ represent variable 3 and 4. Here ρ_g does not appear because it can be deduced from P_g. Since both volume and temperature of the bomb are constant, the density of the gas in the bomb is only a function of gas pressure.

Thus:

Table 5.3.1 Orthogonal design table for test conditions

Test No.	1	2	3	4	5	6	7	8	9
P_{inj} (ΔP)	P_1	P_1	P_1	P_2	P_2	P_2	P_3	P_3	P_3
P_g (ρ_g)	P_{g1}	P_{g2}	P_{g3}	P_{g1}	P_{g2}	P_{g3}	P_{g1}	P_{g2}	P_{g3}
D_0	D_{01}	D_{02}	D_{03}	D_{02}	D_{03}	D_{01}	D_{03}	D_{01}	D_{02}
γ	γ_1	γ_2	γ_3	γ_3	γ_1	γ_2	γ_2	γ_3	γ_1

To simulate the combustion chamber working condition of a Ruxton 6APC engine, the values of the above parameters are:

P_1 =180 bar	P_{g1} =55 bar	D_{01} =0.37 mm	γ_1 =0
P_2 =210 bar	P_{g2} =50 bar	D_{02} =0.35 mm	γ_2 =5%
P_3 =150 bar	P_{g3} =45 bar	D_{03} =0.39 mm	γ_3 =10%

For the consideration of the effect of water percentage on spray penetration which is the main objective of the test, four more tests were conducted to obtain the individual effect of water content on fuel atomisation without any change in the other parameters, see test No. 10 to 13 in table 5.4.

In table 5.4, the contents of test number 1 to 9 are same as the table 5.3.1, but in different order. This is because the tests were carried out in the order of - pure fuel, 5% emulsified fuel and 10% emulsified, etc..

Table 5.4 Test conditions for picturing injection spray

Test No.	1	2	3	4	5	6	7	8	9	10	11	12	13
P_{inj} (bar)	180	210	150	180	210	150	180	210	150	180	180	180	180
P_g (bar)	55	50	45	50	45	55	45	55	50	55	55	55	55
D_0 (mm)	0.37	0.35	0.39	0.39	0.37	0.35	0.35	0.39	0.37	0.37	0.37	0.37	0.37
γ (%)	0	0	0	5	5	5	10	10	10	5	10	15	20

The other test conditions of tests for picturing injection spray:

a). Film used is Kodak Negative Film, its ISO is 250, and the film speed is 6000 fps.

b). Camera lens is 25 mm, and the camera rotary shutter constant is K=5.

c). Exposure time of the camera is T= 0.0333 ms.

d). Injection frequency is 325 injs./min, and one injection volume is approximately 0.70 ml.

e). Gas temperature is 17 °C.

5.2.4 Test Results

According to the experimental results analysis, some important characteristics about emulsified fuel penetration can be summarised as follows:

Compared with a pure fuel spray,

a). The emulsified fuel has a longer spray penetration during the beginning of injection (Fig. 5.7).

b). Its penetration increases as the water percentage increases.

c). The increment of spray penetration decreases as time increases. The spray

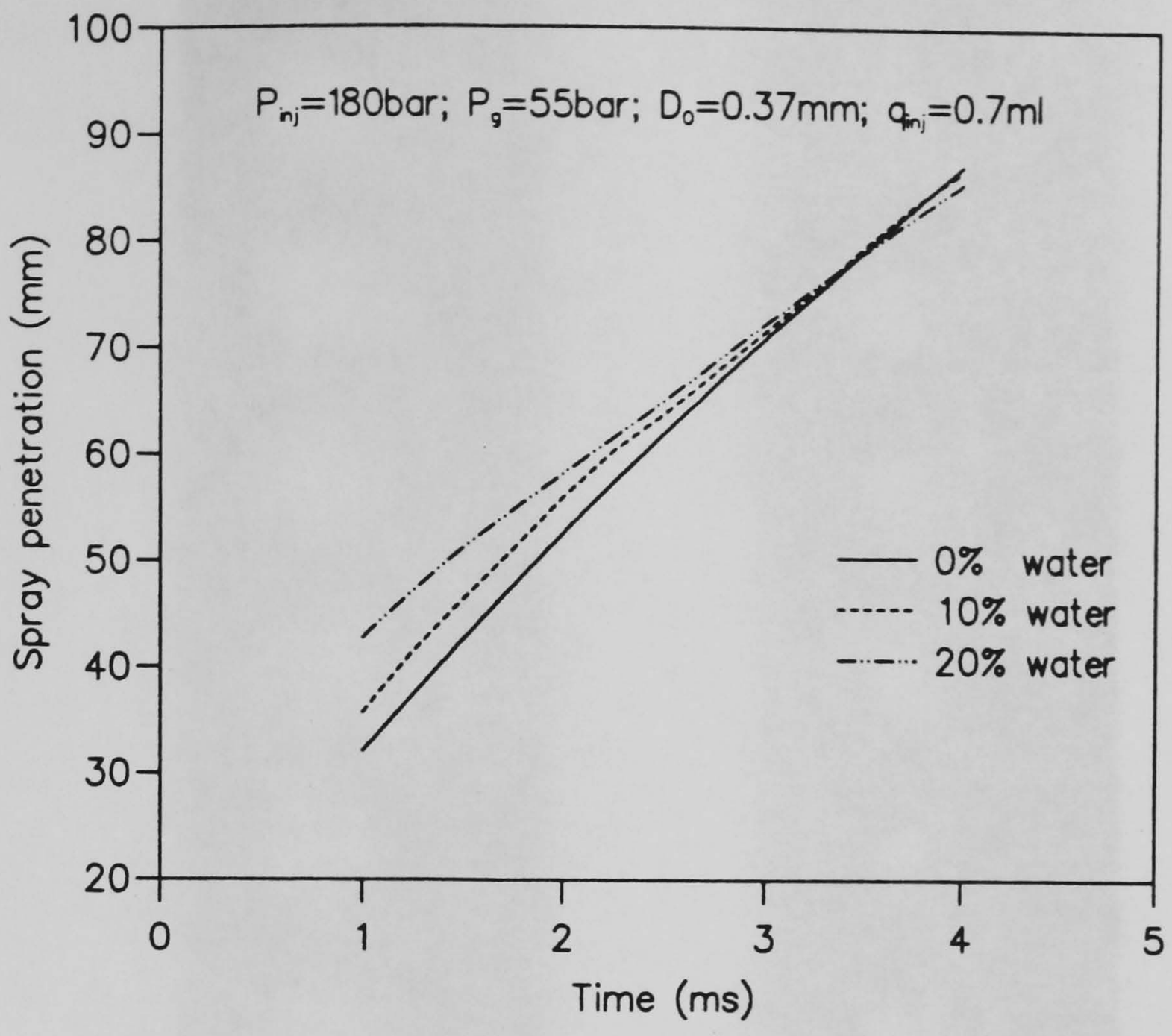

Fig. 5.7 Spray penetration at different water contents

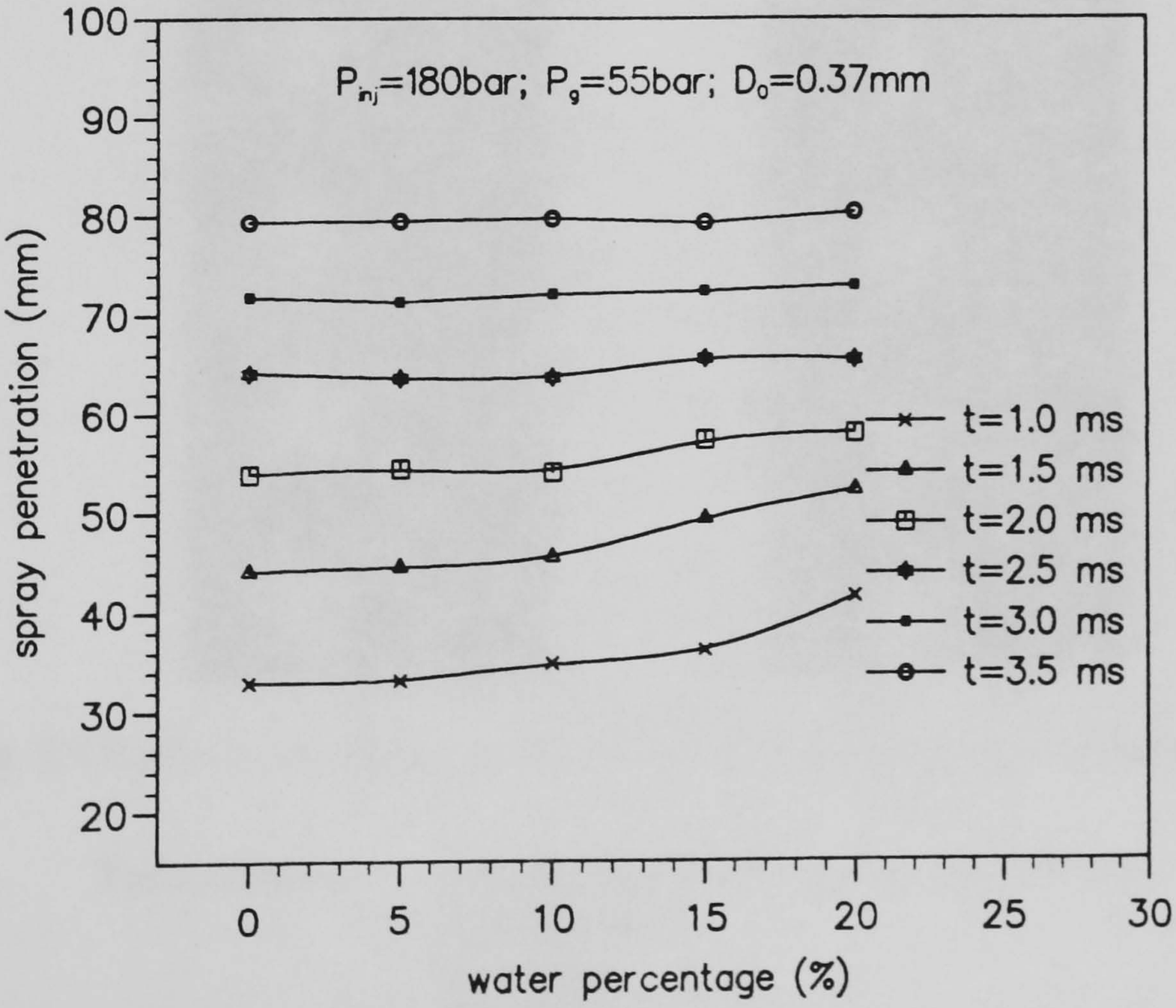

Fig. 5.8 Spray penetration at different times from start of injection

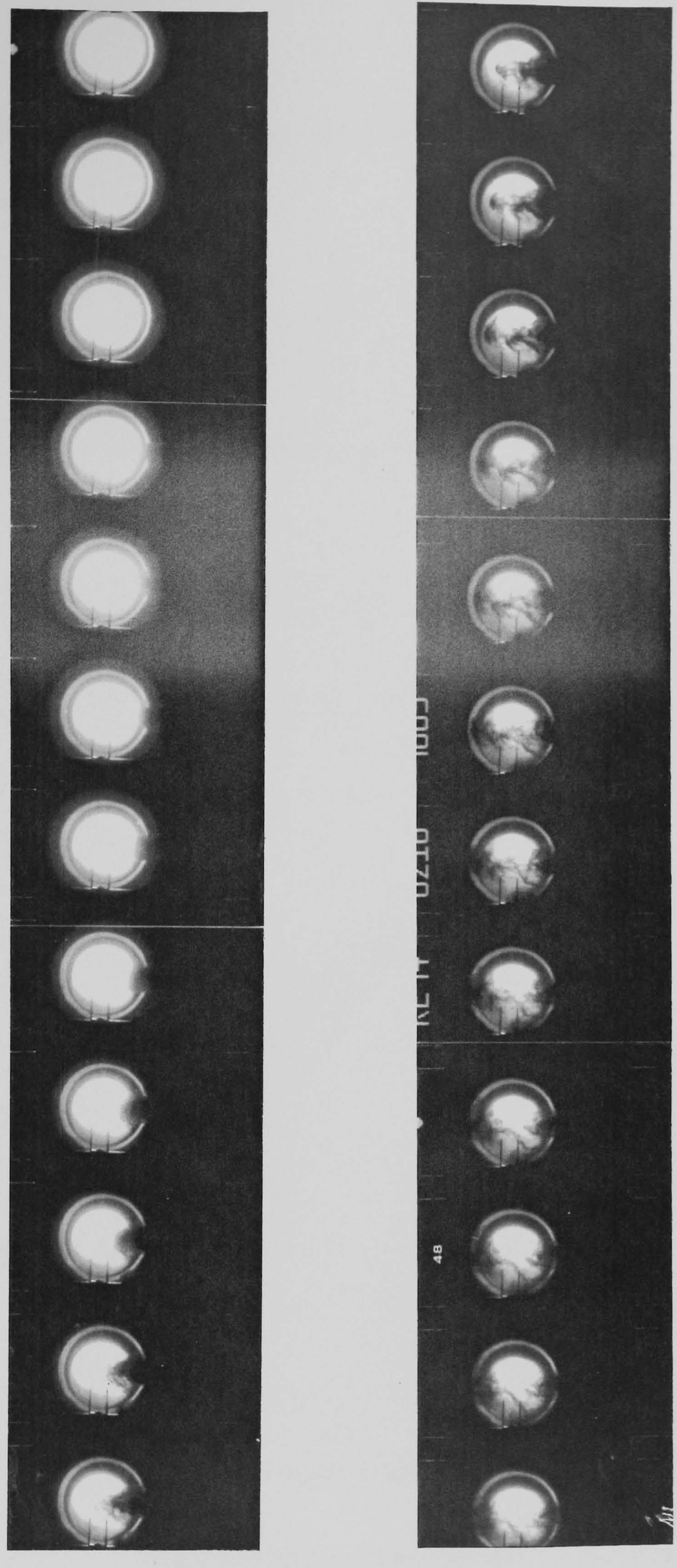

Fig. 5.9 Fuel injection spray obtained from the high speed camera test rig

Test conditions: Fuel sample: 15% water emulsified fuel;
P_{inj}: 180 bar;
P_g: 55 bar;
D_0: 0.37 mm;
Film speed: 6000 frames per second

penetration curves at 1.0 and 1.5 ms are much steeper than the curves at times above 3.0 ms (Fig. 5.8)

d). The emulsified fuel spray is wider, and its edge is blurred. The shape of the spray head is like a mushroom (Fig. 5.9).

e). After the spray breaks up, its head is less dense and more air is combined with the spray.

f). The injection line pressure has no significant change (Fig. 5.10).

The complete test results for spray penetration are presented in Appendix A.

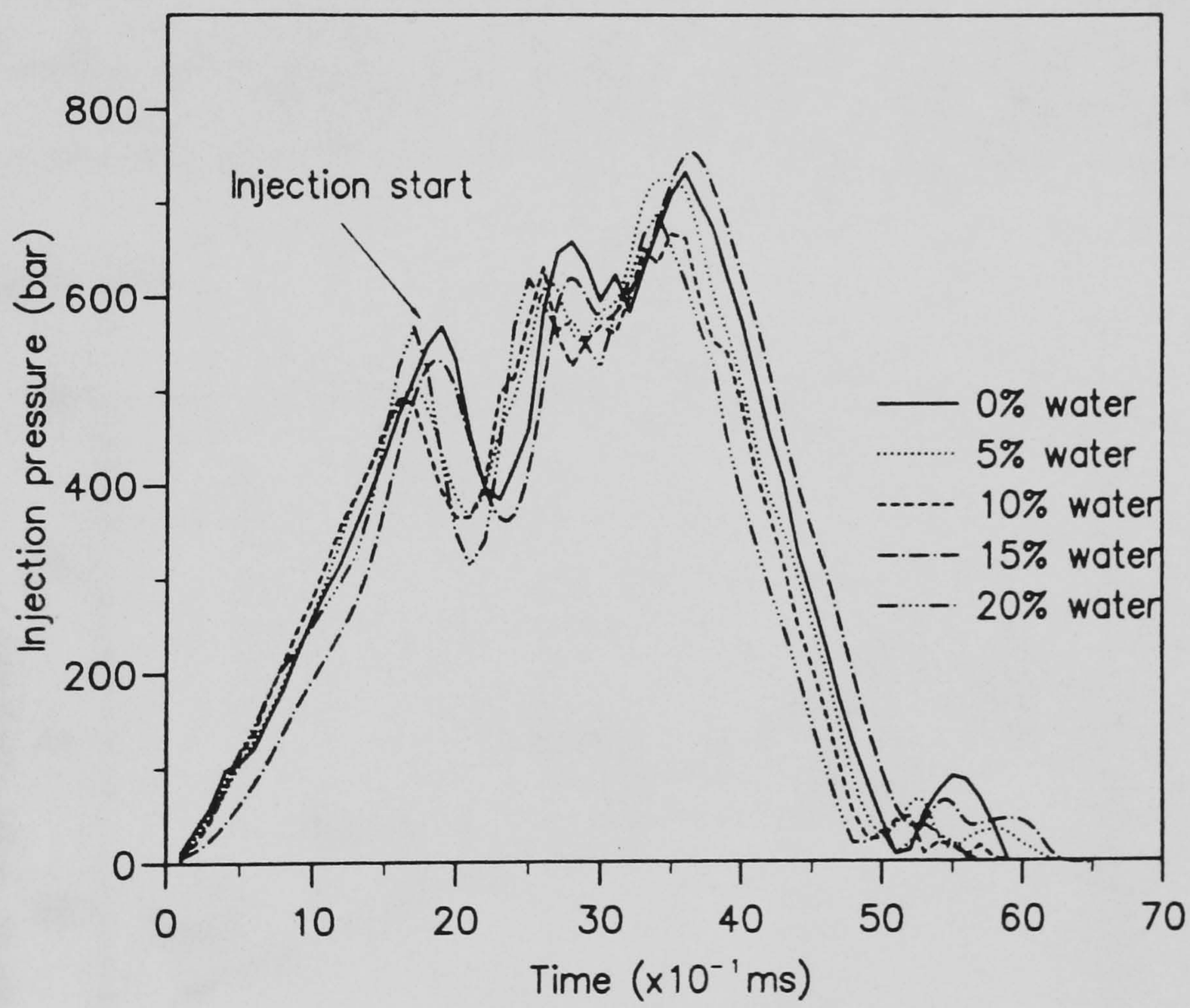

Fig. 5.10 Injection line pressure

5.3 Spray Angle Test Results

Table 5.5 shows the test results for spray angles. The test results indicate that spray angle increases with an increase in pressure drop at the front and back of the nozzle

hole, nozzle hole diameter and gas density. This is well understood and in agreement with the other reports [52]. The weighted order in which the parameters affect the spray angle is nozzle hole diameter, gas density, then injection pressure drop.

Fig. 5.11 shows the results for the addition of water on the spray angle.

Table 5.5 Test results on spray angles.

Test No.	1	2	3	4	5	6	7	8	9	10	11	12	13
P_{inj} (bar)	180	210	150	180	210	150	180	210	150	180	180	180	180
P_g (bar)	55	50	45	50	45	55	45	55	50	55	55	55	55
D_0 (mm)	0.37	0.35	0.39	0.39	0.37	0.35	0.35	0.39	0.37	0.37	0.37	0.37	0.37
γ (%)	0	0	0	5	5	5	10	10	10	15	20	5	10
θ°	21	20	24.5	26	21	22	20	24	21.5	24.5	25	22	23

* θ -- Spray angle.

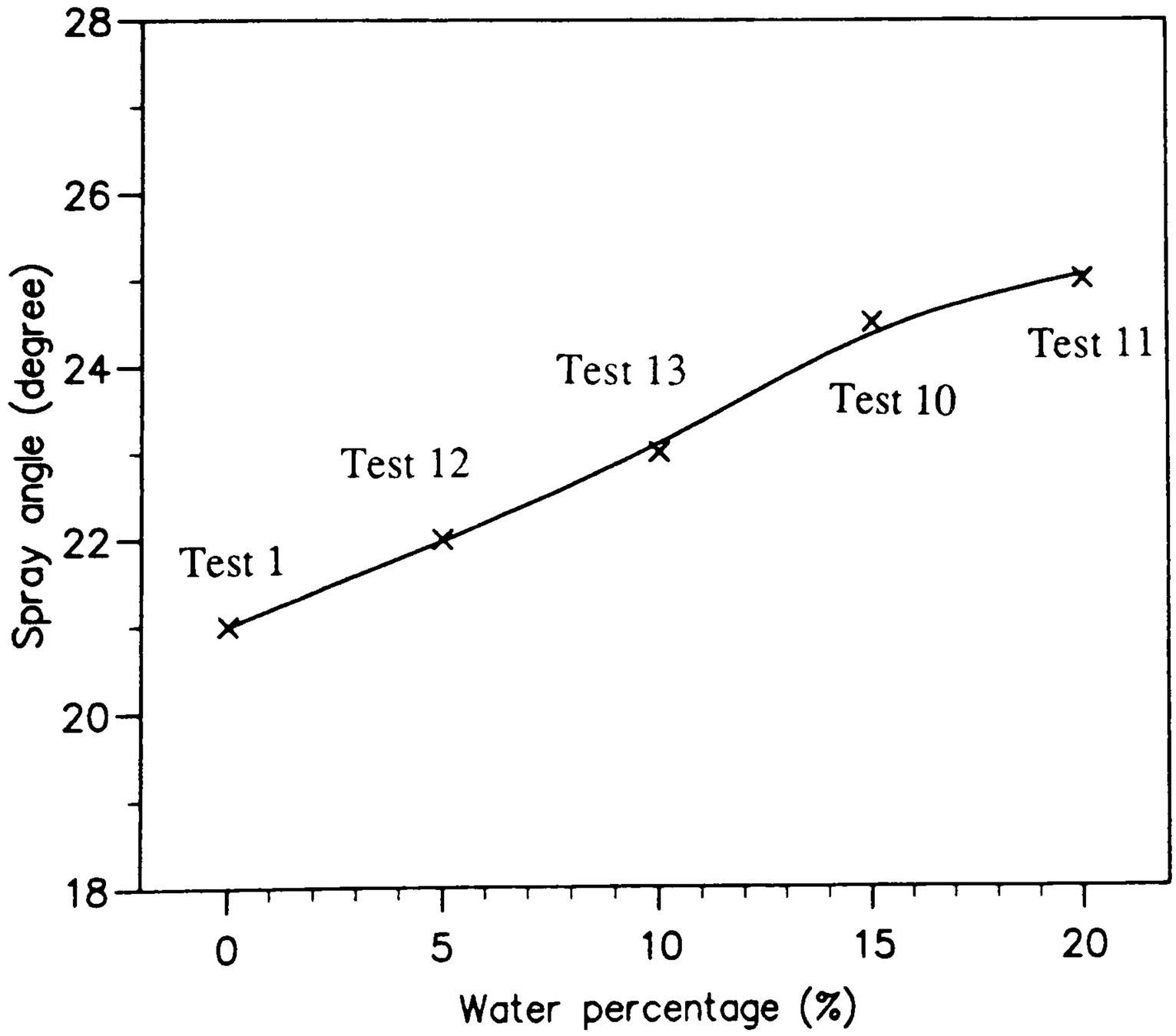

Fig. 5.11 Test results for spray angle.

5.4 Droplet Size And Distribution Test Results

5.4.1 Test Conditions And Instrumentation

In order to obtain an accurate measurement of droplets size, the image of moving droplets should be frozen on the films, i.e. the droplet edges must be distinct, no "comet tail" effects and so on. For this purpose, the following requirements must be satisfied:

a). The camera exposure time has to be extremely short.

b). The real injection field must be enlarged before its imaging on films.

c). The film resolution should be fine enough.

The short exposure time can be achieved by either increasing the film speed or changing the rotary shutter to one with a high shutter constant. Therefore, a shutter with a shutter constant of 40 was used in this test, the film speed being 4,000 frames per second. Thus, the exposure time was $T=1/4{,}000x40 = 6.25x10^{-3}$ ms. In this case, intensive illumination is required. Normal light sources cannot meet this requirement. A condenser lens was fixed on the illumination side of the bomb to concentrate the light beams to a spot upon which the camera was focussed. For enlarging the droplets, a micro-lens with an extension tube was used to achieve up to 1:1 images on the films. In this situation, the droplets could be seen clearly with about 40x film magnification. When the film is enlarged with a large magnification, the grains of film emulsion will appear on the screen if the film grains are not reasonably fine. From this point of view, the film chosen should be as fine as possible. In this test, the film with an ISO number of 68° was used (250° for photographing the whole spray). The light strength for illumination is inversely proportional to the film ISO number. That means the finer the film is, the higher the light strength is required. The use of the condenser lens solved the problems of short exposure time and low film ISO number at the same time.

In this test, the test conditions are mainly the same as the conditions for photographing the whole spray described previously. In addition to these, fuel injection amount is also considered. Therefore, five parameters are considered and each parameter has three test points (see table 5.6). Table 5.7 shows the test conditions orthogonal design table.

Table 5.6 Test conditions for picturing the droplets size

	$P_{inj}(\Delta P)$(bar)	D_0(mm)	$P_g(\rho_g)$(bar)	q(ml)	γ(%)
1	210	0.35	55	0.70	0
2	180	0.37	50	0.55	5
3	150	0.39	45	0.40	10

Table 5.7 The orthogonal design table of test conditions

No.	$P_{inj}(\Delta P)$ bar	$P_g(\rho_g)$ bar(kg/m^3)	D_0 mm	q ml	γ %
1	180(125)	55(62.5)	0.37	0.70	0
2	210(160)	50(56.8)	0.39	0.40	0
3	150(105)	45(51.1)	0.35	0.55	0
4	180(130)	50(56.8)	0.35	0.70	5
5	210(165)	45(51.1)	0.37	0.40	5
6	150(95)	55(62.5)	0.39	0.40	5
7	180(135)	45(51.1)	0.39	0.55	10
8	210(155)	55(62.5)	0.35	0.70	10
9	150(100)	50(56.8)	0.37	0.70	10
10	180(125)	55(62.5)	0.37	0.70	5
11	180(125)	55(62.5)	0.37	0.70	10
12	180(125)	55(62.5)	0.37	0.70	15
13	180(125)	55(62.5)	0.37	0.70	20

Other conditions associated with this test are:

1). Bomb temperature is 17.0 °C,

2). Injection frequency is 325 injs./min,

3). Film speed is 4,000 fps, and camera rotary shutter constant K=40,

4). Fuel dynamic viscosity is 2.975×10^{-3} Ns/m^2, and surface tension is 0.0293 N/m.

The time property of droplets size is not considered in this test. The justification for this is that since the fuel is injected into the "cold" bomb, the vaporisation of fuel droplets can be ignored. After the fuel is injected into the bomb, the droplets size is controlled by its velocity and gas density. The test results show that the effects of velocity and gas density on droplets size are not significant after the droplets have been formed. Normally, in order to obtain the spray droplets size, several points along the whole spray should be measured at the same time. However, it was impossible to do this when the high speed camera was used for this purpose. In any case, the objects imaged on the films are fields instead of points, and the area of the image field is about 63-88 mm^2.

The position where the camera focused on is shown in Fig. 5.12. The central point of the frame is 68mm from the nozzle and 17mm from the spray central line. The reasons for choosing this position are that, if the position is chosen too close to the spray central line or to the nozzle where the fuel spray is too dense and droplets are not yet being formed. If the position is selected far away from the central line or far down stream of the injection where only a few droplets can reach, that would not typify the spray atomisation characteristics. It is reasonable to assume that the spray is symmetrical about its central axis and that the droplets are of the same size in the area of a few millimetres from the position where the camera focuses on. In practice, the fuel ignition spots are within or close to this area. Therefore, the position chosen for picturing the fuel droplets can be considered as characteristic of the whole spray.

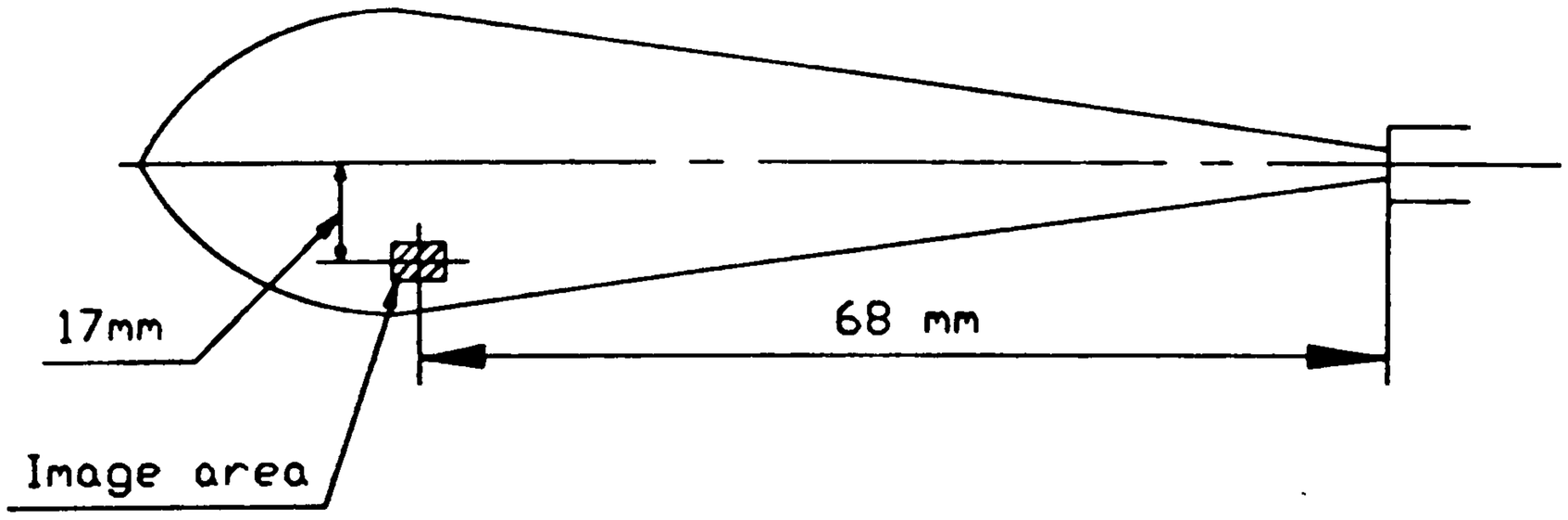

Fig 5.12 Position of shooting the droplets

It is evident that there are huge numbers of droplets in the space where the camera's optical path crosses the fuel spray. Theoretically, all of the droplets in this space should be presented on the films. However, when the micro-lens is used, especially with an extension tube the field depth is extremely short and only the droplets on the focal plane appearing on the films. In this test, the depth of the image field was less than 0.75 mm and the focal plane was set through the spray central line.

5.4.2 Droplets Size Measurement

The Image Analysis System (IAS) AMS OPTOMAX V was used for droplet measurement, which gives the output of individual droplet size or in the form of size ranges (classes). From the data obtained by IAS, the other parameters, such as droplet mean diameter, Sauter mean diameter, droplet size distribution, can be derived.

The data from the IAS can not be used directly to calculate the above parameters, since the droplet size given by the IAS is the droplet size on film. The actual droplets have been scaled down on film, and the reduction scale is unknown. Thus, a reference wire of 25 μm diameter was fixed inside the bomb for size calibration. Therefore, during the measurement of droplet size from film, the magnification factor was not considered. The final result is the measurement obtained from film times the calibration factor as shown in Table 5.8.

Table 5.8 One of droplet size data samples before and after the calibration.

Size classes(μm) Original Data	Size Classes(μm) After Calibration	Count	Count %
0.00 - 2.50	0.00 - 1.78	0	0
2.50 - 5.00	1.78 - 3.56	0	0
5.00 - 7.50	3.56 - 5.34	62	5.8
7.50 - 10.0	5.34 - 7.12	90	8.4
10.0 - 12.5	7.12 - 8.91	83	7.7
12.5 - 15.0	8.91 - 10.68	110	10.2
15.0 - 17.5	10.68 - 12.46	105	9.8
17.5 - 20.0	12.46 - 14.25	74	6.9
20.0 - 22.5	14.25 - 16.03	62	5.8
22.5 - 25.0	16.03 - 17.81	69	6.4
25.0 - 27.5	17.81 - 19.59	58	5.4
27.5 - 30.0	19.59 - 21.37	51	4.7
30.0 - 32.5	21.37 - 23.15	51	4.7
32.5 - 35.0	23.15 - 24.93	31	2.9
35.0 - 37.5	24.93 - 26.72	28	2.6
37.5 - 40.0	26.71 - 28.49	30	2.8
40.0 - 42.5	28.49 - 30.28	25	2.3
42.5 - 45.0	30.28 - 32.06	25	2.3
45.0 - 47.5	32.06 - 33.84	14	1.3
47.5 - 50.0	33.84 - 35.62	27	2.5
50.0 - 52.5	35.62 - 37.41	14	1.3

to be continued

cont. Table 5.8

52.5 - 55.0	37.41 - 39.18	9	0.8
55.0 - 57.5	42.75 - 40.97	15	1.4
57.5 - 60.0	40.97 - 42.75	8	0.7
60.0 - 62.5	42.75 - 44.53	7	0.7
62.5 - 65.0	44.53 - 46.31	7	0.7
65.0 - 67.5	46.31 - 48.09	2	0.2
67.5 - 70.0	48.09 - 49.87	4	0.4
70.0 - 72.5	49.87 - 51.65	3	0.3
72.5 - 75.0	51.65 - 53.44	1	0.1
75.0 - 77.5	53.44 - 55.21	1	0.1
77.5 - 80.0	55.21 - 56.99	2	0.2
80.0 - 82.5	56.99 - 58.78	1	0.1
82.5 - 85.0	58.78 - 60.56	2	0.2
85.0 - 87.5	60.56 - 62.34	1	0.1
87.5 - 90.0	62.34 - 64.12	0	0
90.0 - 92.5	64.12 - 65.91	1	0.1
92.5 - 95.0	65.91 - 67.68	0	0
95.0 - 97.5	67.68 - 69.46	0	0
97.5 - 100	69.46 - 71.24	0	0

* Other test data on droplet diameter are presented in Appendix B

Test conditions for the above table:

Injection pressure: 180 bar

Gas pressure: 55 bar

Gas density: 62.5 kg/m^3

Nozzle diameter: 0.37 mm

Water content: 10% by volume

Injection amount: 0.70 ml

At each test condition, only one frame was chosen for the measurement. On one frame, there were about 800 to 1100 countable droplets. This number was big enough to form statistical information for droplet size and distribution. It took about 3 hours to complete one frame's measurements by the IAS. In order to measure the droplets at the same times after injection, effort has been made to try to measure the frames which are at the same positions from the beginning of the injection under all test conditions.

5.4.3 Test Results

Fig. 5.13 gives two samples of prints showing fuel droplets and their distributions in fuel sprays. The analysis of experimental data on droplet size indicates that for pure fuel, the numbers of droplets at the two ends of the measurement range are bigger than those of the emulsified fuels as shown in Figs. 5.14(a-e). As water content increases the number of middle size droplets increases. So the droplet diameter size in emulsified fuel spray is "more" homogeneous. Equivalently, on the diagram of droplet distribution, the curve for pure fuel is higher than that of the emulsified fuels at the small droplet end (less than 20 μm). When the droplet diameter is bigger than 45 μm, it becomes high again. The middle part of the curve gets high as water content increases. The number of the emulsified fuel droplets becomes zero when droplet diameter is greater than about 55 μm, while for the pure fuel, this occurs at about 70 μm. This causes the mean droplet diameter of the pure fuel spray to be smaller, while its Sauter mean diameter is greater compared to emulsified fuels at the same test conditions.

Table 5.9 shows the test results on droplet diameters, alternatively, Fig. 5.15 illustrates graphically these results. The test results for droplet diameters indicate that the droplet mean diameter increases as the water contents increase, while the Sauter mean diameter decreases when water percentages increase.

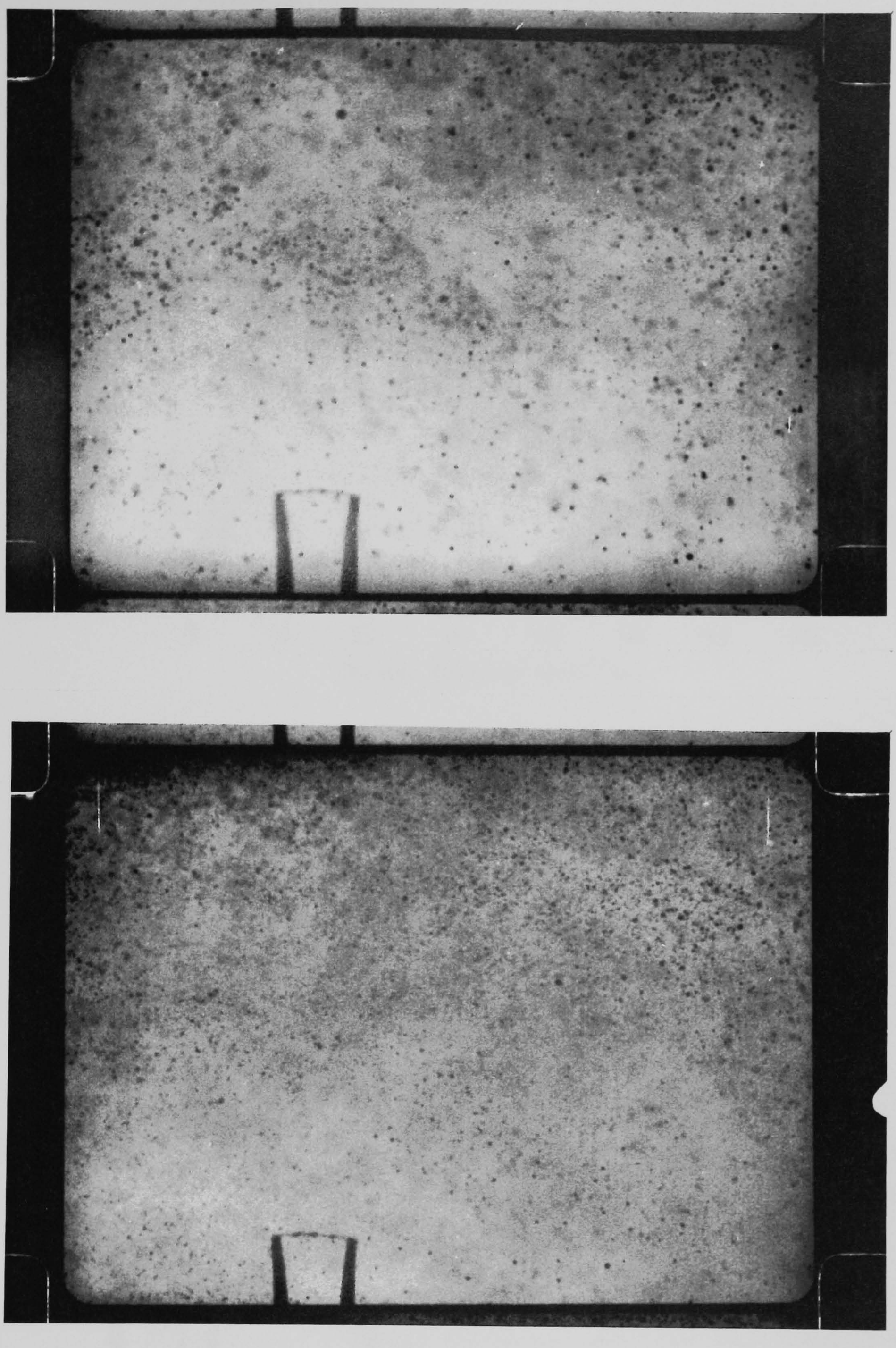

Fig. 5.13 Droplet spacing in two fuel types

Above: pure fuel; Bottom: emulsified fuel with 10% water.
Test conditions: P_{inj}= 180 bar; P_g= 55 bar; D_0= 0.37 mm; q= 0.70 ml.
Camera-- NAC-E10 16mm high speed camera; Lens-- TAMRON SP 90mm F/2.5 with an extension tube; Film-- Kodak Eastman 7231™ Plus-X Negative film; Exposure time-- 6.25×10^{-3} ms.

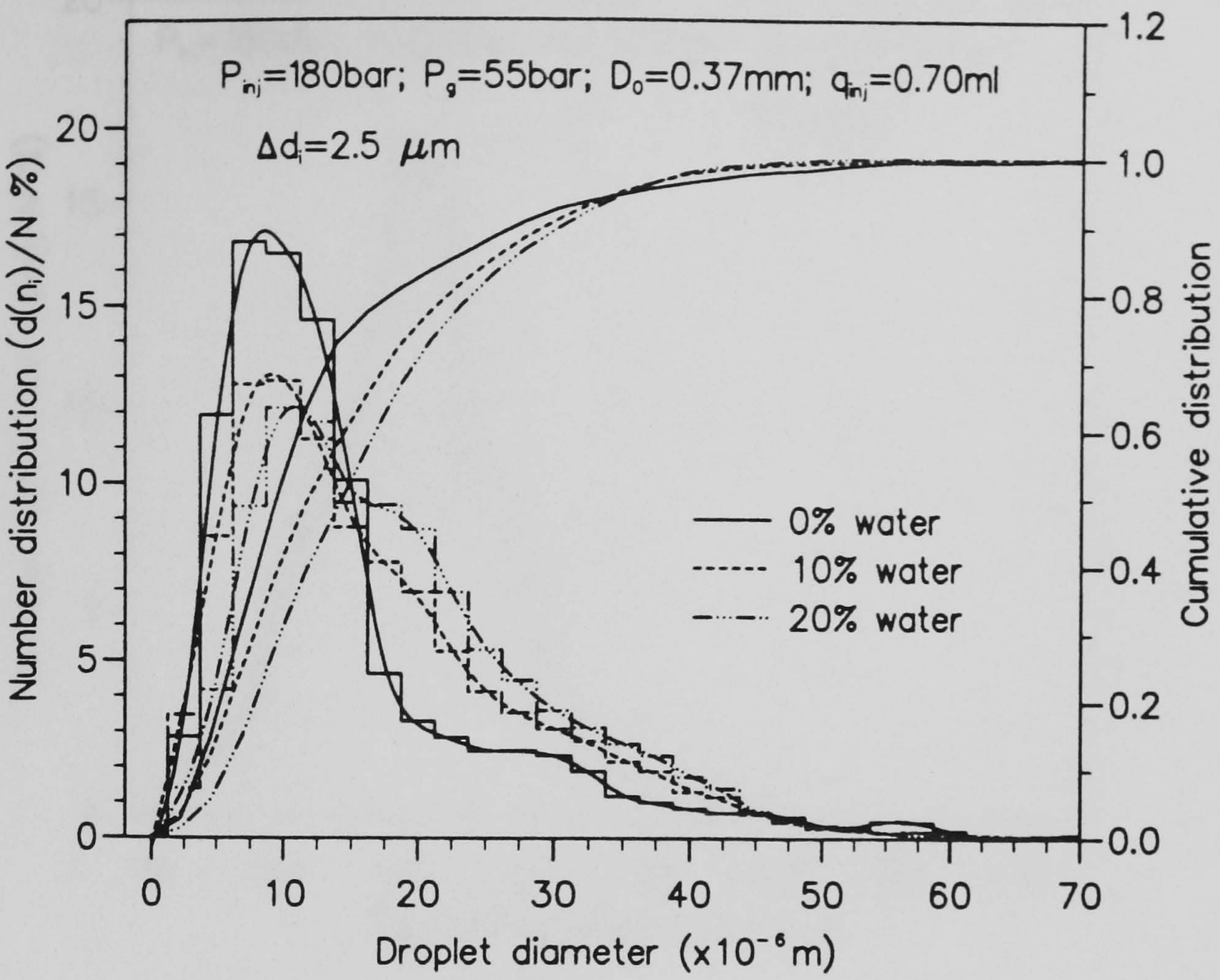

Fig. 5.14(a) Number distribution comparison of droplet diameter for three types of emulsified fuels

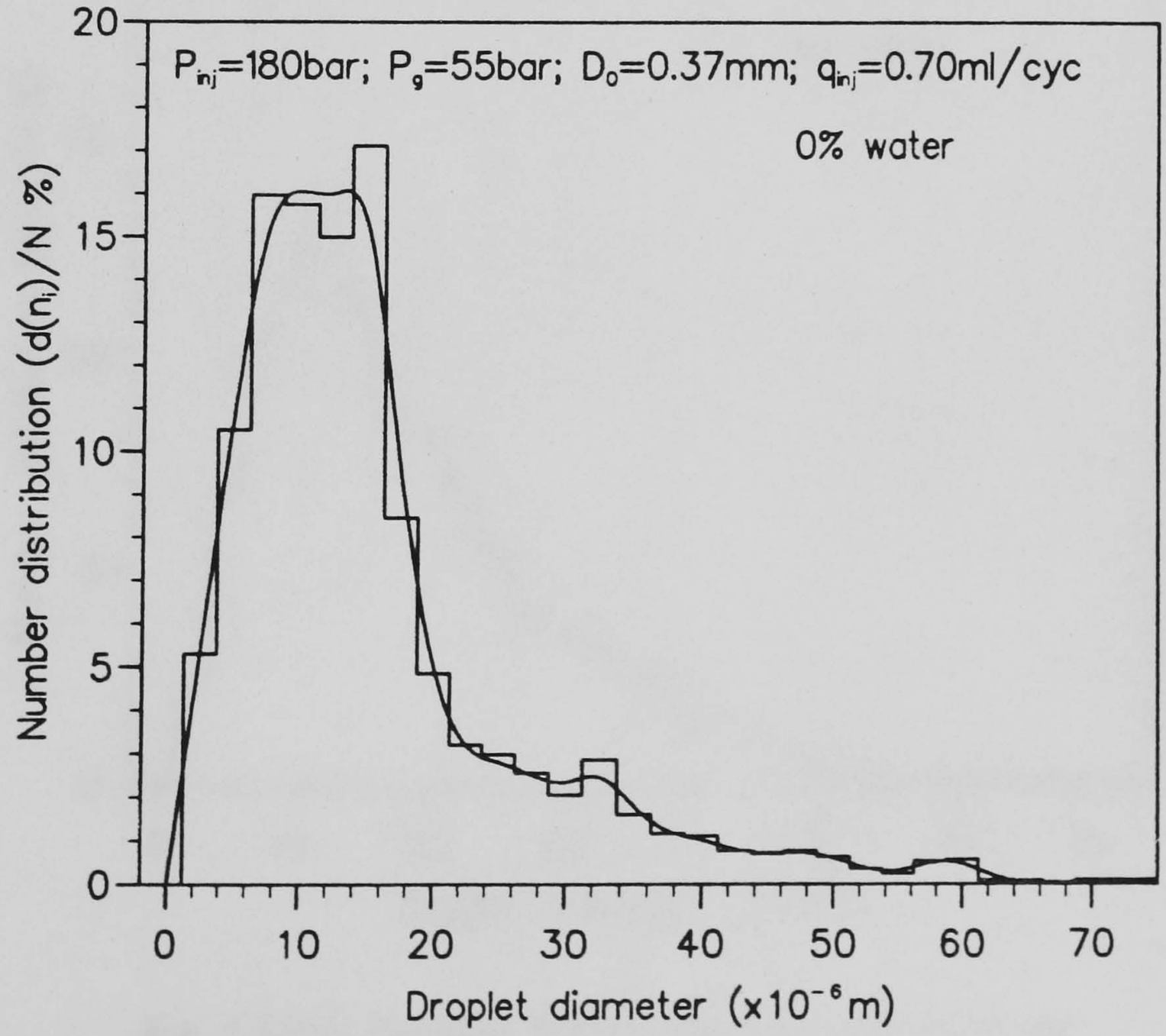

Fig. 5.14(b) Number distribution of droplet diameter for pure fuel

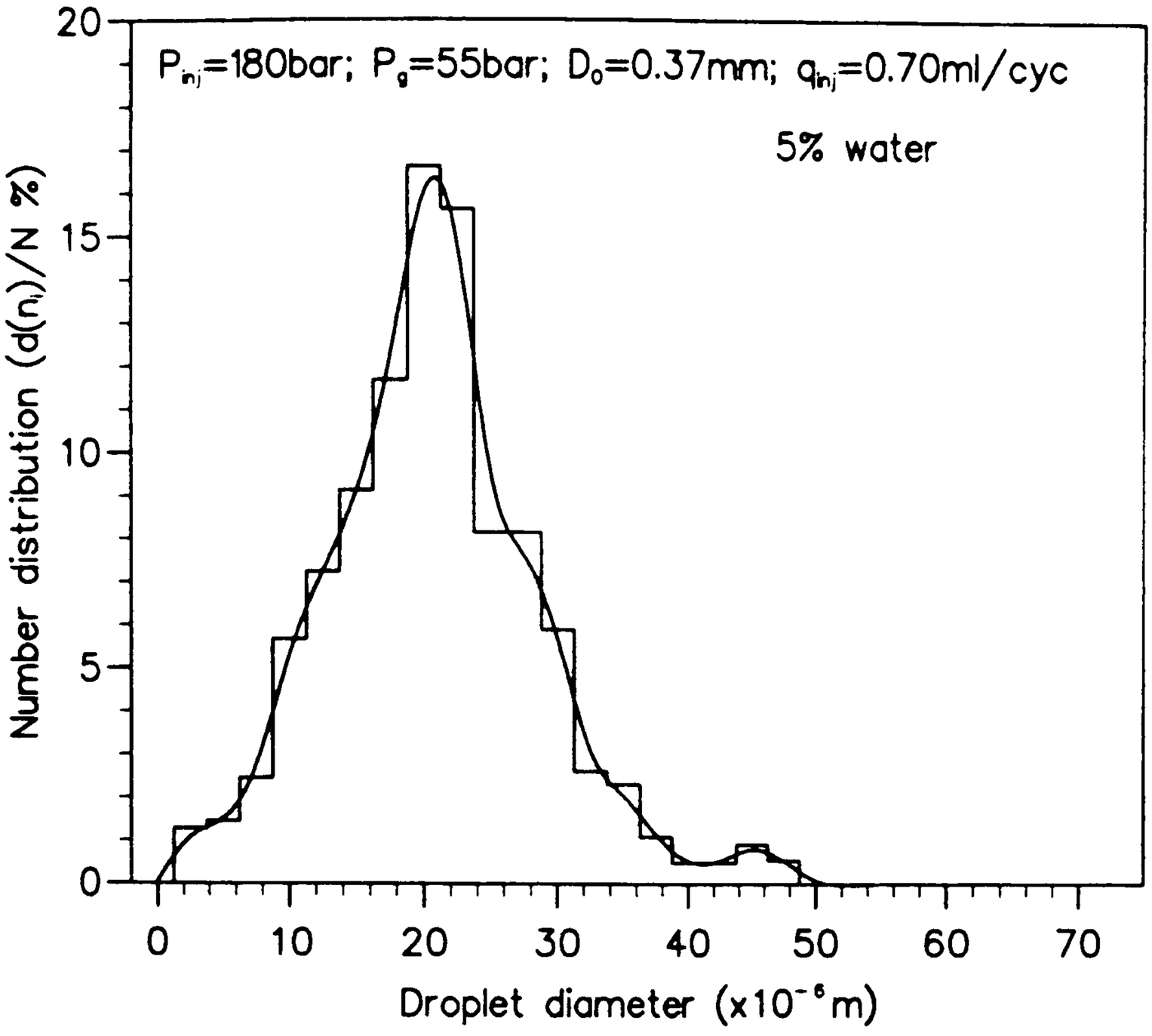

Fig. 5.14(c) Number distribution of droplet diameter

for 5% emulsified fuel

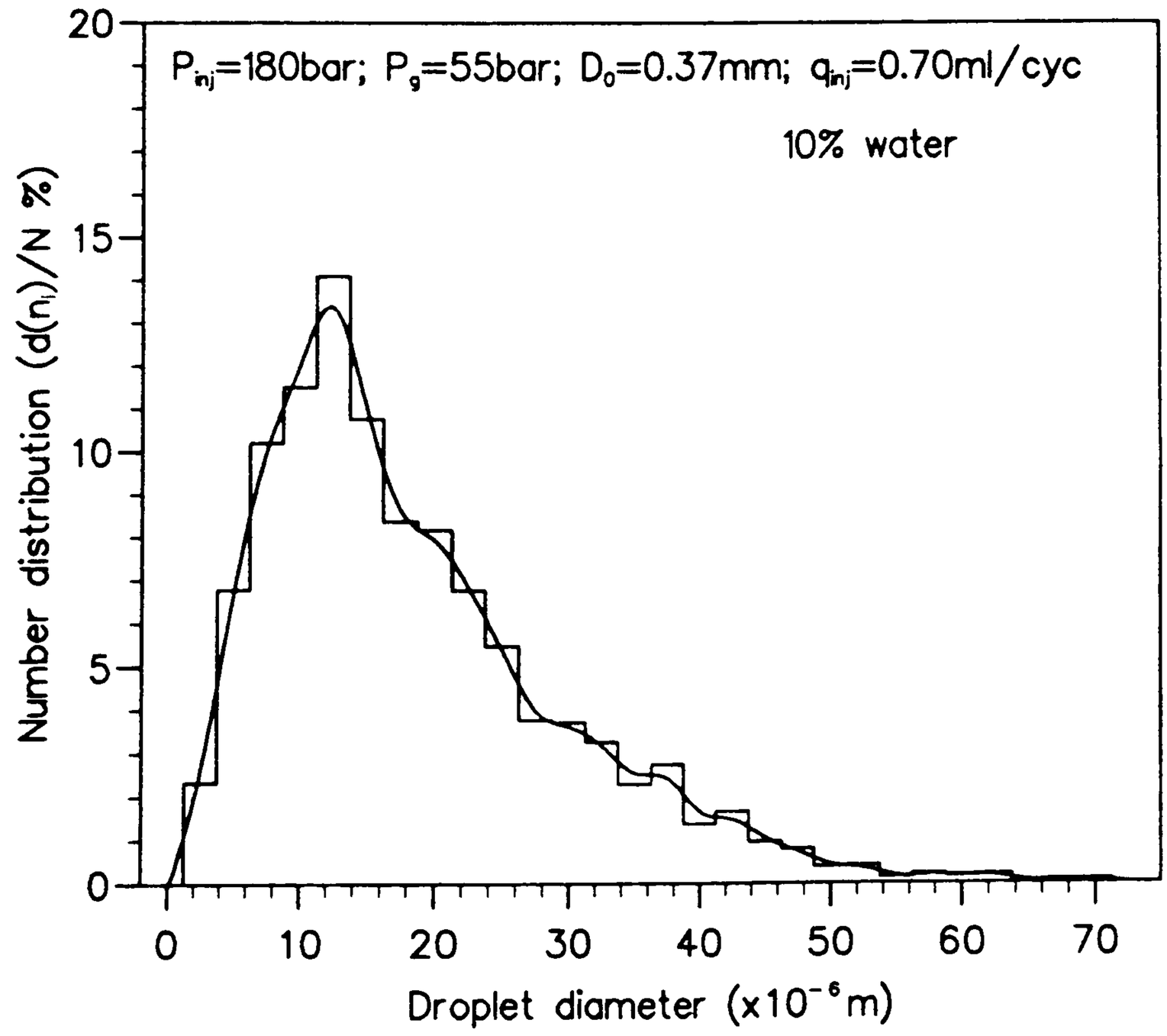

Fig. 5.14(d) Number distribution of droplet diameter

for 10% emulsified fuel

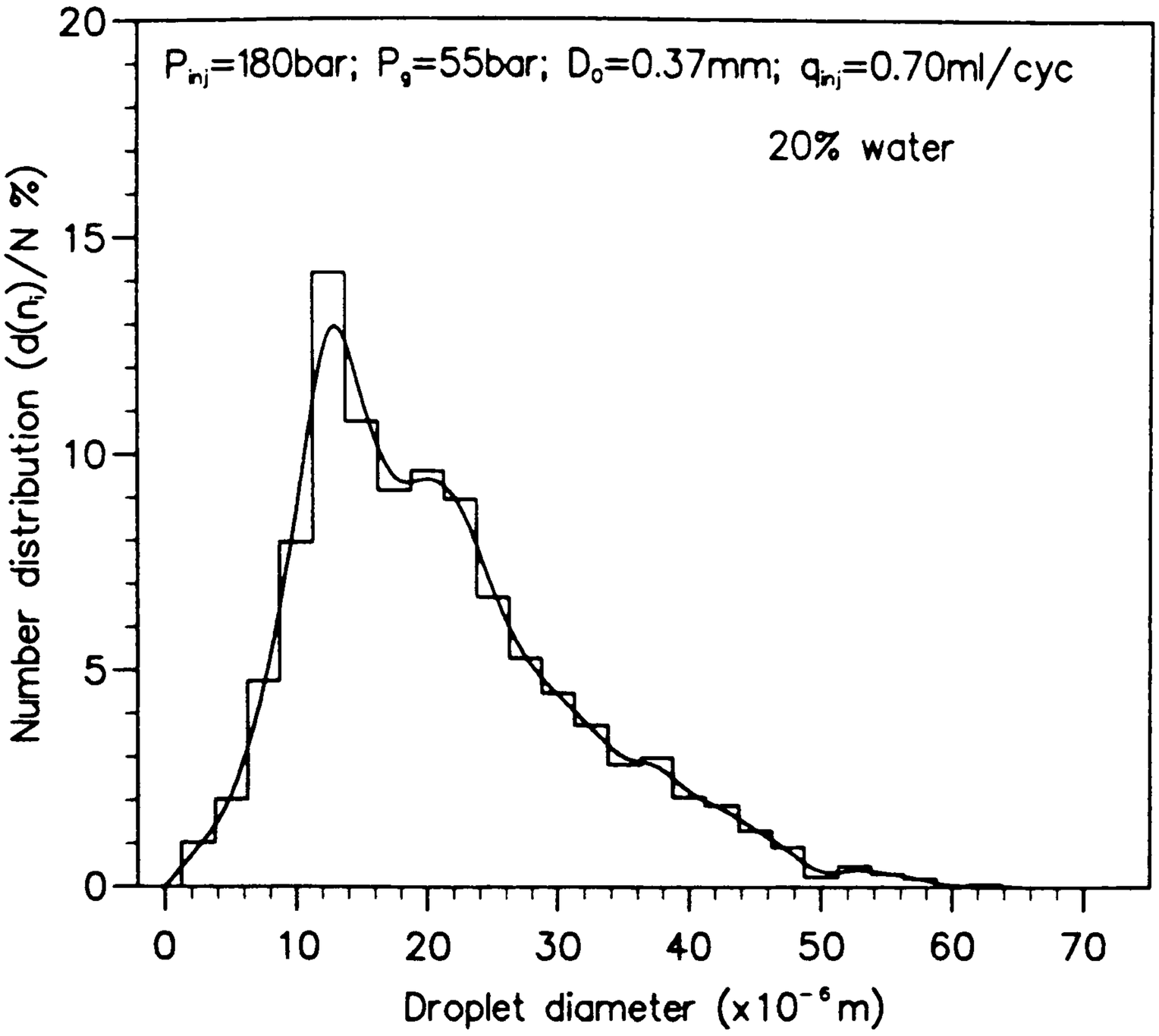

Fig. 5.14(e) Number distribution of droplet diameter for 20% emulsified fuel

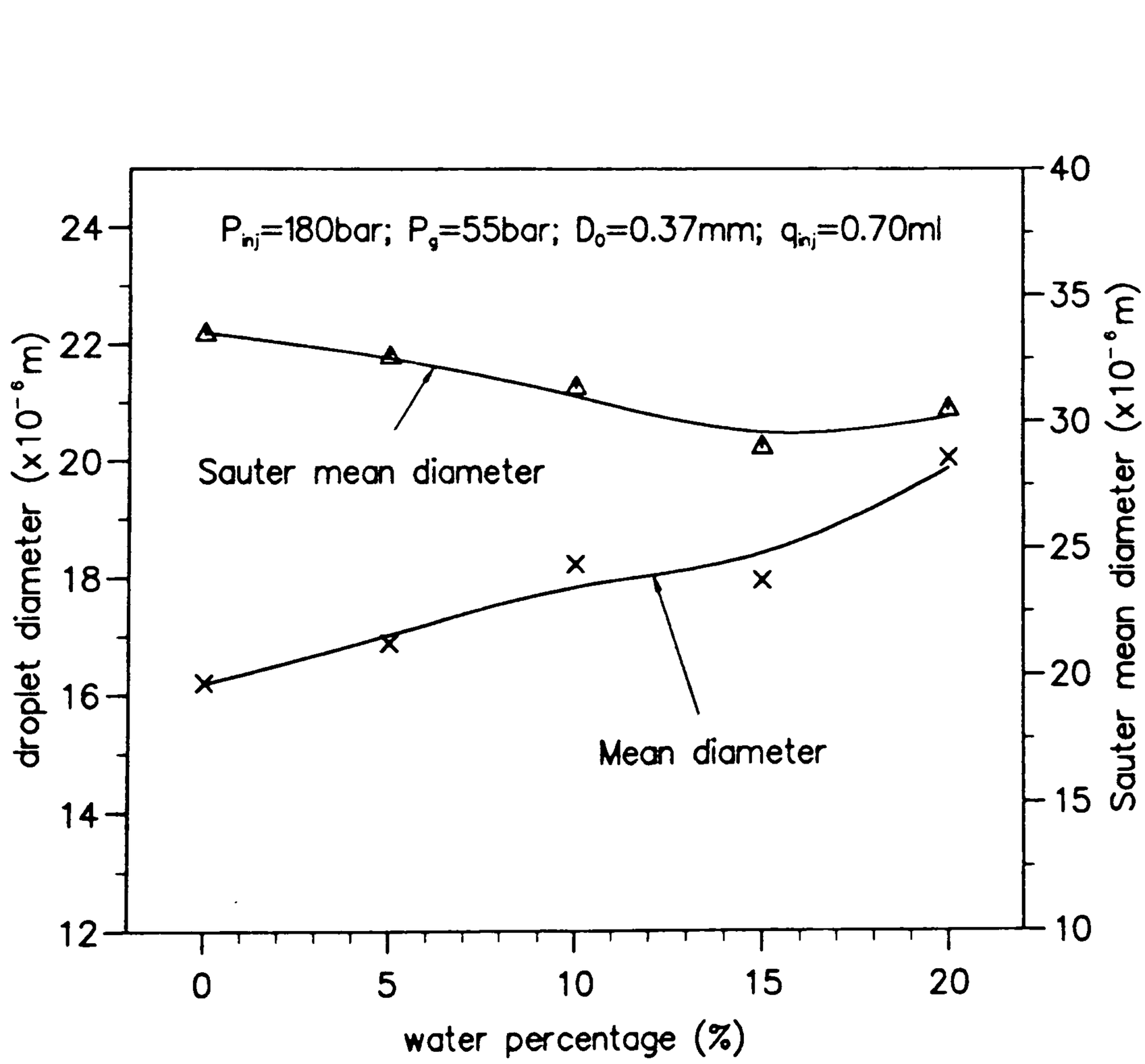

Fig. 5.15 Droplet diameters from test results

Table 5.9 Test results on droplet diameters

Test No.	P_{inj} (bar)	P_g (bar)	D_0 (mm)	γ (%)	q (ml)	D_{10}^{*}(μm)	D_{32} (μm)
1	180	55	0.37	0	0.70	16.04	33.90
2	210	50	0.39	0	0.40	15.45	25.65
3	150	45	0.35	0	0.55	15.66	23.77
4	180	50	0.35	5	0.55	17.35	24.40
5	210	45	0.37	5	0.70	17.67	27.89
6	150	55	0.39	5	0.40	19.10	25.57
7	180	45	0.39	10	0.40	21.46	31.74
8	210	55	0.35	10	0.55	16.07	23.38
9	150	50	0.37	10	0.70	18.19	27.79
10	180	55	0.37	15	0.70	16.80	24.87
11	180	55	0.37	20	0.70	17.51	31.03
12	180	55	0.37	5	0.70	15.16	29.32
13	180	55	0.37	10	0.70	19.34	29.03

* D_{10} -- Mean droplet diameter,

D_{32} -- The Sauter mean diameter.

5.5 Test Results Discussion

5.5.1 Spray Penetration And Angle Discussion

The test results obtained for spray penetration indicate that the emulsified fuel possesses a higher velocity, at the beginning of injection. This is in agreement with the theoretical discussion in chapter 2 which stated that the emulsified fuel will have a high injection efficiency and high momentum.

As mentioned above, the resistance of spray progress for emulsified fuel increases as fuel viscosity increases since $C_f \propto \nu^{1/2}$. However, at the beginning of injection, the spray is quite dense and the contact surface of the fuel to the air is relatively small. Thus the resistance effect is not significant. In other words, during this period the increment of resistance due to the increase in viscosity is less significant than the increment of penetrating energy obtained by the spray. Because there is

no atomization at the beginning of injection, the spray can be considered as a liquid jet, its volume flow rate is proportional to the jet velocity (assuming that the discharge efficiencies of the nozzle are the same for pure fuel and emulsified fuels). Therefore, the higher velocity implies that the amount of emulsified fuel injected into the combustion chamber during this period is more than that of the pure fuel. As the spray develops further, it begins to break up and the contact surface of the fuel to air becomes large. The resistance (friction) effect dominates the penetration event and the increment of spray penetration gets smaller compared with the pure fuel. The increase in friction force between fuel and gas also causes an increase in turbulence strength at the surface of the spray, results in more gas being involved in the fuel spray. This makes the head of the spray wider (a mushroom shape) and less dense than that of pure fuel (see Fig. 5.9). These phenomena are favourable in the formation of fuel/air mixture and improves the engine combustion processes (see section 5.6.1).

5.5.2 Droplet Size And Its Distribution Discussion

The test results related to droplet size obtained on the high speed test rig are basically in agreement with the results obtained in the fundamental study of atomisation. The reduction in large diameter droplets in emulsified fuel spray confirms the discussion in 2.3.4.

As discussed in section 2.3.4, during the fuel atomisation process and after the individual fuel droplets are formed, the large droplets will break down again at high shear rates. In the meantime, for an emulsified fuel droplet, the existence of water can promote this break-up process. Because of the reduction in large diameter droplets, emulsified fuel sprays possess a small Sauter mean diameter, which implies emulsified fuel sprays have a large total surface area. This is very important for improving engine combustion.

In Fig. 5.14(a) at the small diameter droplets end, the curve for the pure fuel is very steep. This is because the tests were carried out in the "cold bomb", and there was no vaporisation of the fuel droplets. If the test were carried out in a "hot bomb", the situation would be changed, since some of the small droplets would vaporise immediately. The droplets distribution curves would be smoother.

5.6 Emulsified Fuel Combustion And Emissions

5.6.1 Emulsified Fuel Combustion

To discuss the effects of emulsified fuel on the combustion processes, it is necessary here to briefly mention the diesel engine combustion processes.

The overall compression-ignition diesel combustion process can be defined as follows and it is identified on the typical heat-release rate diagram for a direct injection (DI) engine shown in Fig. 5.16 [70].

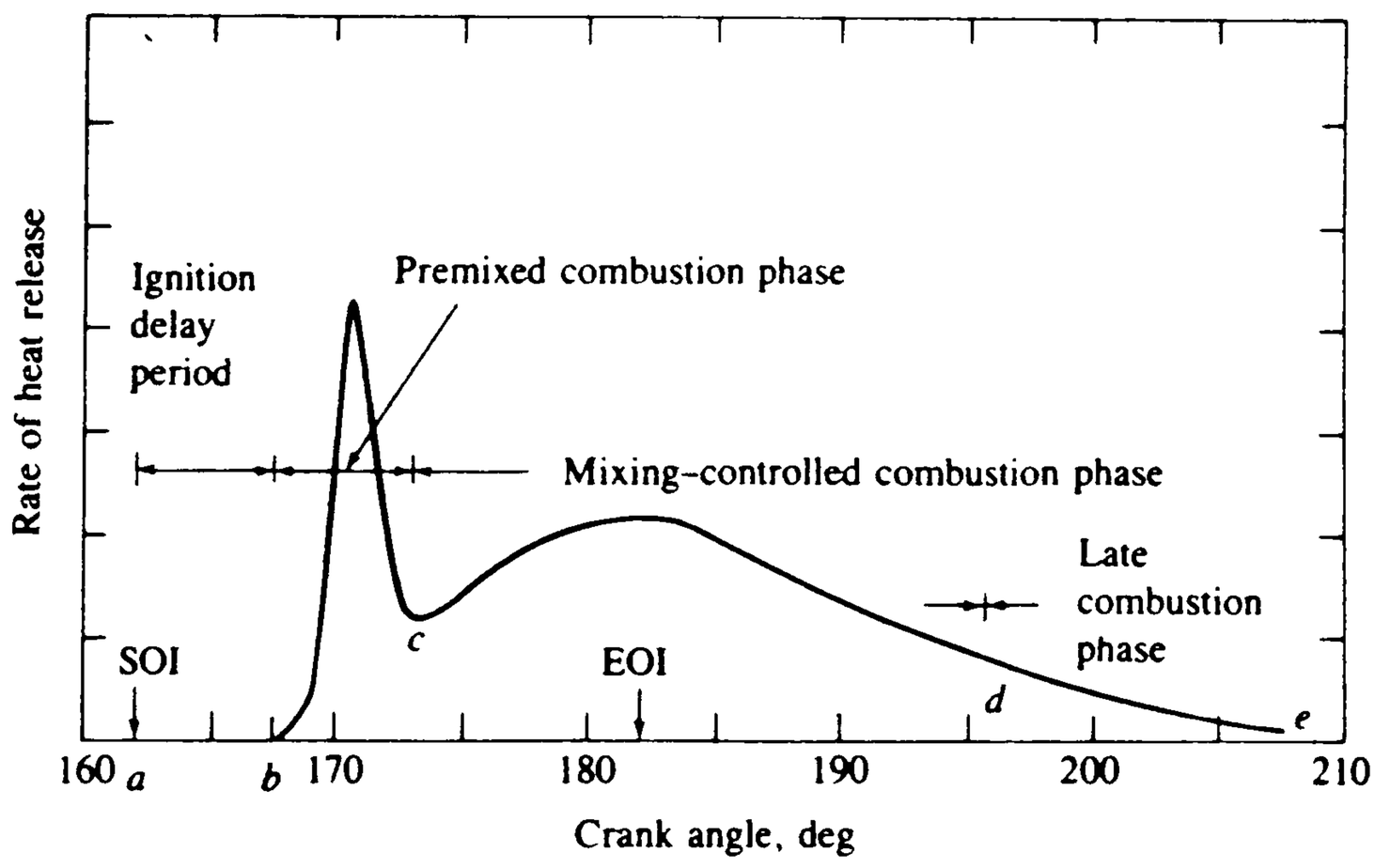

Fig. 5.16 Typical DI engine heat-release-rate diagram identifying diesel combustion phases.

1). Ignition delay (ab) The period between the start of fuel injection into the combustion chamber and the start of combustion.

2). Premixed or rapid combustion phase (bc) In this phase, combustion of the fuel which has mixed with air to within the flammability limits during the ignition delay period occurs rapidly in a few crank angle degrees. When this mixture is added to the fuel which becomes ready for burning and burns during this phase, the high heat-release rates are characteristic of this phase result.

3). Mixing-controlled combustion phase (cd) Once the fuel and air which premixed during the ignition delay have been consumed, the burning rate is controlled by the rate at which the mixture becomes available for burning, i.e. the fuel vapour-air mixing process. The heat-release rate may or may not reach a second (usually lower) peak in this phase; it decreases as this phase proceeds.

4) Late combustion phase (de) Heat release continues at a lower rate well into the expansion stroke. The kinetics of final burn out processes become slower as the temperature of the cylinder gases fall during expansion.

In order to increase the engine thermal efficiency, it is preferred that the combustion processes are arranged near the T.D.C. and finish as soon as possible. To this end, in relation to the diagram of heat-release rate vs crank angle degree, efforts have been made to increase the height of the first peak of the heat release curve, and to move the centre of gravity of the diagram toward the T.D.C. .

As discussed above, the amount of emulsified fuel at the beginning of injection is more than that of pure fuel. Both physical and chemical reactions for fuel ignition will take longer. These two factors (more fuel and long ignition delay) lead to an increase of fuel/air mixture amount ready for combustion which further results in an increased heat release ratio at the beginning of the combustion which is useful for shortening the combustion period.

In reference [8], a quantitative description of the air increase in fuel spray subsequent to combustion has been given as follows:

$$\lambda = \frac{G_a \cdot (1+\gamma)}{L_{th} \cdot G_f}$$

Where:

λ - the excess air for emulsified fuel atomising,

G_a,G_f - weight of air and fuel in atomisation,

L_{th} - quantity of theoretical combustion air per unit fuel,

γ - ratio of additional water to fuel oil.

Therefore, it is possible to consider that the air quantity which is supplied for the atomisation within a fixed time is increased as much as the water content γ corresponding to the same quantity of fuel. As a result, the inflammable mixture quantity is increased and thus high combustion rates can be achieved.

To briefly summarise the above discussion, a better air utilization in the combustion chamber can be achieved when emulsified fuels are used as they are characterised by a longer, wider spray and more air is involved in the spray atomisation. There will therefore be a good fuel-air mixing and an improved combustion process. Besides, the large relative surface area of spray will also speed up the combustion process. These are the main reasons why the combustion processes of emulsified fuel are faster and more complete than with pure fuel and this helps in the reduction of engine emissions.

The above results are generally in agreement with Dr. Sheng's test results [13]. But in Dr. Sheng's report, the phenomenon of combustion finishing early was explained by the effect of micro-explosions. All the other reports concerned with the utilization of the emulsified fuel on diesel engines stated that the maximum cylinder pressure increases as the water water increases. Although the pressure increases, the

temperature does not increase due to the vaporization of water which absorbs the heat in the combustion chamber and also due to the increased air involved in the combustion processes.

In Dr. Sheng's report [13], it is said that "the flame region of the emulsified fuel is larger than pure fuel, the angle of the flame region is also much larger, the edge of the emulsion flame is vague and irregular. This phenomenon can be regarded as the macro effect of the micro-explosions. Inside the flame region, many burning lumps can be seen, but they are different from the case of the pure fuel flame".

There are now other explanations for Dr. Sheng's observations. The phenomenon of emulsified fuel possessing a larger flame region and angle is attributed to the characteristics of a larger spray angle. Since the edge of the emulsified fuel spray is blurred and irregular, its flame edge is unclear and irregular. More air is involved into the spray, so there are many burning "lumps" inside the flame region.

The high maximum combustion pressure and the complete and rapid combustion permit the increase in engine thermal efficiency. Apart from this, the presence of water yields more expansive work in the power stroke per unit fuel used. In a sense, the water permits the engine to act in part like a steam engine. The low combustion temperature can also reduce cylinder wall losses. The net result is improved engine efficiency.

When engines run at part load, both injection pressure and gas density decrease. The injection energy is reduced and spray penetration becomes short and spray angle is small. The air in the areas far from the nozzle and between the sprays is not sufficiently utilised. It is evident that emulsified fuel will improve this situation. This gives a good explanation why most of the reports show that the benefits of using emulsified fuel on diesel engines are more significant when the engines run at low loads.

The summary of the above discussion provides the fundamentals or theory for the improvements of diesel engine combustion by using emulsified fuels, which explains the results/observations obtained by previous researchers in this field.

5.6.2 Engine Emissions

5.6.2.1 Diesel Engine Emissions [70,71]

Internal combustion engines are a major source of urban air pollution. The main harmful/pollutant emissions from the internal combustion engine are oxides of nitrogen (NO_x), unburnt or partially burnt hydrocarbons (HC), carbon monoxide (CO) and particles (primary soot with some additional absorbed hydrocarbon material,).

The general mechanisms of formation for these pollutants in diesel engines can be summarized as follows:

1). NO_x is formed when the temperature is very high in the presence of air, mainly during the rapid combustion period. Therefore an increase in the quantity of fuel injected during the ignition delay period increases the maximum temperature and hence the NO_x formation.

Main sources: rich fuel areas.

2). HC is mainly due to fuel which is unburnt because of insufficient temperature. This is the case with fuel near the walls of the combustion chamber ('wall quenching') and with fuel not yet burnt at the end of combustion because of lack in pressure and temperature ('bulk quenching').

Main sources: spray edge (weak fuel areas), large injector sac volume, cold walls and late injection.

(Note that other researchers believe that the leaking of fuel from the injector SAC does not occur in practice)

3). CO is formed when there is a lack of oxygen during combustion, either near full load, or sometimes also at low loads when there is poor mixing of fuel with air.

Main sources: rich fuel areas, too large fuel droplets, insufficient swirl, etc..

4). Soot formation is complex and not fully understood. Soot formed during combustion will be largely governed by local oxygen availability and temperature late in the combustion process. Absorption of hydrocarbons occurs during the whole expansion stroke and continuing in the exhaust system. Particulates are sometimes formed from oil molecules.

Main sources: cold starting, idling and possible low load with low compression ratio engines, oil leaking into combustion chamber.

5.6.2.2 Diesel Engine Emissions Control

As the requirements for environmental protection increase, the emissions regulations for I. C. Engines become more and more strict. At the present time, the new emissions regulations for 1994 in USA and 1996 in Europe [72] have been established. The emphasis on engine emissions has been greatly increased and much research has been done in this field already. Currently, the efforts have been concentrated on the optimization of fuel injection systems and combustion [72,73,74].

Methods for reducing nitric oxides (NOx):

The conventional methods for reducing NO_x are normally contrary to the methods for reducing other emissions. Fig. 5.17 illustrates the conventional methods for reducing engine NO_x emissions.

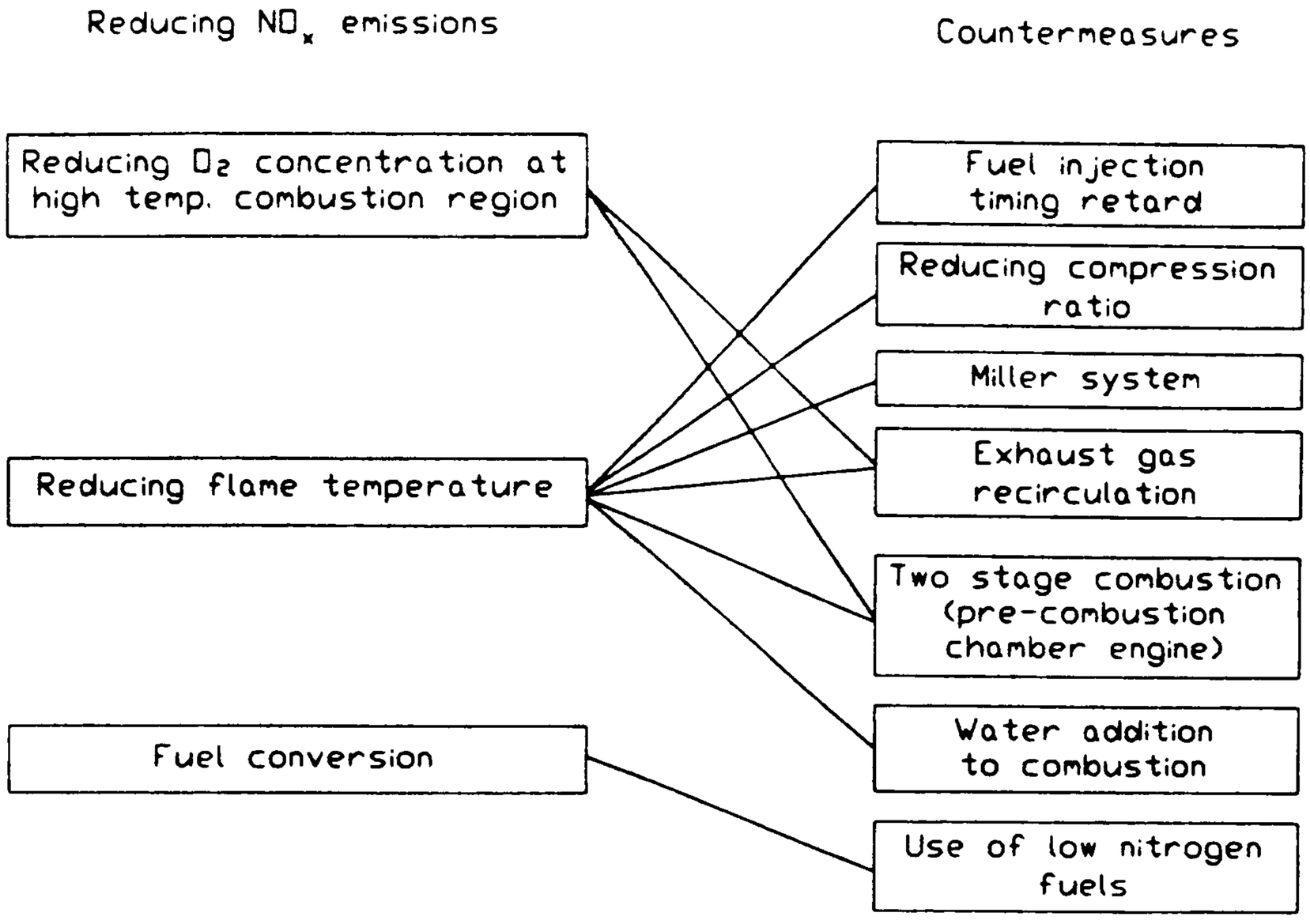

Fig 5.17 Conventional methods for reducing engine NO_x emissions

1). Fuel injection timing retard

It is possible to reduce the explosion temperature and pressure by fuel injection time retard, hence to reduce the formation of NO_x. But the fuel injection delay makes combustion worse, fuel consumption increases as does the formation of black smoke.

2). Reducing compression ratio

A reduction in compression ratio results in low combustion temperature and pressure. However, engine starting and thermal efficiency get worse.

3). Miller system

In the Miller system, the intake valves or ports are closed a little before bottom dead centre (BDC), the charged air expanding as the piston goes toward BDC. Basically, this produces the same effects as a low compression ratio.

4). Exhaust gas recirculation

In this method, a part of the exhaust gas is recirculated and it is mixed with the intake air in order to reduce the flame temperature hence to reduce the formation of NO_x. However, this cannot be used for the engines operated by heavy fuel due to its dirty exhaust gas. The air charging system can be choked, and sulphuric acid corrosion in air cooling systems and intake valves may occur.

5). Two stage combustion (pre-combustion chamber system)

In this system, injected fuel is first ignited and burnt in a pre-combustion chamber with insufficient air, and then the fuel/partially burnt fuel is burnt in the main chamber with sufficient air. This system has been employed for gasoline engines and small diesel engines, and has brought good results for the reduction of NO_x. This system is cannot be used in engines with large cylinder diameter due to the high thermal load on combustion chamber and walls. The maximum cylinder diameter of the pre-combustion chamber in practical use is about 250 mm.

6). Water addition into combustion

Discussion will be presented later.

7). Fuel conversion

The emissions of NO_x from a diesel engine consist of two parts. One is so-called 'Fuel NO_x', another is so-called 'Thermal NO_x'. The former is due to the nitrogen component of fuel itself. The latter is caused by the high combustion temperature. It is known that heavy oil contains more nitrogen than diesel fuels and produces

more NO_x. However this only contributes to about 10% of the total NO_x emissions. Therefore, to change from heavy oil to diesel fuel is not very effective for reducing NO_x.

The methods mentioned above for reducing the oxides of nitrogen suffer from the loss of thermal efficiency and possible increases in other harmful emissions. Out of these methods, it is understood that the fuel injection retard and emulsified fuels are the most effective way to restrain the formation of NO_x.

Methods for reducing HC, CO and particulates:

The most common methods used for decreasing the emissions of HC, CO and particulates are exhaust treatment devices and exhaust gas recirculation. These methods influence engine combustion, and result in an increase in fuel consumption.

There is a clear preference to achieve low emissions by improvements to the fuel combustion and injection system, without losing any of the diesel engine fuel consumption advantages, rather than by the use of exhaust recycle and after treatment devices. For this purpose, both the fuel injection equipments and combustion processes of the engines have to be re-optimised. Recently, the research having been undertaken toward this end is concentrated on the following areas: 1). using a small hole diameter nozzle with high fuel injection pressure [72]; 2). utilizing the electronic unit injector (EUI) with a by-pass valve [73]; 3). reducing injector sac volume [74].

The mechanisms of the above measures for reducing harmful emissions are discussed as follows:

1). The use of a small hole diameter with high injection pressure provides a fine fuel atomisation. Generally speaking, the fine fuel atomisation leads to better air utilisation, improved combustion and therefore leads to a reduction in HC,

CO, NO_x and unburnt hydrocarbon particulates (soots). The small hole diameter results in a longer injection period, which lowers the combustion temperature hence minimising NO_x formation.

2). For the conventional injector, the injection fuel is shut off by the spring loaded needle valve. At the end of injection, the injection line pressure is relatively low. The fuel injected into the combustion chamber during this period cannot be well atomised. Also the air available for this portion of fuel combustion is insufficient. This is one of the main sources for HC, CO and soots formation.

In the EUI system, the injection fuel is cut off by a solenoid operated needle valve, and the remaining pressure in the pressure line is released by a by-pass valve. This overcomes the problems of late injection experienced with conventional injectors and greatly reduces the emissions of HC, CO and soots.

3). The fuel trapped in the sac volume after injection will drop into the combustion chamber. Its combustion conditions are worse than those for late injected fuel, and it may even be exhausted in an unburnt state. Therefore, the reduction of sac volume directly minimises the unburnt hydrocarbon emissions. At present, a zero sac volume nozzle has been developed, and will be available to the market soon [74].

To summarise the above discussion, the improvements or optimization of fuel injection systems and combustion can minimise all the engine emissions without losing engine thermal efficiency. In particular, they are more effective in reducing the formations of HC, CO and particles.

5.6.2.3 The Reduction Of Harmful Engine Emissions By The Addition Of Water Into Combustion Process

The addition of water into the combustion process is very effective in reducing NO_x formation. There are two ways to do this: 1). injecting water directly into

the engine intake pipes or the combustion chamber; 2). mixing the water with fuel oil with an emulsifier, and then injecting the emulsified fuel into the combustion chamber at a high pressure.

For the direct injection of water into the combustion chamber, the water is injected during the fuel combustion period. The reduction of NO_x is very significant since the vaporisation of this water lowers the combustion temperature. However, the fuel combustion becomes worse as water content increases. Also there is a question about the durability of the high pressure water injection system.

The use of emulsified fuels in diesel engines improves the combustion and reduces the emissions dramatically, except for the hydrocarbons. It is reported [5] that reductions of 24% to 52% in NO_x have been achieved in some medium speed engine applications. In high speed diesel engine tests, CO decreased as much as 28% at high speed and load. Smoke capacity was decreased as much as 50% at idle conditions and exhaust temperature decreased 5% over the whole operating range. All reports concerning the HC emissions agreed that HC increased slightly. The mechanisms of engine emission reductions by using W/O emulsified fuels are:

a). NO_x:

The major contribution to the reduction of NO_x is the lower combustion temperature. This lower combustion temperature results from several factors: a. The vaporisation of water absorbs heat from the air and combustion; b. More air involved in combustion provides a cooling function; c. Large flame region limits the increase in local temperature.

b). CO:

More air available for combustion curbs CO formation. The decrease in large size fuel droplets also prevents its formation, and the presence of water provides a source of OH radicals. It has been suggested [24] that the water gas reaction removes a part of the CO as follows:

$$CO + OH \Leftrightarrow CO_2 + H$$

or $$CO + H_2O \Leftrightarrow CO_2 + H_2$$

$$H + H_2O \Leftrightarrow H_2 + OH$$

c). HC:

As mentioned above, it is reported that HC emissions are slightly increased when an engine burns W/O emulsified fuels. This is perhaps because of the lower combustion temperature, especially at the edges of the spray and at combustion chamber walls where there are effects of 'water quenching'. However, rapid combustion can minimise HC formation during the period of late-combustion.

d). Soots:

The good fuel atomisation, better fuel-air mixing and reduction in large droplets result in a better fuel combustion process hence a reduction in soot formation. Clearly the generation of free carbon is curbed by the water gas reaction and soot particles formed can be burnt by the following reaction:

$$2C + 2OH \Rightarrow 2CO + H_2$$

CHAPTER SIX:

MATHEMATICAL REGRESSION

6.1 A Brief Discussion Of Multidimensional Linear Regression

In chapter three, a non-dimensional expression for spray penetration was deduced from the similarity theory. For the following mathematical regression discussion, it is necessary to briefly repeat it here.

It was stated in chapter three that the non-dimensional expression for spray penetration is :

$$\frac{S}{D_0} = C \cdot K_1^{B_1} \cdot K_2^{B_2} \cdot K_3^{B_3} \cdot K_4^{B_4} \cdot K_5^{B_5} \cdot K_6 \qquad ---6.1$$

where:

S -- spray penetration,

D_0-- diameter of nozzle hole,

C -- constant,

B_i (i=1,...,5) -- exponential constants,

$$K_1 = \frac{\Delta P \cdot D_0^2 \cdot \rho_g}{\mu_f^2}, \qquad K_2 = \frac{\sigma_f \cdot D_0 \cdot \rho_g}{\mu_f^2},$$

$$K_3 = \frac{\rho_f}{\rho_g}, \qquad K_4 = \frac{L_0}{D_0},$$

$$K_5 = \frac{t}{t_0}, \qquad K_6 = f(\gamma).$$

Because the length of nozzle hole was not considered in the tests, K_4 should be removed from Eq. 6.1.

Rewriting $K_4=t/t_0$, $K_5=f(\gamma)$ and,

taking logs of both sides of equation 6.1,

gives:

$$\ln\frac{S}{D_0} = \ln C + B_1 \cdot lnK_1 + B_2 \cdot \ln K_2 + \cdots + lnK_5 \qquad ---6.2$$

let:

$$\begin{aligned} Y &= \ln(S/D_0)\ , \\ B_0 &= \ln C\ , \\ X_i &= \ln K_i\ , \qquad i=1,...,5 \end{aligned}$$

then:

$$Y = B_0 + B_1 \cdot X_1 + B_2 \cdot X_2 + B_3 \cdot X_3 + B_4 \cdot X_4 + X_5 \qquad ---6.3$$

Now it is necessary to define the function $K_5=f(\gamma)$. From the experimental results analysis, it is known that the spray penetration increases as the water percentage increases. The curve S-γ could be fitted by the natural exponent (see Fig. 5.8), i.e.

$$S \propto e^{c_1\gamma} \qquad ---6.4$$

It is also noticed that the increase in penetration with the increase of water content is a function of time. As the time increases, the increment of penetration becomes smaller.

Considering the time effect and rewriting Eq. 6.4,

gives:

$$S \propto e^{c_1 \cdot \gamma \cdot \left(\frac{t}{t_0}\right)^{c_2}} \qquad ---6.5$$

Then K_5 in Eq. 6.2 is:

$$K_5 = e^{c_1 \cdot \gamma \cdot \left(\frac{t}{t_0}\right)^{c_2}}$$

$X_5 = \ln K_5 = c_1 \cdot \gamma \cdot \left(\frac{t}{t_0}\right)^{c_2}$. Replacing X_5 with $c_1\gamma\left(\frac{t}{t_0}\right)^{c_2}$ in equation 6.3,

gives:

$$Y = B_0 + B_1X_1 + B_2X_2 + B_3X_3 + B_4X_4 + c_1\gamma\left(\frac{t}{t_0}\right)^{c_2} \qquad ---6.6$$

This is a non-linear expression due to the existence of $\left(\frac{t}{t_0}\right)^{c_2}$, and can be expressed in

the form of a series. When Taylor's series is employed toward this end, the expression

of a^x is:

$$a^x = 1 + \frac{\ln a}{1}x + \frac{(\ln a)^2}{2!}x^2 +, \ldots, + \frac{(\ln a)^n}{n!}x^n + \ldots$$

$$(a > 0, -\infty < x < +\infty)$$

Referring to Eq. 6.6, x and a in the above equation are respectively represented by C_2

and (t/t_0) in the following discussion. When $a > 0$, a^x is known as a "well-behaved"

function. The high order items in the above series can be removed, and their remainder

error is:

$$R(x) = \frac{[\ln(a)]^{n+1} \cdot x^{n+1}}{(n+1)!}$$

Since $0<a=(t/t_0)<=1$, the maximum error exists when $a=a_{min}$. In the tests, t=1.0-3.5ms and t_0=3.5ms. Thus, $(t/t_0)_{min}$=0.285. To simplify the regression process, high order terms of n>2 are removed giving a maximum error of 16.9%. Therefore it can be taken that,

$$\left(\frac{t}{t_0}\right)^{C_2} = 1 + \ln\left(\frac{t}{t_0}\right)\cdot C_2 + \left[\ln\left(\frac{t}{t_0}\right)\right]^2 \cdot \frac{C_2^2}{2} \qquad ---6.7$$

Substituting $\left(\frac{t}{t_0}\right)^{C_2}$ from Eq. 6.7 into Eq. 6.6,

gives:

$$Y = B_0 + B_1X_1 + B_2X_2 + B_3X_3 + B_4X_4 + C_1\gamma + C_1C_2\gamma\ln(t/t_0) + C_1C_2^2\gamma[\ln(t/t_0)]^2/2 \qquad ---6.8$$

Let:

$B_5 = C_1$,

$B_6 = C_1C_2$,

$B_7 = C_1C_2^{\,2}$,

$X_5 = \gamma$,

$X_6 = \gamma\ln(t/t_0)$,

$X_7 = \gamma[\ln(t/t_0)]^2/2$.

then:

$$Y = B_0 + B_1X_1 +, \ldots, +B_7X_7 \qquad ---6.8.1$$

This is a standard multidimensional linear regression expression. In the process of regression calculation, B_7X_7 was ignored, since C_1 and C_2 could be determined from B_5 and B_6. The existence of B_7 would cause "self-locking" when determining C_1 and C_2.

Now rewriting Eq. 6.8 in matrix form, we have:

$$y_i = \sum_{j=0}^{n} x_{ij} \cdot b_j \qquad x_{i,0}=1;\ i=1,...,m. \qquad ---6.9$$

where, m is the number of test points or reading adopting points.

n is the experimental variables.

The target of regression is to determine the constant factors b_j.

Introducing,

$$[Y]=[y_1,...,y_m]^T,$$

$$[X]=[x_{ij}], \qquad i=1,...,m; \quad j=0,1,...,n.$$

$$[B]=[b_1,...,b_n]^T.$$

Then Eq. 6.9 can be written as:

$$[Y]=[X][B] \qquad --- 6.9.1$$

$$[X]^T[Y]=[X]^T[X][B]$$

$$\{[X]^T[X]\}^{-1}[X]^T[Y]=[B]$$

then:

$$[B]=\{[X]^T[X]\}^{-1}[X]^T[Y]$$

Such, b_i (i=1,..,n) are finally worked out from the Matrix calculation.

6.2 Spray Penetration Regression

The original input data is presented in Appendix C.

The calculation results for [B] are:

b_0= 17.874006
b_1= 0.1754497
b_2=-1.179359
b_3=-0.8508729
b_4= 0.5943661
b_5= 0.2435608
b_6=-0.3804321

Referring to the Eq. 6.6,

then:

B_0=EXP(17.874006)= 5.788×10^7
B_1= 0.1754497
B_2=-1.179359
B_3=-0.8508729
B_4= 0.5943661
C_1= 0.2435608
C_2=b_6/b_5=-1.561959

Then referring to Eqs. (6.1) and (6.6),

$$\frac{S}{D_0} = 5.788 \times 10^7 \left(\frac{\Delta P \cdot D_0^2 \cdot \rho_g}{\mu_f^2} \right)^{0.175} \cdot \left(\frac{\sigma_f \cdot D_0 \cdot \rho_g}{\mu_f^2} \right)^{-1.179} \cdot \left(\frac{\rho_f}{\rho_g} \right)^{-0.851} \cdot \left(\frac{t}{t_0} \right)^{0.594} \cdot e^{0.244 \cdot \gamma \cdot \left(\frac{t}{t_0} \right)^{-1.562}} \quad \text{---6.10}$$

Taking μ_f, ρ_g, σ_f and t_0 as constants (see Appendix D),

gives:

$$S = 66.01 \cdot \frac{\Delta P^{0.176} \cdot D_0^{0.172} \cdot t^{0.594}}{\rho_g^{0.153}} \cdot e^{1.426 \cdot \gamma \cdot t^{-1.562}} \quad \text{---6.11}$$

where the parameters' units are:

S -- mm,
ΔP -- MPa,
D_0 -- mm,
t -- ms,
ρ_g -- kg/m^3.
γ -- in form of percentage (e.g. 10% water, γ=0.10).

Two Alternative Models For Spray Penetration

In chapter three, fuel properties, e.g. fuel surface tension, viscosity and density, were considered for developing the mathematical model of spray penetration. After the resulting expression had been developed (Eq. 6.10), the parameters of fuel properties were converted into the constant. These parameters could be ignored at the beginning of setting up the model (see Appendix D), that is, only the parameters of ΔP, D_0, ρ_g, γ and t are considered. From this point of view, two alternative models can be developed (the deduction of these two models is presented in Appendix D) for simulating the spray penetration as follows:

$$\frac{S_2}{D_0} = f\left(\frac{\Delta P \cdot t^2}{D_0^2 \cdot \rho_g}, \gamma\right) \qquad ---6.12$$

and

$$\frac{S_3}{D_0} = \left(\frac{\Delta P}{D_0^2 \cdot \rho_g \cdot g}, \frac{t}{t_0}, \gamma\right) \qquad ---6.13$$

where g is the gravitational acceleration, and t_0 is the duration of injection.

Their resulting regression expressions are:

$$S_2 = 87.87\left(\frac{\Delta P}{\rho_g}\right)^{0.287} \cdot D_0^{0.425} \cdot t^{0.575} \cdot e^{0.755 \cdot \gamma \cdot t^{-1.267}} \qquad ---6.14$$

$$S_3 = 112.22\left(\frac{\Delta P}{\rho_g}\right)^{0.227} \cdot D_0^{0.773} \cdot t^{0.589} \cdot e^{1.25 \cdot \gamma \cdot t^{-1.378}} \qquad ---6.15$$

The units of the parameters are the same as for Eq. 6.11.

In equations 6.11, 6.14 and 6.15, the last term on the right hand side is the modifying factor for emulsified fuel and shows the effects of water content on fuel spray penetration. The spray penetration is increased when γ increases. When γ=0, the term

$f(\gamma)=1$, and the above equations are the pure fuel spray penetration expressions. When γ is fixed, $f(\gamma)$ becomes smaller as time increases, which indicates the increment of spray penetration is decreased as time increases.

The differences, among these three equations, are the different constants and the exponential terms for the variables P, ρ_g and D_0. This is because the product of $\frac{\Delta P}{D_0 \cdot \rho_g \cdot g}$ is a non-dimensional item, and the different exponential terms result in different constant factors. Their total product results are the same.

General speaking, all three models are acceptable for fitting the experimental results. The model which fits the experimental results most closely should be chosen as the best fitting model. Normally the best fitting model is chosen by the comparison of the models' estimates or errors.

The root mean square error of the above models are:

Model 1: e=5.934%,

Model 2: e=4.441%,

Model 3: e=4.701%.

Therefore, model 2 is the best fitting model, since its error is smaller than that of the other two models.

6.3 Spray Angle Regression

The following equation has been developed in Chapter three as a general expression for the spray angle.

$$\theta = C \cdot R_e^{a_1} \cdot \left(\frac{\rho_g}{\rho_f}\right)^{a_2} \cdot f(\gamma) \qquad ---3.34 repeat$$

Where $f(\gamma)$ is the effect of water on the spray angle.

From Fig. 5.11, it is recognized that the effect of water on spray angle can be represented by an exponential function. Therefore Eq. 3.34 can be rewritten as follow:

$$\theta = C \cdot R_e^{a_1} \cdot \left(\frac{\rho_g}{\rho_f}\right)^{a_2} \cdot e^{a_3 \gamma} \qquad ---6.16$$

where: C, a_1, a_2 and a_3 are constants.

From the experimental data regression, the four constants in the above equation are determined as follows:

$$C = 6.18$$

$$a_1 = 0.177$$

$$a_2 = 0.186$$

$$a_3 = 0.733$$

Therefore:

$$\theta = 6.18 \cdot R_e^{0.177}\left(\frac{\rho_g}{\rho_f}\right)^{0.186} \cdot e^{0.733\gamma} \qquad ---6.17$$

the units of the parameters in Eq. 6.17 are:

θ -- degree(°)

ρ_g,ρ_f -- kg/m^3

γ -- in the form of percentage (i.e. 5% water, γ=0.05)

6.4 Sauter Mean Diameter Regression

In chapter three, a general simulation model (Eq. 3.13) for the Sauter mean diameter has been developed, which included all the parameters influencing the fuel droplets formation. In this test, only the following parameters are considered for the Sauter mean diameter regression. They are:

ΔP -- pressure drop cross the nozzle hole,

D_0 -- nozzle diameter,

ρ_g -- gas density,

q -- injection quantity,

γ -- water percentage in fuel by volume.

From the non-dimensional analysis in Appendix E, their non-dimensional relationship is:

$$\frac{D_{32}}{D_0} = f\left(\frac{D_0 \cdot \rho_g \cdot g}{\Delta P}, \frac{q}{D_0^3}, \gamma\right) \qquad ---6.18$$

where g is the gravitational acceleration.

The test results show that the effects of water percentage on the Sauter mean diameter can be expressed by an exponential function.

Therefore,

$$\frac{D_{32}}{D_0} = C \cdot \left(\frac{D_0 \cdot \rho_g \cdot g}{\Delta P}\right)^{B_1} \cdot \left(\frac{q}{D_0^3}\right)^{B_2} \cdot e^{B_3 \cdot \gamma} \qquad ---6.19$$

After the experimental data regression, the constant C and exponential B_i (i=1,2,3) are:

C =34.362

B_1 =0.189

B_2 =0.162

B_3 =-0.595

Then:

$$\frac{D_{32}}{D_0} = 34.362 \cdot \left(\frac{D_0 \cdot \rho_g \cdot g}{\Delta P}\right)^{0.189} \cdot \left(\frac{q}{D_0^3}\right)^{0.162} \cdot e^{-0.595 \cdot \gamma} \qquad ---6.20$$

Combining the D_0 terms and calculating the constant $g^{0.189}$, gives:

$$D_{32} = 52.89 \cdot \left(\frac{\rho_g}{\Delta P}\right)^{0.189} \cdot D_0^{0.703} \cdot q^{0.162} \cdot e^{-0.595 \cdot \gamma} \qquad ---6.21$$

The units of the parameters in the above equation are:

D_{32} -- μm

ρ_g -- kg/m^3

ΔP -- MPa

D_0 -- mm

q -- ml

γ -- %

6.5 Droplet Diameter Distribution Regression

The following equations have been deduced in Chapter three.

$$\frac{d(n_i)}{d(d_i)} \cdot \frac{1}{N} = A \cdot (d_i)^{\alpha} \cdot \exp(-B \cdot d_i^{\beta}) \qquad ---3.17repeat$$

--- The Nakiyama-Tanasava distribution of droplet diameter

The relationships of the parameters A, B, α and β are:

$$A = \frac{\beta}{\Gamma\left(\frac{\alpha+1}{\beta}\right)} \cdot \left[\frac{\Gamma\left(\frac{\alpha+4}{\beta}\right)}{D_{32} \cdot \Gamma\left(\frac{\alpha+3}{\beta}\right)}\right]^{\alpha+1}$$

$$B = \left[\frac{\Gamma\left(\frac{\alpha+4}{\beta}\right)}{D_{32} \cdot \Gamma\left(\frac{\alpha+3}{\beta}\right)}\right]^{\beta}$$

$$\frac{D_{32}}{D_{10}} = f(\alpha, \beta) \qquad ---3.32repeat$$

where D_{32} and D_{10} are determined from the experimental data.

Now, there are three equations for four unknown parameters, which means that there are, theoretically, infinite solutions for A, B, α and β. To determine A, B, α and β, most of the researchers use the method of assuming one parameter is known, then solving the other three parameters, e.g. Hiroyasa [69] assumed α=3, K.Takeuchi [69] took α=2 and X.Gao [52] set $\alpha=\beta-1$. The best way to solve them is to regress A, B, α and β with the experimental data.

However, the regression of Eq. 3.17 involves a non-linear problem. Perhaps that is the reason why most of the researchers do not use mathematical regression. The following part of this section illustrates a regression method for determining A, B, α and β.

From the previous work done in this area, it is known that the value range for β is about 0 to 5, to avoid the non-linear exponent item d_i^{β}, it is advantageous to first fix a value for β within 0 to 5 and then to regress the other three parameters, subsequently, to fix another value for β with a very small step (supposing 0.01) increasing or decreasing. To this end, there are 500 set solutions for parameters A, B, α and β. Any one set of them could possibly be the most accurate model. The method of selecting the most accurate model is to compare the sum of the squares of deviation of the experimental and model data. The one which has the minimum error should be chosen as the best model.

Table 6.1 shows the regression results of the parameters A, B, α and β for Eq. 3.32 with different water contents.

In table 6.1, parameters A, B, α and β vary with water content. Relationships between water contents and A, B, α and β can be expressed in a mathematical function form shown as follows:

$$
\begin{aligned}
A &= a_0 + a_1\gamma + a_2\gamma^2 + a_3\gamma^3 + \cdots \\
B &= b_0 + b_1\gamma + b_2\gamma^2 + b_3\gamma^3 + \cdots \\
\alpha &= \alpha_0 + \alpha_1\gamma + \alpha_2\gamma^2 + \alpha_3\gamma^3 + \cdots \\
\beta &= \beta_0 + \beta_1\gamma + \beta_2\gamma^2 + \beta_3\gamma^3 + \cdots
\end{aligned}
\qquad \text{---6.22}
$$

Ignoring the higher order terms, and solving the a_i, b_i, α_i and β_i for the above equations gives:

$$
\begin{aligned}
A &= 7.708 - 126.27\gamma + 1436.08\gamma^2 - 4485\gamma^3 \\
B &= 3.483 - 25.773\gamma + 433.5\gamma^2 - 119.06\gamma^3 \\
\alpha &= 4.198 - 23.240\gamma + 413.75\gamma^2 - 1064.25\gamma^3 \\
\beta &= 0.45 - 0.307\gamma - 5.644\gamma^2 + 15.648\gamma^3
\end{aligned}
\qquad \text{---6.23}
$$

Substituting Eq. 6.23 into Eq. 3.17 will form a completed expression of droplet size distribution for emulsified fuels. When γ=0, it is the expression for pure fuel.

Table 6.1 The regression results of the parameters A, B, α and β

Water %	A	α	B	β
0	7.708	4.198	3.483	0.450
10	4.956	4.947	4.122	0.440
15	5.940	6.429	5.597	0.422
20	4.010	7.585	6.717	0.411

6.6 Comparison Of Models With Experimental Results

Figs. 6.1(1-13) illustrate the comparison of the mathematical model with the test results for spray penetration at all the test conditions. Generally, the model gives a very good fit to the test results. However, at some test points there are deviations between the model and test results. This is reasonable, since the model is regressed from the data of 13 test conditions. It takes account of all these tests at the same time and gives the best fit to all the experimental results instead of any particular one.

The time range for obtaining the data from films is about 1.0 ms to 3.5 ms after injection start. The data before and after this time range shown in these diagrams are produced by mathematical interpolation.

The purpose of developing a model is to express a physical phenomenon mathematically. With a developed model, one can predict the effects of any considered parameters on the physical event, which is difficult to realise in practice.

Figs. 6.2 to 6.4 show the effects of each parameter on spray penetration within a certain parameter range.

On these diagrams, the gas density does not appear, but is represented by the gas pressure. The relationship between P_g and ρ_g is $\rho_g=P_g/(RxT)$, where R is the gas constant; T is the gas temperature.

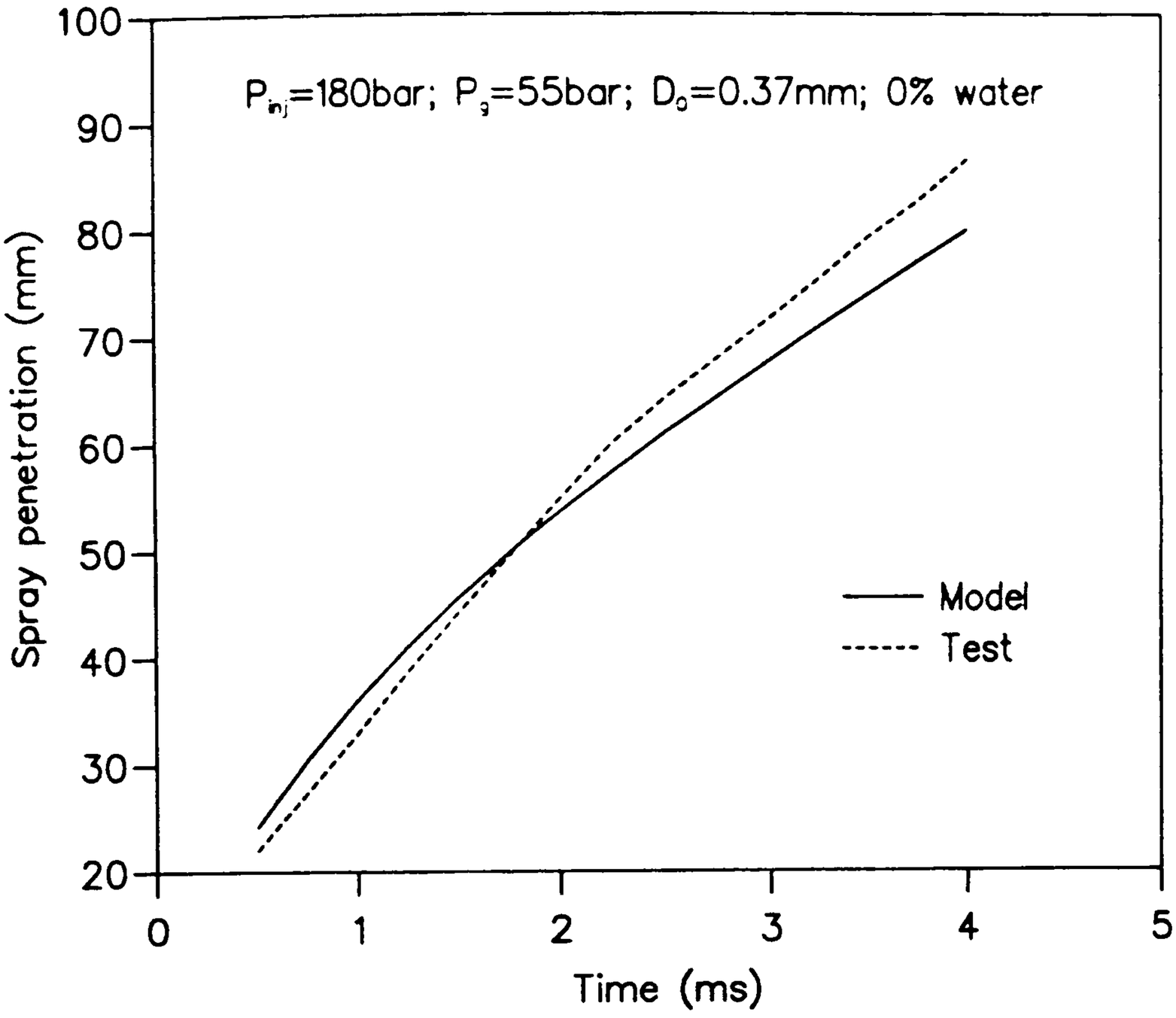

Fig. 6.1(1) Comparison between model and test results for spray penetration

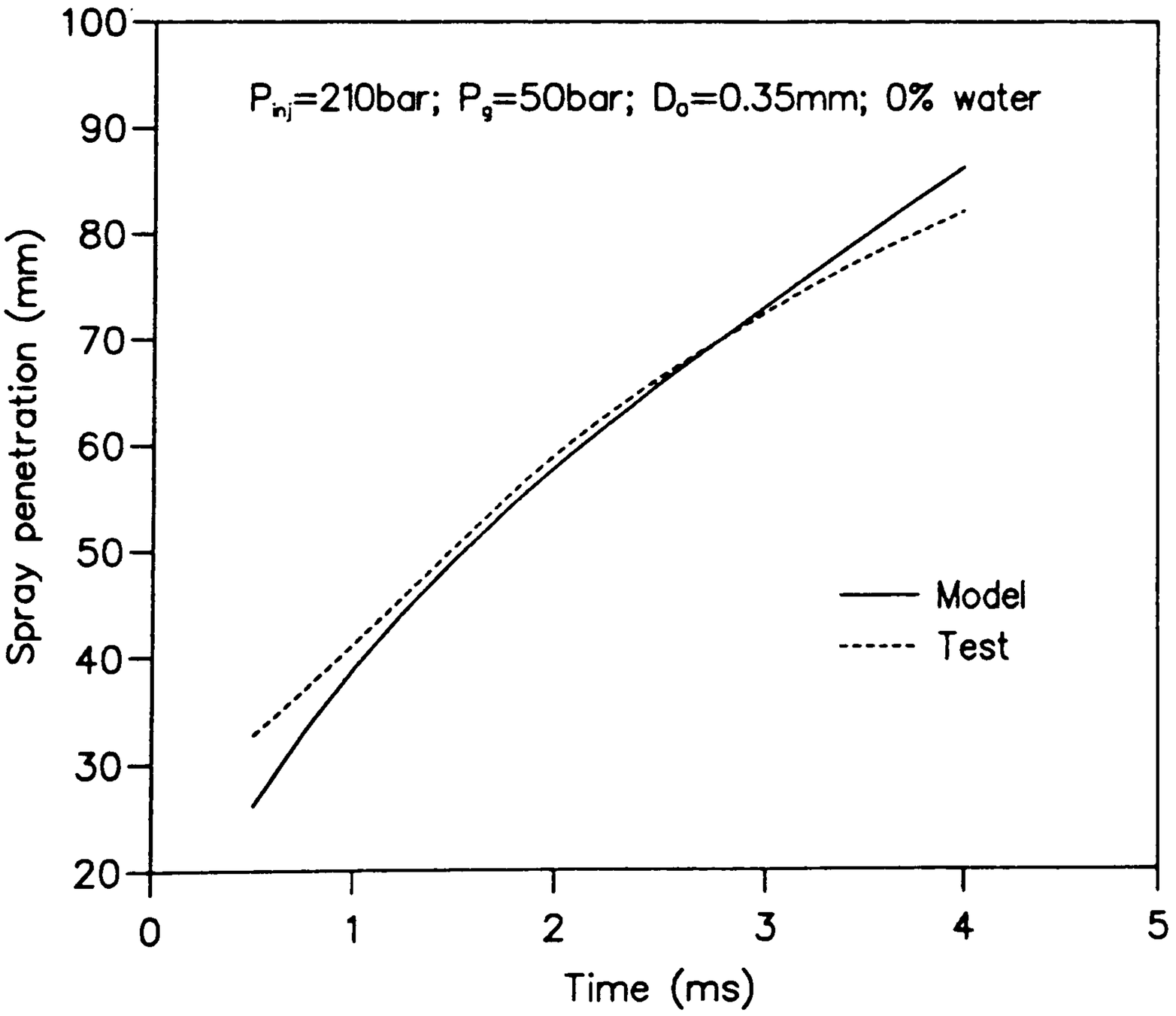

Fig. 6.1(2)

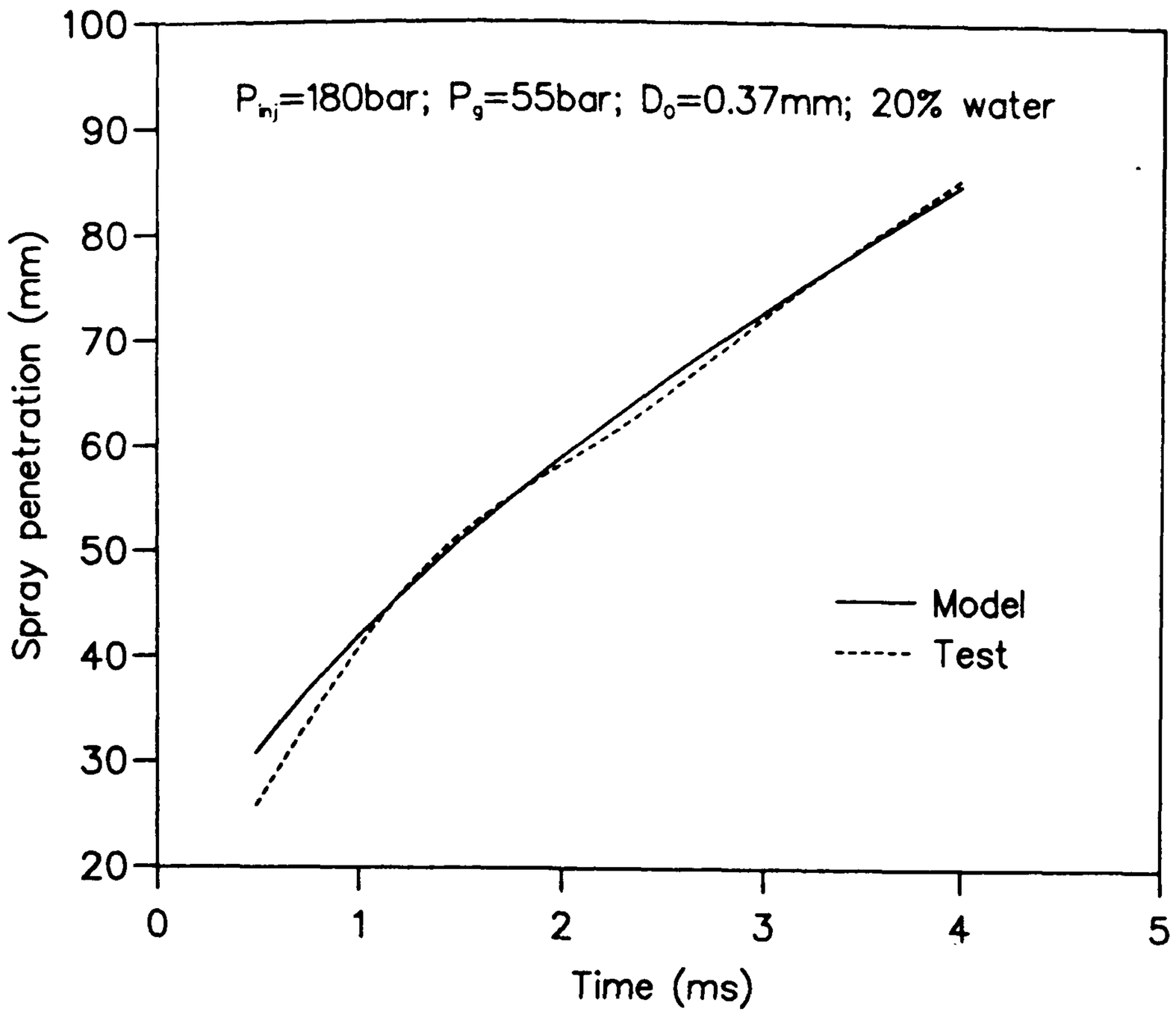

Fig. 6.1(3)

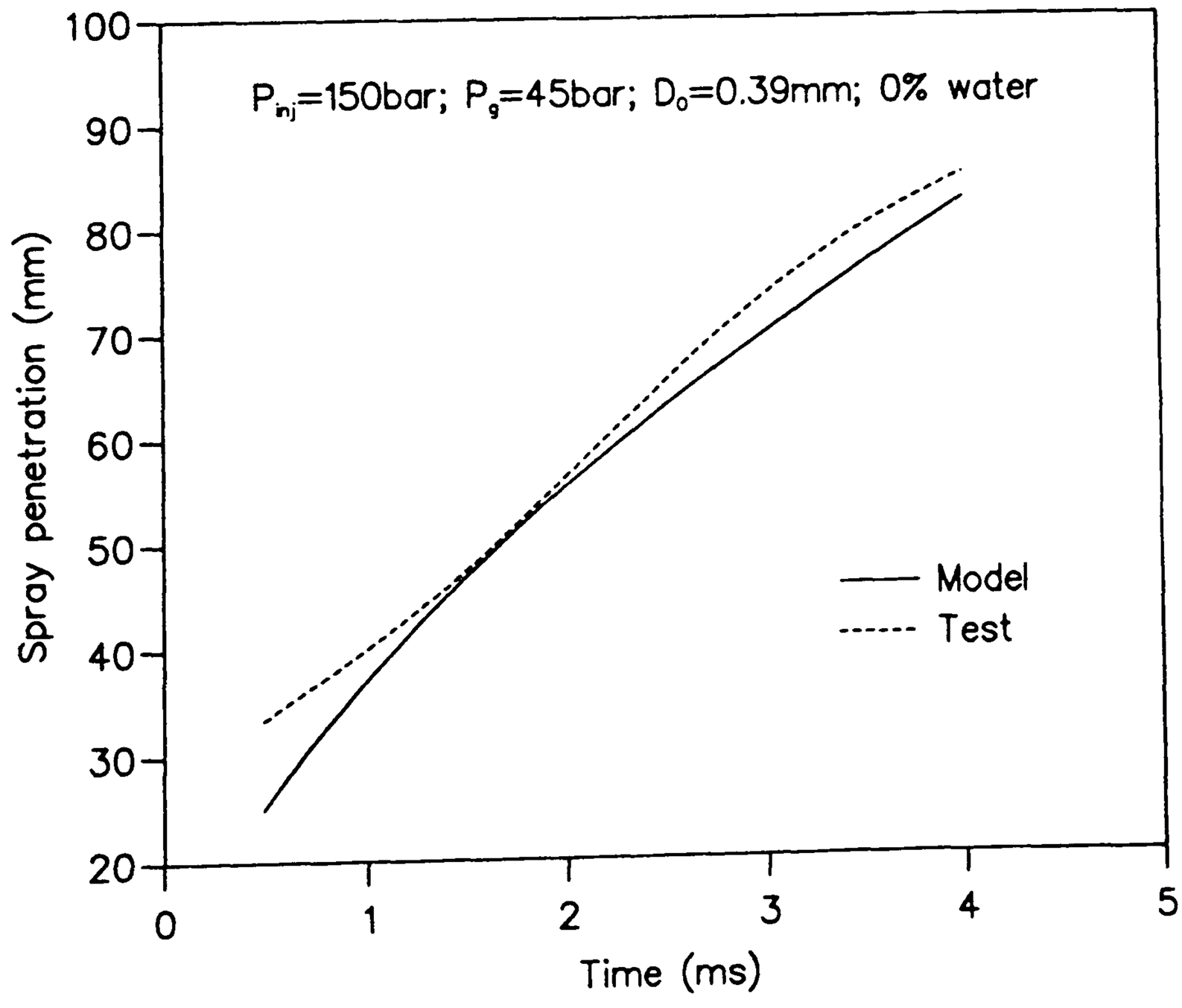

Fig. 6.1(4)

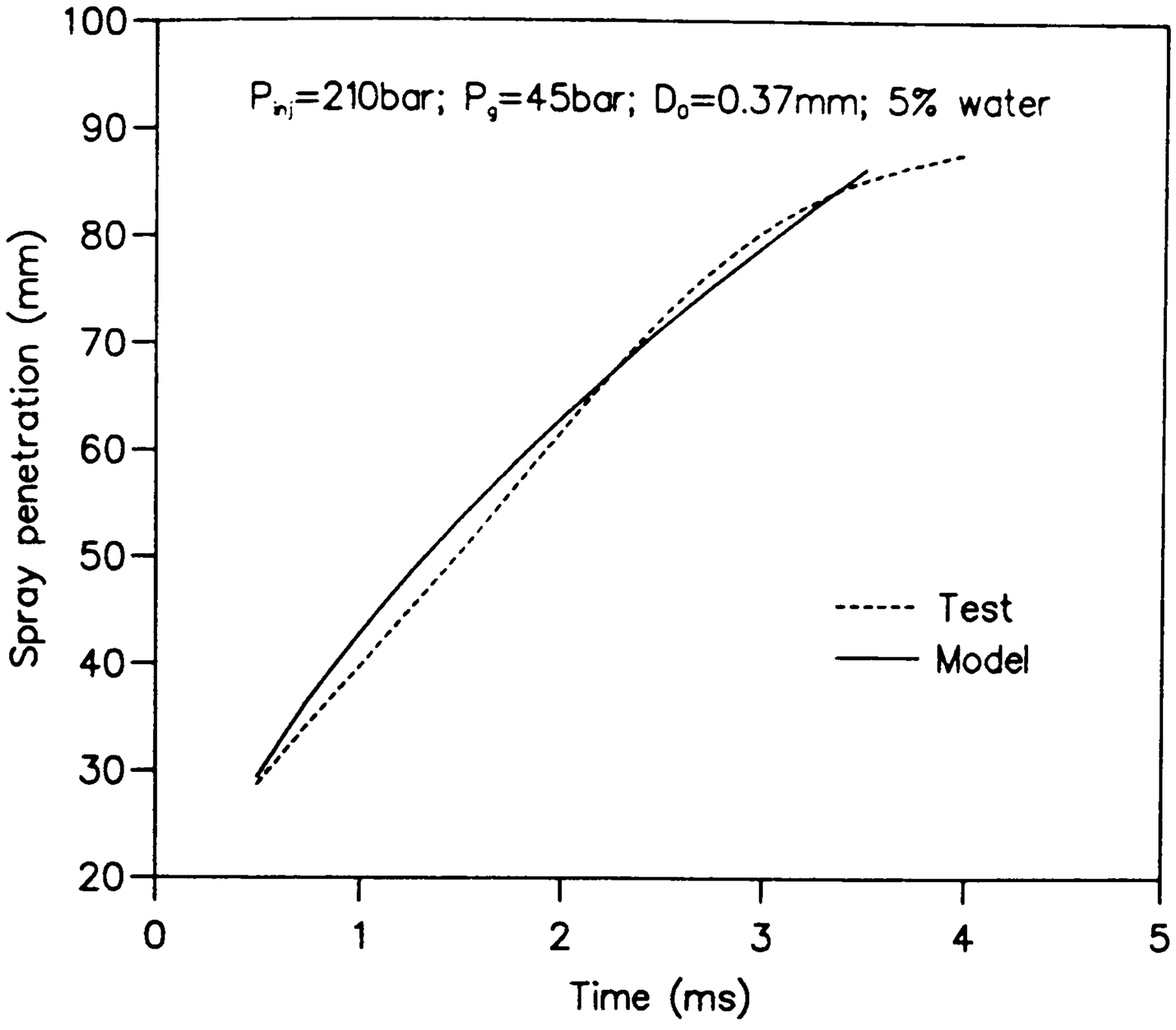

Fig. 6.1(5)

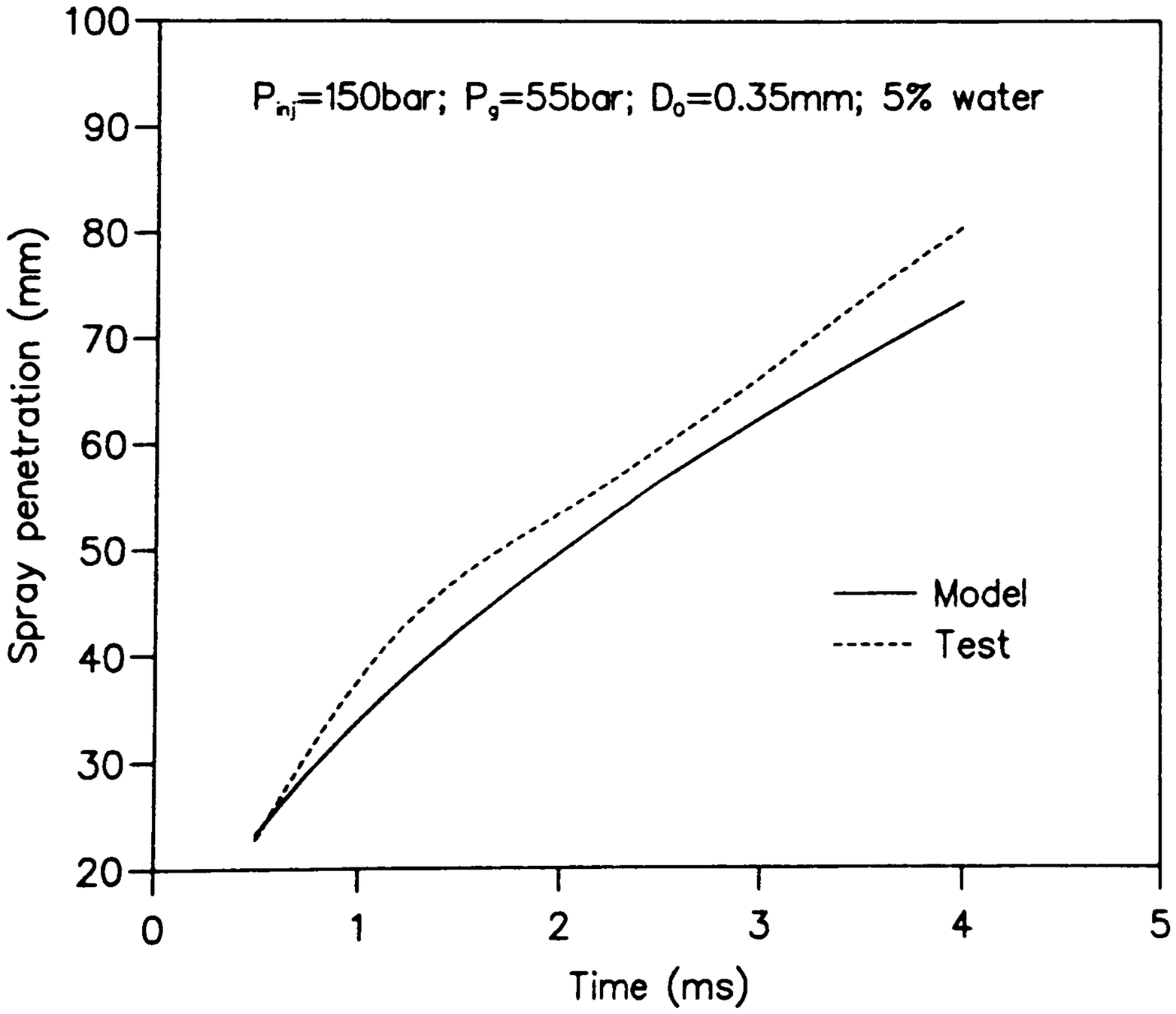

Fig. 6.1(6)

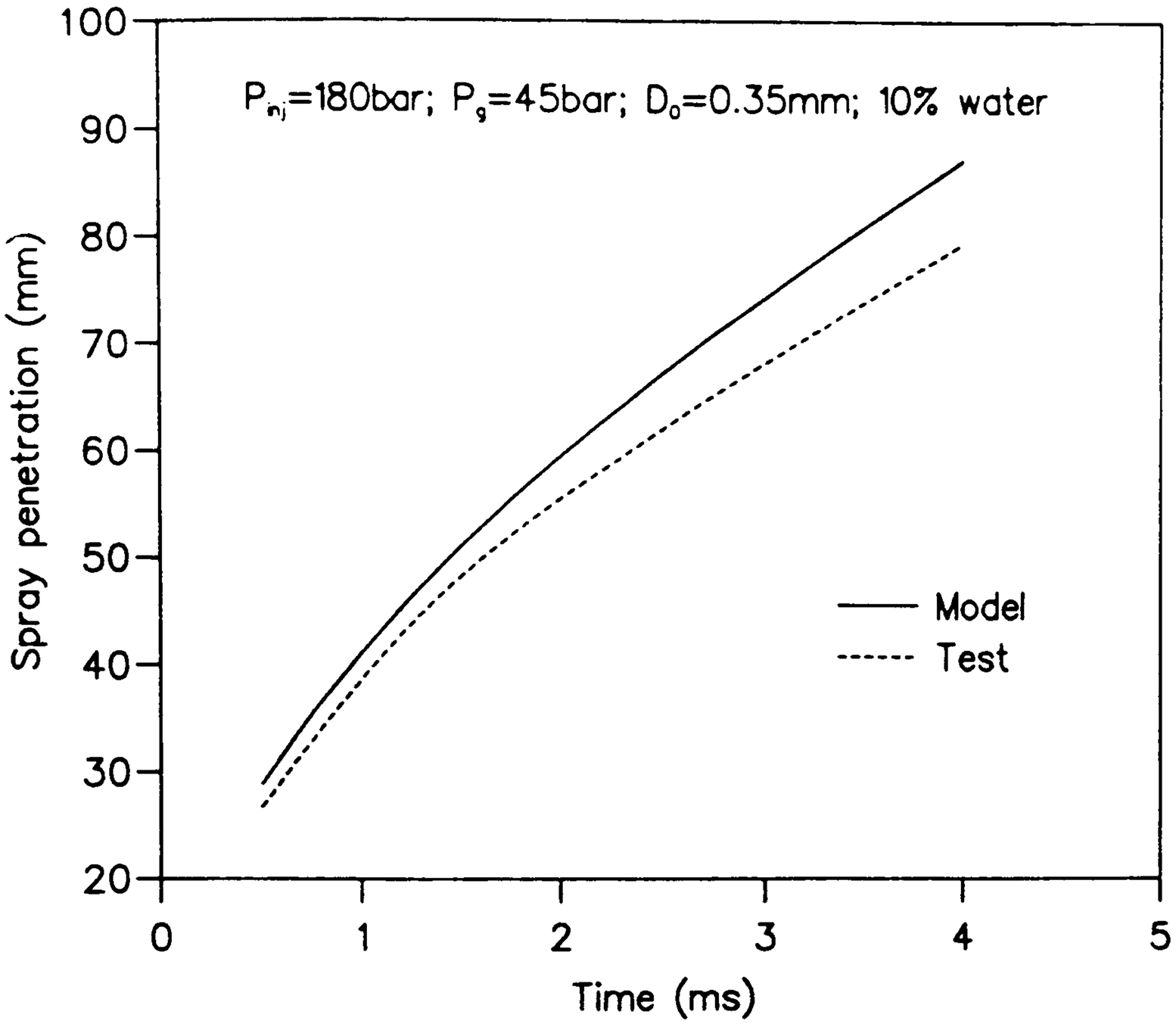

Fig. 6.1(7)

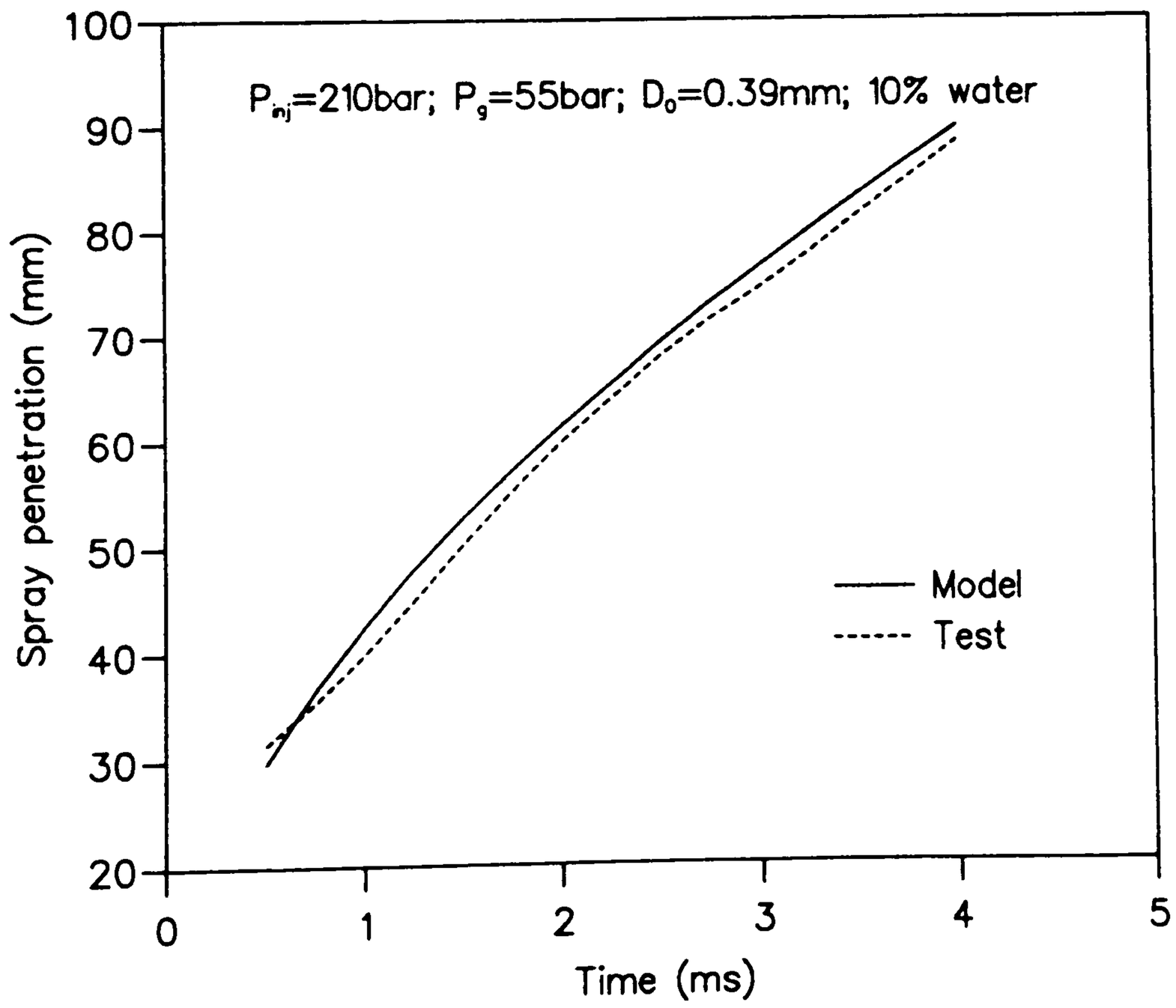

Fig. 6.1(8)

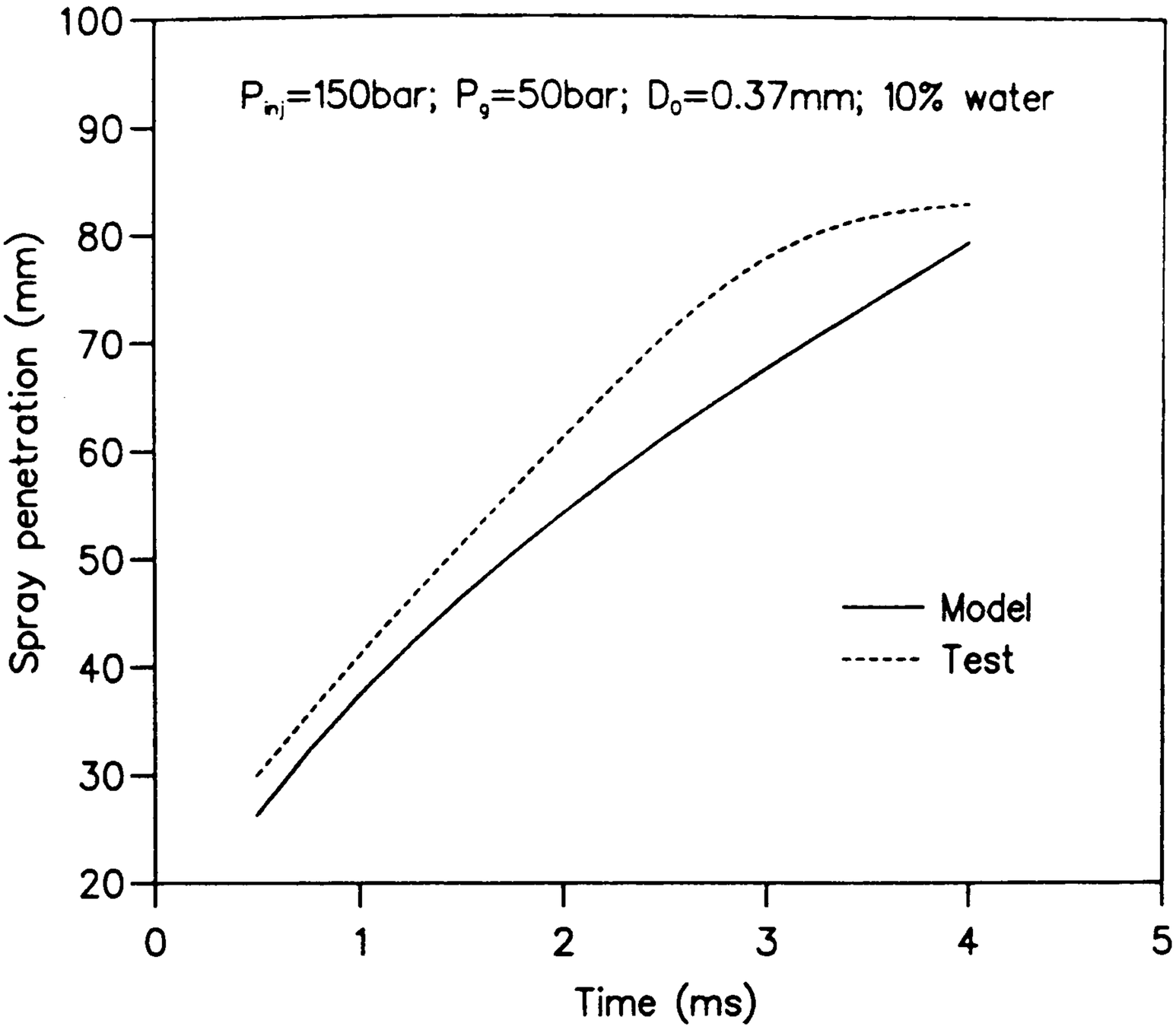

Fig. 6.1(9)

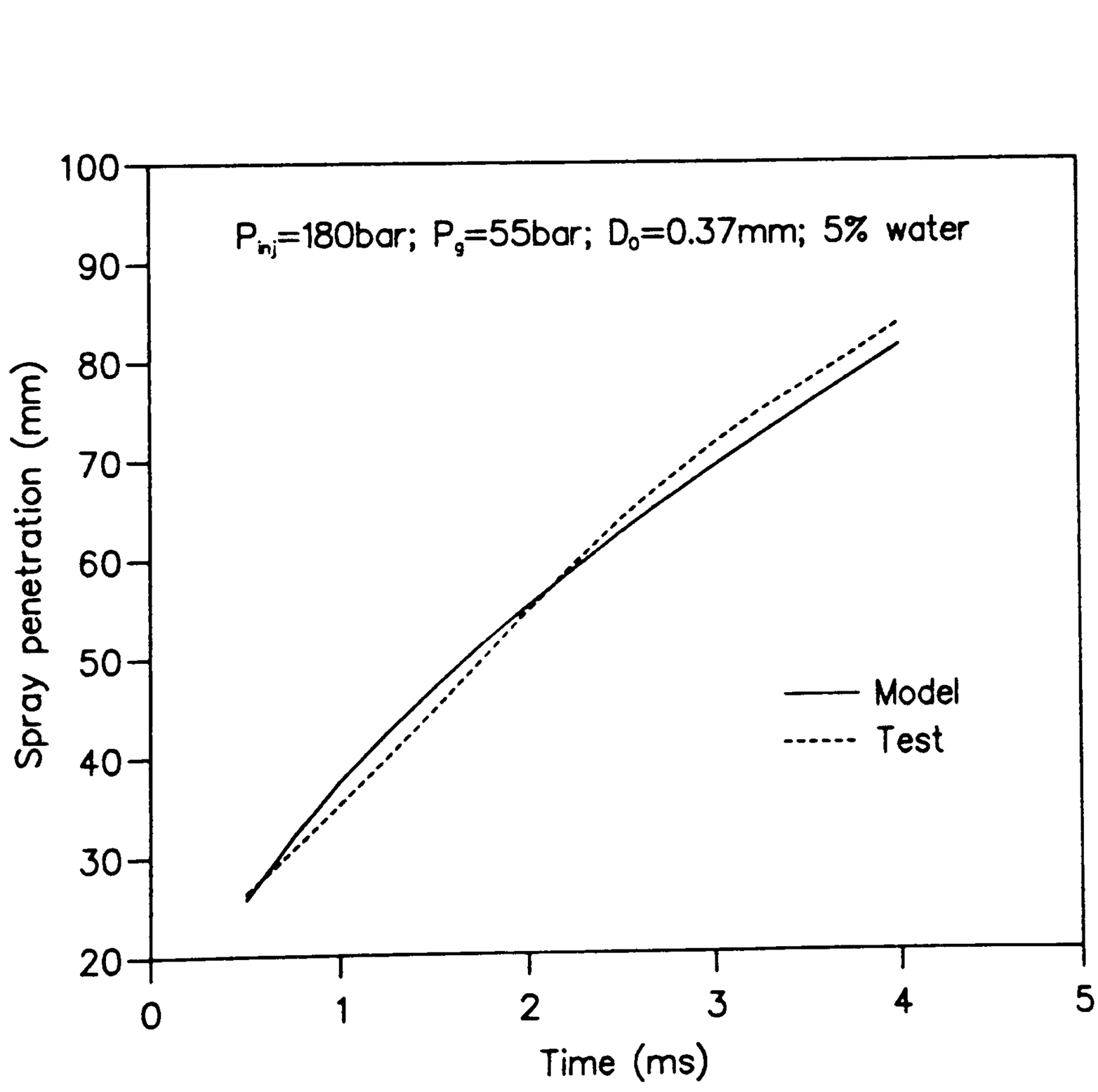

Fig. 6.1(10)

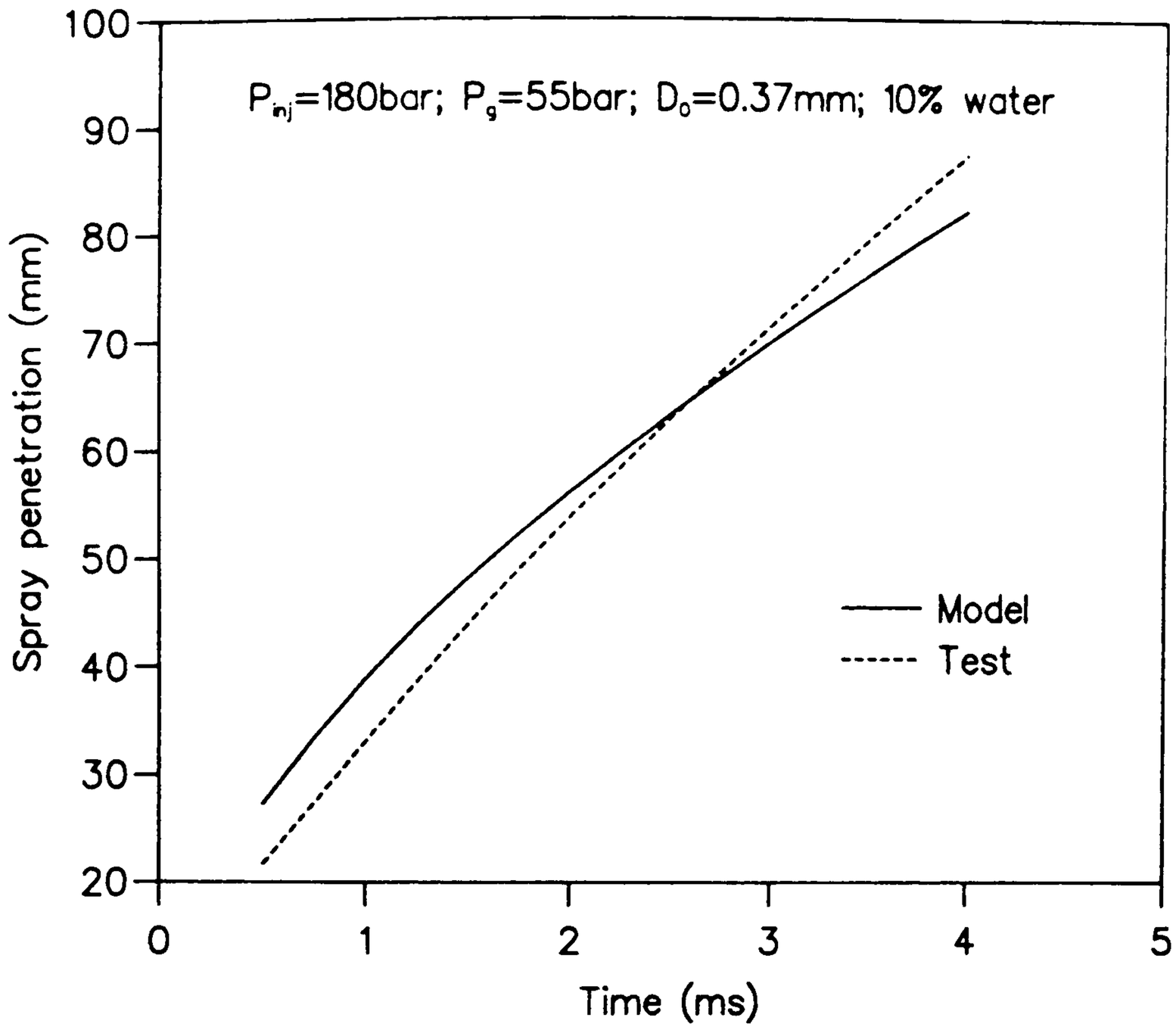

Fig. 6.1(11)

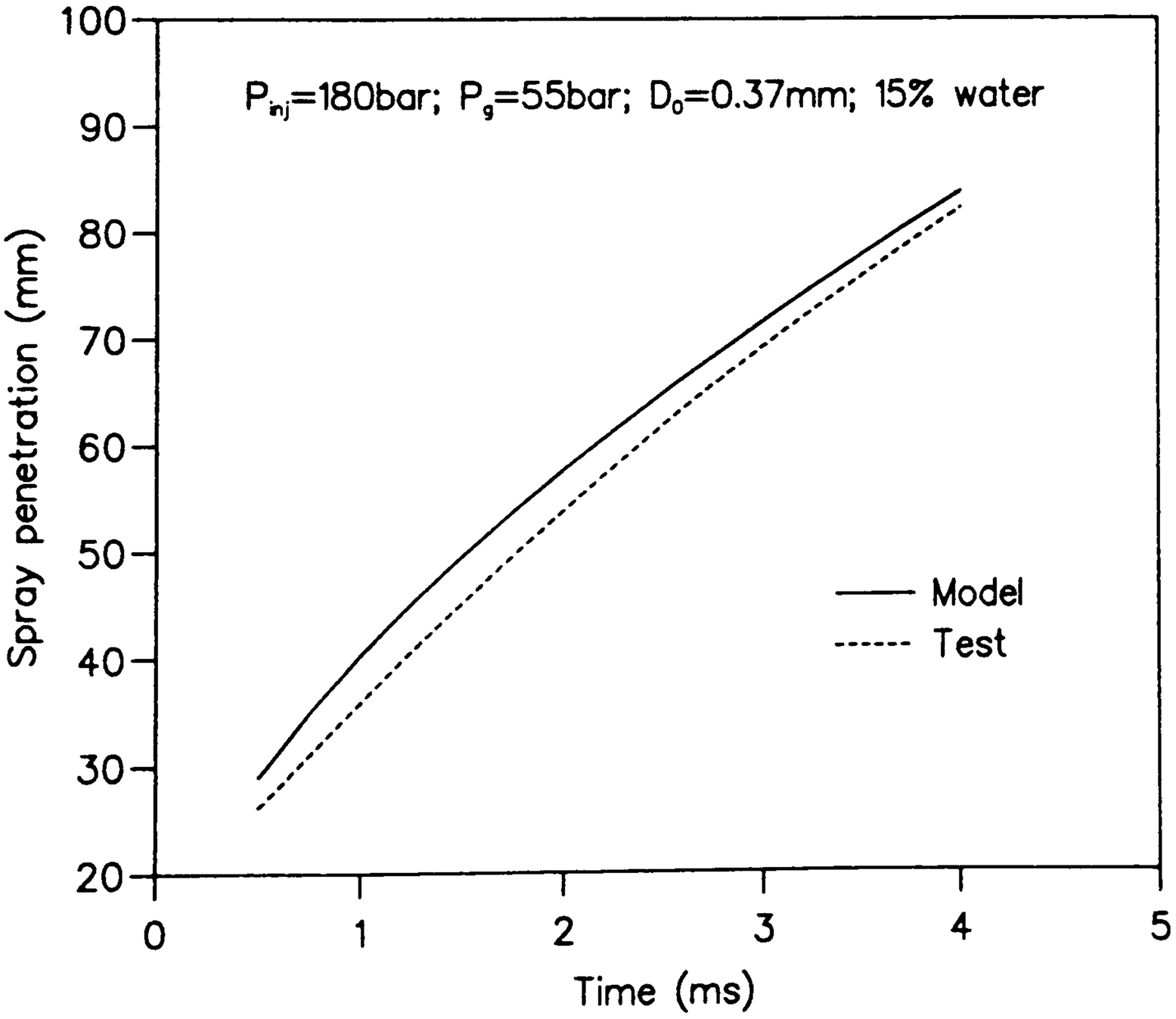

Fig. 6.1(12)

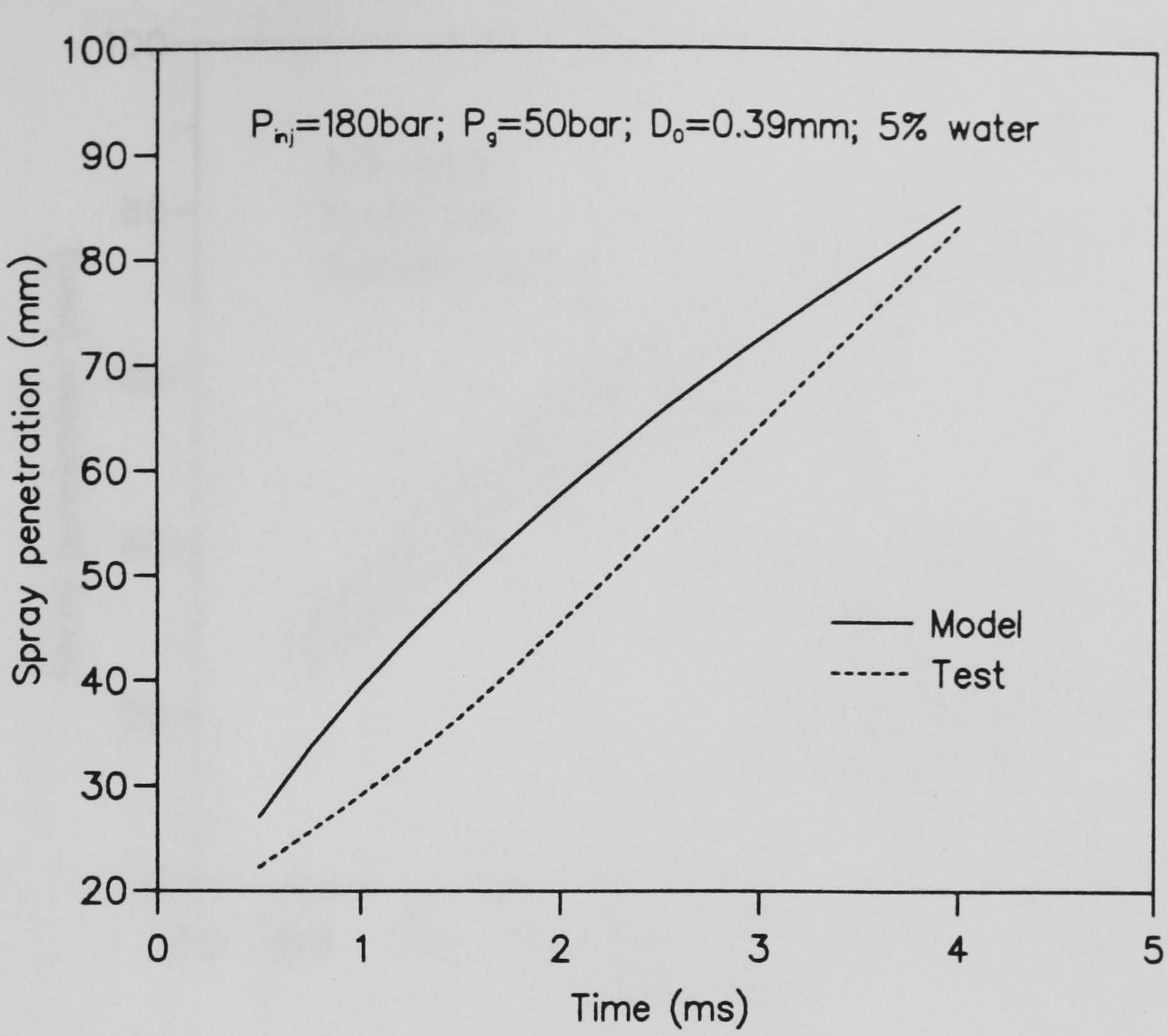

Fig. 6.1(13)

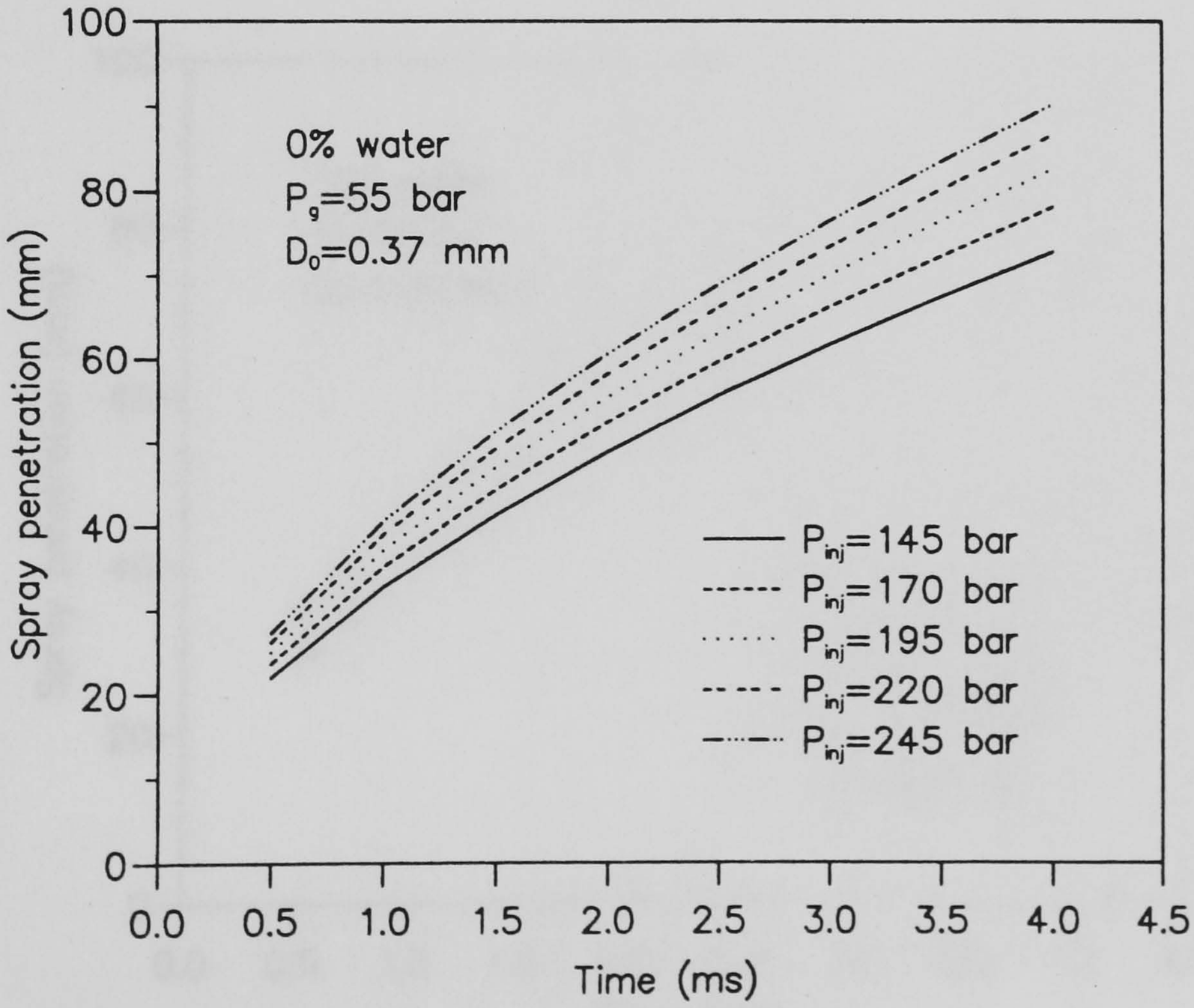

Fig. 6.2(1) Spray penetration (model 2) at different injection pressures

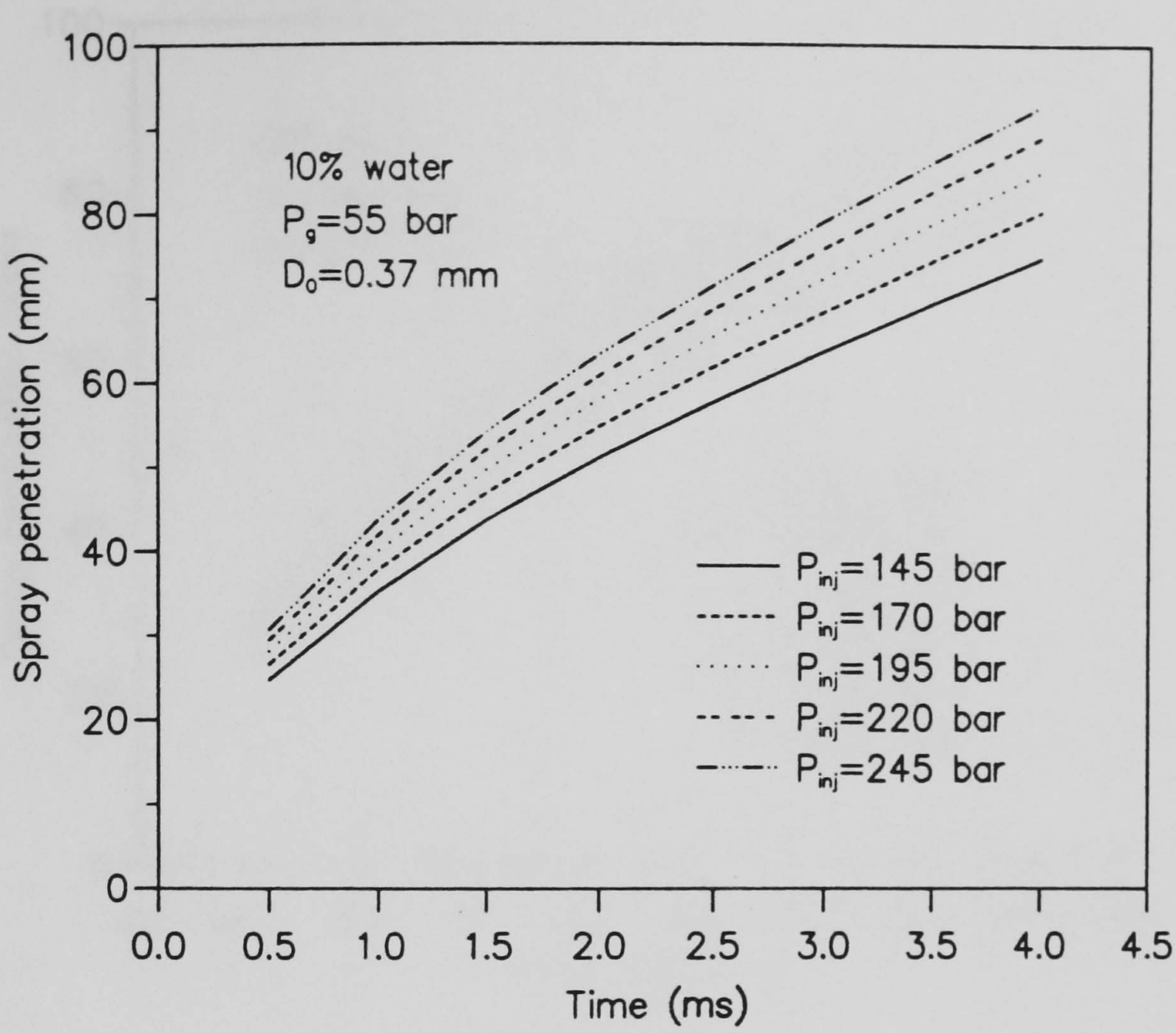

Fig. 6.2(2)

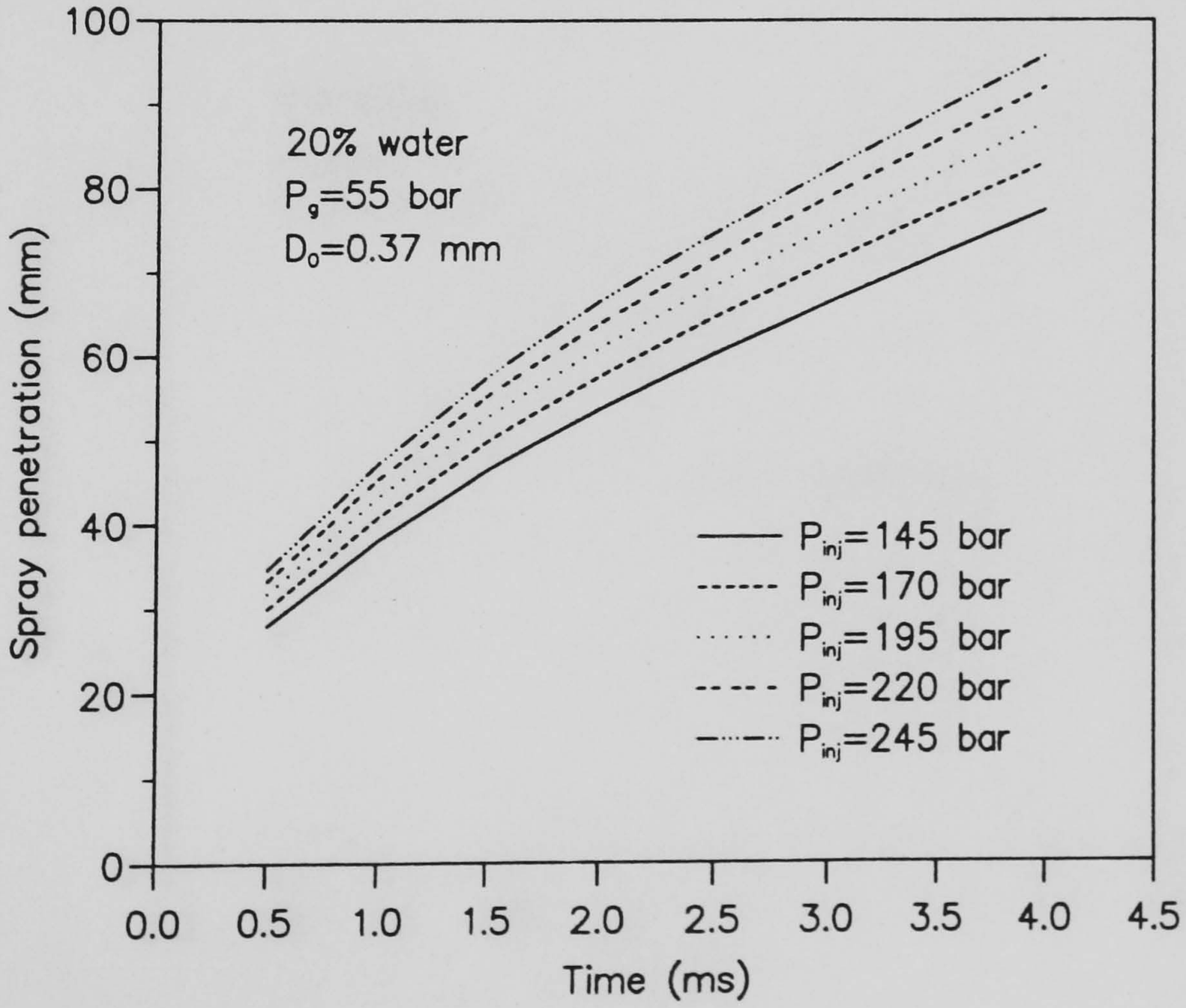

Fig. 6.2(3)

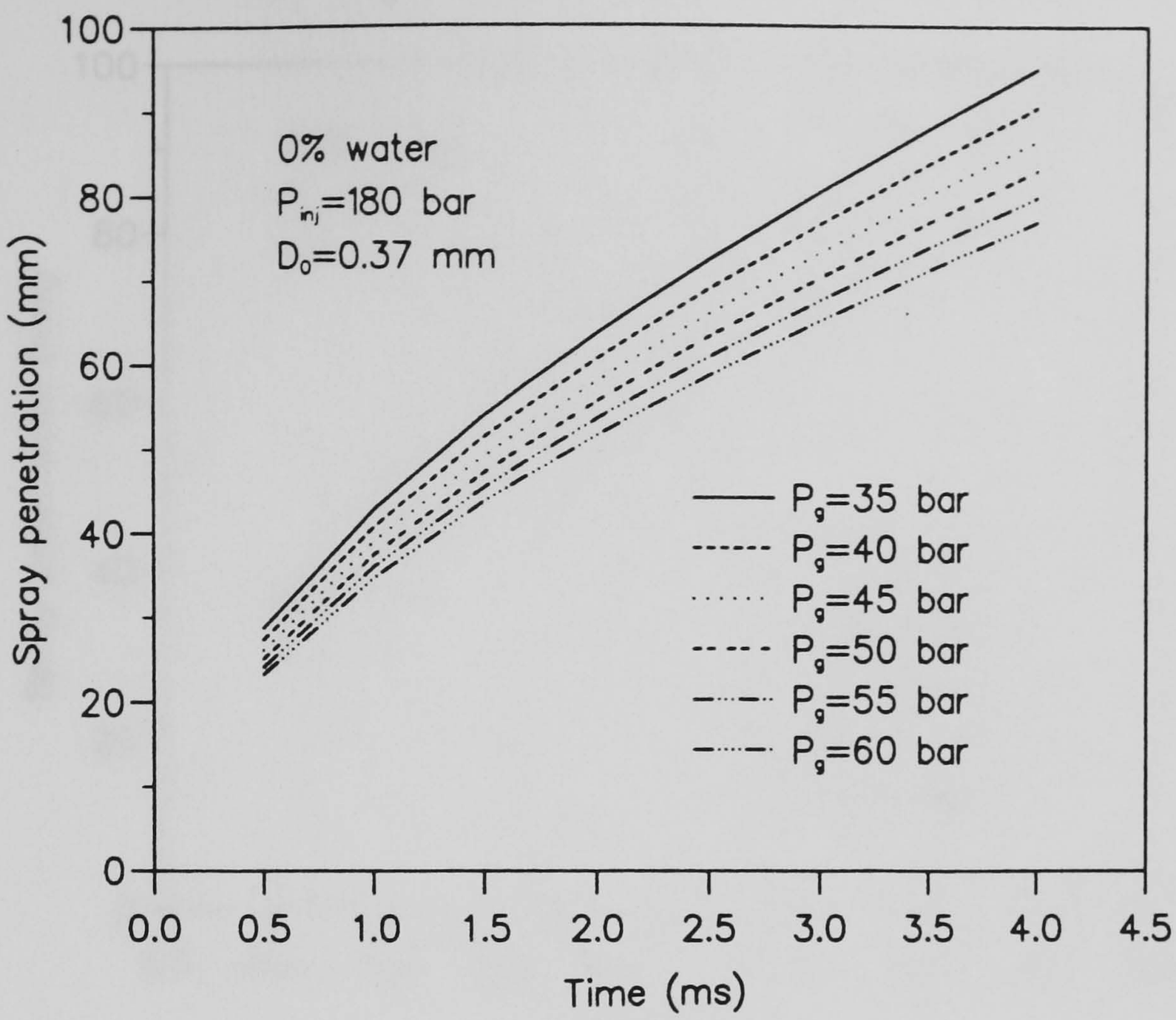

Fig. 6.3(1) Spray penetration (model 2) at different gas pressures

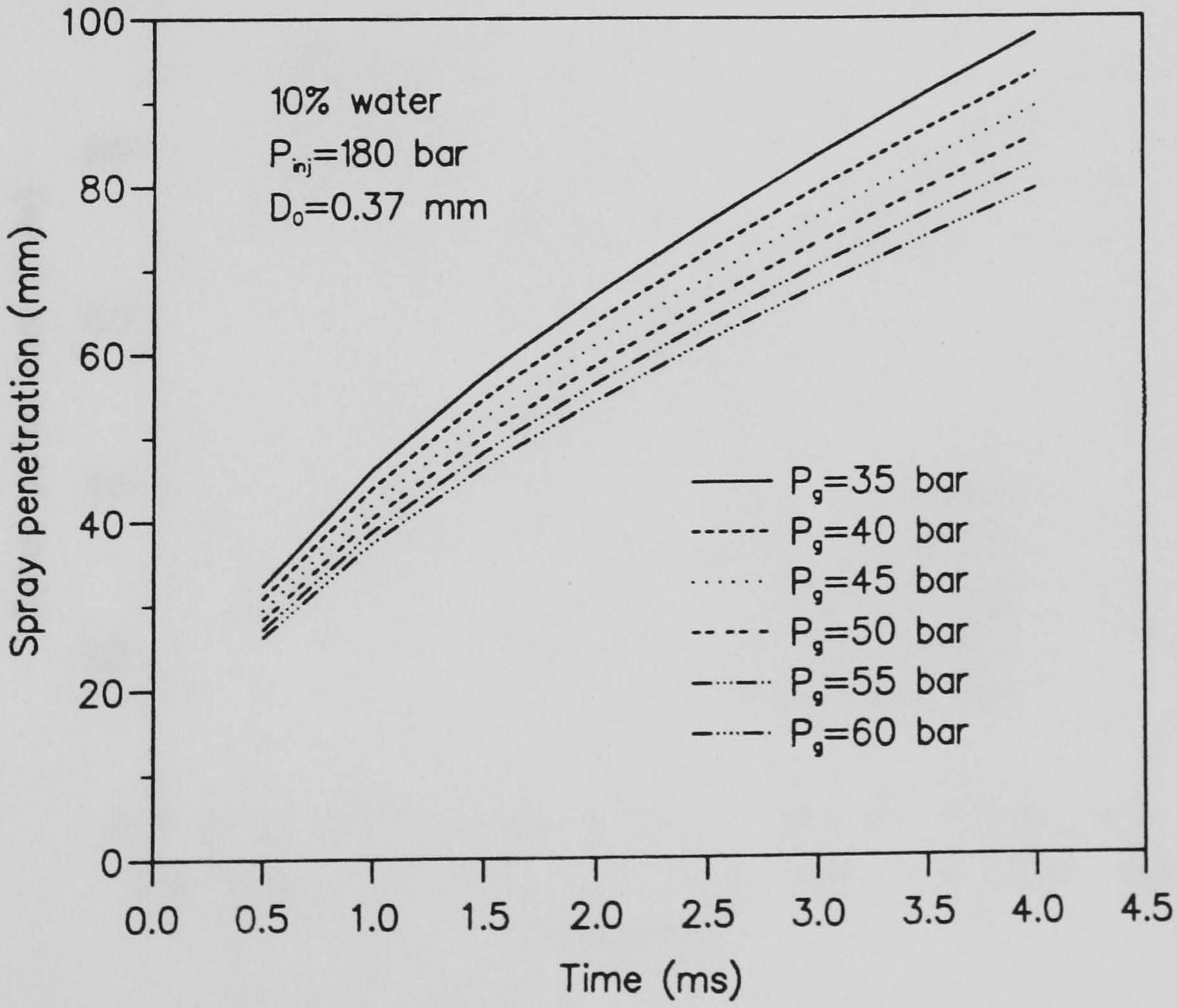

Fig. 6.3(2)

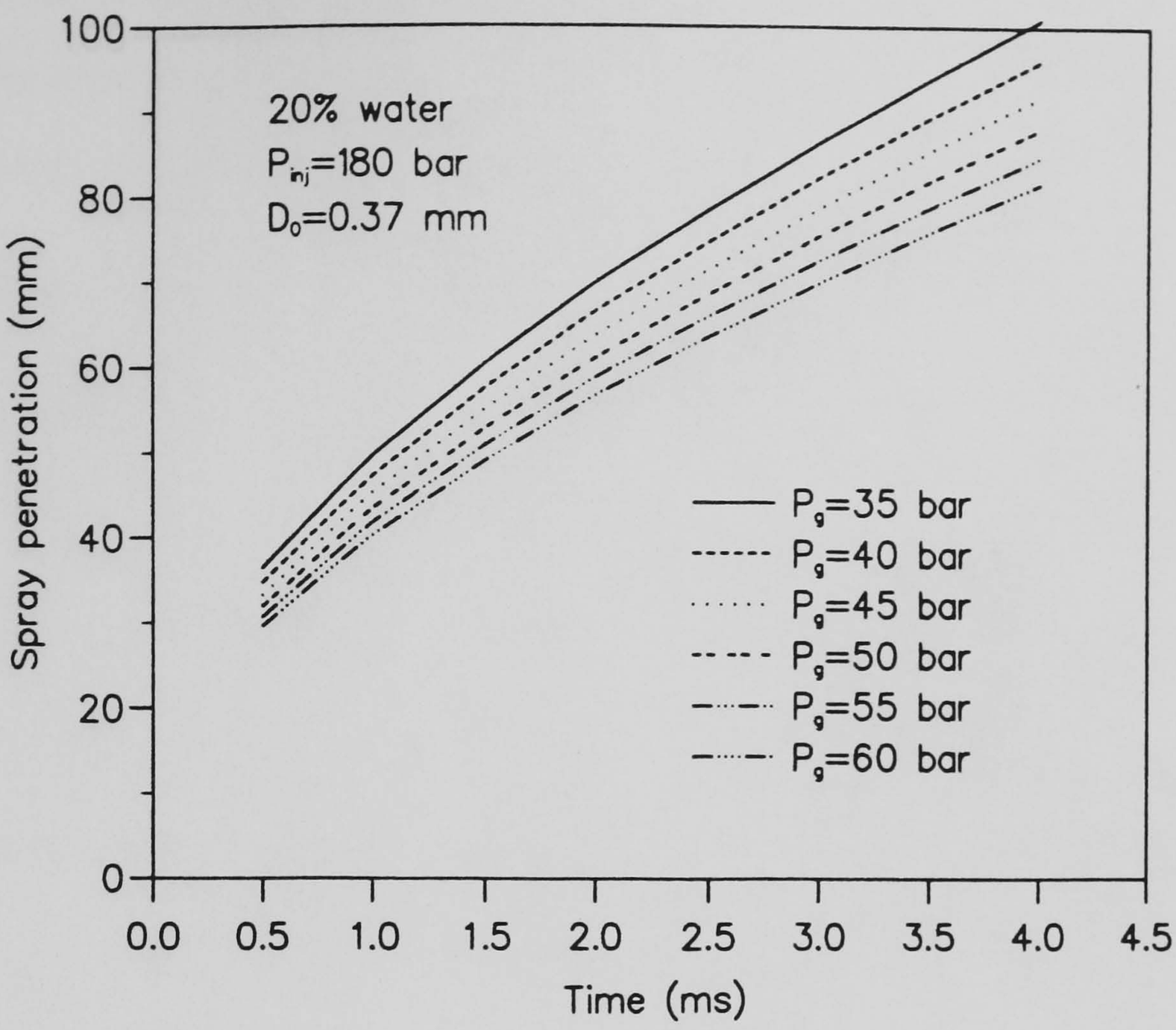

Fig. 6.3(3)

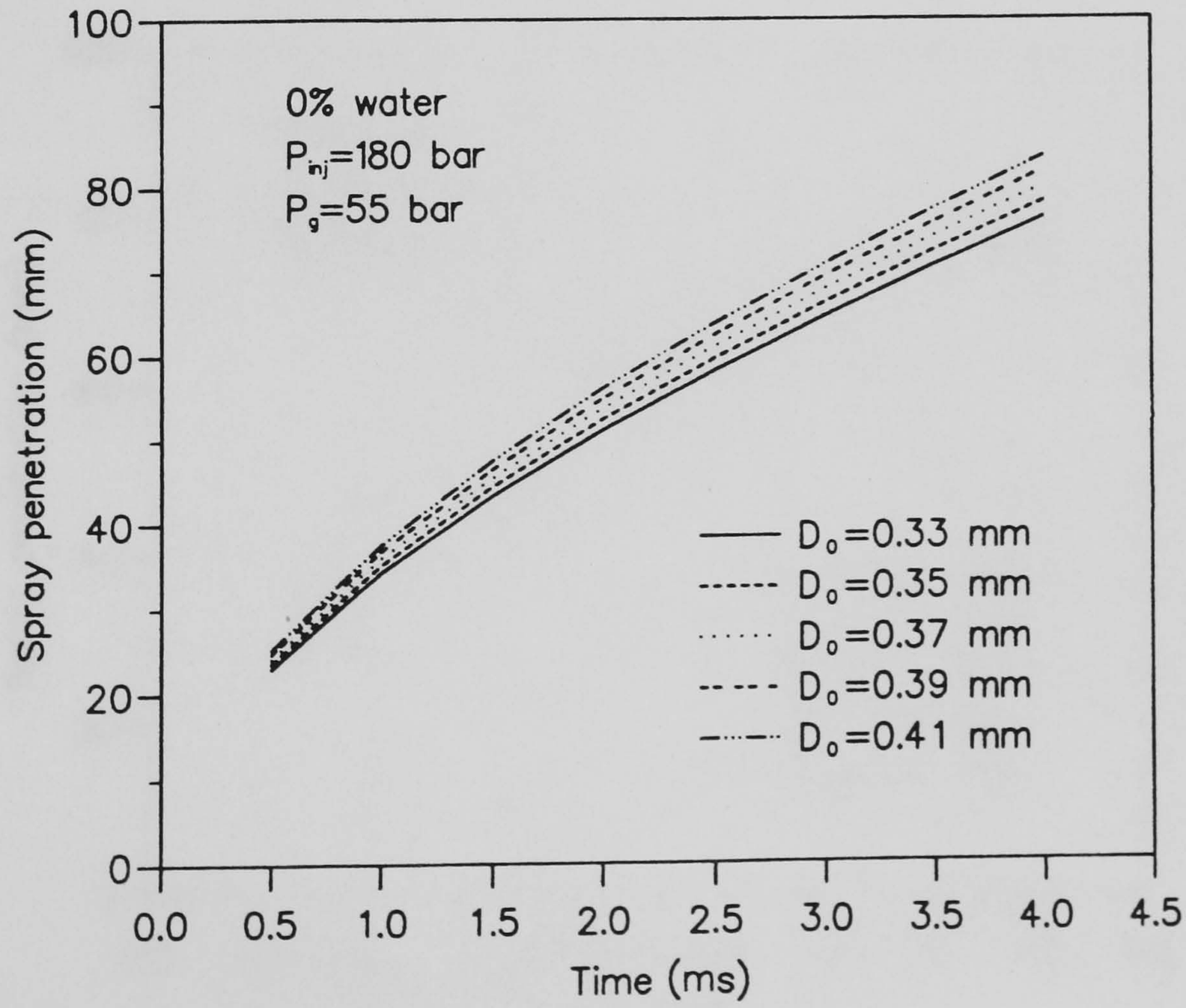

Fig. 6.4(1) Spray penetration (model 2) at different nozzle diameters

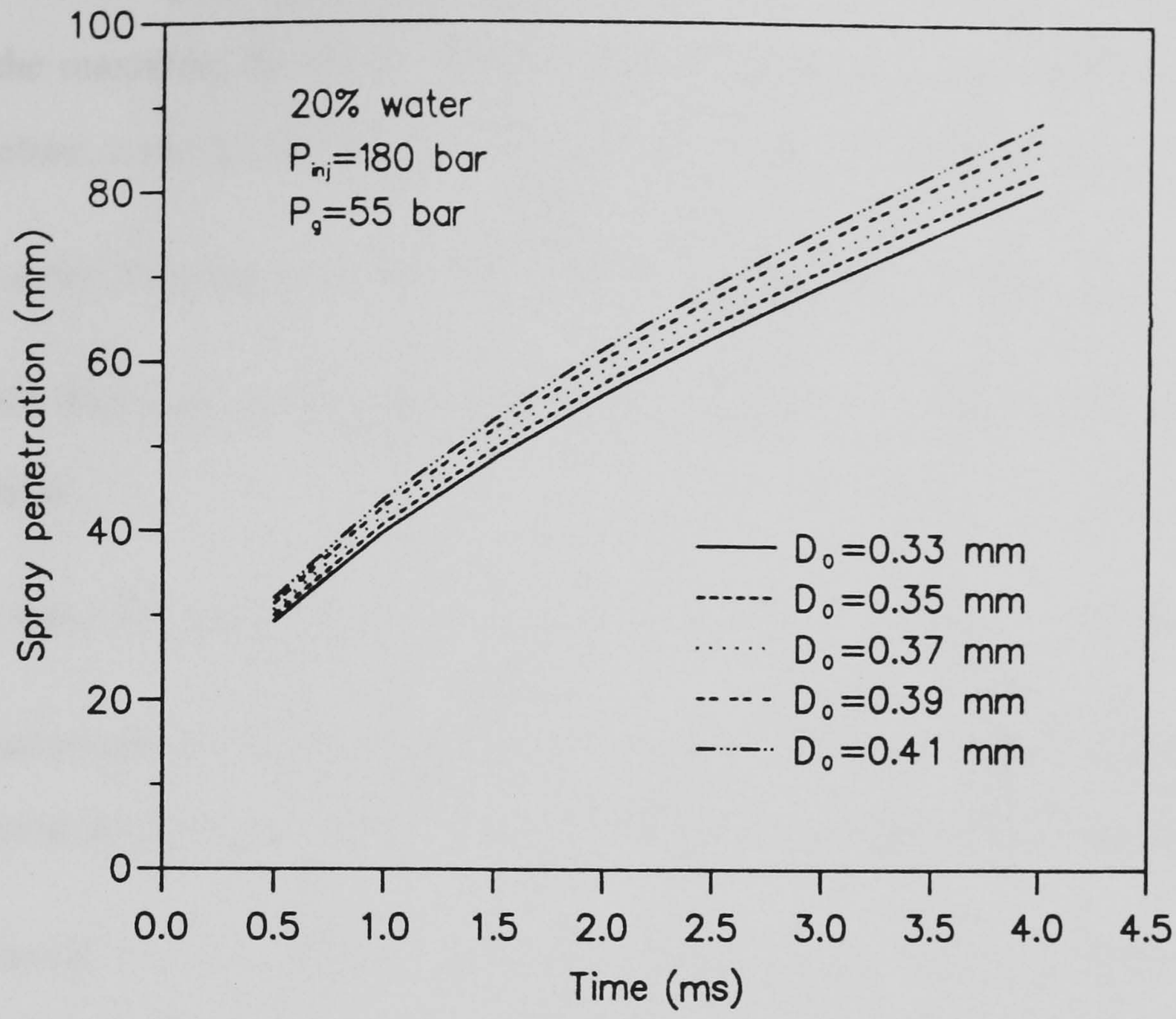

Fig. 6.4(2)

Fig. 6.4(3)

Fig. 6.5 is the spray angle comparison between the model and the test results. It shows that the maximum deviation of the test from the model is about half of one degree. Therefore, it can be said that the model gives a 'good' fit to the experimental results.

Figs. 6.6(1-3) present the effect of each test parameter on the spray angle.

Fig. 6.7 illustrates the comparison between model and test curves for the Sauter Mean Diameter.

Figs. 6.8(1-4) present the effects of test parameters on the Sauter mean diameter.

The set of curves shown in figures 6.9(1-3) are the comparisons of the model with test results on droplet diameter distributions. The model is the Nukiyama-Tanasawa model.

The model fits the emulsified fuel curves with some acceptable deviations. For the pure fuel (Fig. 6.9(1)), the deviation is 15.37%. This is because the test curve is very steep at the small size droplet end (see the stair-case diagram Fig. 5.14(a)). The model simulates the slope/tangent at the very beginning of the curve, which results in a large deviation at the top of the curve. The model only gives the general tendency of the curves for all test conditions. It does not simulate the oscillations of the test curves. This means that the four control parameters (A, B, α and β) used in the N-T droplet distribution are not enough to simulate the oscillations of the test curves.

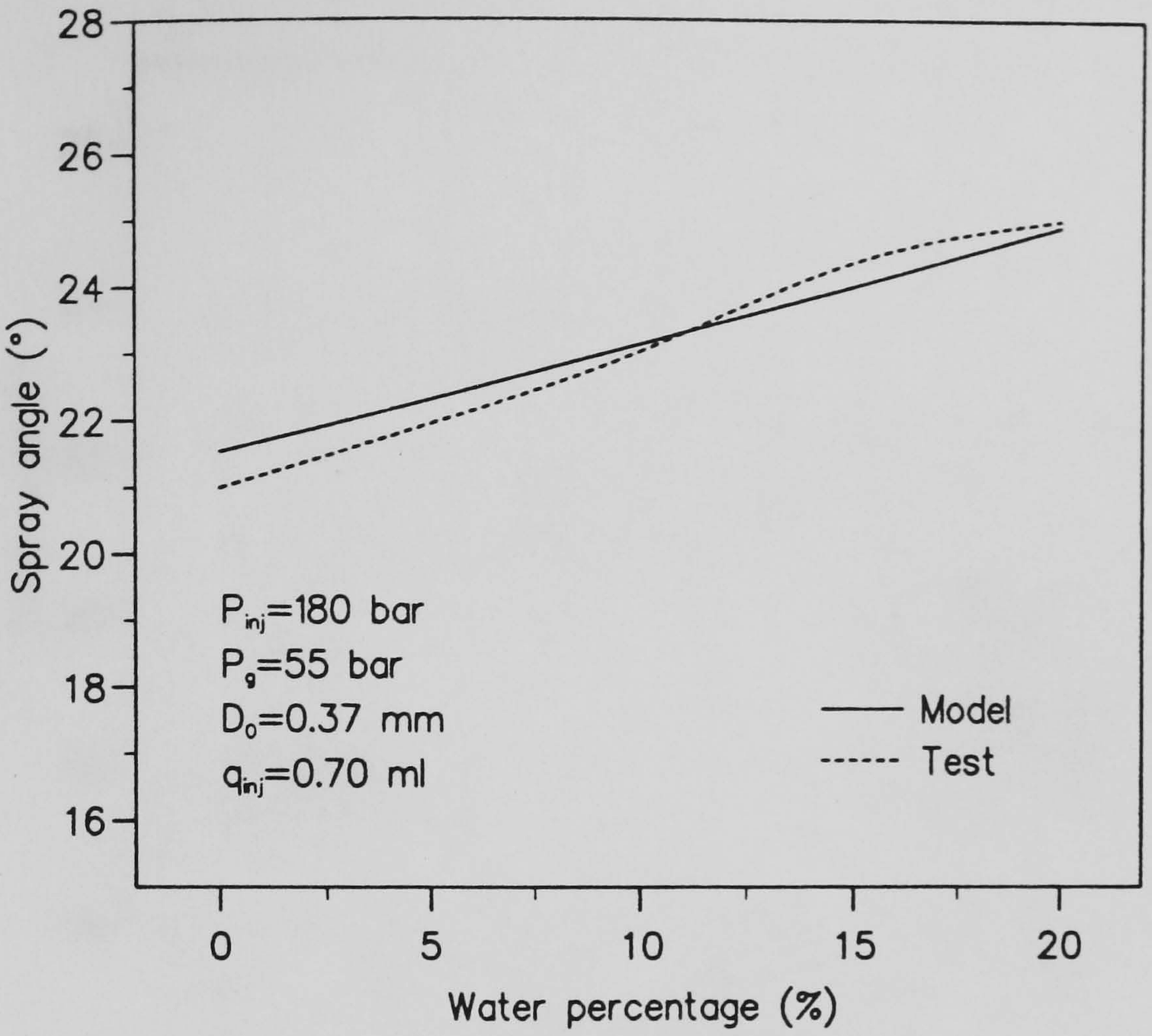

Fig. 6.5 Comparison between model and test results for the spray angle

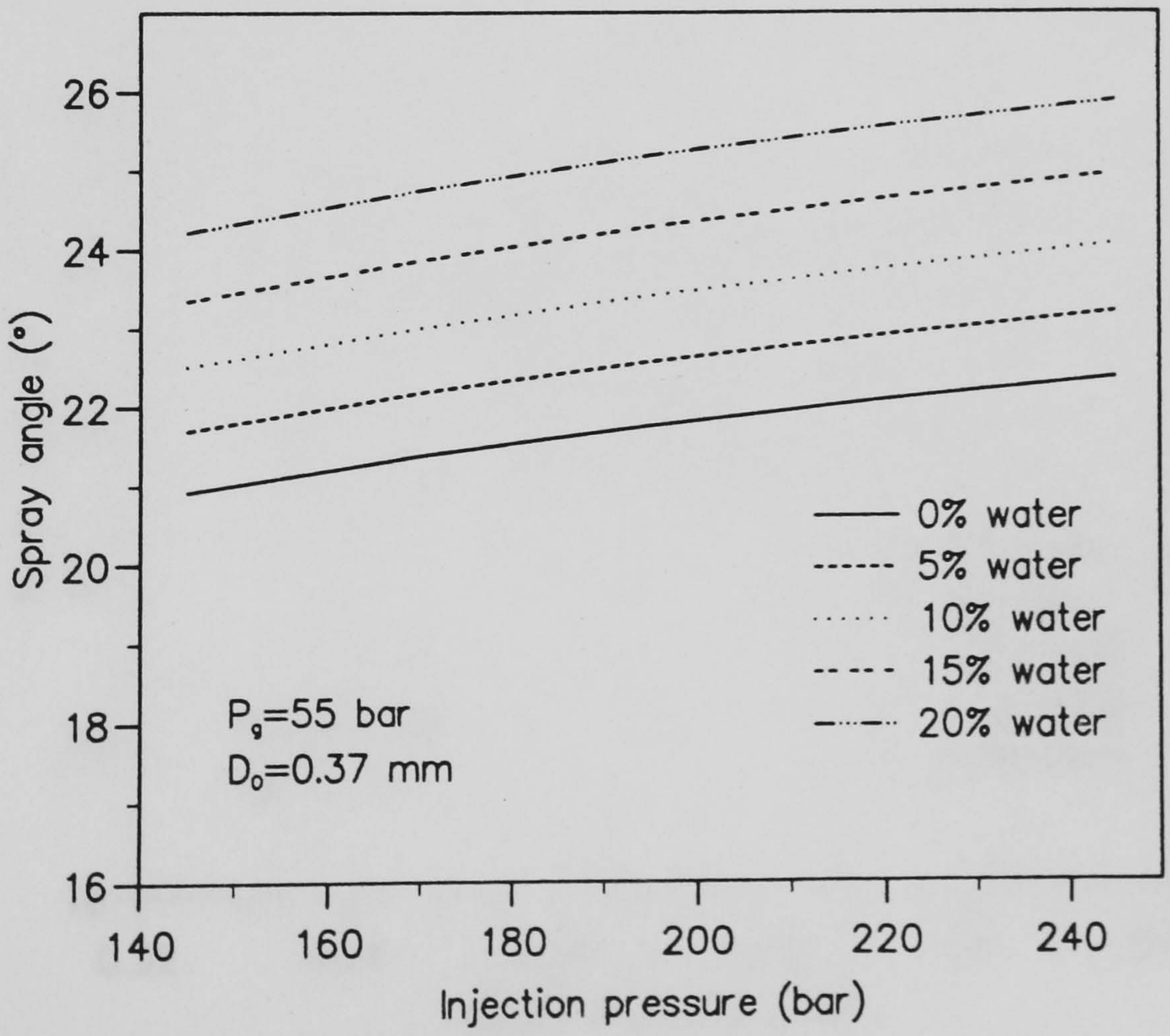

Fig. 6.6(1) Spray angle changes with different injection pressures

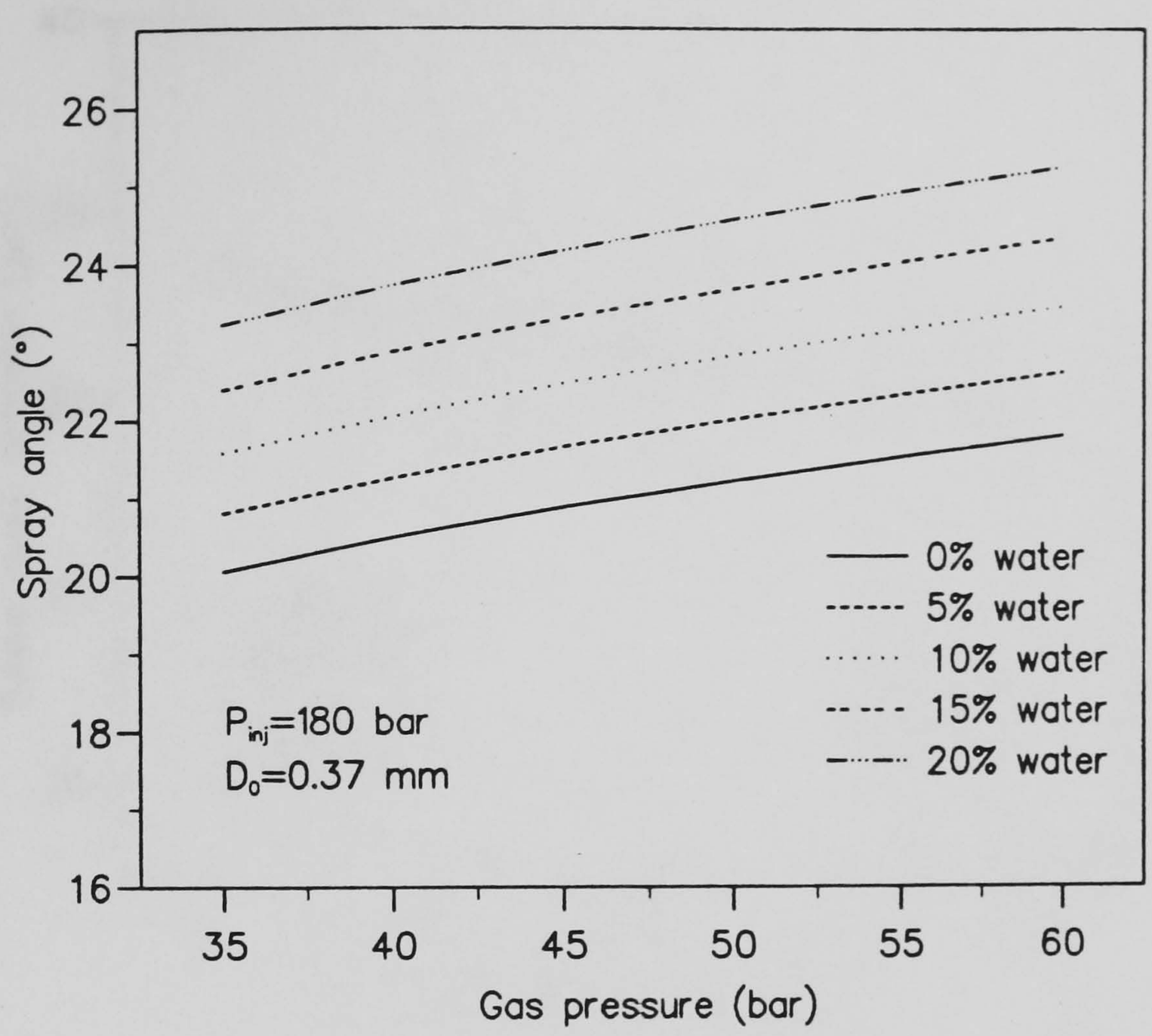

Fig. 6.6(2) Spray angle changes with different gas pressures

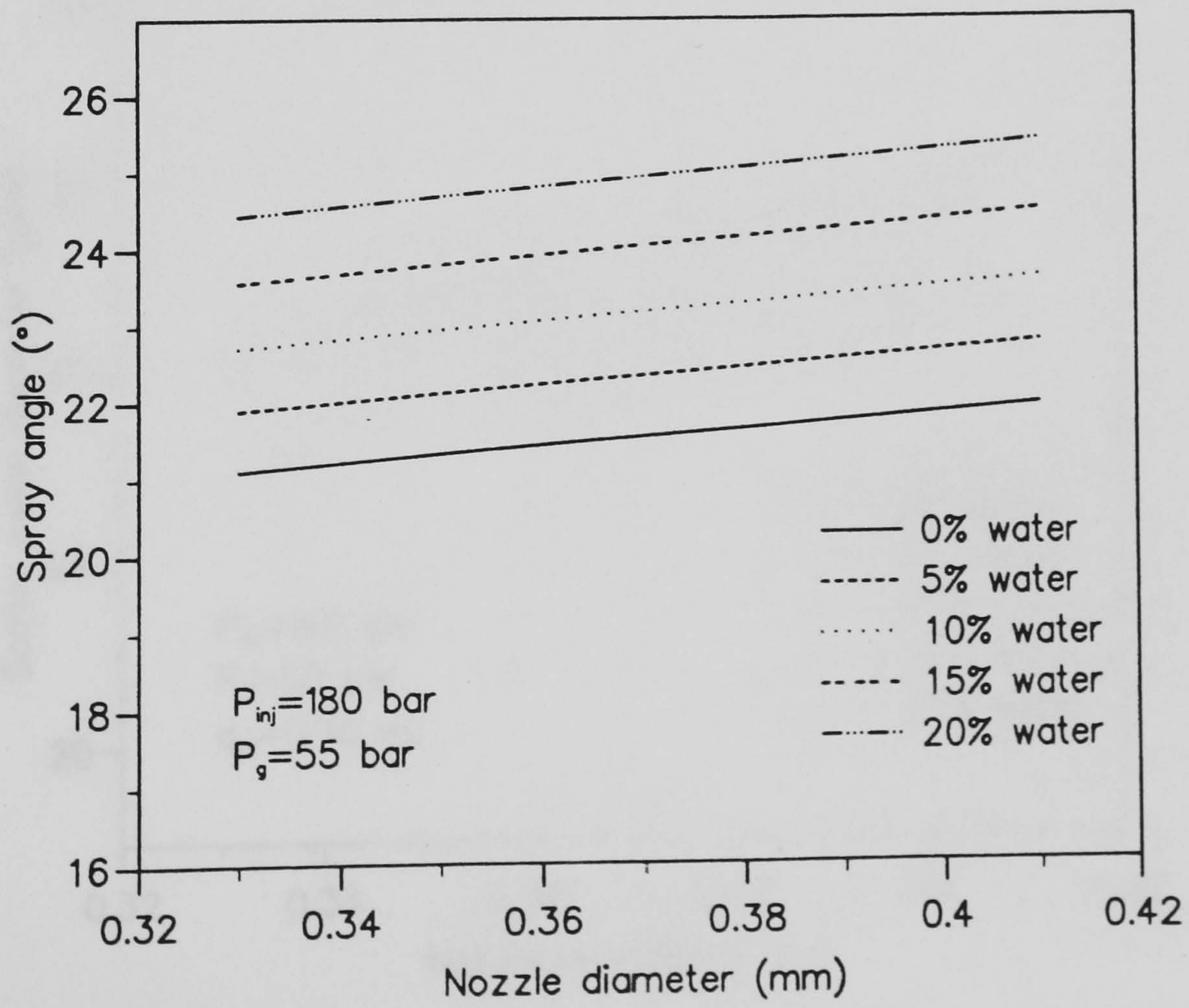

Fig. 6.6(3) Spray angle changes with different nozzle diameters

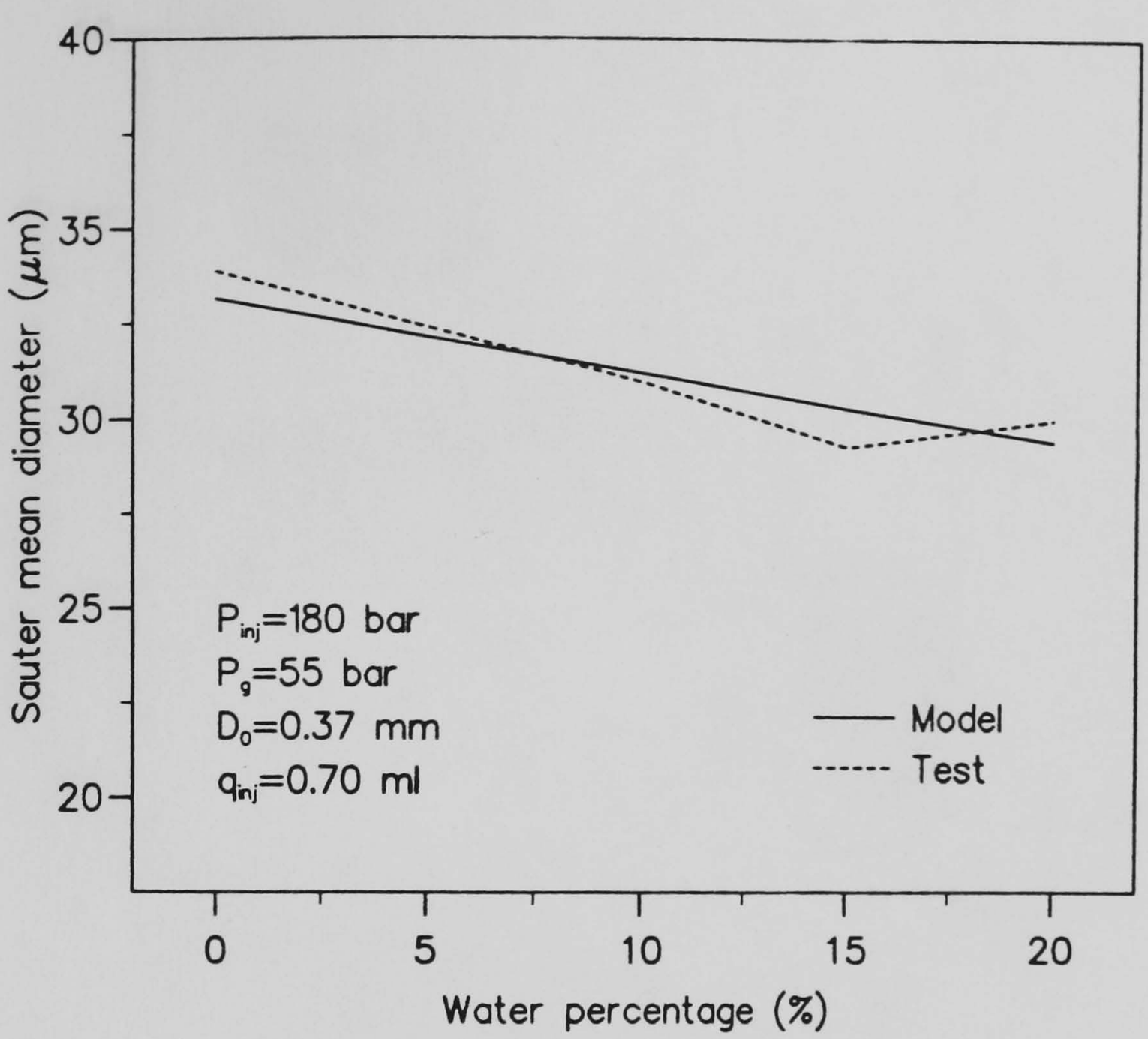

Fig. 6.7 Comparison between model and test curve for the Sauter mean diameter

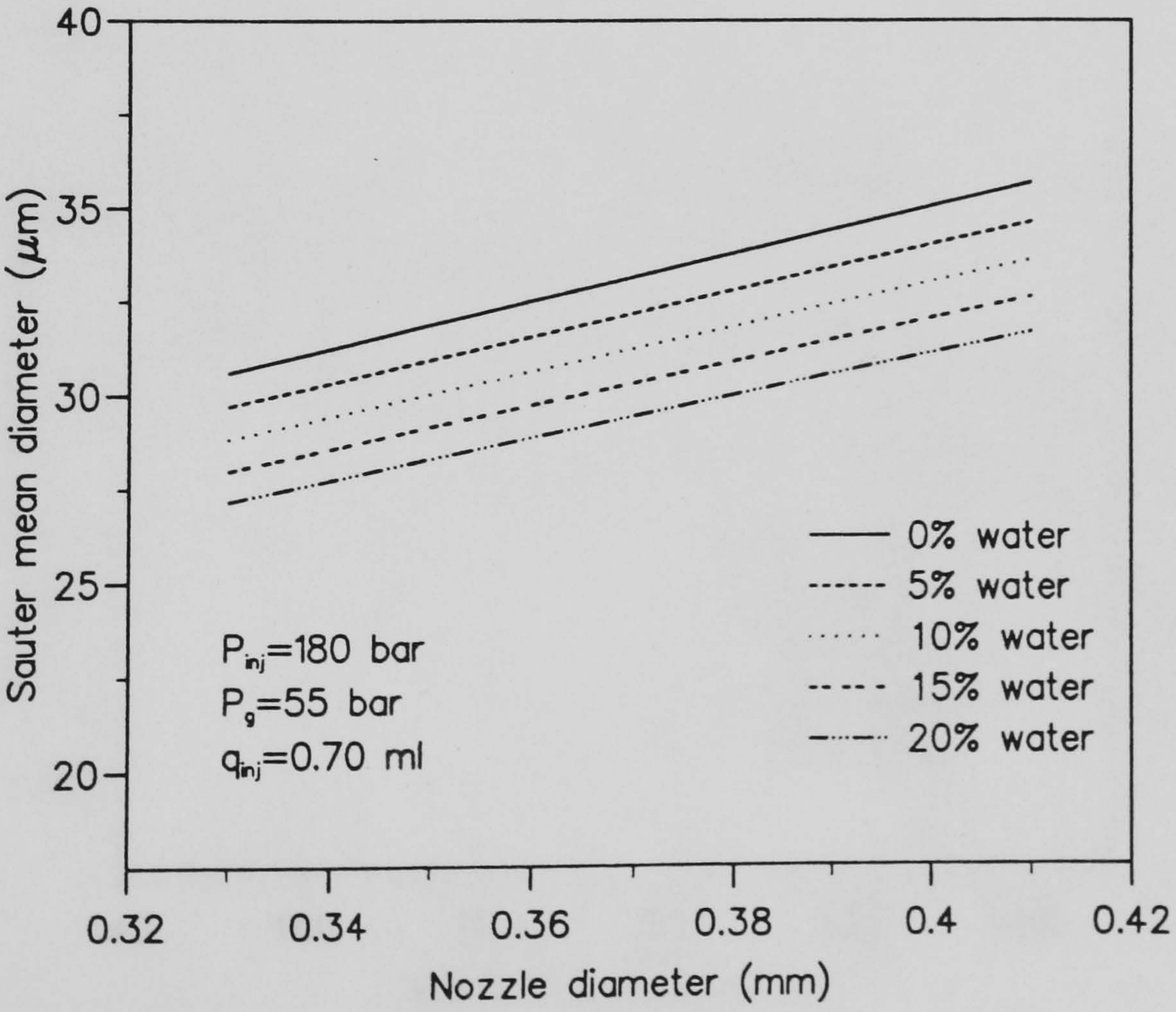

Fig. 6.8(1) Curves of Sauter mean diameter vs. nozzle diameter

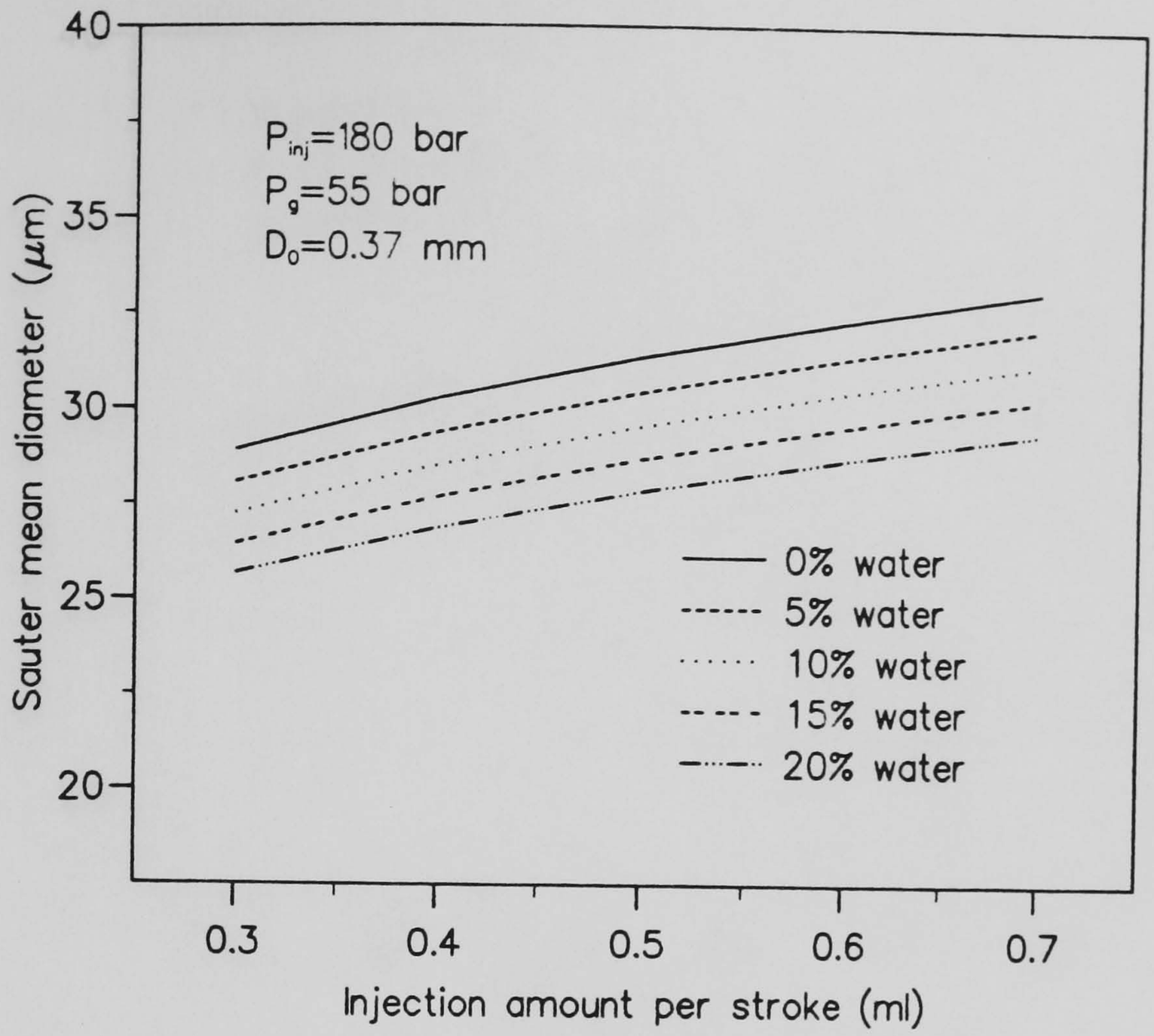

Fig. 6.8(2) Curves of Sauter mean diameter vs. injection amount

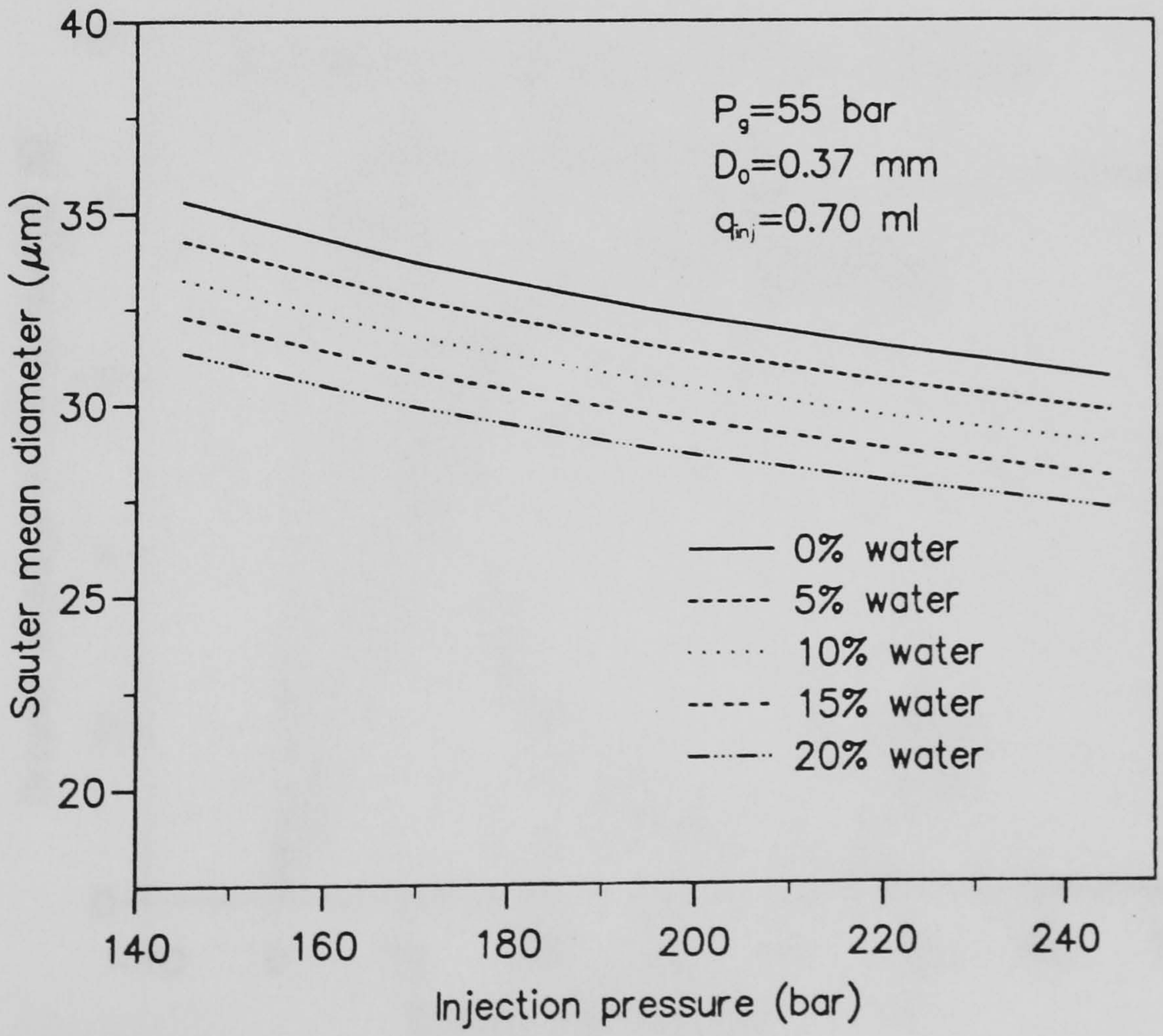

Fig. 6.8(3) Curves of Sauter mean diameter vs. injection pressure

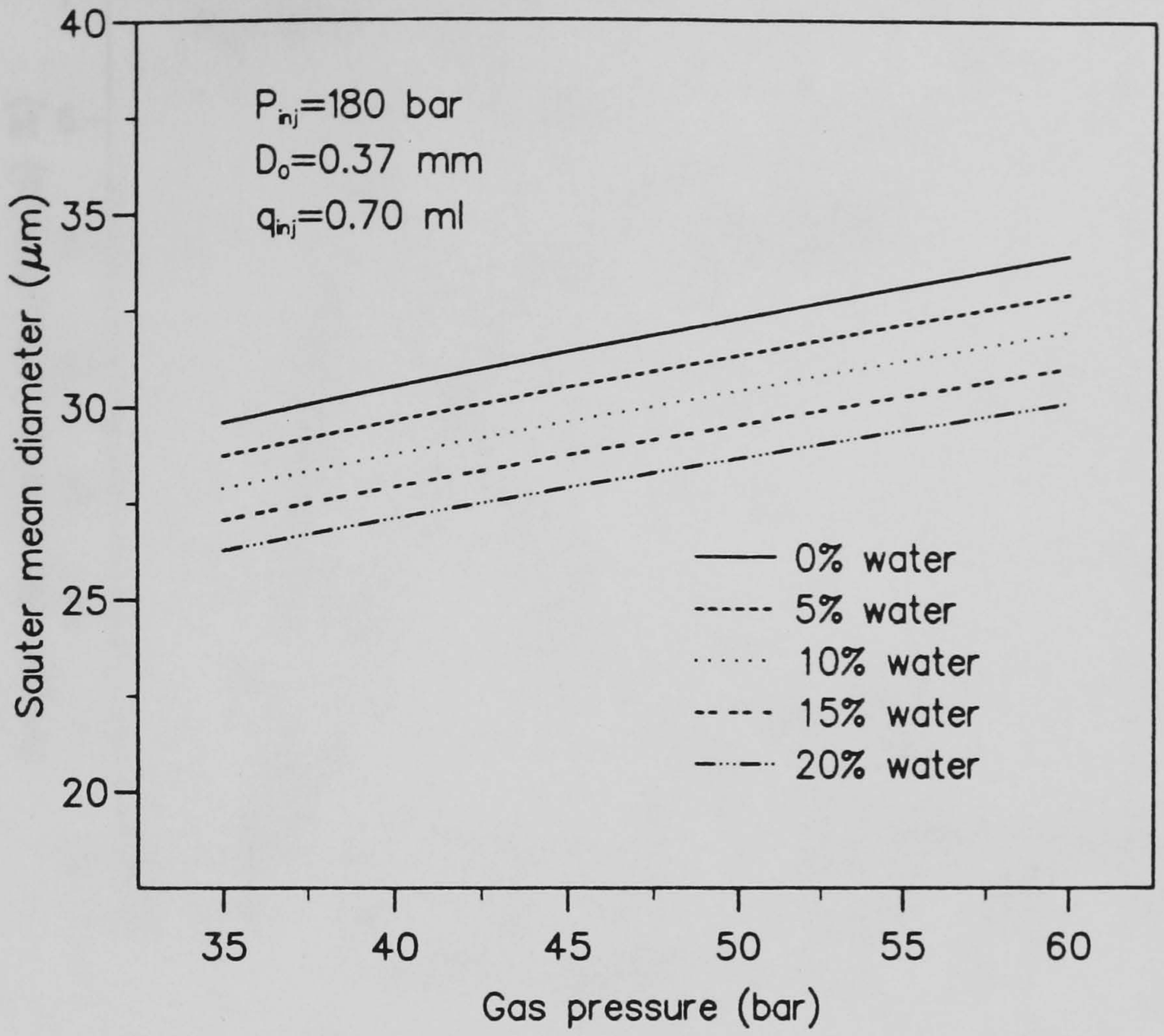

Fig. 6.8(4) Curves of Sauter mean diameter vs. gas pressure

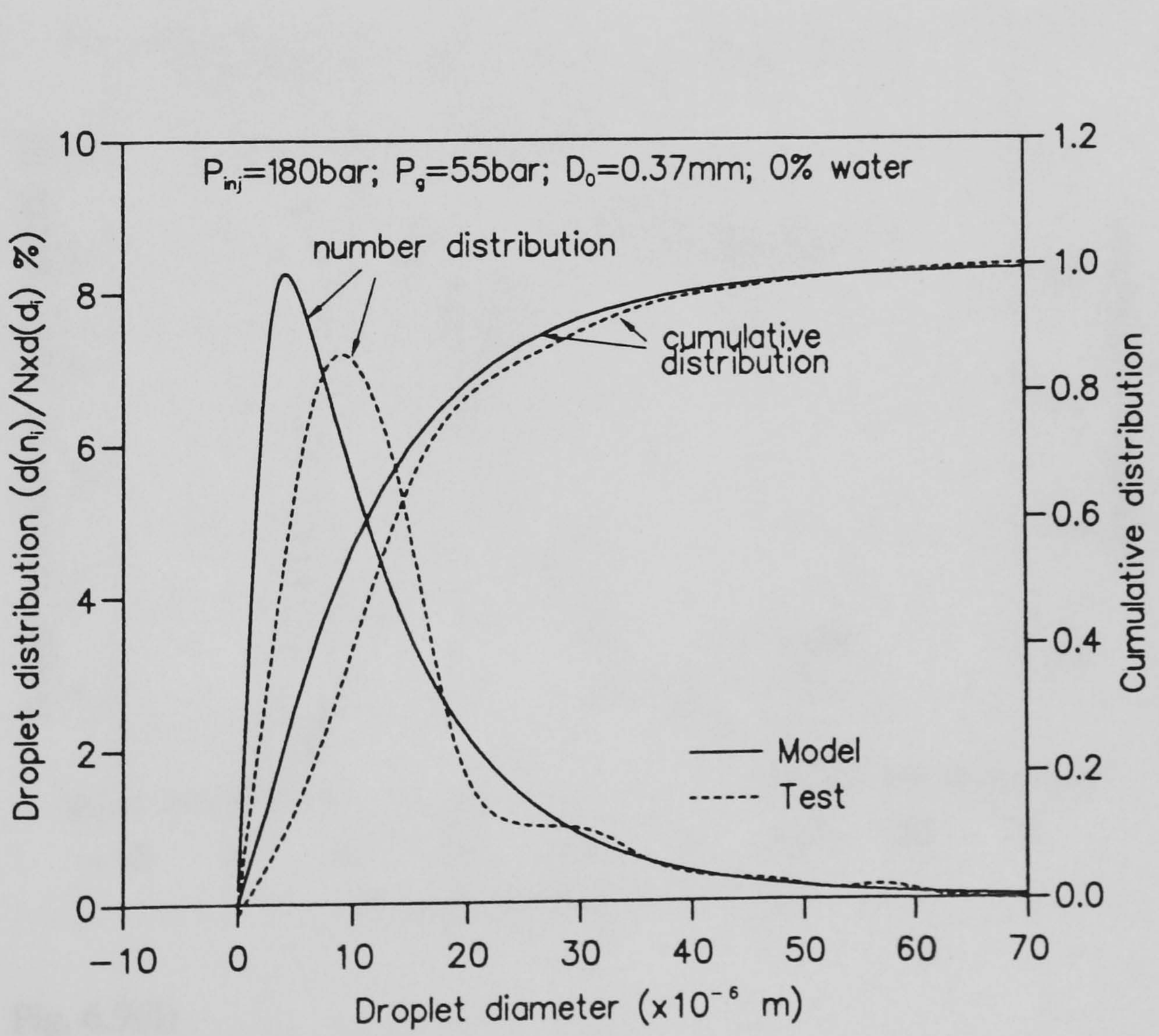

Fig. 6.9(1) Comparison droplet distributions between model and test curve

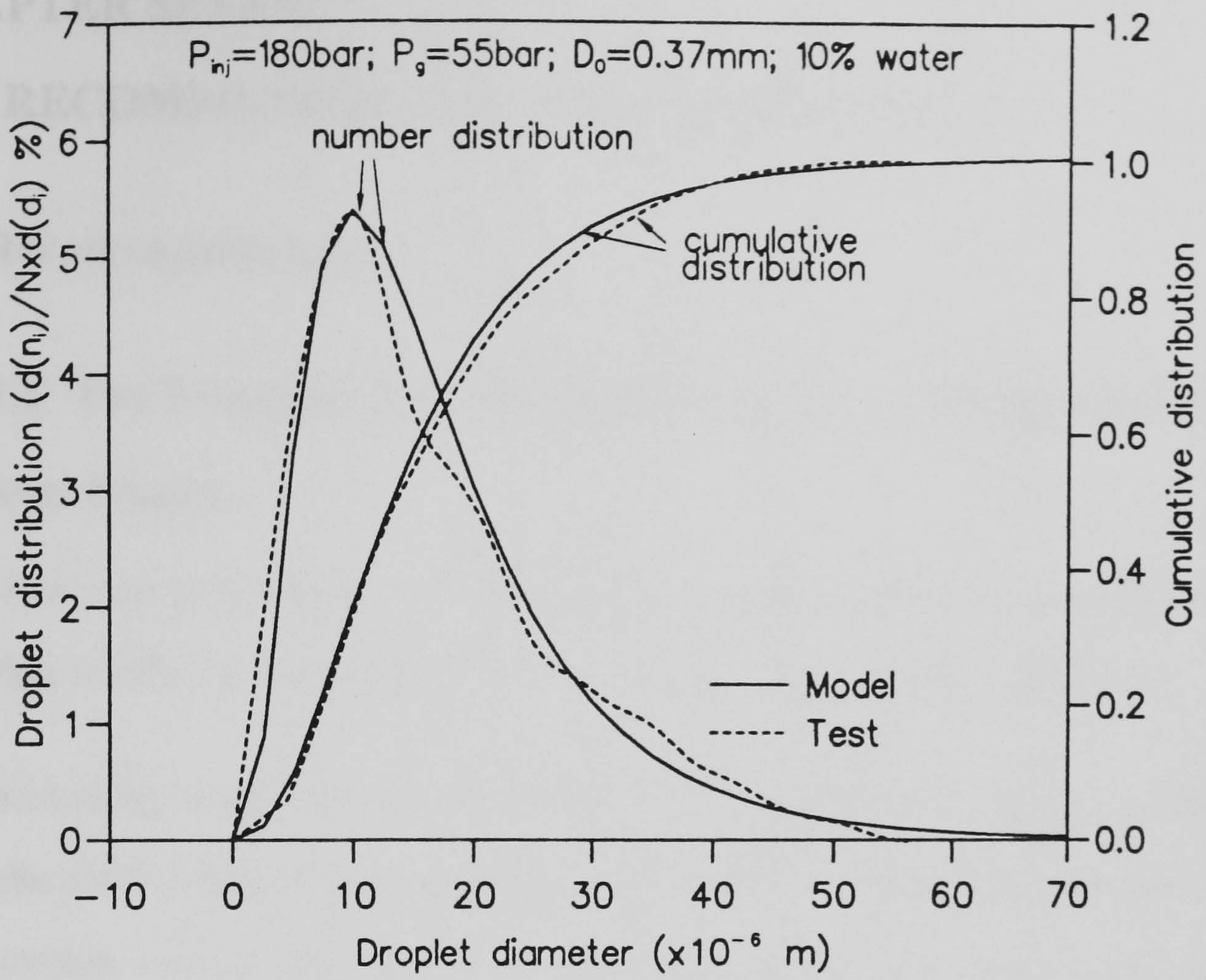

Fig. 6.9(2)

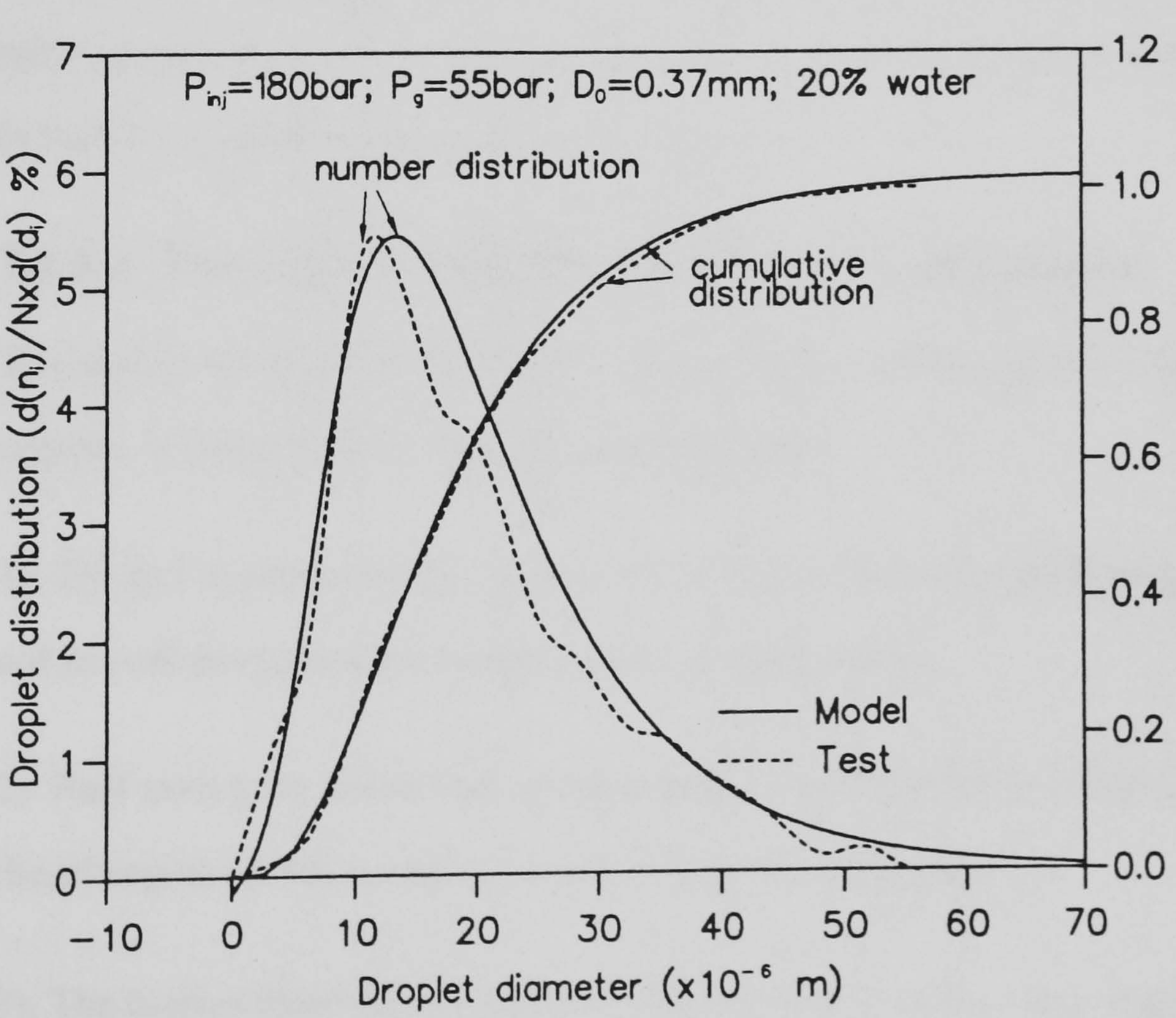

Fig. 6.9(3)

CHAPTER SEVEN:

RECOMMENDATIONS AND CONCLUSIONS

7.1 Recommendations

7.1.1 The Prospects For The Application Of Emulsified Fuels To Diesel Engines

To look into the future use of W/O emulsions in diesel engines, it is worthwhile to review briefly the past applications which have been stated in Chapter one.

The investigation of burning emulsified fuels in diesel engines was a favoured topic in the 1970's and at the beginning of the 1980's. The initial purposes of this utilisation were to reduce the engine fuel consumption and to use heavy oils on board ships, largely stimulated by the energy crisis at the beginning of the 1970's. In the meantime, the studies also found that the use of emulsified fuels could reduce harmful emissions and result in a cleaner exhaust system. Nowadays, emulsified fuels have been practically used on board ships.

7.1.1.1 The Use Of Emulsified Fuels For Road Vehicles

The application of emulsified fuels to road vehicles, which are driven by diesel engines, is more difficult. The reasons for this are:

1). The techniques of providing emulsified fuels to the road vehicle engines are not so well developed for the on board ship applications.

2). Fuel saving for small high speed engines, especially for in-direct injection diesel engines is not so significant as in large diesel engines.

3). The current emissions control methods can meet the emissions regulations.

The first of these is the main obstruction for road vehicles to use emulsified fuels. The technical problems rise from several aspects:

a). How to ensure what is injected into the engine combustion chamber is a homogeneous mixed emulsion rather than separated water and fuel. The separation process of water from fuel oil is very quick, and only takes seconds. The emulsifier should be fitted immediately before the high pressure pump, and is probably limited by the space available.

b). The ideal water content varies with engine loads and the loads of road vehicles change constantly. Even though a quick response flow rate controller is available, the fuel trapped in the fuel line from the emulsifier to the injectors needs time to be consumed or replaced by the 'new' emulsion. In other words, probably the engine will always run with non optimum water content emulsified fuel.

c). The space available for arranging the emulsifier and water tank may be limited.

The second point concerns the fuel consumption and its cost. Compared with a ship or a large power plant, a road vehicle's fuel consumption is very small. The small percentage fuel saving would seem to be not worthwhile to balance the cost of equipment and the difficulties in providing the emulsified fuels

As discussed in the previous chapters, the use of emulsified fuels in diesel engines results in a large reduction in harmful emissions, except those of the hydrocarbons. From this point of view, it seems that the profit for the reduction of harmful emissions is more than that of the fuel saving. However this has not been sufficiently notified by the automotive manufacture industries. They would not like to invest the extra cost for getting further clean exhausts, since the current methods for controlling the engine emissions can satisfy the requirements of the emissions regulations. At present, the U.S.A. has established new emissions regulations US 1994, in which the emissions specifications are more rigid than the present one. Fig 7.1 illustrates todays development status of a quiescent

combustion system [75] for particulate emissions. In the emissions regulations US 1994, the requirement of NO_x emissions for the heavy-duty trunks is less than 5 g/bhp-h.

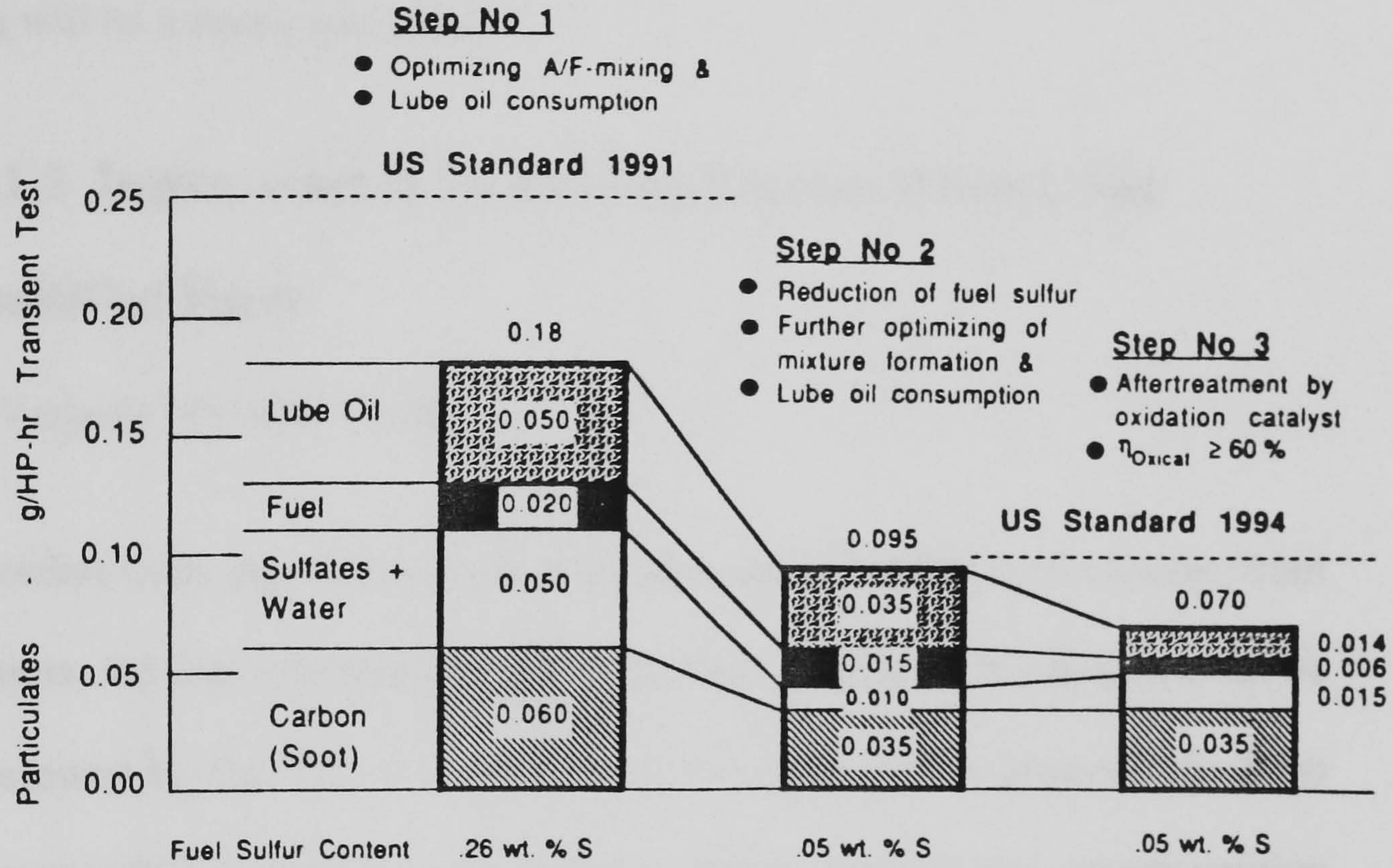

Fig 7.1 US 1994 particulate emissions regulations for HD trucks

As discussed in 5.6.2.2, efforts have been concentrated on improvements to the injection systems and combustion chambers to meet the emissions regulations of US 1994. It is reported that these approaches just about meet the regulatory requirements. However, the requirements for environmental protection are being continuously increased and the intervals of renewing emissions regulations are shorter and shorter. It has been predicted [75] that beyond 1994, further emissions reductions may be required for the conflicting components of NO_x and HC. To meet the further requirements of environmental protection, alternative fuels for diesel engines have been recommended for the purposes of engine emission reductions and energy source saving.

If the problems mentioned above, for using emulsified fuels for road vehicles, can be solved or partially solved, then the utilisation of emulsified fuels will be more acceptable to the automotive manufacturers. Vice versa, if the emissions regulations become even more restrictive, it will force the automotive industries to invest in techniques or alternative fuels for diesel engines where emulsified fuels will be a strong competitor.

7.1.1.2 Improvements To Existing Engines When Using Emulsified Fuels

1). Variable Injection Timing

According to the injection spray characteristics of emulsified fuels obtained from the tests, the fuel injection rate (I.R.) and heat release (H.R.) diagram can be represented by Fig. 7.2. It is understood (see discussion in previous chapters) that emulsified fuels possess the features of high injection rate, longer ignition delay and fast combustion when compared to fuel oil. The longer ignition delay results in a higher heat release rate at the pre-mixed (rapid) combustion phase and a higher combustion pressure in existing engines. The characteristics of high fuel injection rate and a fast combustion process allow the engine to employ the method of injection timing retard to lower the maximum cylinder pressure. Due to the fast and improved combustion process of emulsified fuel, the late fuel injection would not cause poorer combustion, low engine thermal efficiency and high exhaust temperature, as happen when an engine burns fuel oil.

As shown in Fig. 7.3, with a moderate injection timing delay, the maximum cylinder pressure (P) can be lowered and combustion may finish at about the same time as fuel oil or even earlier.

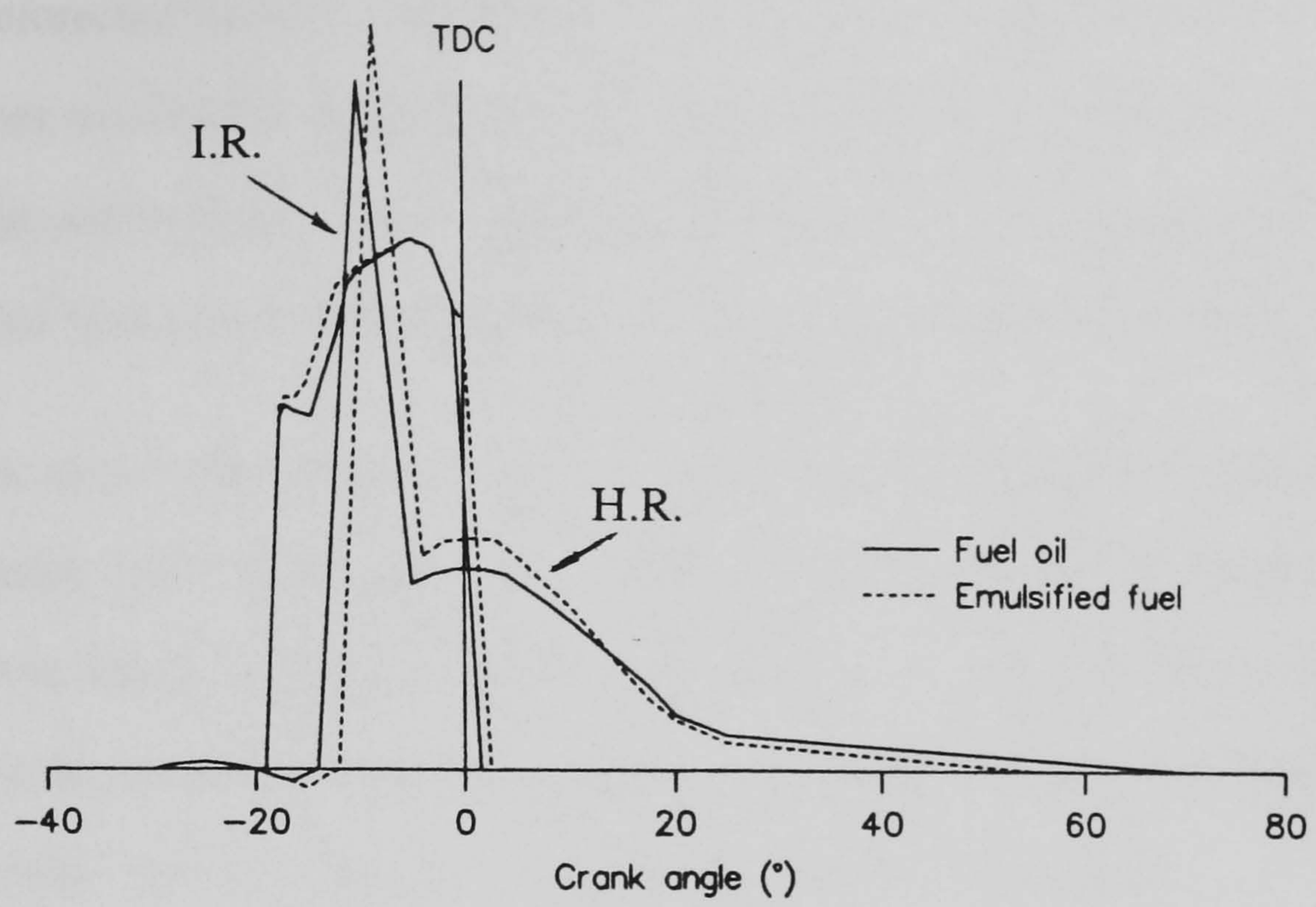

Fig. 7.2 Comparison of injection rate and heat release rate between emulsified fuel and fuel oil

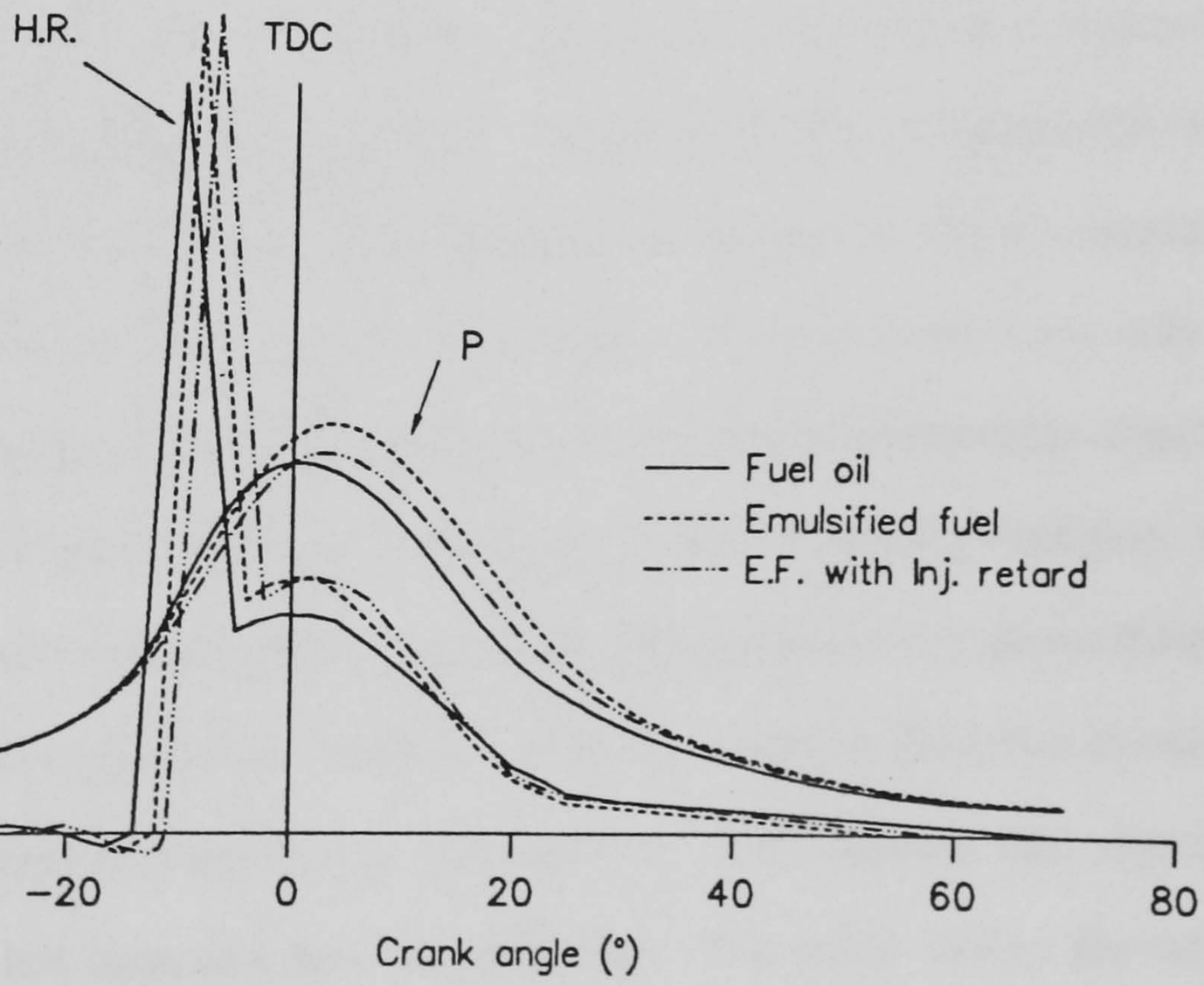

Fig. 7.3 Heat release and cylinder pressure diagram of emulsified fuel with injection timing retard

The lowered combustion temperature produces a significant reduction in NO_x emissions and the presence of water in combustion also curbs NO_x formation. Therefore, the use of emulsified fuels with injection timing retard in the existing engines would reduce the NO_x emissions dramatically and would not lead to poorer combustion. This is particularly beneficial for turbo-charged diesel engines because turbo-charged engines have high mechanical and thermal loads.

In the above discussion, if the term "injection timing retard" is replaced by "variable injection timing", i.e. to use emulsified fuels accompanied with the variable injection timing device in existing engines, that would effectively solve the problems of high mechanical load and emissions when the engine runs at high loads and also improve the engine performance at low loads.

2). Improvement Of Injection Systems

The existing fuel injection systems are not designed for use with emulsified fuels. The volumetric calorific value is lowered by the presence of water. To apply emulsified fuels to existing engines and keep the engines generating the same power as when burning fuel oils, the water content added to fuel is limited by the existing injection pump and systems. Therefore the fuel pump and injection systems should be remodelled with a larger injection capacity, and it is necessary to strengthen the cam driving systems as well. The cam should not only be designed to enlarge the pump delivery capacity, but also to optimize the injection systems in order to match the characteristics of emulsified fuel atomisation. For example, the use of emulsified fuels in existing engines causes high mechanical loads due to the long ignition delay. The pump should be designed to reduce the fuel injection amount during this period. This sounds like injection timing-retard, but basically they are different. The latter moves the whole injection rate profile towards T.D.C.. The former is optimized with a different injection rate profile, i.e. decreased injection rate during the period of ignition

delay and increased injection rate after combustion start. For existing engines, the increase in the fuel amount injected after ignition start results in a worse combustion and a low thermal efficiency, since the fuel injected during this period can not obtain sufficient air for combustion (it is surrounded/blocked by the flame gas). When emulsified fuel is used, the situation is different. As emulsified fuels possess larger atomising momentum, it may penetrate and break up the flame regions, reaching the fresh air in the areas "remote" from the injector. Therefore this provides a possibility to permit the late injection of a large fuel amount and this would not cause poorer combustion as would be the case with fuel oil.

3). Reorganisation Of In Cylinder Air Swirl

In medium or small size diesel engines, there is normally a created swirl inside the cylinder to promote the fuel-air mixture formation and fully utilise the limited air for combustion. This is accompanied by a sacrifice of engine thermal efficiency. In order to minimise the thermal loss caused by the swirl, the swirl strength can be reduced when the engine is designed for burning emulsified fuels. The increased air suction effect of emulsified fuel can compensate the effective loss of fuel-air mixture formation caused by the decreased swirl strength.

4). Engine Wear And Erosion

When a diesel engine burns emulsified fuels, the wear and erosion (including cavitation erosion) in fuel injection systems, cylinder liners and piston rings may be increased. When sulphur content in the fuel is high, the sulphides may be formed in the engine exhaust system. There have been only a few reports about the wear and erosion in engines when using emulsified fuels. In reference [3], after 1000 hours running of a test engine, it was found that the wear rates for emulsified fuels tests were nearly the same as the "dry" fuels for the exhaust valve stem, exhaust valve guide, piston skirts, piston compression rings, and the

connecting rod bearings. The cylinder liner wear was heavier than the engine using dry fuel. Two possible heavy wear and deposit areas were identified: a). cylinder liner wear with associated blow-by; b). fuel injection equipment durability. To the author's knowledge, there has been no accurate measurement report about the wear of production engines by emulsified fuels except for visual inspection. Therefore, it is necessary to collect the actual results in test engines and to establish the counter-measures for the mentioned problems.

To summarise the above discussion, the author would like to recommend use of a variable injection timing system (or injection timing retard) for existing engines to burn the emulsified fuels. In fact, Japanese researchers [8] have found that the use of emulsified fuels with injection timing retard could effectively control the engine emissions at high loads, especially for the NO_x emissions and the engine fuel consumption was not bad.

7.1.2 Future Research Work On the application Of W/O Emulsified Fuels In Diesel Engines

Apart from the technical problems for the practical use of emulsified fuels in diesel engines, there still exist other problems which remain to be studied.

1). Real Engine Test

At present, the study of engine performance using emulsified fuels has been reasonably comprehensive, including ship board applications. It has been generally considered that the benefits to engine performance of using emulsified fuels are brought about by the emulsified fuels atomisation and combustion. Some tests on atomisation and combustion have been carried out in constant volume chambers, although they have not necessarily been completed. However, the work done on atomisation studies concerns more than just the combustion. Combustion studies have been limited to the combustion phenomenon observation. No quantitative

description has been given, since the mechanism of hydrocarbon combustion itself is not yet fully understood. What is more, the results obtained from the above tests do not fully match real engine working conditions.

Till now, no one has undertaken tests of emulsified fuels atomisation and combustion on real engines. This has, perhaps, been limited by the lack of suitable measuring techniques and the complex physical phenomena. In 1989, the AVL company developed a High Speed Photography System [38] which allows filming of fuel atomisation and combustion in real engines under realistic conditions. Thus, the obstructions to this field of study are not the measuring techniques but the requirements and interests of the application of emulsified fuels in diesel engines.

2). Emulsified Fuels Properties At High Pressure Condition

A comprehensive study of emulsified fuels as non-Newtonian fluids was done as early as the 1920's [54]. The more specific research on W/O emulsified fuel properties, e.g. viscosity, surface tension and water droplets size etc., was undertaken in the 1980's [22,23]. The previous reports on this aspect, having provided a theory based on the assumption of micro-explosions, gave the W/O emulsions properties associated with temperature at atmosphere pressure. Fuel injection in a diesel engine concerns very high pressure (more than 2,000 kgf/cm^2). At such high pulse pressures, what would happen to the emulsified fuels where fine water droplets are homogeneously distributed at 'low' pressure? Will the individual droplets congregate or further break down? Will the properties still be the same as those at atmosphere pressure? These questions need to be answered to further establish the actual explanation of the effect of emulsified fuel on atomisation and combustion.

3). Modifications To The Developed Models

All the models developed in this project will have to be modified when they are used to simulate the atomisation of emulsified fuels in a real engine, since the models were developed from the tests in a "cold" bomb and the injection rate was not considered. The modifications can be made in two ways. One is to add the effective components into the models based on real engine test results; Another one is to directly change the constants in the models. The temperature effect can also be converted into the parameters of P_g and ρ_g.

Taking the effect of temperature on the Sauter mean diameter (referring to Eq. 6.19) as an example, if the Sauter mean diameter is considered as a function of temperature, the non-dimensional parameter T/T_0 should be included in the developed model. Thus,

$$\frac{D_{32}}{D_0} = C \cdot \left(\frac{D_0 \cdot \rho_g \cdot g}{\Delta P} \right)^{B_1} \cdot \left(\frac{q}{D_0^3} \right)^{B_2} \cdot e^{B_3 \cdot \gamma} \cdot f\left(\frac{T}{T_0} \right)$$

In the above equation, function $f(T/T_0)$, the effect of temperature on the Sauter mean diameter, can be determined from the test results.

For changing the constant in the developed model (referring to Eq. 6.19), a reference temperature, e.g. the mean temperature during the injection period or the temperature at the beginning of the injection (or end of the compression), can be employed as a reference for the constant C. For example, when T_{ref}=t °K, C can be written as C(t). According to the test results, there will be a corresponding C(t) at each T_{ref}. Thus, the resulting expression of the Sauter mean diameter of Eq. 6.21 will become:

$$D_{32} = C(t) \cdot \left(\frac{\rho_g}{\Delta P} \right)^{0.189} \cdot D_0^{0.703} \cdot q^{0.162} \cdot e^{-0.595 \cdot \gamma}$$

7.2 Conclusions

From this water-in-oil emulsified fuels atomisation study, it is clear, from both the tests and mathematical models, that the effects of water on fuel atomisation play a major

role in improving engine performance. It is evident that the test results do not contain any consideration of micro-explosions, since the tests were carried out in a 'cold bomb'. The author does not deny the micro-explosion theory, which was proposed as the major source of the improvement of engines' performance. The point is, as discussed in Chapter one, that the positive effects of micro-explosions may only occur at their limiting conditions which may only be present for a small fraction of the combustion period. The presence of micro-explosions would therefore not be so significant in improving engines' combustion and emissions.

This project testifies that the atomisation of emulsified fuels presents a major contribution to engines' performance improvements, whether micro-explosions occur or not.

REFERENCES:

1) Flanagan B.D., "The potential of burning water in fuel emulsion at sea," The Society of Naval Architects and Marine Engineers, Paper presented at the spring meeting/STAR Symposium, New London, Apr. 1978

2) Volkmar, D.S., et al, "Emulsion production and boiler performance with the Total-Bertin Emulsifier," paper presented at DOT Symposium, Sep. 1978

3) Diana D., et al, "Performance of water emulsified residual fuels in a medium-speed diesel," ASME paper No. 83-DGP-10, 1983

4) Thorp I., et al, "Application of O/W emulsion as a diesel engine fuel," University of Newcastle upon Tyne, U.K., Paper published by North East Coast Institution of Engineers and Shipbuilders, Jan. 1980

5) Patricia A, Strandell, et al, "A review of water emulsified fuel investigations for shipboard applications," Naval Engineers Journal, Mar. 1986

6) Katsoulakos P.S., "Effectiveness of the combustion of emulsified fuels in diesel engine," C84/83 IMechE 1983

7) Minoru Tsukahara, et al, "Influence of fuel properties on the combustion in diesel engine driven by the emulsified fuels," Bulletin of the JSME, Vol.25, No.202, Apr. 1982

8) Kazuya Mitsuhashi, et al, "Application of emulsified fuel on diesel engine," Japan Shipbuilding & Marine Engineering, Vol.13, No.1, 1979

9) Sheng H.Z., et al, "Study of atomization and vaporization of emulsified diesel fuel droplets by laser holography," CSICE 885040, May 1988

10) Sheng H.Z., "The investigation of combustion process of emulsified diesel fuel by high speed photography," CSICE 885047, May 1988

11) Sheng S.Z., "Performance prediction and computation of combustion process of emulsified fuel on D.I. diesel engine," CSUCE 885046, May 1988

12) Sheng S.Z., et al, "The relation Between micro-explosions of emulsified fuel and fuel saving," Thermodynamic Institute of China 884075, Nov. 1988

13) Sheng H.Z., "Micro-explosion and combustion characteristics of water-in-diesel fuel emulsion", IMeche, Seminar on Diesel Fuel injection Systems, Oct. 1989

14) Jordan J.B., et al, "The influence of added water on combustion processes", Communication, Dept. of Fuel and Energy, University of Leeds, U.K., Sept. 1979

15) Hughes F.A., "Emulsifiers for fuel economy", Shipbuilding and Marine Engineering International, Sept. 1982

16) Davies C.B., "Microfelt filters for treating heavy fuel", Shipbuilding and Marine Engineering International, July/Aug. 1979

17) Adge A.M., "Combustion of water impregnated fuels in marine diesel engines", Communication, Dept. of Marine Engineering, University of Newcastle upon Tyne, U.K., July 1980

18) Mellows S., "Combustion of water impregnated fuels in marine diesel engines", Research Proposal, Dept. of Marine Engineering, University of Newcastle upon Tyne, U.K., Dec. 1980

19) Hiroshi Okada, et al., "Soot formation in the combustion of emulsion fuel droplets", Bulletin of the JSME vol. 8 No. 4 Dec. 1980

20) Tsao K.C., et al., "Puffing and micro-explosion phenomena of water emulsion fuels", SAE 860304

21) Cook H., et al., "A preliminary study on the utilization of water-in-oil emulsions in diesel engines", Combustion Science and Technology, Vol. 18 pp211-221 1978

22) Dept. of Marine Engineering, University of Newcastle Upon Tyne, U.K., "The evaluation of emulsified fuel in marine diesel engines", Final report, Dec. 1980

23) Zheng K.Z., "The study of water addition to heavy oil used on middle speed engine", Dalian Maritime University, China, (in Chinese) 10. 1989

24) Doober J., et al, "Emulsion as fuels", Mechanical Engineering, Nov. 1976

25) Toshio Shimada et al, "Investigation on combustion in diesel engines using a constant volume combustion chamber," Bulletin of the JAMS Vol. 22, No.174, Dec. 1979

26) Johnston S.C., et al, "An experimental investigation into the application of spontaneous Raman scattering to spray measurements in an engine," Sandia National Laboratories, Livermore, California

27) Mildred Cohn, et al, "Combustion in a bomb with a fuel-injection system," Report No. 544, National advisory committee for Aeronautics, 1975

28) Hajime Fujimoto, et al, "Investigation on combustion in Medium-speed Marine diesel engine using model chambers," CIMAC, 12th International Congress on Combustion Engines, Feb. 1989

29) Hajime Fujimoto, et al, "Investigation on the characteristics of diesel spray," Bulletin of the JSME, Vol.25, No.200, Feb. 1982

30) Wassenaar H., "Injection phenomena in high-speed diesel engines," Royal Dutch/Shell Laboratory , Delft, N.K., de Bataafsche Petrolem Maatschappij, Feb. 1955

31) Scheid E., et al, "Spray combustion chamber with optical access, ignition zone visualization and first Raman measurements of local Air-Fuel Ratio," SAE, 861121

32) Joe Rife, et al, "Photographic and performance studies of diesel combustion with a Rapid Compression Machine," SAE, 740948

33) Wigley G., et al, "In-cylinder swirl measurement by laser anemometry in a production diesel engine," Engineering Sciences Division, AERE Harwell, AERE-R9651 HL79/3928, Dec. 1979

34) Shiozaki, et al, "Observation of combustion process in D.I. diesel engine via high speed direct and Schlieren photography," SAE, 800025

35) Falcus M., "Photographic studies of diesel combustion in a quiescent combustion chamber," SAE, 831292

36) James F. Sinnamon, et al, "An experimental and analytical study of engine fuel spray trajectories," SAE, 800135

37) Shin Matsuoka, et al, "Application of laser anemometry to a motored diesel engine," SAE, 800965

38) Karimi E.R., "High-speed photography of fuel spray combustion events in a production diesel engine and combustion bomb," C372/012, IMechE, Mar. 1989

39) Kamimoto T., et al, "The measurement of flame temperature and the thermodynamic analysis of combustion processes in a direct injection diesel engine," C96/75 IMechE, Dec. 1974

40) Turns S.R., et al, "An estimation of Quench-Gas Bias in internal combustion engine in-cylinder sampling," Combustion and Flame 39, 97-109, 1980

41) Sinha S.K., "Study of combustion processes of emulsified W/F mixture," Mar. 1975

42) Tishkoff J.M., "Diagnostic measurements of fuel spray dispersion," ASME, 80-W4/HT-35

43) Swithenbank J., et al, "A laser diagnostic technique for the measurement of droplet and particle size distribution," AIAA Paper, No.76-69, AIAA 14th Aerospace Sciences Meeting, Washington D.C., Jan. 1976

44) Norman A. Chigier, "Instrumentation techniques for studying heterogeneous combustion," Dept. of chemical engineering and fuel technology, University of Sheffield, England, Apr. 1977

45) Yule A.J., "Measurement techniques for spray combustion," Dept. of chemical engineering and fuel technology, University of Sheffield, England, Apr. 1977

46) Amann C.A., "A perspective of reciprocating engine diagnostics without laser", Prog. energy combust. Sci. 1983 Vol. 9

47) Saffmann M., et al., "Simulations measurements of size, concentration and velocity of spherical particles by a laser Doppler method", 2nd international symposium on application of laser anemometry to fluid mechanics, 2-4 July 1984 Lisbon

48) Nakayama M., "Studies on luminous and non-lominous flames with spray combuster", Bulletin of the JSME, Vol. 216 June 1983

49) Norman Chigier, "Group combustion models and laser diagnostic methods in sprays: A Review", Combustion and Flames 51, 127-139 1983

50) Wigley G., et al., "Swirl velocity measurements in a firing production diesel engine by laser anemometry", Engineering Sicence Division, AERE Harwell, U.K.

51) Chigier N.A., "The atomisation and burning of liquid fuel sprays", Prog. energy combust. Sci. Vol. 2 1976

52) Gao X.Y., "The investigation of diesel spray with laser technology", Dalian Technological Institute, China, (in Chinese) 1986

53) G.Takeshi, Sato, "Structure of diesel spray," Liquid Atomisation and Spray Systems 3rd Int. Conf. ICLASS-85

54) Sherman P.,«Emulsion Science», 1968

55) 5th short course notes on atomization and spray technology, UMIST, Jan. 1991

56) Bracco F.V., "Modeling of Engine spray", SAE 850394

57) Sirignano W.A., "Fuel droplet vaporisation and spray combustion theory", Prog. energy combust. Sci. 1983 Vol. 9

58) Williams T.J., "Parameters for correlation of penetration results for diesel fuel sprays", Proc. instn Mech. Engrs 1973 Vol. 187 69/73

59) Lee D.W., "The effect of nozzle design and operating conditions on the atomisation and distribution of fuel sprays", Report No. 425, National advisory committee for Aeronautics, 1932

60) Hiroyasu H., et al., "Development and use of a spray combustion modeling to predict diesel engine efficiency and pollutant emissions", Bulletin of the JSME Vol. 26, No.214 April 1983

61) Giffen E., "Pressure calculation for oil engine fuel injection system", Dept. of Mechanical Engineering, King's College, London

62) Brunello C., et al., "Characterisation of transient spray structure in cross flows", CNPM - National Research Council, Peschiera Borromeo, Milano, Italy

63) Bracco F.V., "Introducing a new generation of more detailed and informative combustion models", SAE 741174

64) Reynolds W.C., "Modeling of fluid motions in engines--an introductory overview", Stanford University, California

65) Dent J.C., "A basis for the comparison of various experimental methods for studying spray penetration", SAE 710571

66) Mattavi J.N. and Amann C.A., «Combustion Modeling In Reciprocating Engines», 1980

67) Law C.K., "A model for the combustion of Oil/Water emulsion droplets", Combustion Science and Technology, Vol. 17, pp 29-38, 1977

68) Wilfred E. Baker; Peter S. Westine; Pranklin T. Dodge, «Similarity Methods in Engineering Dynamics», 1973

69) Fu W.B., «Combustion Physics Fundamentals», 1985

70) Heywood J.B., «Internal Combustion Engine Fundamentals», 1988

71) Weaving J.H., «Internal Combustion Engineering: Science and Technology», 1990

72) Tullis S., et al., "Optimising diesel combustion with an EUI system for heavy-duty trucks", Seminar on Diesel Fuel Injection Systems, I Mech E, Birmingham, 14-15, April 1992

73) Yang M.G., "Characteristics of an electronic pump-pipe-injector system with electromagnetic spill control", Seminar on Diesel Fuel Injection Systems, I Mech E, Birmingham, 14-15, April 1992

74) Farra-Khan J.R., et al., "Influence of nozzle sac volume on diesel spray droplet size", Seminar on Diesel Fuel Injection Systems, I Mech E, Birmingham, 14-15, April 1992

75) Zelenka P., "Ways toward the clean heavy duty diesel", SAE 900602

BIBLIOGRAPHIES:

1) Izumi S., et al., "Effects of fuel injection mode on residual fuel combustion in high speed marine diesel engine", Faculty of Engineering, Nagaski University, Japan

2) Khan I.M., et al., "Factors affecting smoke and gaseous emissions from direct injection engines and a method of calculation", SAE 730169

3) James N. Mattavi and Charles A. Amann, «Combustion Modeling In Rreciprocating Engines», 1980

4) N.C. Markatos, «Computer Simulation In Reciprocating Engines», 1989

5) Randall McMullan, «Practical AutoCAD», 1989

APPENDIX A:

DATA OF SPRAY PENETRATION AFTER SMOOTHING

Table A.1 Test data of spray penetration after smoothing

Time	Spray penetration (mm)												
(ms)	No. 1	2	3	4	5	6	7	8	9	10	11	12	13
0.75	27.51	33.31	33.67	33.25	35.83	31.52	33.19	31.43	34.92	36.14	33.11	33.20	33.70
1.00	32.93	37.61	37.31	34.89	41.90	39.35	39.53	39.29	36.71	41.58	41.44	39.48	39.42
1.25	38.65	43.31	40.30	40.07	46.36	44.09	44.44	44.64	42.91	45.95	48.28	45.36	44.32
1.50	44.11	48.36	42.95	46.22	52.24	50.12	48.49	49.88	47.09	49.40	52.17	50.83	49.16
1.75	49.46	53.95	45.29	51.30	55.26	52.33	52.09	54.99	50.71	52.95	55.14	55.91	54.11
2.00	54.92	62.58	51.21	55.26	58.69	56.06	55.41	59.78	54.91	57.69	57.94	59.33	59.06
2.25	60.17	66.37	56.74	60.01	64.46	59.71	58.40	63.93	60.17	62.57	60.83	63.67	63.74
2.50	64.75	68.78	61.13	64.38	69.38	62.58	61.93	67.89	65.44	66.58	64.38	67.67	67.92
2.75	68.13	71.12	65.23	68.63	72.85	65.87	65.37	71.37	70.58	69.56	68.46	71.37	71.74
3.00	71.81	76.53	69.84	73.66	73.88	66.97	68.59	74.43	75.62	75.58	72.80	74.75	75.65
3.25	75.51	78.16	74.17	77.94	77.85	74.09	73.89	77.79	80.00	78.81	76.47	79.55	79,80
3.50	79.44	79.70	78.49	83.64	81.74	77.29	76.73	81.42	82.51	81.95	79.12	82.84	82.38

The test conditions for each corresponding test No. have been shown in Table 5.4.

There are 13 test points and, at each test point, 12 readings are obtained. Therefore, there are in total 156 (13x12) readings in Table A.1. This number will be represented by the parameter "i" in Appendix C.

APPENDIX B:

TEST DATA OF DROPLET DIAMETERS AFTER CALIBRATION

Table B.1 Droplets number count

Size Classes (μm)	Count				
	Test 1	Test 9	Test 11	Test 12	Test 13
0.0 - 2.5	0.0000	0.0000	0.0000	0.0000	0.0000
2.5 - 5.0	1.5350	10.4915	25.0182	7.4304	9.6845
5.0 - 7.5	165.4976	38.9126	109.6154	54.9888	44.9830
7.5 - 10.0	163.2637	86.3363	123.5280	82.1632	75.3885
10.0 - 12.5	155.4429	149.7379	151.3168	157.0367	134.2112
12.5 - 15.0	177.4260	122.8768	115.6128	156.8688	101.7888
15.0 - 17.5	87.6990	106.8077	89.9661	120.5313	86.7380
17.5 - 20.0	50.2980	89.0169	87.7718	76.8928	90.9830
20.0 - 22.5	33.1591	76.4029	72.8070	60.8336	84.8592
22.5 - 25.0	30.9532	60.2112	58.9459	44.1280	63.3677
25.0 - 27.5	26.5975	47.9452	40.4739	47.4704	50.0169
27.5 - 30.0	21.3197	30.3514	39.9120	26.1456	42.4570
30.0 - 32.5	29.7177	23.0163	35.0880	23.7088	35.3670
32.5 - 35.0	16.5507	14.8422	24.5795	22.5152	26.8077
35.0 - 37.5	12.1123	22.9466	29.4544	20.6304	28.3853
37.5 - 40.0	11.5507	7.5267	14.7021	11.2320	19.7015
40.0 - 42.5	7.9251	7.5776	17.8585	9.0528	17.8240
42.5 - 45.0	7.2246	1.7197	10.3683	9.8976	12.3155
45.0 - 47.5	7.9064	1.2803	8.5078	3.6192	8.6480
47.5 - 50.0	6.5320	0.6669	4.1408	2.6976	2.1402
50.0 - 52.5	3.6630	1.4035	4.4029	0.1568	4.5443
52.5 - 55.0	2.6084	1.4035	1.4035	0.6688	2.7888
55.0 - 57.5	5.4586	0.0000	2.2810	1.8720	1.7549
57.5 - 60.0	5.7738	0.0000	1.8070	2.7008	0.2451
60.0 - 62.5	1.0094	0.0000	2.1226	1.7120	0.6845
62.5 - 65.0	0.7754	0.0000	0.4035	0.0464	0.0000
65.0 - 67.5	0.2434	0.0000	0.9120	0.7328	0.0000

Cont-ed

Cont. Table B.1

67.5 - 70.0	1.0094	0.0000	0.8950	0.0000	0.0000
70.0 - 72.5	1.0094	0.0000	0.0000	0.0000	0.0000
72.5 - 75.0	1.0094	0.0000	0.0000	0.0000	0.0000
75.0 - 75.5	0.0000	0.0000	0.0000	0.0000	0.0000
Total	1036	892	1074	947	946

Table B.2 Droplets number count percentage

Size Classes (μm)	Count %				
	Test 1	Test 9	Test 11	Test 12	Test 13
0.0 - 2.5	0.0000	0.0000	0.0000	0.0000	0.0000
2.5 - 5.0	0.1482	1.1762	2.3294	0.7846	1.0237
5.0 - 7.5	15.9747	4.3624	10.2063	5.8066	4.7551
7.5 - 10.0	15.7590	9.6790	11.5017	8.6762	7.9692
10.0 - 12.5	15.0041	16.7868	14.0891	16.5826	14.1872
12.5 - 15.0	17.1261	13.7754	10.7647	16.5648	10.7599
15.0 - 17.5	8.4652	11.9740	8.3767	12.7277	9,1689
17.5 - 20.0	4.8550	9.9795	8.1724	8.1196	9.6177
20.0 - 22.5	3.2007	8.5653	6.7791	6.4238	8.9703
22.5 - 25.0	2.9878	6.7501	5.4884	4.6598	6.6985
25.0 - 27.5	2.5673	5.3750	3.7685	5.0127	5.2872
27.5 - 30.0	2.0579	3.4026	3.7162	2.7609	4.4881
30.0 - 32.5	2.8685	2.5803	3.2670	2.5036	3.7386
32.5 - 35.0	1.5976	1.6639	2.2886	2.3775	2.8338
35.0 - 37.5	1.1691	1.4514	2.7425	2.1785	2.0006
37.5 - 40.0	1.1149	0.8438	1.3689	1.1861	2.0826
40.0 - 42.5	0.7650	0.8495	1.6628	0.9559	1.8841
42.5 - 45.0	0.6974	0.1928	0.9654	1.0452	1.3019
45.0 - 47.5	0.7632	0.1435	0.7922	0.3822	0.9142
47.5 - 50.0	0.6305	0.0748	0.3855	0.2849	0.2262
50.0 - 52.5	0.3536	0.1573	0.4100	0.0166	0.4804
52.5 - 55.0	0.2518	0.1573	0.1307	0.0706	0.2948

Cont-ed

Cont. Table B.2

55.0 - 57.5	0.5269	0.0000	0.2124	0.1977	0.1855
57.5 - 60.0	0.5573	0.0000	0.1683	0.2852	0.0259
60.0 - 62.5	0.0974	0.0000	0.1976	0.1808	0.0724
62.5 - 65.0	0.0748	0.0000	0.0376	0.0049	0.0000
65.0 - 67.5	0.0235	0.0000	0.0849	0.0774	0.0000
67.5 - 70.0	0.0974	0.0000	0.0833	0.0000	0.0000
70.0 - 72.5	0.0974	0.0000	0.0000	0.0000	0.0000
72.5 - 75.0	0.0974	0.0000	0.0000	0.0000	0.0000
75.0 - 75.5	0.0000	0.0000	0.0000	0.0000	0.0000

Test conditions for table B.1 and B.2 are:

Test No.	P_{inj} (bar)	P_g (bar)	D_0 (mm)	q_{inj} (ml)	γ (%)
1	180	55	0.37	0.70	0
9	150	50	0.37	0.70	10
11	180	55	0.37	0.70	10
12	180	55	0.37	0.70	15
13	180	55	0.37	0.70	20

P_{inj}: injection pressure,

P_g: gas pressure,

D_0: nozzle diameter,

q_{inj}: fuel injection amount,

γ: water content,

1). The scale of charge amplifier was 1.00,

2). The camera lens was a micro-lens and the rotary shutter constant was 40,

3). The bomb gas temperature was 17.0°C; the injection frequency was 325

injs./min; and the film speed is 4,000 fps,

4). The fuel dynamic viscosity ($\rho_f \cdot \nu_f$) was 850(kg/m^3) x $3.5x10^{-6}(m^2/s)$ = $2.975x10^{-3}$ (Ns/m^2), and its surface tension was 0.0239 (N/m).

APPENDIX C:

INPUT DATA FOR SPRAY PENETRATION REGRESSION

From equation 6.9:

$$Y = B_0 + B_1X_1 +, \ldots, +B_6X_6$$

$Y = \ln(S_i/D_0)$, where "i" (i=156, see Appendix A) is the number of readings obtained.

B_j (j=0,1,...,6) are the unknown terms,

$X_{ij} = \ln K_{ij}$, j=1,...,6

$$K_{i1} = \frac{\Delta P \cdot D_0^2 \cdot \rho_g}{\mu_f^2}, \qquad K_{i2} = \frac{\sigma_f \cdot D_0 \cdot \rho_g}{\mu_f^2},$$

$$K_{i3} = \frac{\rho_f}{\rho_g}, \qquad K_{i4} = \frac{t_i}{t_0},$$

$$K_{i5} = \gamma, \qquad K_{i6} = \gamma \ln\left(\frac{t_i}{t_0}\right).$$

The original input data for K_{ij} are shown in table C.1.

Table C.1 The original input data for parameter K_{ij}

Test No.	ΔP (Mpa)	ρ_g (kg/m^3)	D_0 (mm)	γ
1	12.25	62.50	0.37	0.00
2	15.68	56.80	0.35	0.00
3	10.29	51.10	0.39	0.00
4	12.74	56.80	0.39	0.05

Cont-ed

Cont. Table C.1

5	16.11	51.10	0.37	0.05
6	9.31	62.50	0.35	0.05
7	13.25	51.10	0.35	0.10
8	15.19	62.50	0.39	0.10
9	9.80	56.80	0.37	0.10
10	12.25	62.50	0.37	0.15
11	12.25	62.50	0.37	0.20
12	12.25	62.50	0.37	0.05
13	12.25	62.50	0.37	0.10

The values for the other parameters in K_{ij}, (j=1,...,6) are:

μ_f (fuel dynamic viscosity) =2.975×10^{-3} (Ns/m^2),

σ_f (fuel surface tension) =0.0239 (N/m),

ρ_f (fuel density) =$850(kg/m^3)$,

t_0 (time of injection duration) =3.2 (ms).

The values for S_i and t_i (spray penetration at time t_i) are same as the table A.1 in Appendix A

APPENDIX D:

TWO ALTERNATIVE MATHEMATICAL MODELS FOR SPRAY PENETRATION

In Chapter three, one of the spray penetration models has been developed, which firstly considered the parameters of fuel viscosity, surface tension and density, then merged them into the constant shown as follows:

$$\frac{S}{D_0} = 5.788 \times 10^7 \left(\frac{\Delta P \cdot D_0^2 \cdot \rho_g}{\mu_f^2} \right)^{0.175} \cdot \left(\frac{\sigma_f \cdot D_0 \cdot \rho_g}{\mu_f^2} \right)^{-1.179} \cdot \left(\frac{\rho_f}{\rho_g} \right)^{-0.851} \cdot \left(\frac{t}{t_0} \right)^{0.594} \cdot e^{0.244 \cdot \gamma \cdot \left(\frac{t}{t_0} \right)^{-1.562}}$$

Taking μ_f, ρ_g, σ_f and t_0 as constants,

gives:

$$S = 66.01 \cdot \frac{\Delta P^{0.176} \cdot D_0^{0.172} \cdot t^{0.594}}{\rho_g^{0.153}} \cdot e^{1.426 \cdot \gamma \cdot t^{-1.562}} \qquad ---6.11 repeat$$

The following discussion develops the spray penetration models without the parameters μ_f, ρ_g, σ_f and t_0.

Alternative model I:

In this model, only the parameters of injection pressure, nozzle diameter, gas density and time are considered. Their dimensional matrix is:

	a_1	a_2	a_3	a_4	a_5
	S	ΔP	D_0	ρ_g	t
L	1	-1	1	-3	0
M	0	1	0	1	0
T	0	-2	0	0	1

* L represents the length dimension,
  M represents the mass dimension,
  T represents the time dimension.

The dimensional determinant of the above matrix is:

$$\begin{aligned} 0 &= a_1 - a_2 + a_3 - 3a_4 \\ 0 &= a_2 + a_4 \\ 0 &= -2a_2 + a_5 \end{aligned}$$

Applying the "PI" theory, and assuming that a_1 and a_2 are known, gives

$$\begin{aligned} a_3 &= -2a_2 - a_1 \\ a_4 &= -a_2 \\ a_5 &= 2a_2 \end{aligned}$$

Substituting for a_3, a_4 and a_5 in a statement of dimensional homogeneity plus collecting exponents with the same coefficients, gives:

$$\left(\frac{S}{D_0}\right)^{a_1} \cdot \left(\frac{\Delta P \cdot t^2}{D_0^2 \cdot \rho_g}\right)^{a_2} = M^0 \cdot L^0 \cdot T^0$$

Let:

$$\pi_1 = \frac{S}{D_0} \qquad \pi_2 = \frac{\Delta P \cdot t^2}{D_0^2 \cdot \rho_g}$$

and including the non-dimensional parameter γ,

$$\pi_3 = \gamma$$

then:

$$\frac{S}{D_0} = f\left(\frac{\Delta P \cdot t^2}{D_0^2 \cdot \rho_g}, \gamma\right)$$

Alternative model II:

The parameters considered for developing model II are injection pressure, nozzle diameter and gas density. Their dimensional matrix is:

	a_1	a_2	a_3	a_4
	S	$\Delta P/g^*$	D_0	ρ_g
L	1	-2	1	-3
M	0	1	0	1
T	0	0	0	0

* g is the gravitational acceleration (m/s^2).

Applying the "PI" theory, and assuming a_1 and a_2 are known,

$$\left(\frac{S}{D_0}\right)^{a_1} \cdot \left(\frac{\Delta P/g}{\rho_g \cdot D_0^2}\right)^{a_2} = M^0 \cdot L^0 \cdot T^0$$

Plus the non-dimensional parameters $\frac{t}{t_0}$ and γ, gives:

$$\frac{S}{D_0} = f\left(\frac{\Delta P/g}{\rho_g \cdot D_0^2}, \frac{t}{t_0}, \gamma\right)$$

The mathematical regression results for these two alternative models have been shown in Chapter six. It was found that the alternative model I gives the "best" fit to the test results.

APPENDIX E:

AN ALTERNATIVE SIMULATION MODEL FOR SAUTER MEAN DIAMETER

Parameters considered in the tests:

ΔP -- pressure drop cross the nozzle hole,

D_0 -- nozzle diameter,

ρ_g -- gas density,

q -- injection amount,

γ -- water percentage in fuel by volume.

The dimensional matrix for the above parameters is:

	a_1	a_2	a_3	a_4	a_5
	D_{32}	$\Delta P/g^*$	D_0	ρ_g	q
L	1	-2	1	-3	3
M	0	1	0	1	0
T	0	0	0	0	0

* g is the gravitational acceleration (m/s^2).

The rank of the matrix is 2, supposing a_1, a_4 and a_5 are known and applying the non-dimensional theory L= M= T= 0, gives:

$a_2 = -a_4$

$a_3 = -a_1 + a_4 - a_5$

Then

$$\left(\frac{D_{32}}{D_0}\right)^{a_1} \cdot \left(\frac{\rho_g \cdot D_0 \cdot g}{\Delta P}\right)^{a_4} \cdot \left(\frac{q}{D_0^3}\right)^{a_5} = L^0 \cdot M^0 \cdot T^0$$

Assuming:

$$\pi_1 = \frac{D_{32}}{D_0}$$

$$\pi_2 = \frac{\rho_g \cdot D_0 \cdot g}{\Delta P}$$

$$\pi_3 = \frac{q}{D_0^3}$$

and including the non-dimensional parameter γ,

$$\pi_4 = \gamma$$

gives:

$$\frac{D_{32}}{D_0} = f\left(\frac{D_0 \cdot \rho_g \cdot g}{\Delta P}, \frac{q}{D_0^3}, \gamma\right)$$

where g is the gravitational acceleration.